NASA CONTRACTOR REPORT

NASA CR-2531

NASA CR-

ANALYTIC AND EXPERIMENTAL EVALUATION OF FLOWING AIR TEST CONDITIONS FOR SELECTED METALLICS IN A SHUTTLE TPS APPLICATION

John W. Schaefer, Henry Tong, Kimble J. Clark, Kurt E. Suchsland, and Gary J. Neuner

Prepared by
ACUREX CORPORATION
Mountain View, Calif.
for Langley Research Center

NATIONAL AERONAUTICS AND SPACE ADMINISTRATION • WASHINGTON, D. C. • AUGUST 1975

1. Report No.	2. Government Accession No.	3. Recipient's Catalog No.
NASA CR-2531		

4. Title and Subtitle	5. Report Date
ANALYTIC AND EXPERIMENTAL EVALUATION OF FLOWING AIR TEST CONDITIONS FOR SELECTED METALLICS IN A SHUTTLE TPS APPLICATION	AUGUST 1975
	6. Performing Organization Code

7. Author(s)	8. Performing Organization Report No.
John W. Schaefer, Henry Tong, Kimble J. Clark, Kurt E. Suchsland, and Gary J. Neuner	

9. Performing Organization Name and Address	10. Work Unit No.
Acurex Corporation Aerotherm Division Mountain View, CA	506-16-43-01
	11. Contract or Grant No. NAS1-10913
	13. Type of Report and Period Covered Contractor Report

12. Sponsoring Agency Name and Address	14. Sponsoring Agency Code
National Aeronautics & Space Administration Washington, DC 20546	

15. Supplementary Notes

FINAL REPORT

16. Abstract

A detailed experimental and analytical evaluation was performed to define the response of TD nickel chromium alloy (20 percent chromium) and coated columbium (R512E on Cb-752 and VH-109 on WC129Y)to shuttle orbiter reentry heating. Flight conditions important to the response of these TPS materials were calculated, and test conditions appropriate to simulation of these flight conditions in flowing air ground test facilities were defined. The response characteristics of these metallics were then evaluated for the flight and representative ground test conditions by analytical techniques employing appropriate thermochemical and thermal response computer codes and by experimental techniques employing an arc heater flowing air test facility and flat face stagnation point and wedge test models. These results were analyzed to define the ground test requirements to obtain valid TPS response characteristics for application to flight.

For both material types in the range of conditions appropriate to the shuttle application, the surface thermochemical response resulted in a small rate of change of mass and a negligible energy contribution.

The thermal response in terms of surface temperature was controlled by the net heat flux to the surface; this net flux was influenced significantly by the surface catalycity and surface emissivity. The surface catalycity must be accounted for in defining simulation test conditions so that proper heat flux levels to, and therefore surface temperatures of, the test samples are achieved.

17. Key Words (Suggested by Author(s))	18. Distribution Statement
Heat shielding Plasma jets TDNi-20Cr Coated niobium Space shuttle orbiter	Unclassified - Unlimited Category 26

19. Security Classif. (of this report)	20. Security Classif. (of this page)	21. No. of Pages	22. Price*
Unclassified	Unclassified	194	$7.00

*For sale by the National Technical Information Service, Springfield, Virginia 22151

FOREWORD

This report was prepared by the Aerotherm Division of Acurex Corporation under National Aeronautics and Space Administration Contract No. NAS1-10913, and describes an extensive experimental and analytical study of the response of bare and coated high temperature metallic alloys to shuttle orbiter vehicle reentry heating conditions. This work was sponsored by the Langley Research Center. The Aerotherm Program Manager and principal investigator was Mr. John W. Schaefer. The authors gratefully acknowledge the support of the other Aerotherm personnel who contributed to the program.

SUMMARY

A detailed experimental and analytical evaluation was performed to define the response of TD nickel chromium alloy (20 percent chromium) and coated columbium (R512E on Cb-752 and VH-109 on WC1269) to shuttle orbiter reentry heating. Flight conditions important to the response of these TPS materials were calculated, and test conditions appropriate to simulation of these flight conditions in flowing air ground test facilities were defined. The response characteristics of these metallics were then evaluated for the flight and representative ground test conditions by analytical techniques employing appropriate thermochemical and thermal response computer codes and by experimental techniques employing an arc heater flowing air test facility and flat face stagnation point and wedge test models. These results were analyzed to define the ground test requirements to obtain valid TPS response characteristics for application to flight.

For both material types in the range of conditions appropriate to the shuttle application, the surface thermochemical response resulted in a small rate of change of mass and a negligible energy contribution. This response for TD NiCr was characterized by subsurface kinetic oxidation of the base material to form an oxide film (Reference 1) and the diffusion controlled surface oxidation of this oxide film. A continuous buildup of this film, and the corresponding continuous depletion of the base material, occurred at a very slow rate. The thermochemical response for coated columbium was characterized (from diffusion-controlled thermochemical analysis) by the formation of condensed surface oxides and the volatilization of these oxides. The surface oxides formed were computed to be Cb_2O_5* and HfO_2* (for R512E and VH-109, respectively). A continuous slow buildup of these condensed oxides occurred. The oxide coating on TD NiCr and the two coated Cb coatings were partially noncatalytic (from experiment). The relative ranking in order of decreasing surface catalycity was TD NiCr, R512E, and VH-109, although differences between material types were small. The thermal response in terms of surface temperature was controlled by the net heat flux to the surface; this net flux was influenced significantly by the surface catalycity and surface emissivity.

Although the surface thermochemical response depends on pressure and enthalpy, a set of simulation test conditions which duplicates flight heat

flux at a pressure and enthalpy within, say, an order of magnitude of those of flight was determined to be acceptable on macroscopic thermochemical terms. This derives from the small magnitude of the thermochemical mass and energy effects. The microscopic surface response may vary considerably over this order of magnitude range and its effect on surface catalycity and surface emissivity must be considered. Surface catalytic response was a complicated function of the simulation test conditions, primarily enthalpy, pressure, and boundary layer characteristics, and it strongly affected the net flux to the surface and therefore the surface temperature. The surface catalycity must be accounted for in defining simulation test conditions so that proper heat flux levels to, and therefore surface temperatures of, the test samples are achieved. The thermal response was dependent on the net flux to the surface; the related limit on simulation test conditions was only that this flux be achieved within the other constraints defined above.

TABLE OF CONTENTS

TABLE OF CONTENTS (concluded)

LIST OF FIGURES

LIST OF FIGURES (concluded)

LIST OF TABLES

LIST OF SYMBOLS[1]

A	area, m^2 (ft^2)
B	pre-exponential constant
C	constant
C_F	momentum transfer coefficient, kg/m^2sec (lb/ft^2sec)
C_H	heat transfer coefficient, kg/m^2sec (lb/ft^2sec)
C_M	mass transfer coefficient, kg/m^2sec (lb/ft^2sec)
C_p	specific heat, J/kg°K (cal/gm°K or Btu/lb°R)
c_p	specific heat, J/kmol°K (cal/mol°K or Btu/mol°R)
d,D	diameter, m (ft)
E	voltage, V
E_a	activation energy, J/kmol (cal/mol)
f	friction coefficient
h	enthalpy, J/kg (Btu/lb)
K	mass fraction
K_o	constant (see Equation (B-3))
L	length, m (ft)

[1]List applies to main text and all appendices.

Le	Lewis number
$\dot{m}$	mass change rate, kg/m^2sec (lb/ft^2sec)
$\dot{m}_g$	gas flow rate, kg/sec (lb/sec)
$\dot{m}_j$	mass flux of j^{th} species, kg/m^2sec (lb/ft^2sec)
$\dot{m}_w$	water flow rate, kg/sec (lb/sec)
M	molecular weight, kg/kmol (g/mol or lb/mol)
M_e	Mach number
n	exponent
p	pressure, N/m^2 (atm)
Pr	Prandtl number
q	heat flux, W/m^2 (Btu/ft^2sec)
$q_{cat\ wall}$	catalytic wall convective heat flux, W/m^2 (Btu/ft^2sec)
q_{conv}	convective heat flux, W/m^2 (Btu/ft^2sec)
q_{loss}	conduction heat flux loss from surface, W/m^2 (Btu/ft^2sec)
q_{net}	net convective heat flux to surface, W/m^2 (Btu/ft^2sec)
$q_{noncat\ wall}$	fully noncatalytic wall convective heat flux, W/m^2 (Btu/ft^2sec)
$q_{rad\ out}$	radiation heat flux, W/m^2 (Btu/ft^2sec)
r, R	radius, m (ft)

R_B	model body radius, m (ft)
R_{eff}	effective model radius, m (ft)
$\mathscr{R}$	universal gas constant, J/kmol°K (cal/mol°K or Btu/lb°R)
Re_s	Reynolds number based on running length
Re_θ	Reynolds number based on momentum thickness
s	surface running coordinate, m (ft)
T_w	surface temperature, °K (°F or °R)
u_e	edge velocity, m/sec (ft/sec)
V	free stream velocity, m/sec (ft/sec)
y_p	oxide scale thickness, m (ft)
γ	isentropic exponent
ε	emissivity
θ'	dimensionless enthalpy gradient (see Reference A-5)
ν	stoichiometric coefficient
ρ	density, kg/m^3 (lb/ft^3)
σ	Stefan - Boltzmann constant, $W/m^2°K^4$ ($Btu/ft^2sec°R^4$)
τ_w	wall shear, N/m^2 (lb/ft^2)

SUBSCRIPTS

c	catalytic wall
e	edge or exit
eq	equivalent
n	noncatalytic wall
o	total
s	stagnation
tr	transition
w	wall or surface
*	throat
∞	free stream

ANALYTIC AND EXPERIMENTAL EVALUATION OF FLOWING AIR TEST CONDITIONS FOR SELECTED METALLICS IN A SHUTTLE TPS APPLICATION

by

John W. Schaefer, Henry Tong, Kimble J. Clark,
Kurt E. Suchsland, and Gary J. Neuner
Aerotherm Division of Acurex Corporation

SECTION 1

INTRODUCTION

The thermal protection system (TPS) for reusable hypersonic vehicles such as the space shuttle orbiter presents a major technological challenge. Bare and coated high temperature alloys offer an attractive potential for the TPS in some areas of these vehicles. Candidate materials include thoria dispersed nickel chromium alloys and columbium alloys with oxidation inhibiting coatings. Definitive evaluation of these materials in flowing air tests requires proper simulation of the flight environment of their application on the shuttle vehicle. A detailed study which investigates the definition of flight conditions and how they are simulated in ground test facilities is therefore desirable. This report presents the results of such a program for thoria dispersed nickel, 20 percent chromium alloy, and for two coated columbuim systems - R512E coating on Cb-752 alloy and VH-109 coating on C129Y alloy.

Flight conditions important to the response of these TPS materials were determined, and test conditions appropriate to simulation of these flight conditions in flowing air ground test facilities were defined. The response characteristics of these metallics were then evaluated for the flight and representative ground test conditions. This definition was accomplished by analytical techniques employing appropriate thermochemical and thermal response computer codes and by experimental techniques employing an arc heater flowing air test facility and stagnation point and wedge test models. These results were analyzed to define the ground test requirements to obtain valid TPS response characteristics for application to flight.

The program description and the primary program results are presented in the following sections. Additional details are presented in Appendices A through D.

SECTION 2

ENVIRONMENT/TPS INTERACTION

The boundary conditions and related parameters of potential importance to the response of metallics and other TPS material types are:

- Convective heat flux, enthalpy, and heat transfer coefficient
- Reactive species flux, species mass fraction, mass transfer coefficient, and species partial pressure
- Total pressure
- Local Mach number
- Boundary layer type and thickness
- Surface shear

The convective heat flux is the primary controller of the surface temperature response. This heat flux is given by

$$q_{conv} = C_H(h_o - h_w) \tag{1}$$

where h_o is the total (or recovery) enthalpy and h_w is the enthalpy of the air at the surface temperature.

Typically, the heat flux seen by the TPS material surface falls between the two extremes defined by a fully catalytic surface and a fully noncatalytic surface

$$q_{cat\ wall} = C_H(h_o - h_{w_c}) \tag{1a}$$

$$q_{noncat\ wall} = C_H(h_o - h_{w_n}) \tag{1b}$$

where h_{w_c} is the enthalpy of equilibrium air at the surface temperature and h_{w_n} is the wall enthalpy for the noncatalytic surface. This latter enthalpy corresponds to the surface nonequilibrium state for which recombination of the dissociated air does not occur in the boundary layer (frozen boundary layer) or at the surface (fully noncatalytic surface). The actual nonequilibrium state at the surface, independent of any interaction with the surface, is dependent on

the boundary layer characteristics. Typically some equilibration (recombination) of the dissociated species at the boundary layer edge occurs in transport through the boundary layer. The resultant surface air composition then interacts with the surface material and again typically some further equilibration of the dissociated species occurs. These events which control the final nonequilibrium state and therefore the heat flux to the surface (Equation (1)) are a complicated function of many variables including:

- Material surface chemical species and surface characteristic
- Air molecular composition at the boundary layer edge
- Enthalpy, total pressure, mass transfer coefficient, boundary layer characteristics

For metallics, the flux seen by the surface (Equation (1)) is essentially completely removed through radiation from the surface. For the case of simple radiation equilibrium, the surface temperature is therefore given by

$$q_{conv} = q_{rad\ out} = \varepsilon_w \sigma T_w^4 \tag{2}$$

where ε_w is the total hemispherical emissivity of the surface at the surface temperature T_w.

In addition to the primary effect of surface catalycity on the surface temperature, other effects must also be considered in evaluating TPS material response. These effects include:

- Surface thermochemical reactions
- In-depth and/or lateral heat conduction
- Surface emissivity

In the first case, oxidation or other surface thermochemical reactions can be significant contributors (plus or minus) to the surface energy flux. Thus the q_{conv} term of Equation (2) becomes $q_{conv} + q_{chem}$ where q_{chem} is the energy flux due to surface thermochemical reactions. Second, at least a small amount of the incident flux is conducted into the TPS and/or redistributed laterally. Thus the q_{conv} term of Equation (2) must also in general include a conduction term, $- q_{cond}$. For bare and coated metallics, the surface thermochemical reactions and in-depth or lateral conduction (q_{chem} and $-q_{cond}$) typically represent negligible contributions to the surface energy balance. Equation (2) unmodified is therefore an accurate characterization of the heat flux/surface temperature interaction for metallics. Finally, thermal effects on the material surface or surface thermochemical reactions can change the surface emissivity and therefore from Equation (2) change the surface temperature.

The reactive species flux to the surface controls the oxidation rate or surface thermochemical reaction rate for the case of diffusion rate control. This mass flux is given by[1]

$$\dot{m}_j = C_{M_j}(K_{j_e} - K_{j_w}) \tag{3}$$

where j indicates the particular reactive species and K_{j_e} and K_{j_w} indicate the boundary layer edge and wall mass fractions. As discussed above, the air molecular composition at the wall K_{j_w} is also influenced by boundary layer and surface catalycity effects.

For reaction rate control, oxidation or surface thermochemical reactions are controlled by the surface temperature and in some cases by the partial pressures of the reactive species as well. The reaction rate may be expressed by an equation of the form

$$\dot{m}_j = B_j e^{-E_{a_j}/\mathscr{R}T_w} p_j^n \tag{4}$$

where p_j is the partial pressure of the reactive species at the wall, n is an exponent (typically between 0 and 2), and the remainder of the equation is the Arrhenius expression.

The convective heat flux and the mass diffusion or surface reaction rates are in general interrelated in terms of the surface energy balance, the resultant surface temperature, and the oxidation or surface thermochemical reaction rates. Because of the small energy contribution of the last for metallics, their interaction may typically be ignored, however, and Equation (2) and Equations (3) or (4) may be considered independently.

Total pressure influences the response of metallics through its effect on:

---

[1]The transfer coefficients are related, in simplified form, through the relations

$$C_{M_j} = C_M = C_H Le^{2/3}$$

$$C_F = C_H Pr^{2/3}$$

where $C_F = \rho u_e (f/2)$.

- The oxide or other surface species that form due to surface thermochemical reactions
- The molecular composition at the boundary layer edge and at the surface, and the recombination rate in the boundary layer

The boundary layer type and thickness and the local Mach number influence the response of metallics through effects such as:

- Sensitivity to surface roughness or surface waviness and the possible enhanced heating
- Presence of singularity regions due to flow field disturbances
- Recombination rate in the boundary layer

Finally, surface shear or surface pressure gradients may be important to TPS response if the shear or gradients are large enough to cause stresses which result in failure or mechanical removal of the surface material. The surface shear is given by

$$\tau_w = \frac{f}{2} \frac{\rho u_e^2}{g} \tag{5}$$

This response mechanism is typically not significant to the bare and coated metallics.

SECTION 3

ANALYTICAL PROCEDURES

The response characteristics of metallic TPS materials were evaluated through analytical predictions of thermochemical and thermal response. Preliminary to this evaluation, the flight boundary conditions to which these materials are exposed and the appropriate test conditions in ground test flowing air facilities were defined. The procedures employed for this definition and evaluation are presented in this section. Additional details are presented in Appendices A and B.

3.1 FLIGHT AND TEST BOUNDARY CONDITIONS

The flight boundary conditions were defined for a representative shuttle vehicle configuration and trajectory, those of the Grumman H-33 vehicle (Reference 2 and private communication with Grumman Aircraft). An outline drawing of the vehicle is shown in Figure 1 and a typical trajectory for an entry angle-of-attack of 29° is shown in Figure 2. Flight conditions for specific trajectory points which were analyzed are shown in Table 1. Aerothermodynamic conditions on the windward side of this vehicle were predicted on the fuselage symmetry plane and the 40 percent semi-span plane of the wing. In addition, heat transfer distributions on the windward side of the fuselage forward of the wing-body junction were estimated.

The primary test configurations for reentry simulation testing are flat face stagnation point models, wedge models, and nozzle models as shown in the typical examples of Figure 3. These configurations accept flat panel test samples which are the most convenient test configuration. Aerothermal conditions were predicted for typical flat-face stagnation point and wedge models for a number of different approaches to ground test simulation.[1] Since it is not possible to duplicate all flight conditions in ground tests, each approach corresponds to a sacrifice in the duplication of one or more of the various flight conditions (Section 2). The four basic simulation approaches considered were:

- Type 1 - Heat flux, heat and mass transfer coefficient, enthalpy species flux, and environment the same as flight
- Type 2 - Heat flux, stagnation pressure, reactive species concentration (partial pressure), and environment the same as flight.

[1]No tests were performed under this program for the nozzle test configuration and therefore no predictions of test conditions were made.

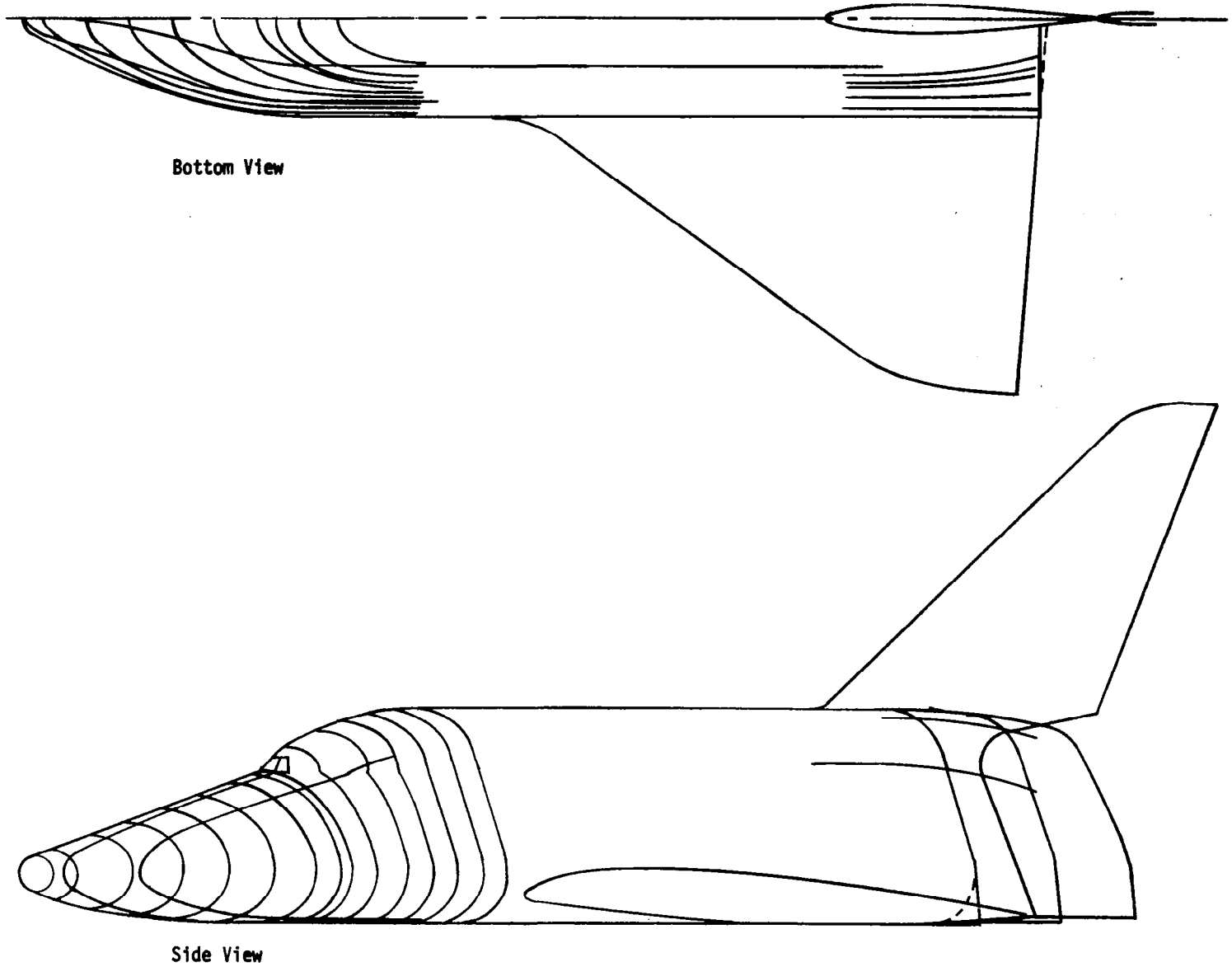

Figure 1. Baseline Shuttle Vehicle Configuration

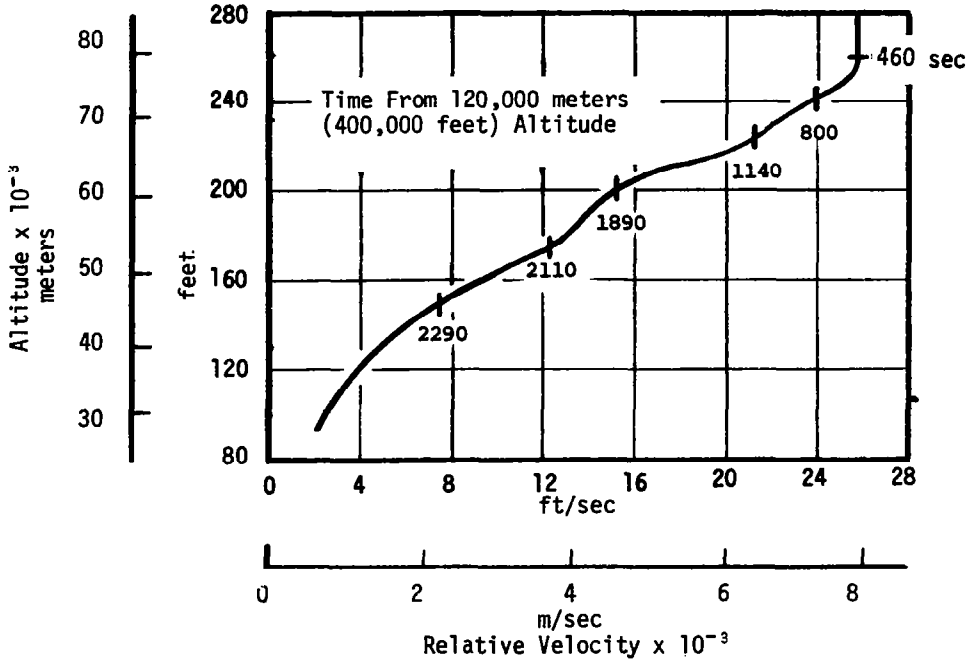

Figure 2. Baseline Reentry Trajectory

TABLE 1

TRAJECTORY INFORMATION FOR DEFINITION OF FLIGHT CONDITIONS
a) SI Units

Case	Time From Start of Reentry (sec)	Altitude (1000 m)	Mach Number	Static Pressure (N/m^2)	Stagnation Pressure (N/m^2)	Stagnation Enthalpy (J/kg)	Wing Leading Edge Pressure (N/m^2)
1	460	77.7	28.2	1.56	1.60×10^3	5.5×10^7	7.46×10^2
2	800	73.2	25.1	3.37	2.74×10^3	4.8×10^7	1.28×10^3
3	1140	68.6	21.4	6.83	4.03×10^3	3.8×10^7	1.88×10^3
4	1890	61.0	14.4	19.75	5.30×10^3	1.9×10^7	4.26×10^3
5	2110	53.3	11.6	52.69	9.15×10^3	1.4×10^7	4.26×10^3
6	2290	45.7	7.1	135.5	9.00×10^3	0.53×10^7	4.19×10^3

TABLE 1 (CONCLUDED)

b) Conventional Units

Case	Time From Start of Reentry (sec)	Altitude (1000 ft)	Mach Number	Static Pressure (atm)	Stagnation Pressure (atm)	Stagnation Enthalpy (Btu/lb)	Wing Leading Edge Pressure (atm)
1	460	255	28.2	1.54×10^{-5}	0.0158	13,170	.00736
2	800	240	25.1	3.33×10^{-5}	0.0270	11,390	.0126
3	1140	225	21.4	6.74×10^{-5}	0.0398	9,010	.0186
4	1890	200	14.4	1.95×10^{-4}	0.0523	4,650	.0244
5	2110	175	11.6	5.20×10^{-4}	0.0903	3,230	.0420
6	2290	150	7.1	1.34×10^{-3}	0.0888	1,270	.0414

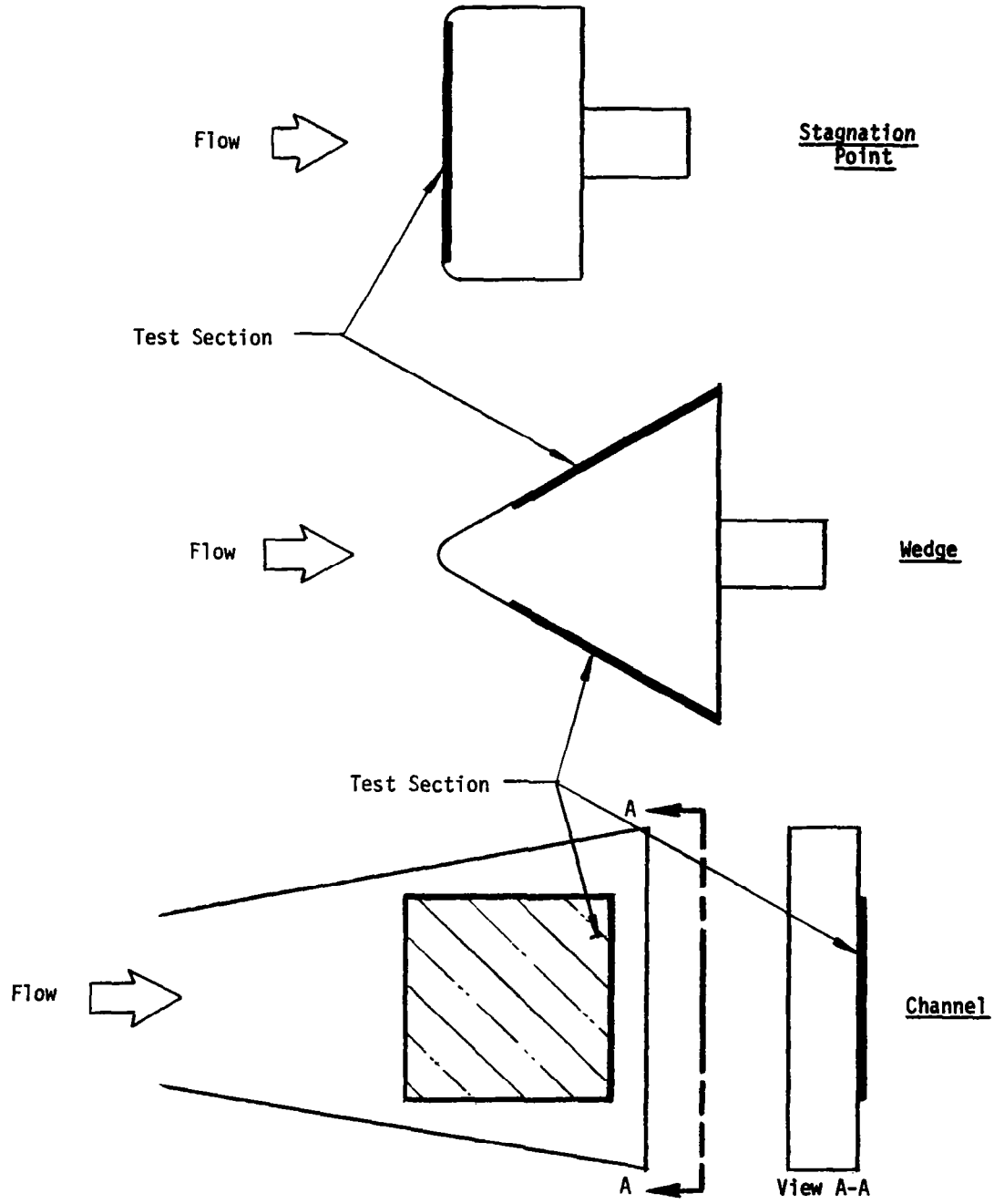

Figure 3. Typical Shuttle TPS Test Configurations

- Type 3 - Heat flux, species flux, and stagnation pressure the same as flight
- Type 1-2 - Compromise between types 1 and 2 which optimizes test capabilities

Note that heat flux is always duplicated since it is the critical response parameter (Section 2). Note also that type 1 simulation results in a sacrifice of total and partial pressure simulation, type 2 simulation results in a sacrifice in enthalpy and species flux simulation, type 3 simulation results in a sacrifice in enthalpy, partial pressure, and environment (non-air) simulation, and type 1-2 simulation falls between the type 1 and type 2 simulations and results in at least a small sacrifice in most variables.

The analysis procedures employed for definition of both the flight and test boundary conditions were similar. Pressure and Mach number distributions were defined using conventional flow field approximation procedures. The boundary layer parameters, including the computation of heat flux, were predicted with the Aerotherm Boundary Layer Integral Matrix Procedure (BLIMP) code (Reference 3).[1] The BLIMP code treats the nonsimilar, compressible, chemically reacting, multicomponent, two-dimensional, laminar or turbulent boundary layer. It computes its own boundary layer edge conditions from the distributions of pressure, and allows for transition from laminar to turbulent flow. For the flight case, an appropriate boundary layer transition criterion was developed and employed in the computations. In the analysis of boundary conditions, the surface of the vehicle and models was assumed to be smooth and the boundary layer was assumed to be in chemical equilibrium, this latter assumption also being equivalent to the assumption of a fully catalytic wall. The maximum possible reduction in flux resulting

[1]For simplified calculations of test model heat flux only, approximate equations may be employed. For a stagnation point model (Reference 4)

$$q_{conv} = 0.042 \sqrt{\frac{p_s}{R_{eff}}} (h_o - h_w) \tag{6}$$

where $R_{eff} = 3.78\ R_B$ for a flat face model at typical test stream Mach numbers (Reference 5). For a wedge model (private communication with Langley Research Center)

$$q_{conv} = 0.021 \sqrt{\frac{p_e}{s}} (h_o - h_w) \tag{7}$$

where s is the wedge surface running length.

from a completely frozen boundary layer and a fully noncatalytic wall was also computed, however.

3.2 THERMOCHEMICAL AND THERMAL RESPONSE

The thermochemical and thermal responses of TD NiCr and coated Cb were computed using the thermochemical models and the computation procedures presented in the following subsections.

3.2.1 Thermochemical Models

The thermochemical response model employed for TD NiCr was that of Reference 1. Accordingly, the main features of the thermochemical response of TD NiCr are:

- Subsurface oxidation of the base metal
- Surface oxidation of the exposed oxide film

The oxide scale which initially forms on bare TD NiCr is mostly NiO*[1] with a thin subscale of Cr_2O_3*. However, once the Cr_2O_3* subscale is established, and this occurs quite early in the time scale of interest in this work, further growth of the NiO* scale is prevented because diffusion of Ni is blocked by the Cr_2O_3* subscale. Thereafter the primary subsurface oxidation mode is the formation of Cr_2O_3*, which is assumed to follow a parabolic oxidation law. The usual parabolic oxidation formulation ignores the microscopic details of the oxidation process and considers the consumption of oxygen from a global point of view; e.g., for the formulation of Cr_2O_3* the overall reaction is

$$2Cr^* + 3/2\ O_2 \rightarrow Cr_2O_3^* \qquad (8)$$

In reality, however, the growth of the oxide scale proceeds via complex microscopic processes involving:

- Conversion of oxygen molecules residing on the exposed surface to atomic anions which then diffuse through the existing oxide scale and combine with metal cations
- Diffusion of metal cations through the scale to the surface where they combine with available oxygen anions.

At present it is not definitely known whether cation or anion diffusion dominates the TD NiCr oxidation process. However, in the present work the details are not

[1]An asterisk after a chemical species indicates the condensed phase.

important since an empirical parabolic law is available (Reference 1) for treating the global process specified by Equation (8). The law is termed parabolic since an Arrhenius-type kinetics equation characterizes the rate of consumption of oxygen (kg O_2/m^2sec) in the formation of the oxide scale

$$\dot{m}_{O_2} = \frac{B}{y_p} e^{-E_a/\mathcal{R} T_w} \tag{9}$$

where y_p is the thickness of the oxide scale, E_a is the activation energy for formation of the oxide species, T_w is the wall temperature, $\mathcal{R}$ is the universal gas constant, and B is a constant. The values of B for the special cases of Cr_2O_3* and NiO* scale formation are presented in Appendix B.

For oxidation of the exposed surface of the Cr_2O_3* scale, the primary reactions are (from the analysis technique of Section 3.2.2)

$$2Cr_2O_3* + O_2 \rightarrow 4CrO_2 \tag{10}$$

$$2Cr_2O_3* + 3O_2 \rightarrow 4CrO_2 \tag{11}$$

and these reactions can be expected to be diffusion rate controlled (as opposed to reaction rate controlled).

For the coated Cb systems, the basic thermochemical response characteristic is the oxidation of the coating to form condensed and volatile oxides of the several coating species (again from the analysis techniques of Section 3.2.2). The steady state coating loss mechanism is apparently the volatilization of the condensed oxides, e.g., $HfO_2* \rightarrow HfO + 1/2O_2$. These surface reactions can also be expected to be diffusion rate controlled.

3.2.2 Calculation Procedures

A two-step computational procedure was used to determine the response of TD NiCr and coated Cb for multiple cycle heating/cooling boundary conditions. First, the Aerotherm Chemical Equilibrium (ACE) computer code (References 6 and 7) was used to determine the thermochemical ablation rate of the surface exposed to the heating environment for the range of surface temperatures and pressures. Then, using the results of these computations, a surface recession versus surface temperature table was generated. This table was utilized by either the Charring Material Ablation (CMA) or Oxide Film Formation and Ablation (OFFA) computer codes (Reference 8) to compute essentially all thermochemical and thermal events occurring at and below the exposed surface. This procedure is summarized in the flow diagram of Figure 4.

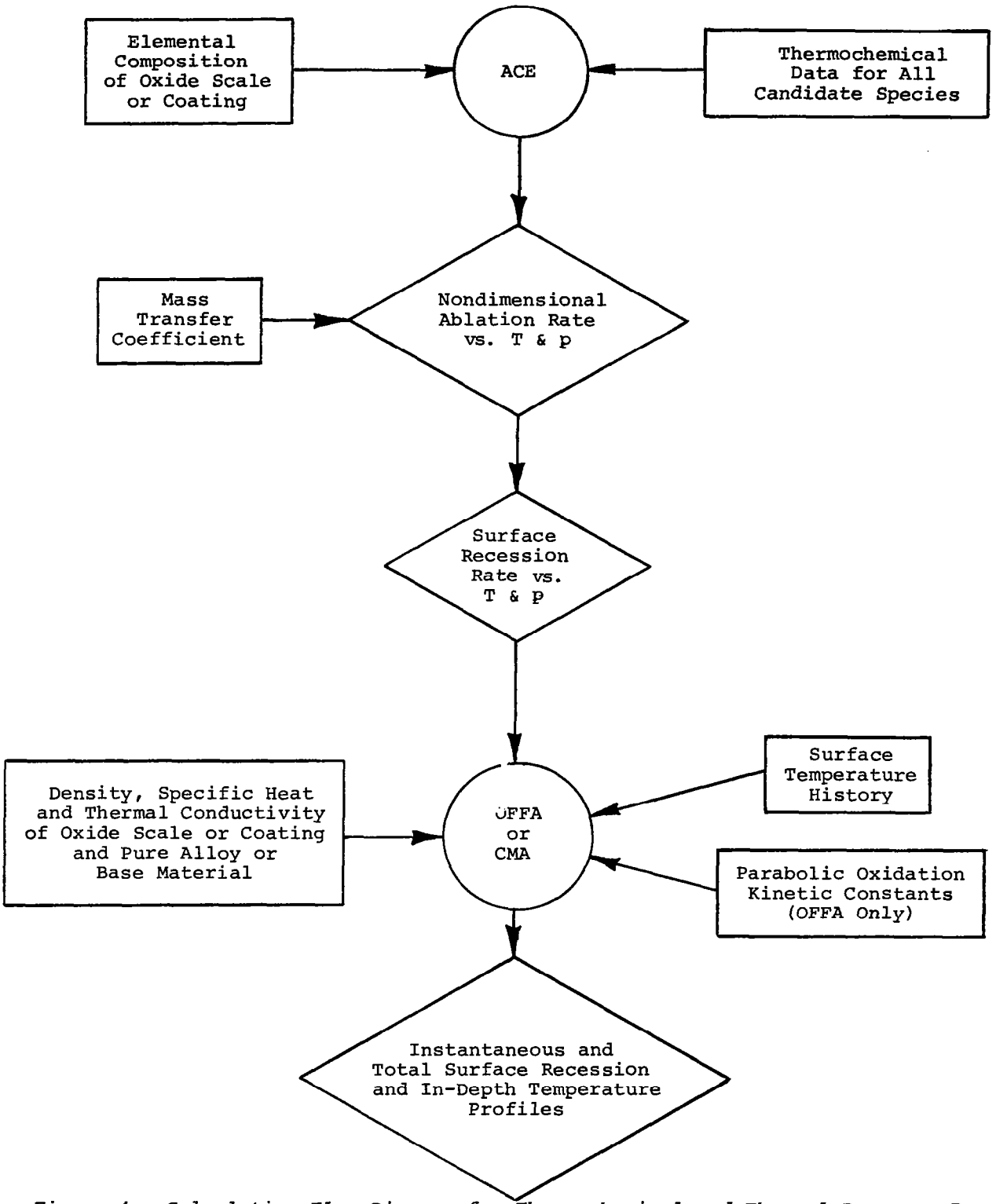

Figure 4. Calculation Flow Diagram for Thermochemical and Thermal Response Predictions

The Aerotherm CMA code determines the thermochemical and thermal response of a decomposing material, accounting for transient heat conduction and pyrolysis with the associated complexities of internal pyrolysis gas flow. In addition, the CMA code accepts as a boundary condition a surface which is undergoing combustion (chemical corrosion) or erosion. The CMA code was used to predict the response of coated columbium.

The phenomena of oxide film formation introduces additional features which are not treated by the CMA code. Hence, modifications were introduced into the CMA code to allow treatment of this special problem. This modified version of CMA is called the OFFA code and was used to compute the response of TD NiCr. The OFFA code incorporates the parabolic oxidation kinetics model discussed above.

The ACE code performs as one of its many options a chemical species mass balance at the gas/solid interface of a material undergoing thermochemical ablation. The mass balance is considered in normalized form, thus eliminating the requirement for explicit values of the boundary layer mass transfer coefficient as input data. Once nondimensional ablation rates have been computed for a range of surface temperatures and pressures, values of the mass transfer coefficient can then be used to deduce explicit values of the surface ablation rate. As already mentioned in the preceding section, chemical equilibrium was assumed for the heterogeneous reactions at both the surface of the oxide scale on TD NiCr and the surface of the coated columbium systems.

In order to carry out the above calculation procedures, a wide variety of thermochemical, thermophysical, and transport property data is required. The computation flow diagram of Figure 4 delineates where the various data are required at each step of the calculation process. The particular input data used for prediction of the response of TD NiCr and the coated Cb systems are presented in Appendix B.

SECTION 4

EXPERIMENTAL PROCEDURES

Metallic TPS materials were tested in a flowing air arc heater test facility employing stagnation point and wedge test model configurations. The description of this test setup, the test samples, and the test procedures are presented in this section. Additional details are presented in Appendix C.

4.1 FACILITY DESCRIPTION

The tests were performed in the Aerotherm 1.5-MW arc plasma facility, and the hyperthermal test stream was generated by the Aerotherm 300-kw constrictor arc heater for the stagnation point model tests and the Aerotherm 1.5-MW constrictor arc heater for the wedge model tests. The basic arc heater configuration for both units is shown schematically in Figure 5. The primary test gas was high purity nitrogen and the secondary gas was high purity oxygen in the proper amounts to yield the required test gas compositions.

The conical test nozzle had a throat diameter of 0.025 meters (1.0 inch) and an exit diameter of 0.203 meters (8.0 inches). The arc heater, plenum, and nozzle assembly were mounted on the vacuum test chamber to which the nozzle exhausted. This chamber also contained the model sting mechanisms and other necessary support equipment.

4.2 MODEL AND TEST SAMPLE CONFIGURATIONS

The model configurations employed in the test program were flat face stagnation point models with 0.121 and 0.032-meter (4.75 and 1.25-inch) body diameters, and a 30° half angle wedge model with a 0.013-meter (0.5-inch) nose radius as shown in Figures 6 and 7. The size and configuration of the large stagnation point model and of the wedge model allowed the maximum practical test sample size consistent with uniform property distributions on the test samples for the 0.203-meter (8-inch) diameter test stream. All test samples were flat panel sections with retention tabs for mounting on the models. The nominal test sample dimensions were 0.102 and 0.017-meter (4.00 and 0.65-inch) diameter (flat face stagnation point models) and 0.112 x 0.097 meters (4.40 x 3.80 inches) (wedge model). For the wedge model, the first 0.023 meters (0.90 inches) of the test sample was considered to be a thermal and flow field transition region, providing

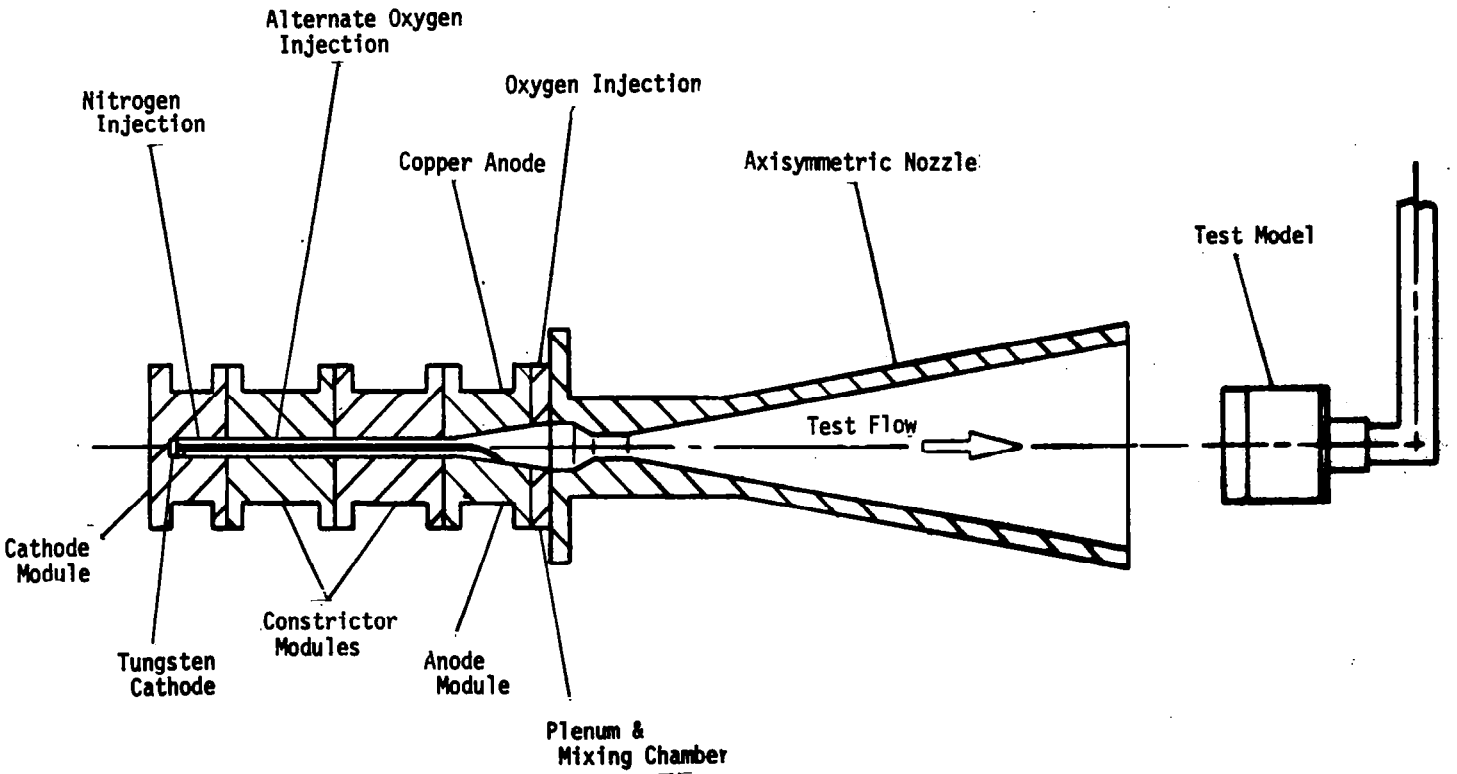

Figure 5. Aerotherm Constrictor Arc Heater and Overall Test Setup

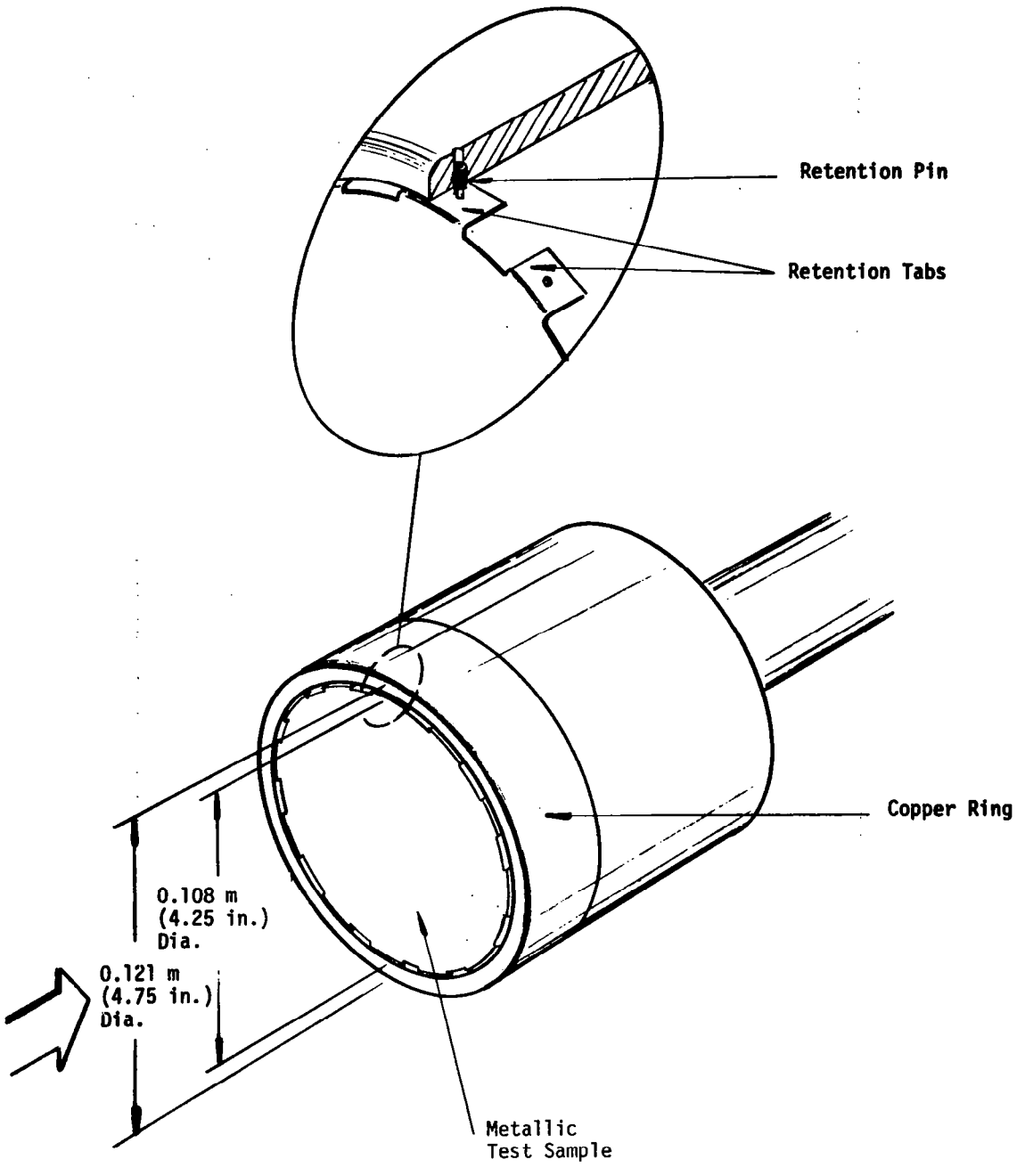

Figure 6. Typical Flat Face Stagnation Point Model

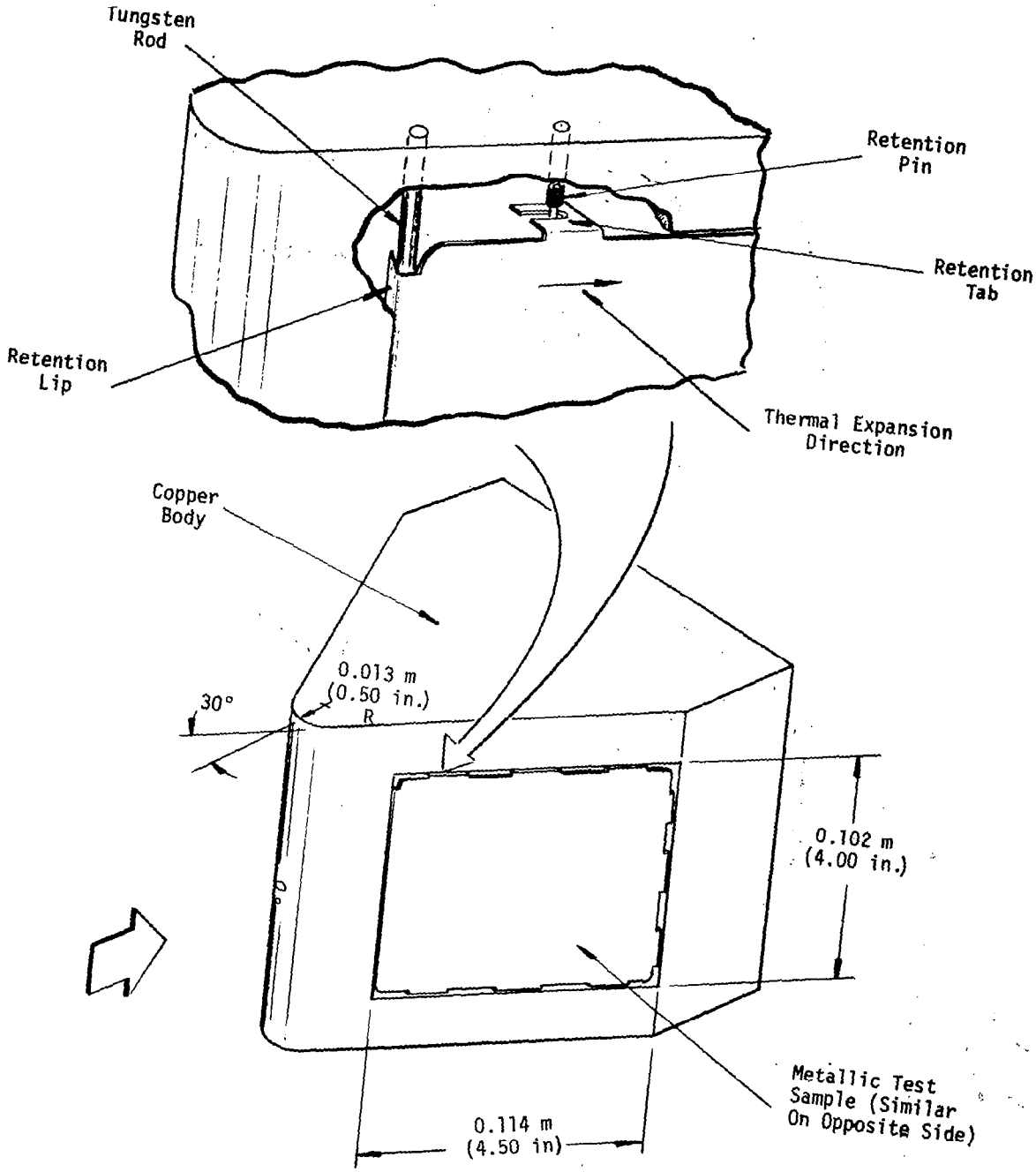

Figure 7. 30° Half Angle Wedge Model

an active test sample of 0.089 x 0.097 meters (3.50 x 3.80 inches). The wedge test sample occupied the surface running length interval (referenced from the stagnation line) from 0.031 to 0.142 meters (1.20 to 5.60 inches) for the complete sample and 0.053 to 0.142 meters (2.10 to 5.60 inches) for the active sample.

For all models, the test sample plus backup insulator was 0.025 meters (1 inch) thick. The backup insulator was Silfrax, which is a pure silica foam with a nominal density of 481 kg/m^3 (30 lb/ft^3).

All model designs incorporated a quick test sample change capability for optimum testing efficiency. The test samples were removed simply by removing the retention pins which engaged the tabs on the test samples (Figures 6 and 7). For the wedge model, a transverse tungsten rod across the entire width of the model retained the leading edge of the test sample. This approach allowed for free transverse thermal expansion with no loss in retention. The backup insulator remained untouched and in place during sample removal and installation. Spring-loaded thermocouples were used to eliminate the requirement for disconnecting instrumentation leads.

4.3 INSTRUMENTATION AND DATA REDUCTION

Instrumentation was provided and data reduction was performed to define arc heater and facility operating conditions, model boundary conditions, and test sample response (see Appendix C). The boundary conditions to which the test samples were exposed were defined by centerline total enthalpy, stagnation or wedge pressure, and convective heat flux for both a catalytic wall and a non-catalytic wall. These measurements were made with calibration models and probes, including calorimeter and pressure tap instrumented models with identical configurations to the test sample models.

The test sample response was defined quantitatively by measurements of surface temperature, surface recession, and weight loss, and qualitatively by photography. Surface temperature was measured with optical pyrometers, one of which was mounted on an oscillating mechanism which alternately viewed five locations on the large test samples throughout each test. Back surface temperature was measured with spring-loaded thermocouples, and the temperature distribution in the backup insulator was measured at three depths below the surface throughout each test. Surface recession and weight loss were measured after test with a non-contact microscope micrometer (required to insure no disturbance to the delicate coatings and oxide films) and a semi-micro analytic balance, respectively. Qualitative test sample response was defined by pre- and post-test color photography.

4.4 TEST PROCEDURE

Prior to the test sample tests, a calibration test series was performed to define the facility operating conditions required to achieve the desired test and model boundary conditions, and to completely characterize these test and model boundary conditions (Section 4.3). Model tests of the metallic test samples were then performed at the nominal test conditions presented in Table 2. The indicated heat flux - surface temperature correspondence applies for a fully catalytic surface with a surface emissivity of 0.85. The nominal surface temperatures were 1370° K (2000° F) for TD NiCr and 1590° K (2400° F) for coated Cb with variations below nominal for TD NiCr and above and below nominal for coated Cb. The simulation types (Section 3.1) were as follows:

- TD NiCr
  - Stagnation point - types 1-2, 3
  - Wedge - types 1-2, 3
- Coated Cb
  - Stagnation point - types 1, 1-2, 3
  - Wedge - type 1

Because of the low pressure required, no type 1 tests for TD NiCr were scheduled.[1] The pressure for all types 1-2 and 3 tests is only slightly below the flight pressure and was chosen to optimize arc heater and facility operating conditions.

Two samples were tested at each test condition; the nominal procedures for the stagnation point models and for the wedge models are presented in Figure 8. For the stagnation point tests, the first model was tested at the nominal heat flux of Table 2. If the surface temperature was significantly lower than nominal, the second model was tested at the heat flux which yielded the nominal surface temperature of Table 2. For the wedge tests, the test heat flux was necessarily lower than nominal in all cases to prevent failures on the upstream part of the test sample where the heat fluxes were significantly higher (Appendix C, Section 5.1.2).

[1]This low pressure is within the Aerotherm operating envelope only for small model diameters for which considerable diffuser action can be achieved.

TABLE 2

NOMINAL TEST CONDITIONS

a) SI Units

Material	Model Configuration[a]	Convective Heat Flux (W/m^2)	Surface Temperature (°K)	Simulation Type	Total Enthalpy (J/kg)	Stagnation or Local Pressure (N/m^2)
TD NiCr	4 3/4 SP	1.59×10^5	1370.	1-2	1.42×10^7	1013.
				3		
		6.36×10^4	1090.	1-2	6.28×10^6	
	1 1/4 SP	1.59×10^5	1370.		8.37×10^6	
R512E/Cb-752	4 3/4 SP	2.95×10^5	1590.	1	4.77×10^7	203.
and				1-2	2.47×10^7	1013.
VH-109/C12-Y				3		
		1.59×10^5	1370.	1-2	1.42×10^7	
		4.31×10^5	1760.		3.60×10^7	
	1 1/4 SP	2.95×10^5	1590.		1.38×10^7	
TD NiCr	W	1.59×10^5	1370.	1	4.77×10^7	203.
				1-2	1.80×10^7	1013.
				3		
R512E/Cb-752 and VH-109/C129Y		2.95×10^5	1590.	1	4.77×10^7	608.

[a] 4 3/4 SP → 0.121-meter diameter flat face stagnation point model

1 1/4 SP → 0.0318-meter diameter flat face stagnation point model

W → wedge model

TABLE 2 (CONCLUDED)

b) Conventional Units

Material	Model Configuration[a]	Convective Heat Flux (Btu/ft²sec)	Surface Temperature (°F)	Simulation Type	Total Enthalpy (Btu/lb)	Stagnation or Local Pressure (atm)
TD NiCr	4 3/4 SP	14.0	2000.	1-2	3400.	0.010
				3		
		5.6	1500.	1-2	1500.	
	1 1/4 SP	14.0	2000.		2000.	
R512E/Cb-752 and VH-109/C129Y	4 3/4 SP	26.0	2400.	1	11,400.	0.002
				1-2	5900.	0.010
				3		
		14.0	2000.	1-2	3400.	
		38.0	2700.		8600.	
	1 1/4 SP	26.0	2400.		3300.	
TD NiCr	W	14.0	2000.	1	11,400.	0.002
				1-2	4300.	0.010
				3		
R512E/Cb-752 and VH-109/C129Y		26.0	2400.	1	11,400.	0.006

[a] 4 3/4 SP → 4.75-inch diameter flat face stagnation point model
1 1/4 SP → 1.24-inch diameter flat face stagnation point model
W → wedge model

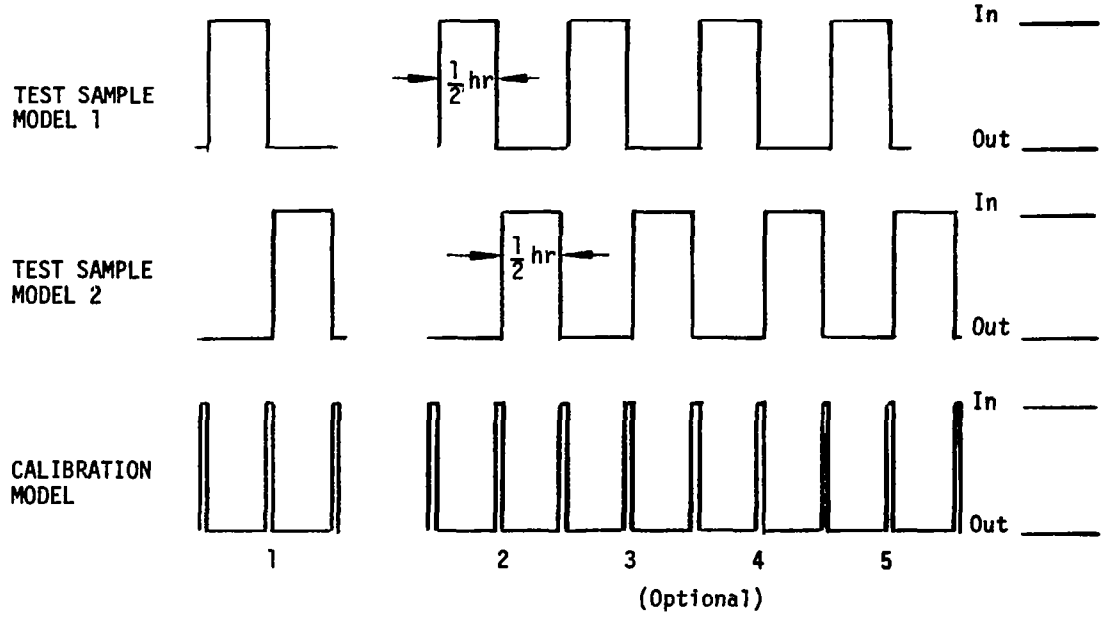

Stagnation Point Models

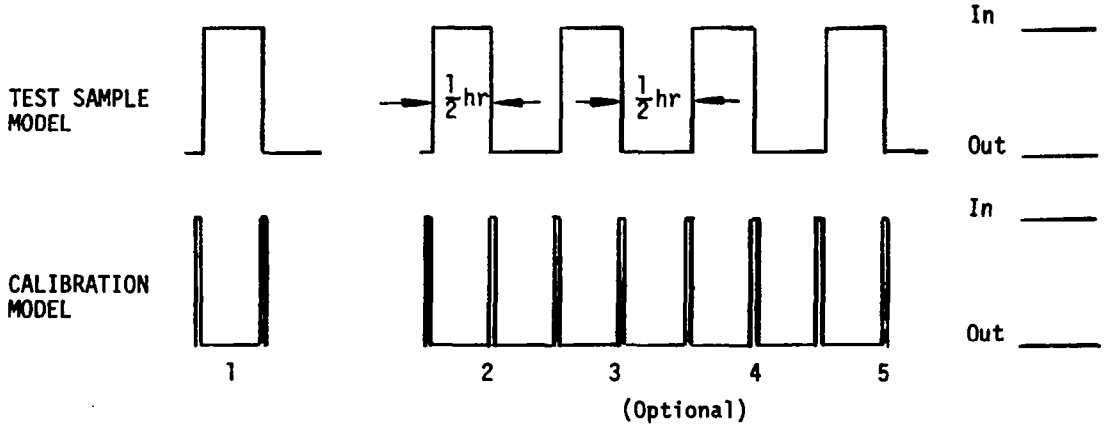

Wedge Model

Figure 8. Cyclic Test Procedure

SECTION 5

RESULTS AND DISCUSSION

The response characteristics of TD NiCr and coated Cb were defined for flight conditions and for representative ground test conditions. This definition for flight conditions was accomplished by analytical techniques; this definition for ground simulation test conditions was accomplished by both analytical and experimental techniques. These results were correlated to define the validity of the analytic and test techniques and to recommend the optimum test approach for evaluating metallic TPS response for application to flight. The overall program results, together with the actual flight conditions and the appropriate simulation test conditions, are presented and discussed in this section. Additional details are included in Appendices A through C.

5.1 FLIGHT AND TEST BOUNDARY CONDITIONS

The flight boundary conditions were defined for the fuselage windward symmetry plane and the wing windward 40 percent semi-span plane of the H-33 vehicle, and test boundary conditions were defined for flat-face stagnation point models with a range of body diameters and for a wedge model. The analysis procedures employed are outlined in Section 3.1; the results are presented in the following subsections.

5.1.1 Flight Conditions

The vehicle stagnation conditions and wing leading edge pressure are included in Table 1. The latter corresponds to the geometric leading edge (referenced to the 29° angle of attack) and is less than the stagnation pressure due to the transverse flow along the stagnation line caused by the sweep of the wing.

The pressure ratio (local pressure over stagnation pressure) is presented in Figure 9 versus surface running length for the fuselage symmetry plane and wing 40 percent semi-span plane. Note that this pressure ratio is insensitive to Mach number and therefore to time during the entry trajectory within the flow field assumptions employed.

The computed results for all other flight conditions are presented in Figures 10 and 11 versus surface running length for the fuselage and wing, respectively. The regions of application for TD NiCr and coated Cb are indicated,

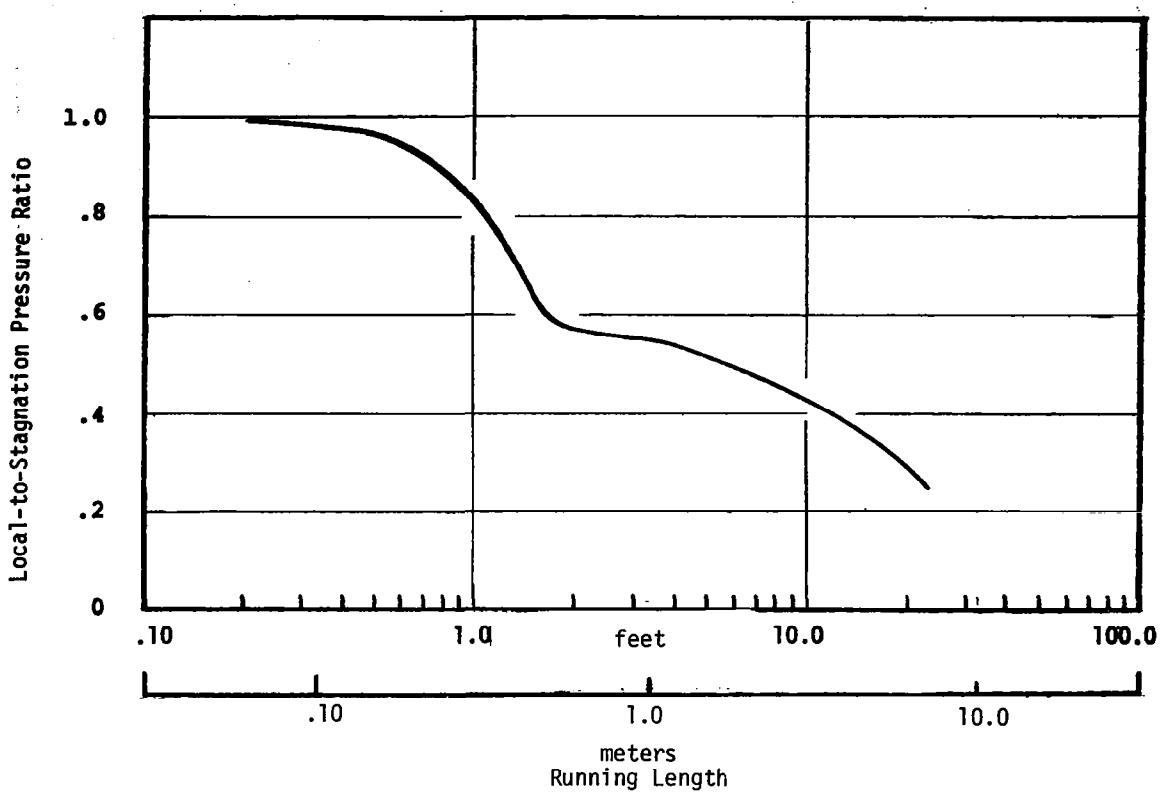

Fuselage Windward Centerline

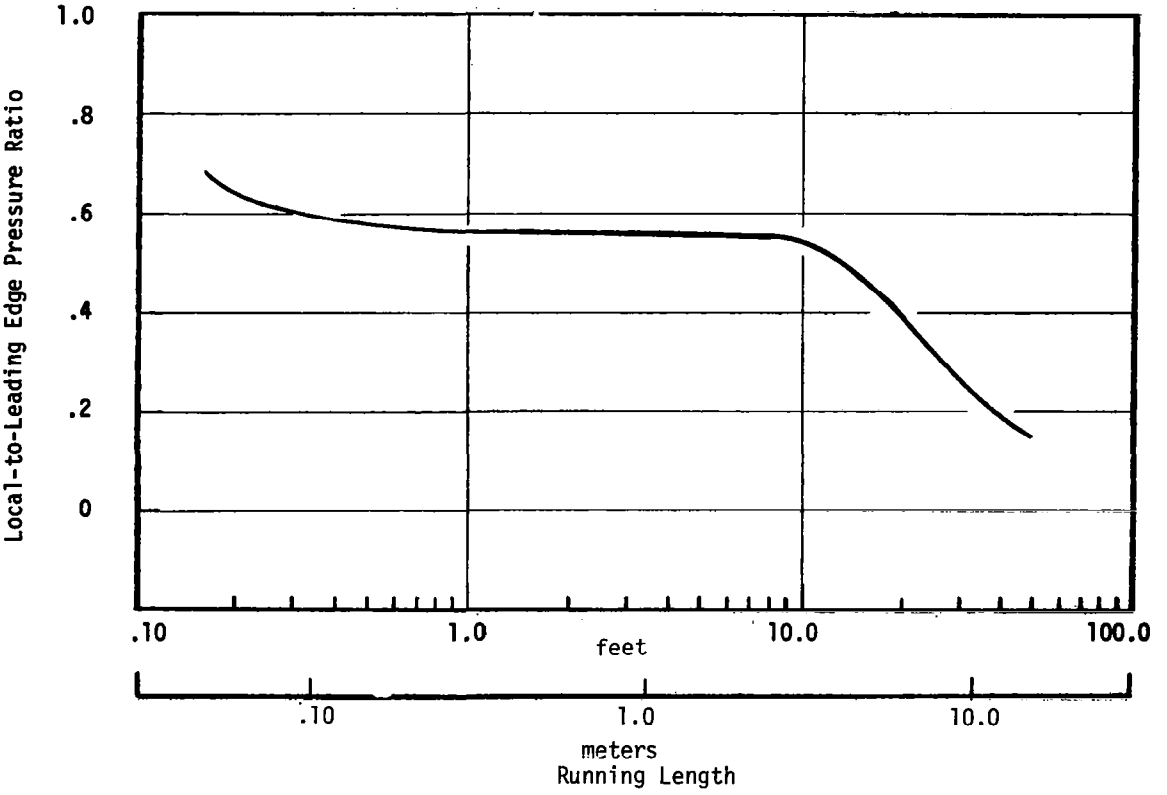

Wing 40 Percent Semi-Span

Figure 9. Vehicle Pressure Distributions

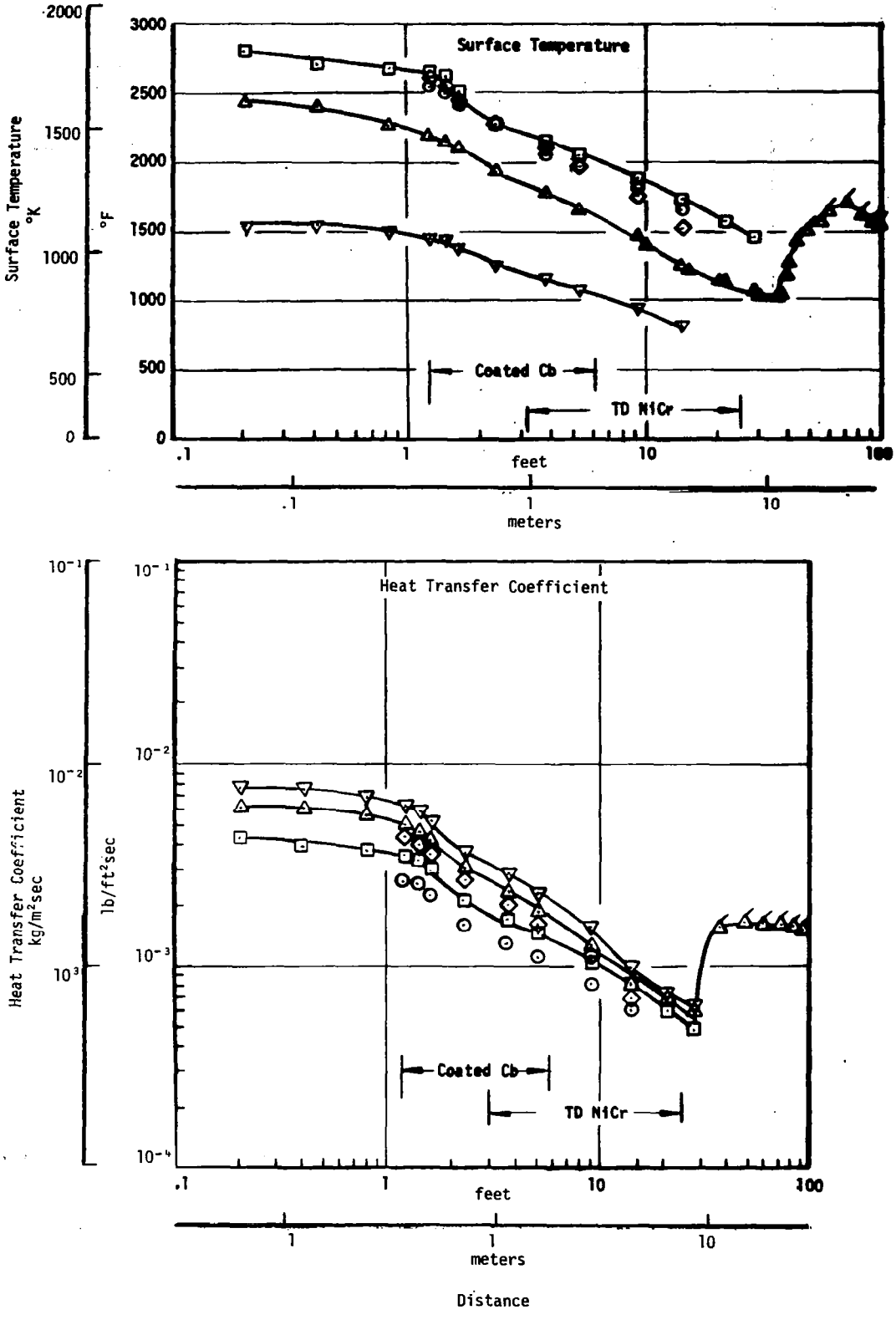

Figure 10. Flight Conditions on H33 Vehicle Fuselage Centerline

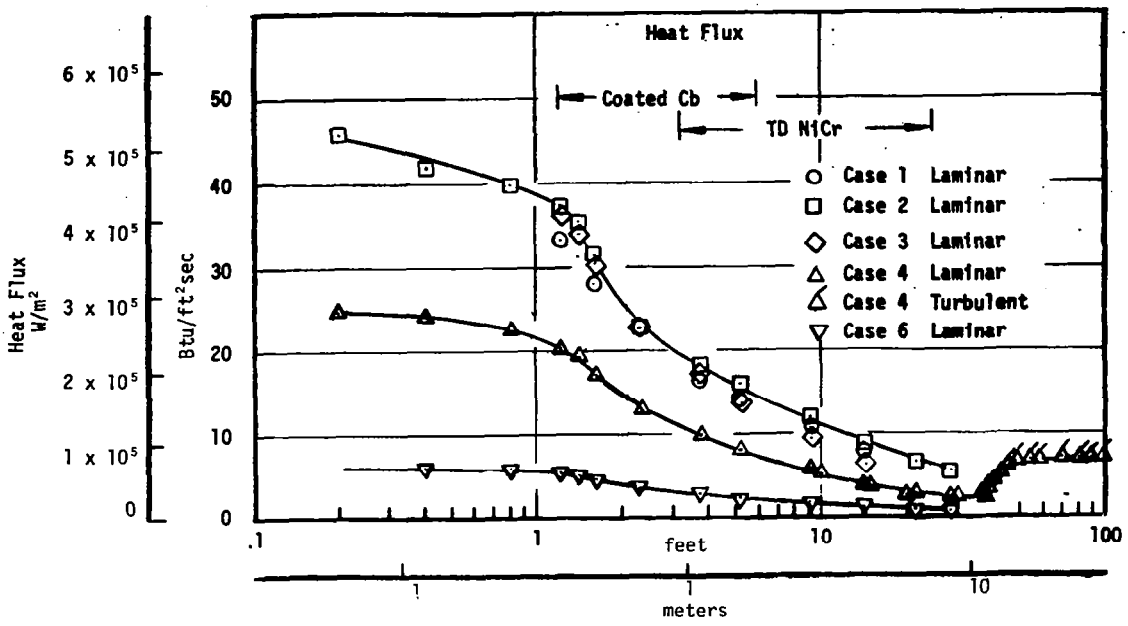

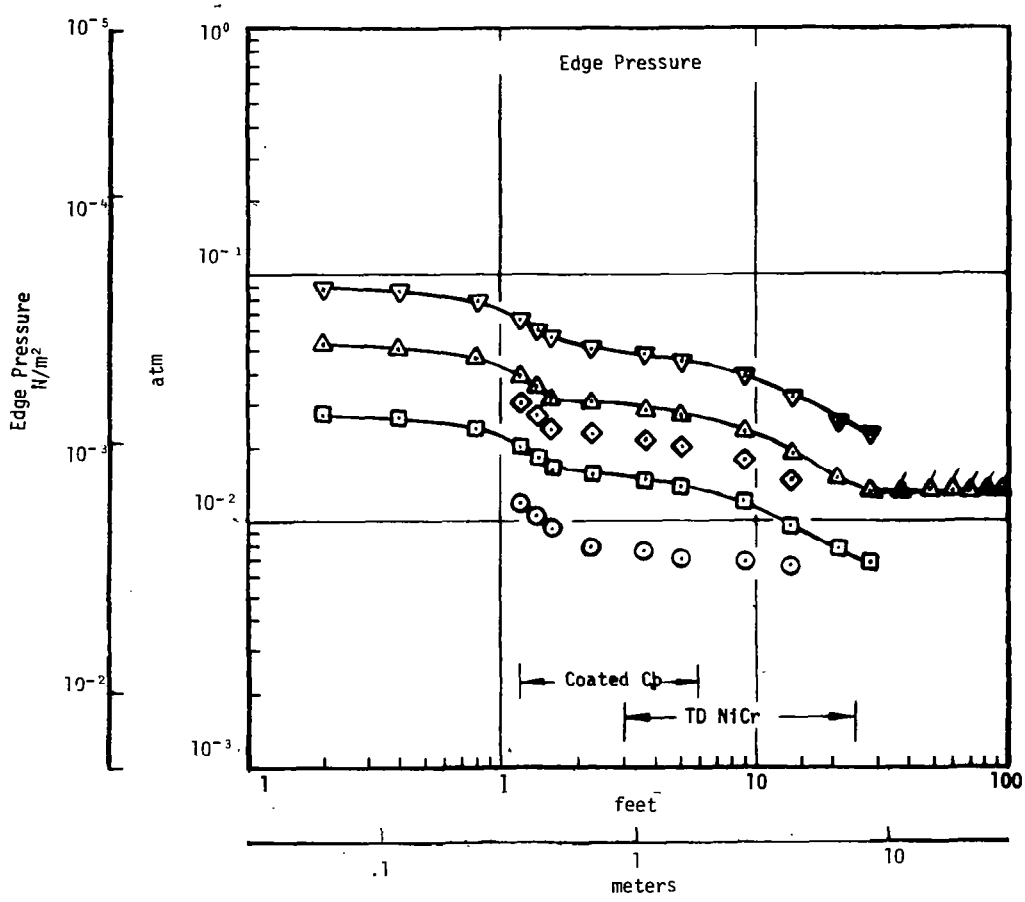

Distance

Figure 10. Continued

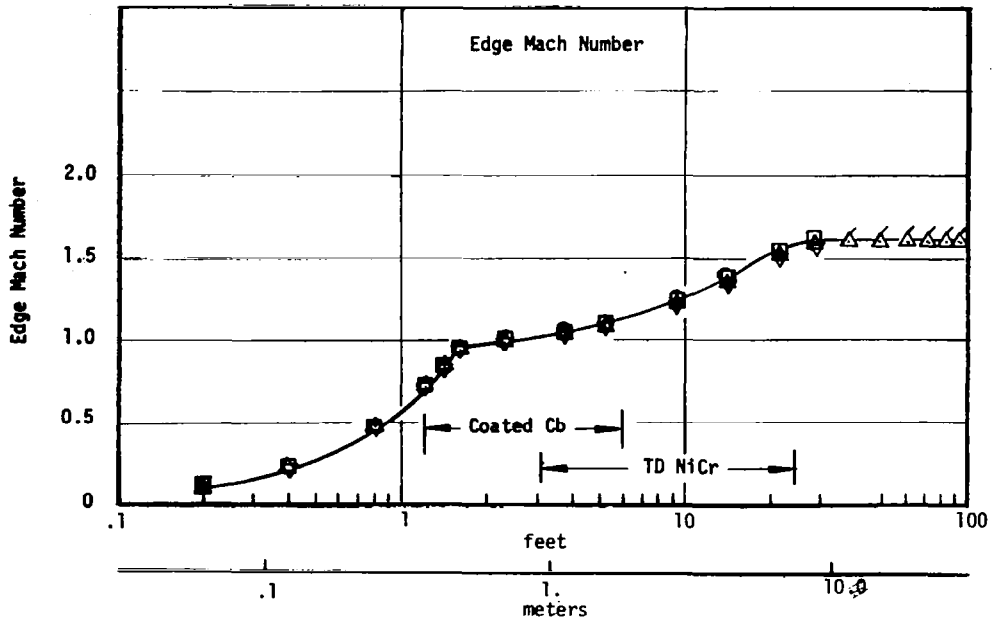

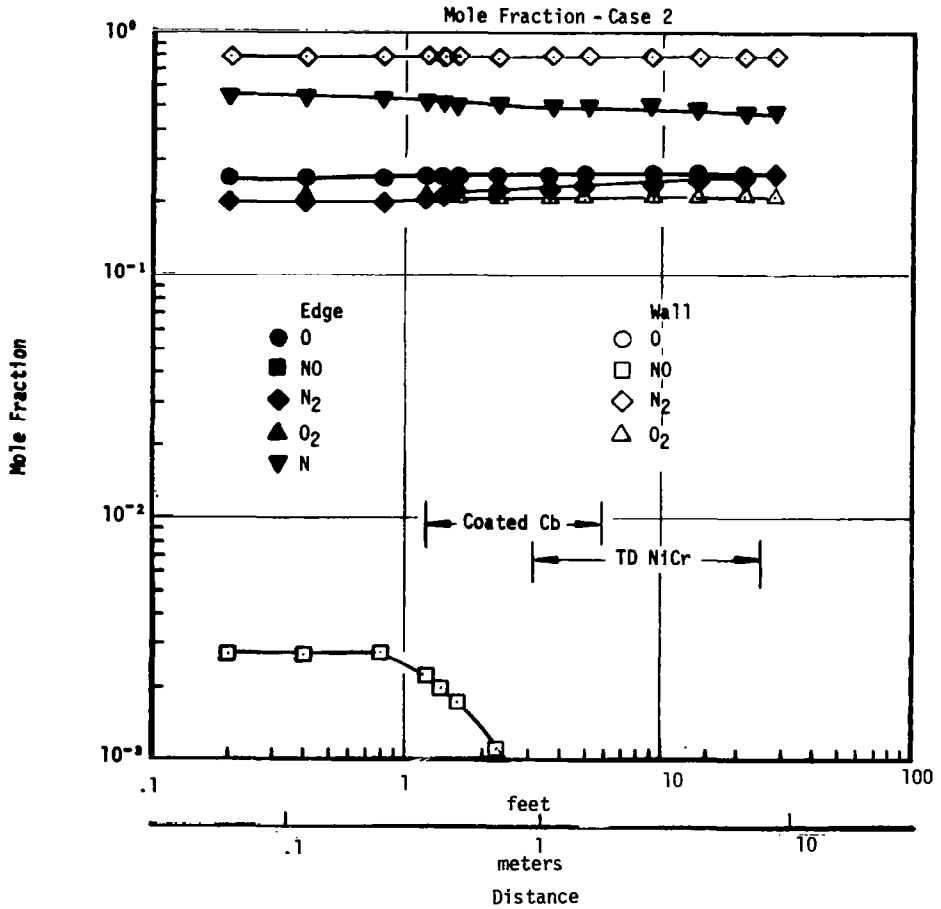

Figure 10. Continued

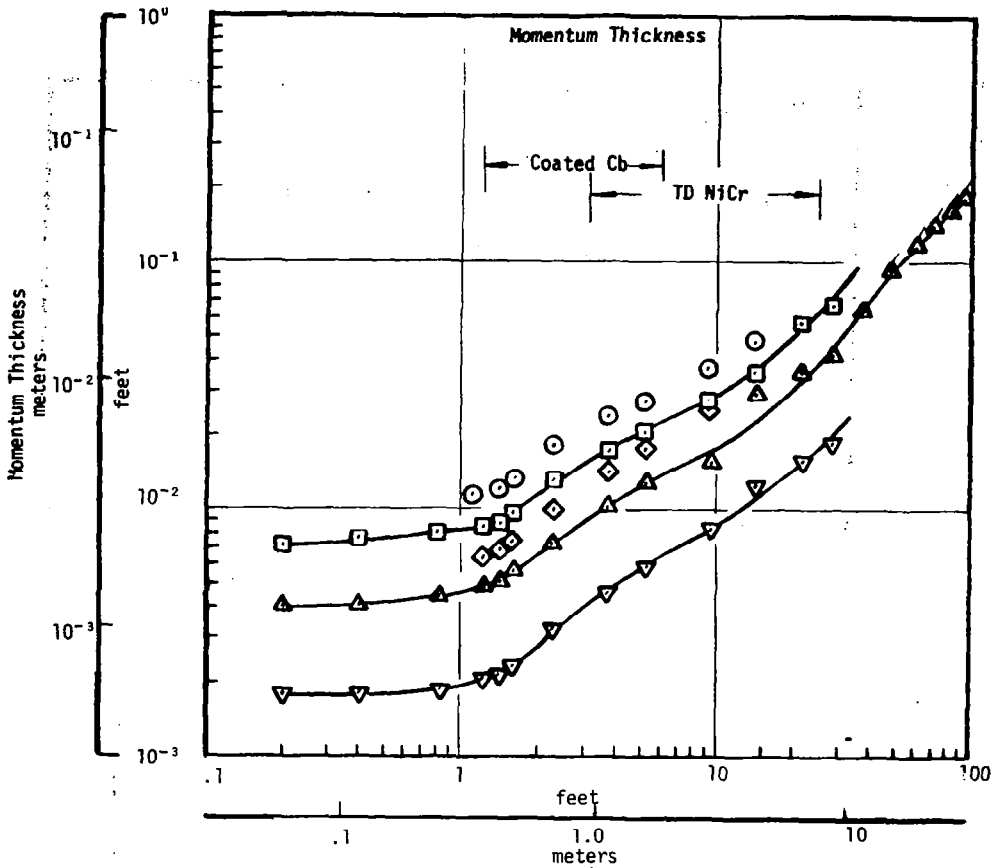

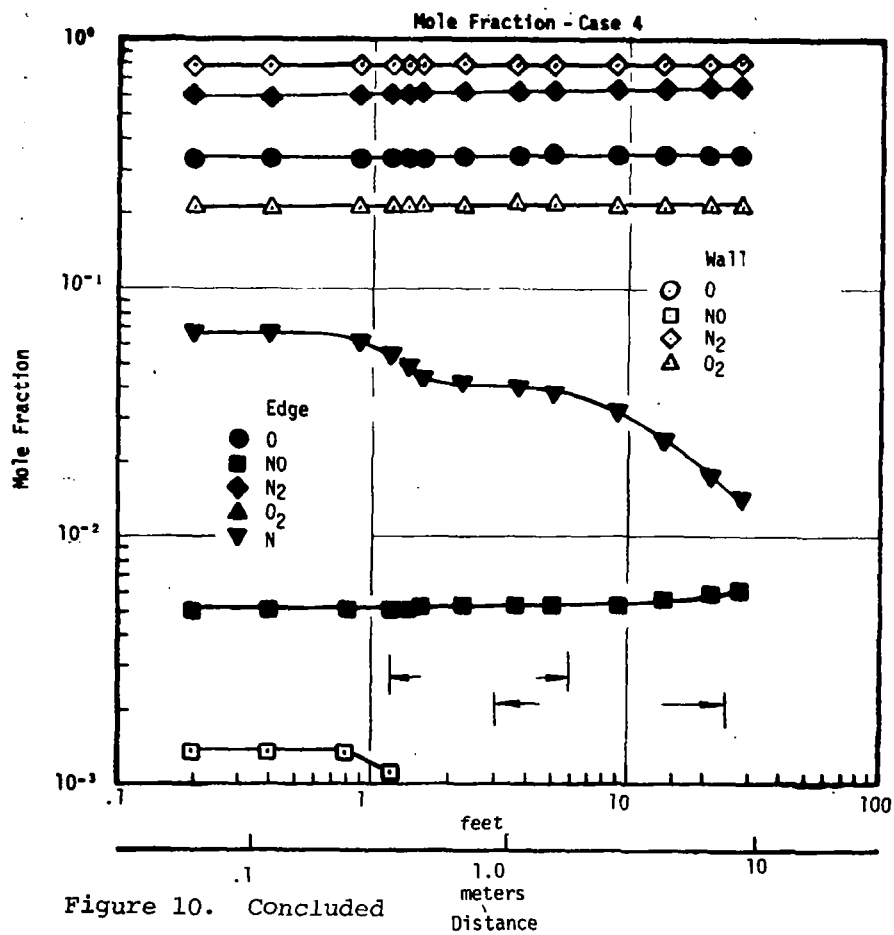

Figure 10. Concluded

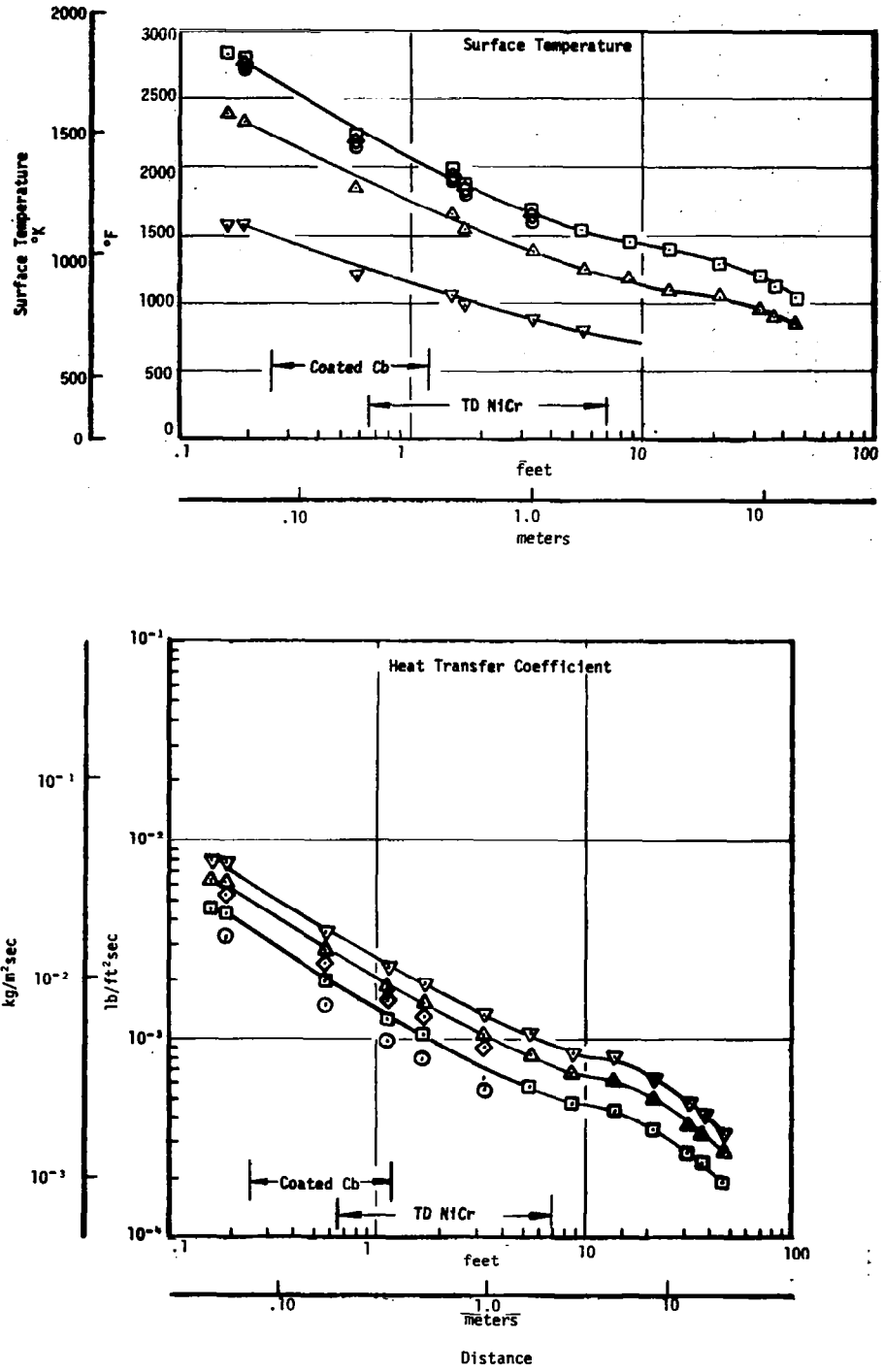

Figure 11. Flight Conditions on H33 Vehicle Wing at 40 Percent Semi-Span Location

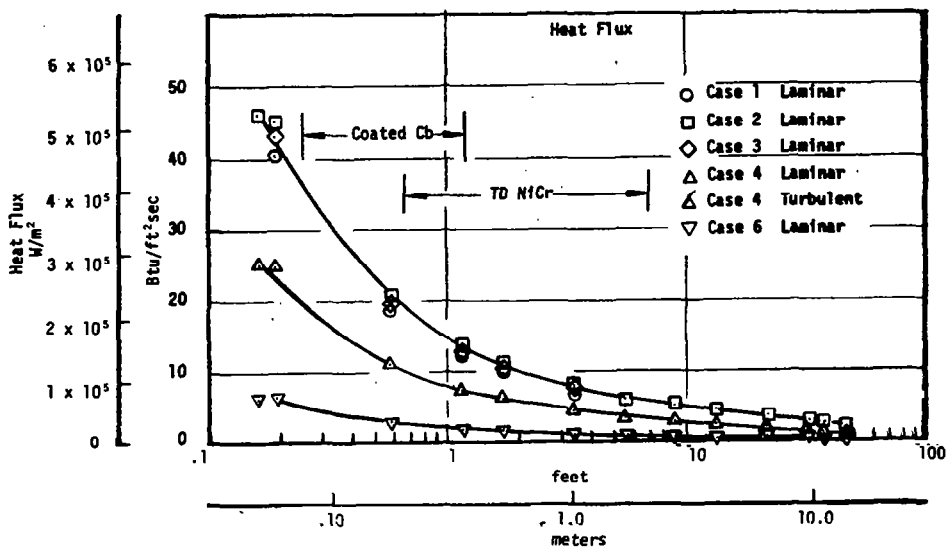

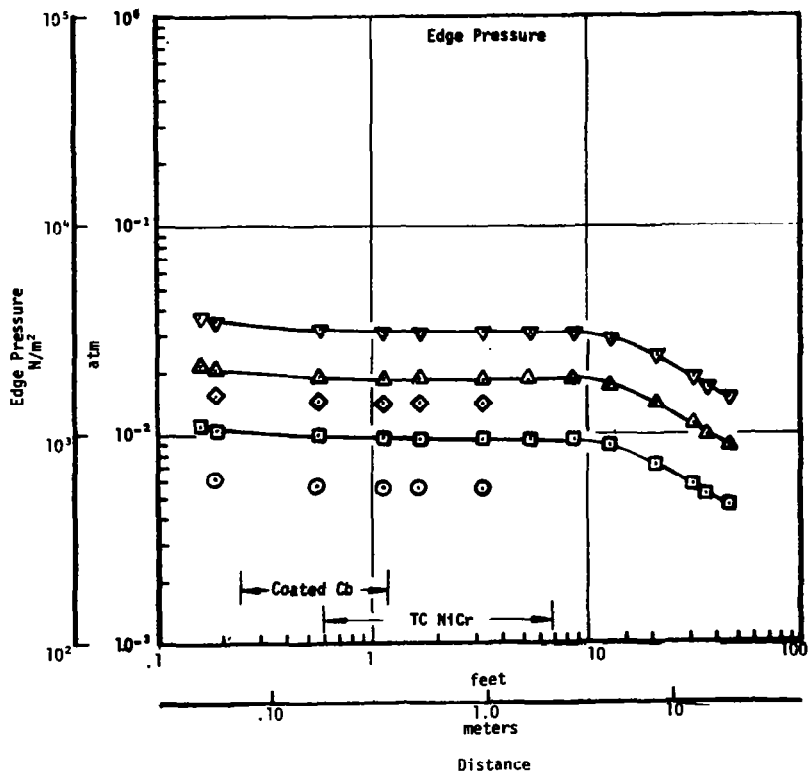

Figure 11. Continued

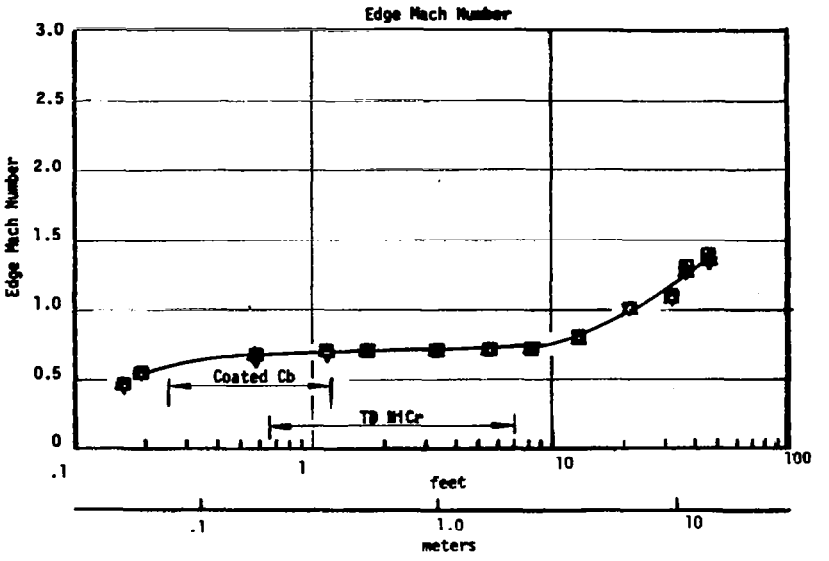

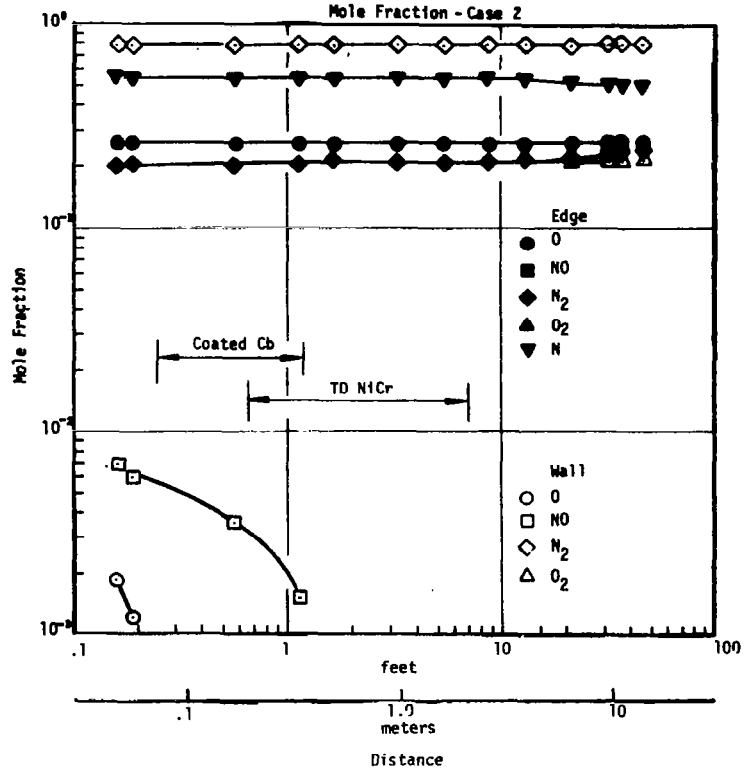

Figure 11. Continued

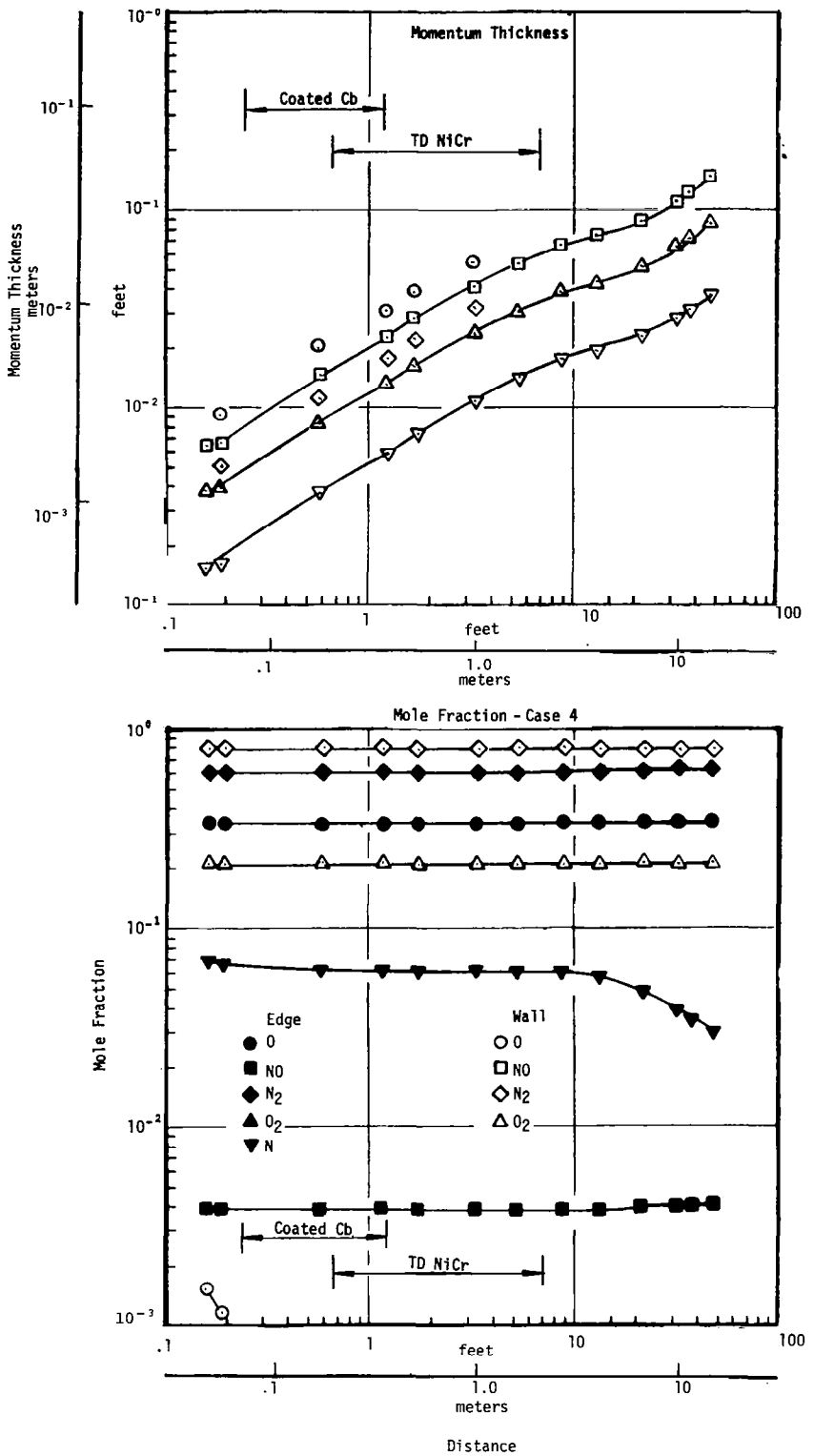

Figure 11. Concluded

these regions corresponding to the fully catalytic wall heat flux and resultant surface temperature presented. Peak heating corresponds approximately to case 2, which is 800 seconds into the reentry trajectory (Table 1). Transition to turbulent flow is not expected to occur on the vehicle until well after peak heating (θ > 1800 seconds).

In order to allow an evaluation of test simulation conditions, a set of reference conditions for both TD NiCr and coated Cb were defined and are presented in Table 3. These conditions were for peak heating and at the locations for which the surface temperatures were 1370° K and 1590° K (2000° F and 2400 °F), respectively. Except for Mach number, these conditions were essentially the same for both the fuselage centerline and the 40 percent semi-span location on the wing (Figures 10 and 11).

5.1.2 Test Boundary Conditions

The definition of test boundary conditions assumed that heat flux is duplicated at the peak heating values appropriate to the application of the metallic TPS materials (Table 3). This boundary condition definition was performed for the following model configurations (e.g., see Figures 6 and 7):

- Flat face stagnation models
  - 0.121-meter (4.75-inch) body diameter with 0.0032-meter (0.125-inch) corner radius
  - 0.032-meter (1.25-inch) body diameter with 0.0032-meter (0.125-inch) corner radius
  - 0.0095-meter (0.375-inch) body diameter
- Wedge model - 30° half angle with 0.013-meter (0.5-inch) nose radius

where the first stagnation point model and the wedge model are appropriate to testing in a nominal 1 MW test facility and the last two stagnation point models are appropriate to testing in a nominal 100 kw test facility.

Typical computed distributions of properties on the test models are presented in Figures 12 and 13 for the stagnation point and wedge models, respectively. The stagnation point configuration provides laminar, subsonic ($M \approx 0$) conditions on the test model. The heat flux, pressure, and momentum thickness are approximately constant, and the Mach number and shear are increasing with radial distance. The wedge configuration provides laminar, supersonic ($M > 1$) conditions on the test model. The pressure and Mach number are constant (downstream of the nose region), and the heat flux and wall shear are decreasing ($\sim s^{-1/2}$) and the momentum thickness increasing with running length from the stagnation line.

TABLE 3
REFERENCE FLIGHT CONDITIONS
a) SI Units

Flight Parameter	TD NiCr	Coated Cb
Total Enthalpy - J/kg	4.8×10^7	4.8×10^7
Catalytic Wall Heat Flux - W/m^2	1.59×10^5	2.95×10^5
Pressure - atm	.012	.012
Heat Transfer Coefficient - lb/ft^2sec	.0013	.0024
Elemental Mass Fraction of O_2	.235	.235
Partial Pressure of O_2 - N/m^2	0	0
Partial Pressure of O^2 - N/m^2	3.14×10^2	3.14×10^2
Local Mach Number (Fuselage/Wing)	1.25/.70	1.00/.70
Momentum Thickness - meters	6.71×10^{-3}	4.27×10^{-3}
Shear - N/m^2	8.62	14.36
Ratio of Fully Noncatalytic Wall to Fully Catalytic Wall Heat Flux	.25	.25

TABLE 3 (CONCLUDED)
b) Conventional Units

Flight Parameter	TD NiCr	Coated Cb
Total Enthalpy - Btu/lb	11,400	11,400
Catalytic Wall Heat Flux - Btu/ft^2sec	14	26
Pressure - atm	.012	.012
Heat Transfer Coefficient - lb/ft^2sec	.0013	.0024
Elemental Mass Fraction of O_2	.235	.235
Partial Pressure of O_2 - atm^2	0	0
Partial Pressure of O^2 - atm	.0031	.0031
Local Mach Number (Fuselage/Wing)	1.25/.70	1.00/.70
Momentum Thickness - feet	.022	.014
Shear - lb/ft^2	.18	.30
Ratio of Fully Noncatalytic Wall to Fully Catalytic Wall Heat Flux	.25	.25

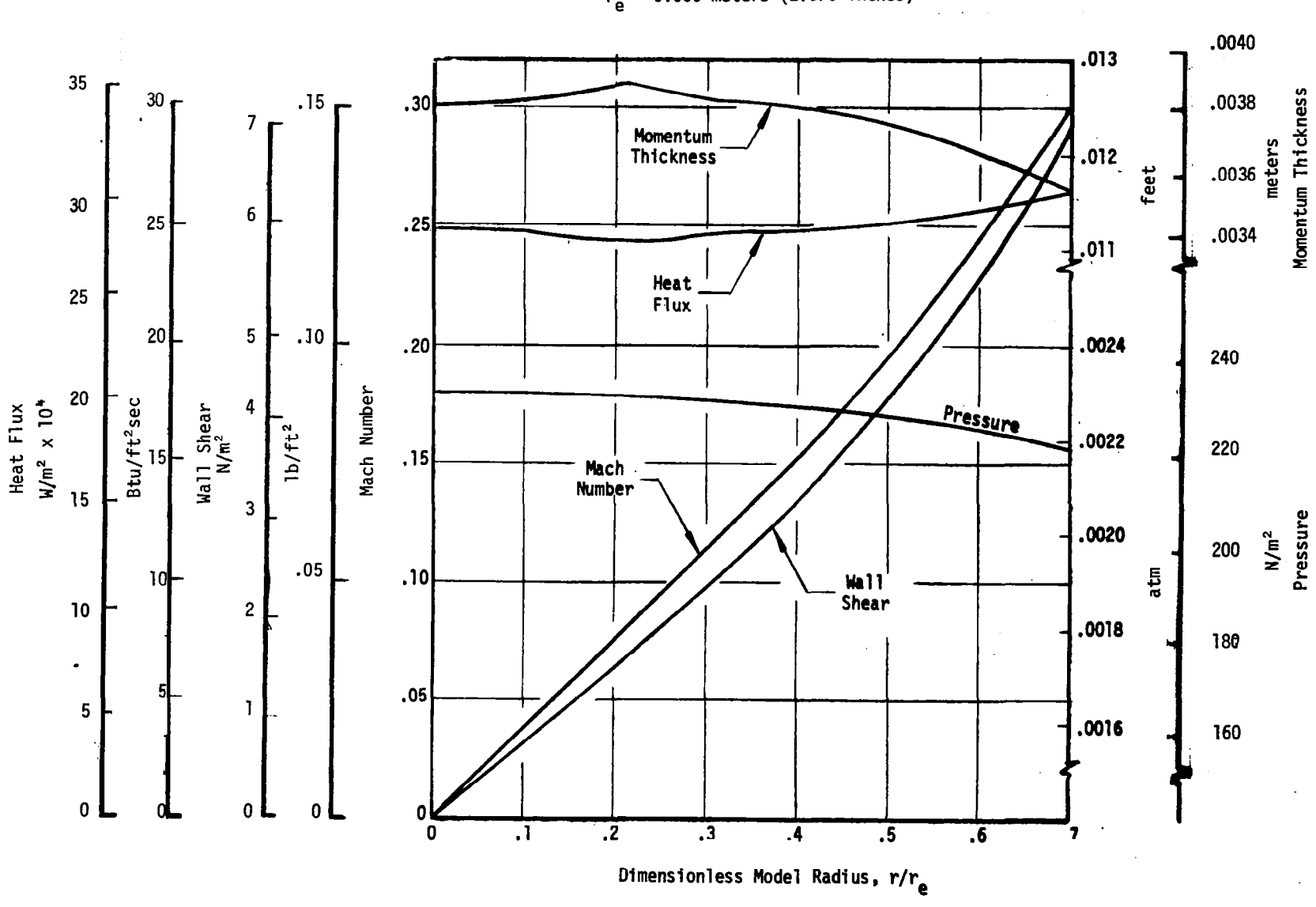

Figure 12. Typical Property Distributions on the Stagnation Point Model

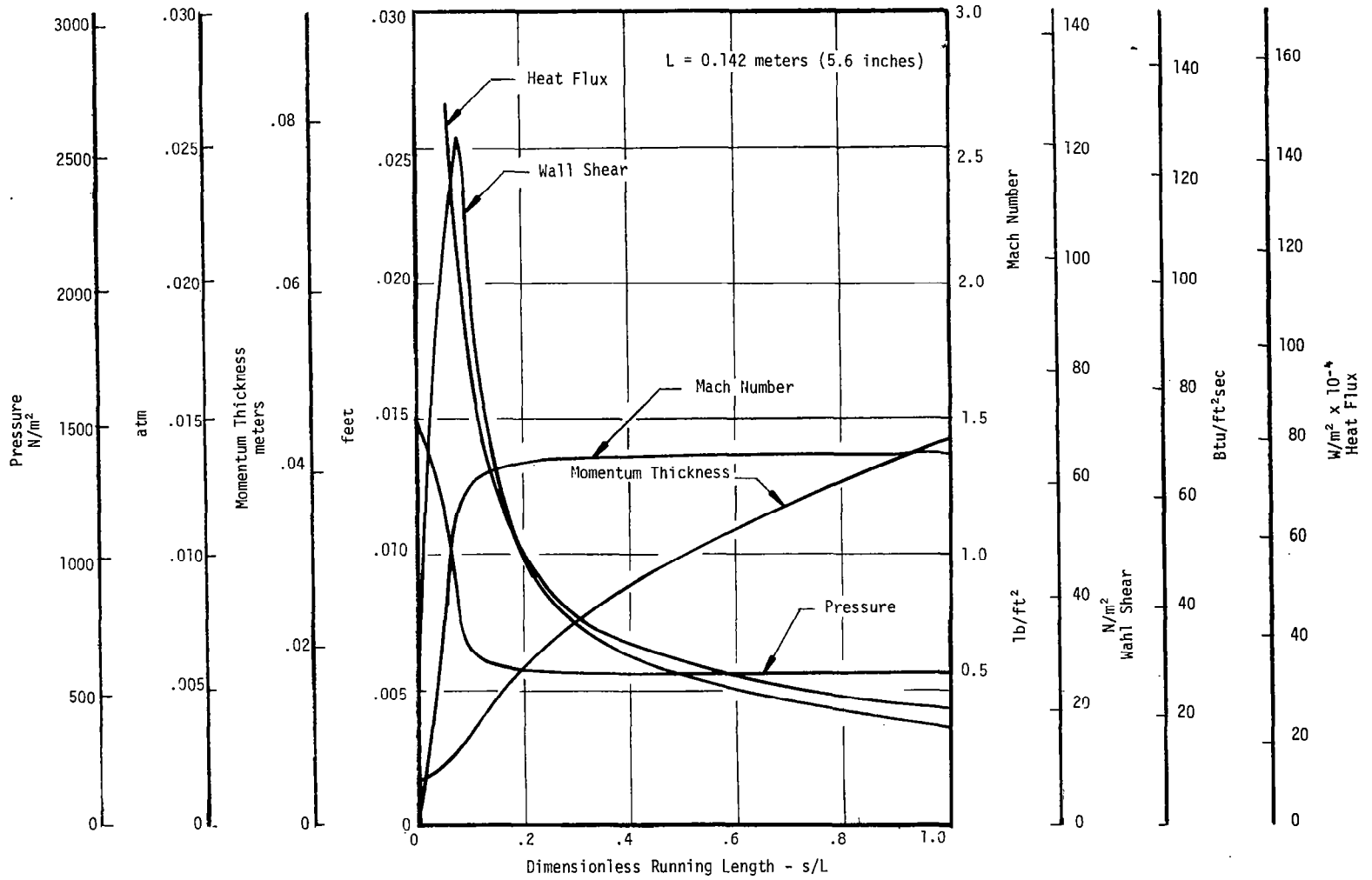

Figure 13. Typical Property Distributions on the Wedge Model

For purposes of defining reference conditions on all models at all simulation test conditions, the following locations were employed:

- Stagnation point model - $r/r_e = 0.25$
- Wedge - $s/L = 0.69$

where the wedge location is the center of the active test sample as described in Section 4.2. These results are presented in Tables 4 and 5 for TD NiCr and coated Cb, respectively, and are compared with the calculated flight conditions defined above (Table 3). The comparisons with flight conditions are also summarized qualitatively in Table 6. These results and comparisons are presented for the four simulation types identified in Section 3.1:

- Type 1 - Duplication of all heat transfer and mass transfer parameters (air environment)
- Type 2 - Duplication of heat flux and pressure (air environment)
- Type 3 - Duplication of heat flux, mass flux, and pressure (non-air environment)
- Type 1-2 - Compromise between types 1 and 2, which optimizes test conditions (air environment)

Comparisons between model configurations and flight conditions (Tables 4 through 6) indicate that the wedge configuration provides test conditions which more closely duplicate those of flight. The heat flux on the test sample is variable, however, (Figure 13) and the definition and measurement of test conditions and material response is less accurate because the flow field and boundary conditions are more difficult to accurately characterize.[1] For the stagnation point model, the heat flux is essentially constant (Figure 12), and the flow field and boundary conditions are accurately defined. Note that the quality of simulation decreases with decreasing stagnation point model size (Tables 4 and 5).

Comparisons between simulation types and flight conditions (Tables 4 and 5) indicate that type 1 simulation offers duplication of the most flight conditions. The quality of simulation depends on the important TPS response characteristics, however. If pressure is not significant to the response, type 1 simulation is in fact the most attractive. However, for small diameter models the resultant test pressure may be too low; it may be below the test facility vacuum pumping capacity or it may result in slip or free molecule flow conditions which are unacceptable for TPS materials testing. Type 1-2 simulation represents an attractive compromise for such cases. Type 2 or 3 simulation is attractive in

[1]Also for a given test section size higher arc heater power input is required for the wedge model to achieve the same heat flux as for the stagnation point model.

TABLE 4

TEST CONFIGURATION CONDITIONS

TD NiCr

a) SI Units

Flight or Test Parameter	Flight	Simulation Type 1				Simulation Type 2				Simulation Type 3				Simulation Type 1-2			
		Flat Face Stagnation Point Model			Wedge Model	Flat Face Stagnation Point Model			Wedge Model	Flat Face Stagnation Point Model			Wedge Model	Flat Face Stagnation Point Model			Wedge Model
Model Body Diameter — meters	---	1.21×10^{-1}	3.18×10^{-2}	9.52×10^{-3}	---	1.21×10^{-1}	3.18×10^{-2}	9.52×10^{-3}	---	1.21×10^{-1}	3.18×10^{-2}	9.52×10^{-3}	---	1.21×10^{-1}	3.18×10^{-2}	9.52×10^{-3}	---
Total Enthalpy — J/kg	4.8×10^{7}	4.8×10^{7}	4.8×10^{7}	4.8×10^{7}	4.8×10^{7}	1.4×10^{7}	0.82×10^{7}	0.56×10^{7}	1.7×10^{7}	1.4×10^{7}	0.82×10^{7}	0.56×10^{7}	1.6×10^{7}	1.8×10^{7}	1.0×10^{7}	0.69×10^{7}	2.92×10^{7}
Catalytic Wall Heat Flux — W/m^2	1.59×10^{5}	1.59×10^{5}	1.59×10^{5}	1.59×10^{5}	1.59×10^{5}	1.59×10^{5}	1.59×10^{5}	1.59×10^{5}	1.59×10^{5}	1.59×10^{5}	1.59×10^{5}	1.59×10^{5}	1.59×10^{5}	1.59×10^{5}	1.59×10^{5}	1.59×10^{5}	1.59×10^{5}
Pressure — N/m^2	1.22×10^{3}	7.19×10^{1}	1.21×10^{1}	5.67×10^{0}	2.13×10^{2}	1.22×10^{3}	1.22×10^{3}	1.22×10^{3}	1.22×10^{3}	1.22×10^{3}	1.22×10^{3}	1.22×10^{3}	1.22×10^{3}	6.08×10^{2}	6.08×10^{2}	6.08×10^{2}	6.08×10^{2}
Heat Transfer Coefficient — kg/m sec	6.35×10^{-3}	6.35×10^{-3}	6.35×10^{-3}	6.35×10^{-3}	6.35×10^{-3}	2.59×10^{-2}	1.88×10^{-2}	9.28×10^{-2}	2.05×10^{-1}	2.59×10^{-2}	4.88×10^{-2}	9.28×10^{-2}	2.05×10^{-1}	1.81×10^{-2}	3.56×10^{-2}	3.56×10^{-2}	1.08×10^{-2}
Elemental Mass Fraction of O_2	0.235	0.235	0.235	0.235	0.235	0.235	0.235	0.235	0.235	0.058	0.031	0.016	0.073	0.235	0.235	0.235	0.235
Partial Pressure of O_2 — N/m^2	0	0	0	0	0	0.000	1.32×10^{2}	2.03×10^{2}	0	0	0	0	0	0	3.04×10^{1}	8.11×10^{1}	0
Partial Pressure of O — N/m^2	3.14×10^{2}	2.03×10^{1}	---	---	6.08×10^{1}	4.05×10^{2}	1.92×10^{2}	6.08×10^{1}	4.05×10^{2}	1.11×10^{2}	6.08×10^{1}	2.03×10^{1}	1.42×10^{2}	2.03×10^{2}	1.52×10^{2}	6.08×10^{1}	2.13×10^{2}
Local Mach Number	1.25/0.70	0.10	---	---	1.37	0.10	0.10	0.10	1.37	0.10	0.10	0.10	0.10	1.37	0.10	0.10	0.10
Momentum Thickness — meters	6.7×10^{-3}	6.71×10^{-3}	---	---	5.79×10^{-3}	1.10×10^{-3}	4.27×10^{-4}	2.13×10^{-4}	1.62×10^{-3}	1.22×10^{-3}	5.49×10^{-4}	2.44×10^{-4}	1.71×10^{-3}	1.92×10^{-3}	6.71×10^{-4}	3.35×10^{-4}	3.08×10^{-3}
Shear — N/m^2	8.61	1.05	---	---	12.9	3.26	5.27	8.62	26.8	3.35	5.75	9.10	28.7	2.44	3.97	6.70	21.5
Ratio of Fully Non-catalytic Wall to Fully Catalytic Wall Heat Flux	0.25	0.21	0.19	0.17	0.21	0.44	0.54	0.73	0.44	0.65	0.84	0.90	0.63	0.44	0.43	0.59	0.39

TABLE 4 (CONCLUDED)

b) Conventional Units

Flight or Test Parameter	Flight	Simulation Type 1				Simulation Type 2				Simulation Type 3				Simulation Type 1-2			
		Flat Face Stagnation Point Model			Wedge Model	Flat Face Stagnation Point Model			Wedge Model	Flat Face Stagnation Point Model			Wedge Model	Flat Face Stagnation Point Model			Wedge Model
Model Body Diameter — inch	---	4.75	1.25	0.375	---	4.75	1.25	9.375	---	4.75	1.25	0.375	---	4.75	1.25	0.375	--
Total Enthalpy — Btu/lb	11,400	11,400	11,400	11,400	11,400	3,240	1,960	1 340	3,950	3,240	1,960	1,340	3,950	4380	2520	1640	7000
Catalytic Wall Heat Flux — Btu/ft²sec	14	14	14	14	14	14	14	14	14	14	14	14	14	14	14	14	14
Pressure — atm	0.012	0.00071	0.00019	0.000056	0.0021	0.012	0.012	0.012	0.012	0.012	0.012	0.012	0.012	0.006	0.006	0.006	0.006
Heat Transfer Coefficient — lb/ft²sec	0.0013	0.0013	0.0013	0.0013	0.0013	0.0053	0.010	0.019	0.0042	0.0053	0.010	0.019	0.0042	0.0037	0.0073	0.0134	0.0022
Elemental Mass Fraction of O_2	0.235	0.235	0.235	0.235	0.235	0.235	0.235	0.235	0.235	0.058	0.031	0.016	0.073	0.235	0.235	0.235	0.235
Partial Pressure of O_2 — atm	0	0	0	0	0	0.000	0.0013	0.0020	0	0	0	0	0	0	0.0003	0.0008	0
Partial Pressure of O — atm	0.0031	0.0002	---	---	0.0006	0.0040	0.0019	0.0006	0.0040	0.0011	0.0006	0.0002	0.0014	0.0020	0.0015	0.0006	0.0021
Local Mach Number	1.25/0.70	0.10	---	---	1.37	0.10	0.10	0.10	1.37	0.10	0.10	0.10	0.10	1.37	0.10	0.10	0.10
Momentum Thickness — feet	0.022	0.022	---	---	0.019	0.0036	0.0014	0.0007	0.0053	0.0040	0.0018	0.0008	0.0056	0.0063	0.0022	0.0011	0.0101
Shear — lb/ft²	0.18	0.022	---	---	0.27	0.068	0.11	0.18	0.56	0.070	0.12	0.19	0.60	0.051	0.083	0.14	0.45
Ratio of Fully Non-catalytic Wall to Fully Catalytic Wall Heat Flux	0.25	0.21	0.19	0.17	0.21	0.44	0.54	0.73	0.44	0.65	0.84	0.90	0.63	0.44	0.43	0.59	0.36

TABLE 5
TEST CONFIGURATION CONDITIONS
COATED Cb
a) SI Units

Flight or Test Parameter	Flight	Simulation Type I				Simulation Type 2				Simulation Type 3				Simulation Type 1-2			
		Flat Face Stagnation Point Model			Wedge Model	Flat Face Stagnation Point Model			Wedge Model	Flat Face Stagnation Point Model			Wedge Model	Flat Face Stagnation Point Model			Wedge Model
Model Body Diameter — meters	---	1.21×10^{-1}	3.18×10^{-2}	9.52×10^{-3}	---	1.21×10^{-1}	3.18×10^{-2}	9.52×15^{-3}	---	1.21×10^{-1}	3.18×10^{-2}	9.52×10^{-3}	---	1.21×10^{-1}	3.18×10^{-2}	9.52×10^{-3}	---
Total Enthalpy — J/kg	4.8×10^{7}	4.8×10^{7}	4.8×10^{7}	4.8×10^{7}	4.8×10^{7}	2.30×10^{7}	1.30×10^{7}	0.83×10^{7}	3.16×10^{7}	2.30×10^{7}	1.30×10^{7}	0.83×10^{7}	3.16×10^{7}	3.19×10^{7}	1.74×10^{7}	1.06×10^{7}	
Catalytic Wall Heat Flux — W/m^2	2.95×10^{5}	2.95×10^{5}	2.95×10^{5}	2.95×10^{5}	2.95×10^{5}	2.95×10^{5}	2.95×10^{5}	2.95×10^{5}	2.95×10^{5}	2.94×10^{5}	2.95×10^{5}	2.95×10^{5}	2.95×10^{5}	2.95×10^{5}	2.95×10^{5}	2.95×10^{5}	
Pressure — N/m^2	1.22×10^{2}	2.33×10^{2}	6.38×10^{1}	1.92×10^{1}	5.67×10^{2}	1.22×10^{3}	1.22×10^{3}	1.22×10^{3}	1.22×10^{3}	1.22×10^{3}	1.22×10^{3}	1.22×10^{3}	1.22×10^{3}	6.08×10^{2}	6.08×10^{2}	6.08×10^{2}	
Heat Transfer Coefficient — ko/m^2sec	1.17×10^{-2}	1.17×10^{-2}	1.17×10^{-2}	1.17×10^{-2}	1.17×10^{-2}	2.59×10^{-2}	4.88×10^{-2}	9.28×10^{-2}	1.81×10^{-2}	2.59×10^{-2}	4.88×10^{-2}	9.28×10^{-2}	1.81×10^{-2}	1.81×10^{-2}	3.56×10^{-2}	6.54×10^{-2}	
Elemental Mass Fraction of O_2	0.235	0.235	0.235	0.235	0.235	0.235	0.235	0.235	0.235	0.106	0.056	0.030	0.154	0.235	0.235	0.235	Same as Type 1
Partial Pressure of O_2 — N/m^2	0	0	0	---	0	0	3.04×10^{1}	1.52×10^{2}	0	0	0	0	0	0	0	3.04×10^{1}	
Partial Pressure of O — N/m^2	3.14×10^{2}	6.08×10^{1}	2.03×10^{1}	---	1.52×10^{2}	3.95×10^{2}	3.95×10^{2}	1.92×10^{2}	3.75×10^{2}	1.82×10^{2}	1.11×10^{2}	6.08×10^{1}	2.43×10^{2}	1.82×10^{2}	2.03×10^{2}	1.52×10^{2}	
Local Mach number	1.00/0.70	0.10	0.10	---	1.37	0.10	0.10	0.10	1.37	0.10	0.10	0.10	1.37	0.10	0.10	0.10	
Momentum Thickness — meters	4.27×10^{-3}	3.96×10^{-3}	3.66×10^{-3}	---	3.66×10^{-3}	4.88×10^{-4}	5.49×10^{-4}	2.44×10^{-4}	2.19×10^{-3}	1.46×10^{-3}	6.40×10^{-4}	3.05×10^{-4}	2.22×10^{-3}	2.17×10^{-3}	9.75×10^{-4}	3.66×10^{-4}	
Shear — N/m^2	3.04×10^{4}	4.05×10^{3}	4.05×10^{3}	---	4.76×10^{4}	7.70×10^{3}	1.22×10^{4}	2.03×10^{4}	6.08×10^{4}	7.90×10^{3}	1.42×10^{4}	2.13×10^{4}	6.18×10^{4}	5.57×10^{3}	7.90×10^{3}	1.52×10^{4}	
Ratio of Fully Non-catalytic Wall to Fully Catalytic Wall Heat Flux	0.25	0.21	0.20	0.18	0.24	0.33	0.40	0.49	0.34	0.41	0.65	0.83	0.35	0.29	0.43	0.40	

TABLE 5 (CONCLUDED)

b) Conventional Units

Flight or Test Parameter	Flight	Simulation Type 1				Simulation Type 2				Simulation Type 3				Simulation Type 1-2			
		Flat Face Stagnation Point Model			Wedge Model	Flat Face Stagnation Point Model			Wedge Model	Flat Face Stagnation Point Model			Wedge Model	Flat Face Stagnation Point Model			Wedge Model
Model Body Diameter — inch	---	4.75	1.25	0.375	---	4.75	1.25	0.375	---	4.75	1.25	0.375	---	4.75	1.25	0.375	---
Total Enthalpy — Btu/lb	11,400	11,400	11,400	11,400	11,400	5,510	3,120	1,980	7,550	5,510	3,120	1,980	7,550	7,630	4,160	2,540	
Catalytic Wall Heat Flux Flux — Btu/ft²sec	26	26	26	26	26	26	26	26	26	26	26	26	26	26	26	26	
Pressure — atm	0.012	0.0023	0.00063	0.00019	0.0056	0.012	0.012	0.012	0.012	0.012	0.012	0.012	0.012	0.006	0.006	0.006	
Heat Transfer Coefficient — lb/ft²sec	0.0024	0.0024	0.0024	0.0024	0.0024	0.0053	0.010	0.019	0.0037	0.0053	0.010	0.019	0.0037	0.0037	0.0073	0.0134	
Elemental Mass Fraction of O_2	0.235	0.235	0.235	0.235	0.235	0.235	0.235	0.235	0.235	0.106	0.056	0.030	0.154	0.235	0.235	0.235	Same as Type 1
Partial Pressure of O_2 — atm	0	0	0	---	0	0	0.0003	0.0015	0	0	0	0	0	0	0	0.0003	
Partial Pressure of of O — atm	0.0031	0.0006	0.0002	---	0.0015	0.0039	0.0039	0.0019	0.0037	0.0018	0.0011	0.0006	0.0024	0.0018	0.0020	0.0015	
Local Mach Number	1.00/0.70	0.10	0.10	---	1.37	0.10	0.10	0.10	1.37	0.10	0.10	0.10	1.37	0.10	0.10	0.10	
Momentum Thickness — feet	0.014	0.013	0.012	---	0.012	0.0046	0.0018	0.0008	0.0072	0.0048	0.0021	0.0010	0.0073	0.0070	0.0032	0.0012	
Shear — lb/ft²	0.30	0.040	0.040	---	0.47	0.076	0.12	0.20	0.60	0.078	0.14	0.21	0.61	0.055	0.078	0.15	
Ratio of Fully Non-catalytic Wall to Fully Catalytic Wall Heat Flux	0.25	0.21	0.20	0.18	0.24	0.38	0.40	0.49	0.34	0.41	0.65	0.83	0.35	0.29	0.43	0.40	

TABLE 6
COMPARISON OF TEST AND FLIGHT CONDITIONS

Boundary Condition or Parameter	Type 1		Type 2		Type 3		Type 1-2	
	Stag Pt Model	Wedge Model	Stag Pt Model	Wedge Model	Stag Pt Model	Wedge Model	Stag Pt Model	Wedge Model
Heat Flux	≡	≡	≡	≡	≡	≡	≡	≡
Enthalpy	≡	≡	<<	<	<<	<	<	<
Heat Transfer Coefficient	≡	≡	>>	>	>>	>	>	>
Total Pressure	<<	<	≡	≡	≡	≡	<	<
Partial Pressures	<<	<	=	=	<	<	<	<
Oxygen Mass Fraction	≡	≡	≡	≡	<	<	≡	≡
Mach Number	<	=	<	=	<	=	<	=
Momentum Thickness	=	=	<<	<<	<<	<<	<	<
Shear	<<	>	<	>	<	>	<	>
Catalycity Ratio	=	=	>	>	>	>	>	>
Merits	All heat flux and diffusion controlled mass flux variables duplicated		Total pressure duplicated		Diffusion controlled mass flux and total pressure duplicated at lower enthalpy		Closer-to-flight simulation of all variables not duplicated in other types	
Compromise	Possible differences in surface catalycity effect, pressures may be unreasonably low		Diffusion controlled mass flux enhanced, possible differences in molecular species composition and surface catalycity effect		Possible differences in molecular species composition and surface catalycity effect		Combination of Types 1 and 2	

All symbols indicate test conditions relative to flight conditions: ≡ Same by definition; = Approximately the same; > Greater than; >> Much greater than; < Less than; << Much less than.

cases where pressure, or diffusion controlled mass flux and pressure, respectively, are important to the TPS material response.

The analytic and test results which follow allow a more definitive discussion of test model configuration and simulation type trade-offs and a selection of the most attractive configurations and types.

5.2 ANALYTICAL EVALUATION

The thermochemical and thermal response characteristics of TD NiCr and coated Cb were defined for typical flight and ground test conditions employing the computer techniques presented in Section 3.2. The results are presented in the following subsections.

5.2.1 TD NiCr Thermochemical Response

Based on the simplified constraint of equilibrium surface reactions for the bare TD NiCr alloy, the ACE code predicts that the prevailing surface species (i.e., the primary oxide of the oxide film) is Cr_2O_3* for surface temperatures greater than approximately 1340° K (1950° F) and is NiO* for all lower temperatures. Even though the physical complexities of oxide film formation (Section 3.2.1) are ignored in this prediction, these results agree qualitatively with the detailed model of Section 3.2.1.

At present the OFFA code is capable of treating the formation of only one oxide at a time. Therefore, separate results are presented below for the formation of both NiO* and Cr_2O_3* oxide scales. The Cr_2O_3* results are representative of the overall shuttle application; the NiO* results are representative only of the initial response in the first cycle of exposure.

Figure 14 illustrates the nondimensional ablation rates as a function of surface temperature for both NiO* and Cr_2O_3* films exposed to air at 1013 N/m^2 (0.01 atm). The ACE code was used to obtain these results. The ablation rates are seen to be very strong functions of temperature. Further, in the temperature range of interest, 1370 to 1920° K (2000 to 3000° F), the NiO* film ablates at a rate considerably higher than that for the Cr_2O_3* film. The influence of pressure on the ablation rate was found to be relatively minor; for a 100 percent increase in pressure, B'_c decreases approximately 30 percent when the oxide film is Cr_2O_3*. Note that this result indicates that type 1 simulation is acceptable or even preferred for TD NiCr in that pressure is not an important variable and its effect is such as to yield conservative results thermochemically (lower pressure than flight yields a higher mass loss rate than flight). Further, the mass change rates are sufficiently low that there are no critical thermochemical constraints on the selection of simulation type.

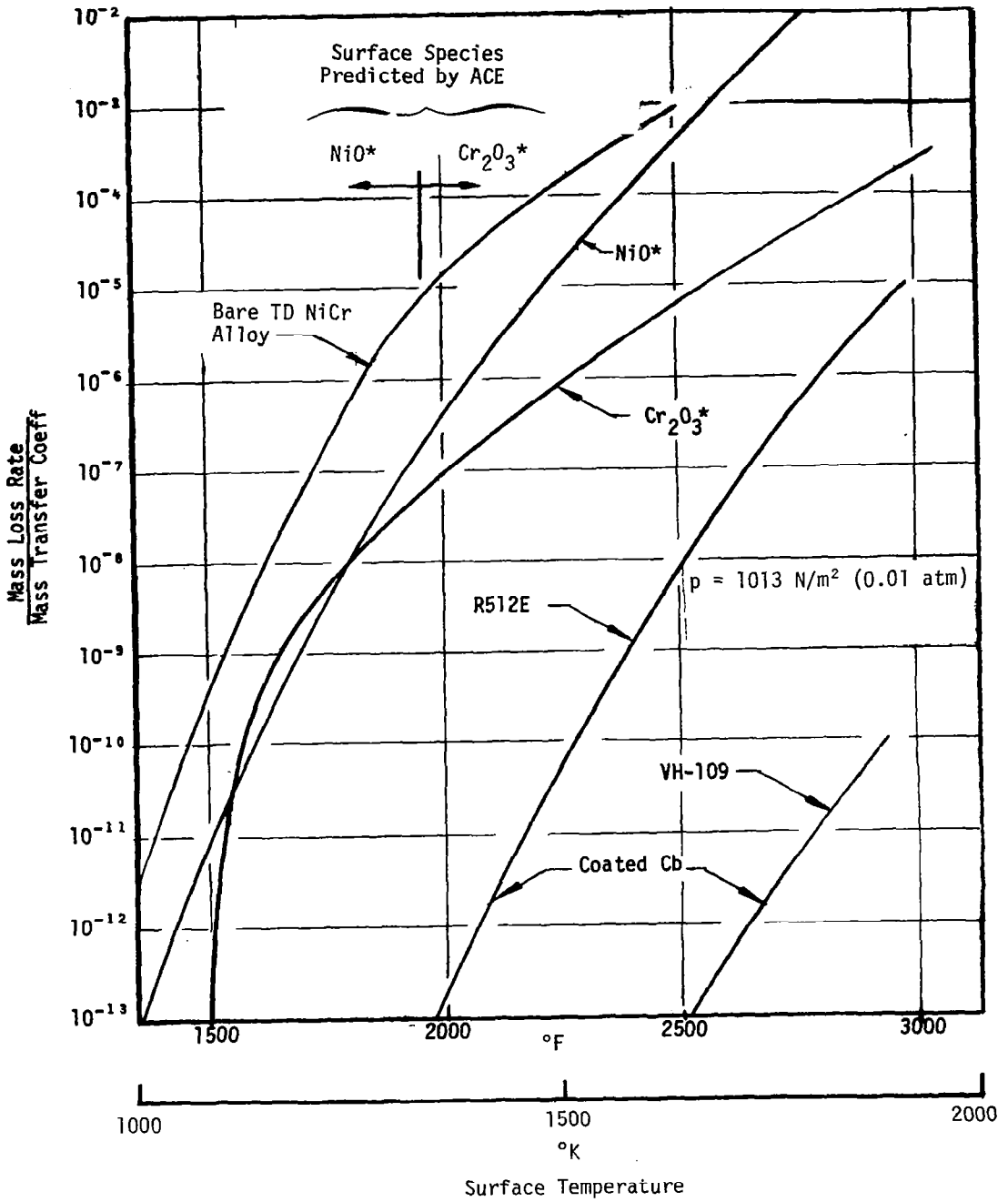

Figure 14. Thermochemical Response of TD NiCr (Bare and with Cr_2O_3* and NiO* Scales) and Coated Columbium (R512E and VH-109)

Also included in Figure 14 is the nondimensional ablation rate predicted by the ACE code for bare TD NiCr in air at 1013 N/m^2 (0.01 atm). In this calculation the elemental composition of the exposed surface was taken to be that of the bare TD NiCr alloy. As noted above, the controlling species is NiO* to about 1340° K (1950° F) and Cr_2O_3* at higher temperatures. This worst case situation, which ignores the effect of the oxide scale, indicates the expected higher mass loss rate.

Figure 15 illustrates the surface movement and film thickness change as computed by the OFFA code for thirty heating/cooling cycles, assuming the oxide film is Cr_2O_3*. The first half of each cycle is comprised of 30 minutes of heating, in which the surface temperature is increased from 290° K to 1370° K (70° F to 2000° F) in the first two minutes and is held constant at 1370° K (2000° F) until 30 minutes have expired. The second half of the cycle is a 30 minute cooldown period during which the surface is assumed to radiate as a black body to the surroundings. The initial oxide thickness was taken to be 3.15×10^{-6} meters (1.24×10^{-4} inches). After thirty cycles, the oxide film thickness has increased by roughly 3 percent and the surface position is essentially unchanged. It is evident that the thermochemical ablation rate for this case (see Figure 15) is smaller than the oxide film formation rate, so that the TD NiCr/Cr_2O_3* composite is predicted to remain intact over many cycles. The similar results assuming an NiO* oxide film are qualitatively and quantitatively similar.

Predictions were also obtained for the response of NiO* and Cr_2O_3* films for higher surface temperatures corresponding to more severe heating conditions. For the Cr_2O_3* film, it was found that even when the surface temperature is as high as 1920° K (3000° F) the predicted thermochemical ablation of the oxide is much smaller than its rate of formation, so that the TD NiCr/Cr_2O_3* composite remains intact over many cycles at the higher temperature. For the NiO* film, however, it was found that at a surface temperature of 1810° K (2800° F) the entire TD NiCr/NiO* composite would be consumed in roughly thirty cycles due to the excessive rate of thermochemical ablation of the exposed surface of the film.

Figure 16 presents the weight gain histories associated with the oxide film histories for a Cr_2O_3* film (Figure 15) and a NiO* film. A net weight gain is predicted for both scales, but the resultant rates are so small as to be negligible in terms of the shuttle application.

5.2.2 Coated Cb Thermochemical Response

The ACE code was also used to compute nondimensional mass loss rates for coated columbium. At a surface temperature of 1590° K (2400° F), this nondimensional ablation rate never exceeded 10^{-9} for both R512E and VH-109 coatings

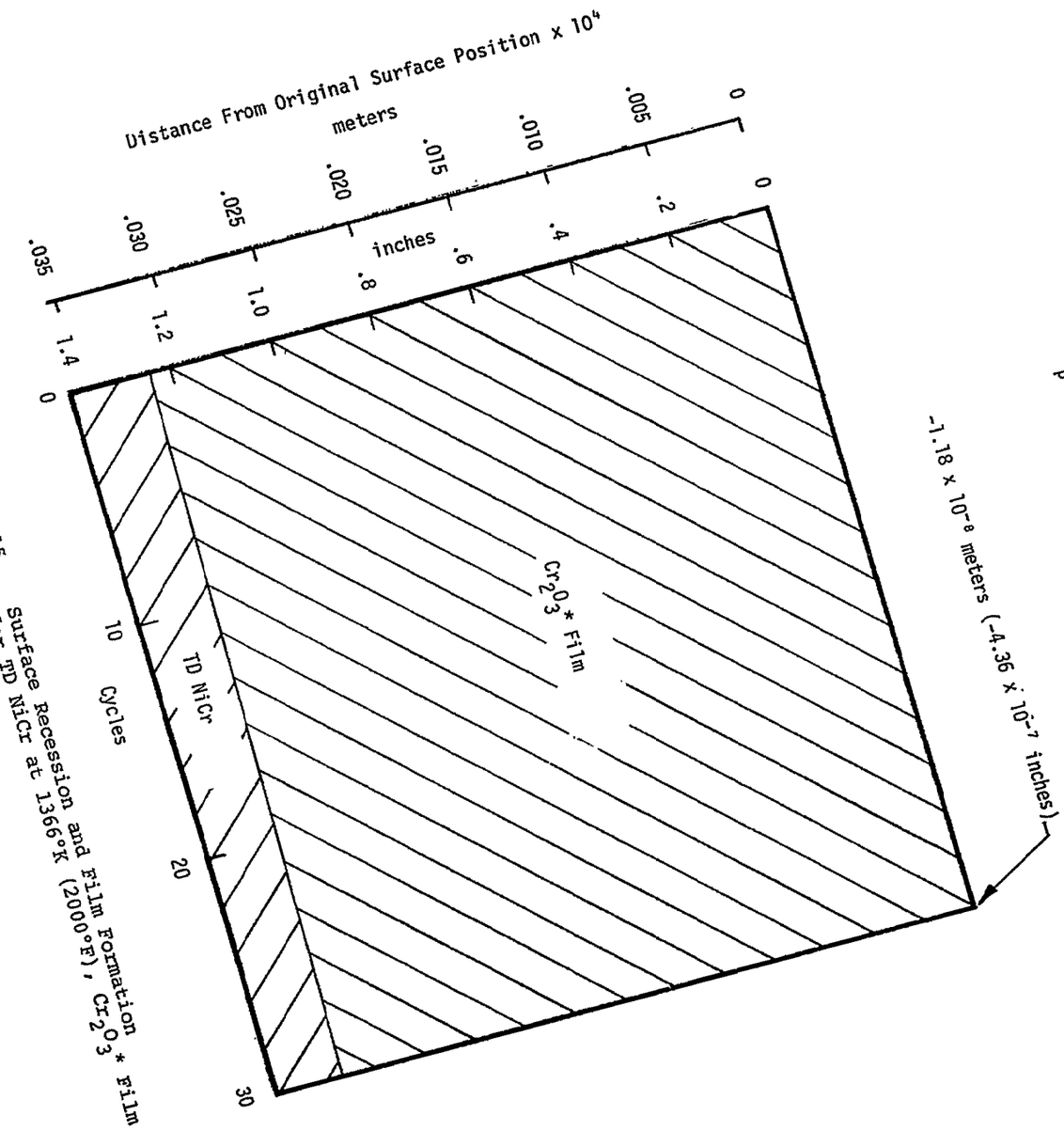

Figure 15. Surface Recession and Film Formation for TD NiCr at 1366°K (2000°F), Cr_2O_3 * Film

T_w = 1366°K (2000°F)
p = 1013 N/m² (0.01 atm)

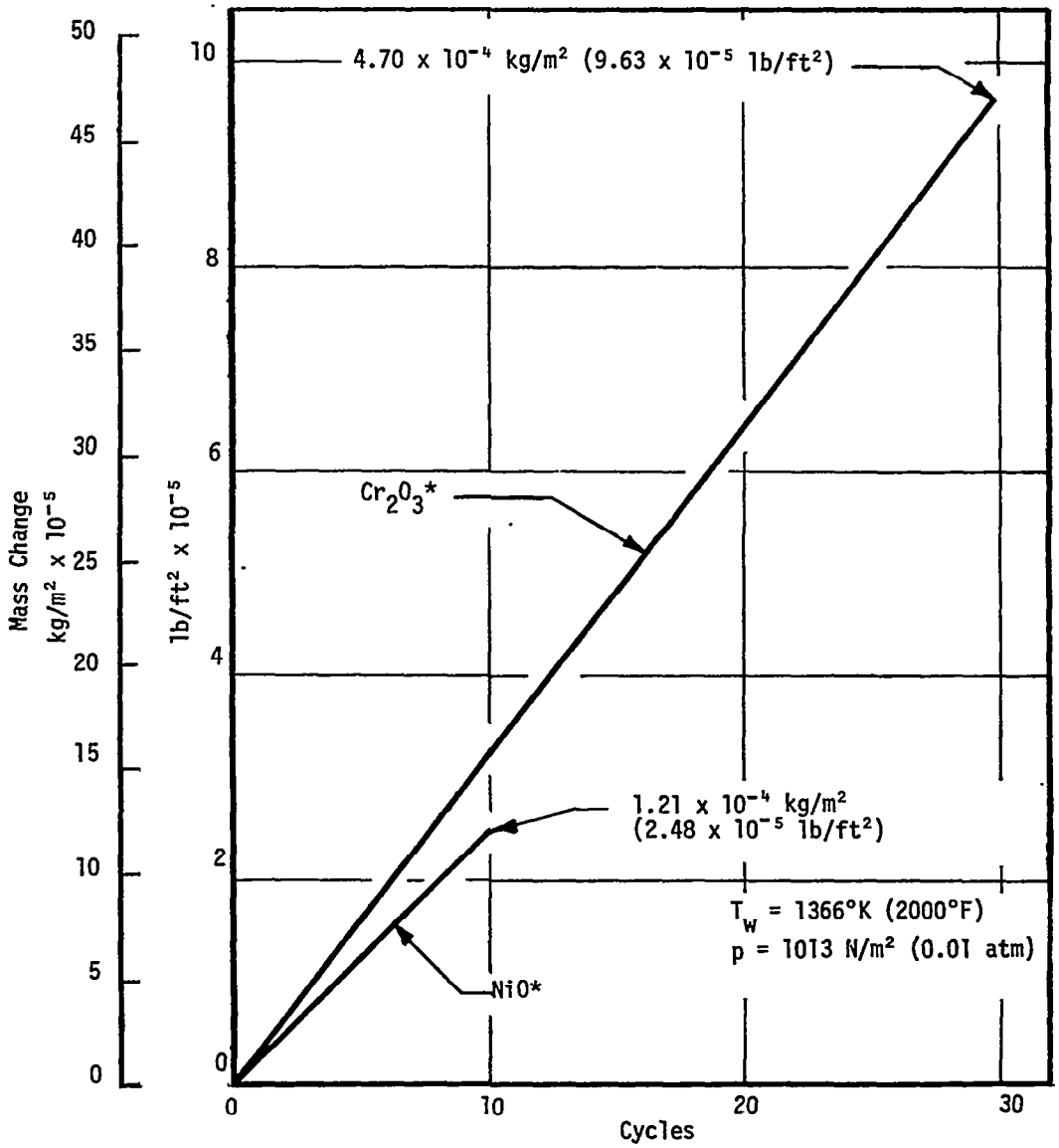

Figure 16. Mass Change for TD NiCr at 1366°K (2000°F)

(see Figure 14). The loss rate for both materials was found to be roughly inversely proportional to pressure for fixed surface temperature. Because of the extremely low ablation rates, surface recession was assumed to be negligible in the CMA code computations of thermal response. The surface species controlling the coatings response, and therefore the prevailing surface species, as predicted by the ACE code were Cb_2O_5* for the R512E coating and HfO_2* for the VH-109 coating. Note that because of the extremely low mass loss rates there are no significant macroscopic thermochemical constraints on the selection of simulation type. Significant differences in microscopic response and surface species may occur however with differences in simulation conditions. Also failure for coated columbiums is typically related to local coating degradation and subsequent catastrophic thermal or oxidation failure of the columbium substrate.

5.2.3 TD NiCr Thermal Response

Figure 17 illustrates one-cycle temperature profile histories for the TD NiCr/Cr_2O_3* composite at the heating rate corresponding to a maximum surface temperature of 1370° K (2000° F). During the first half of the cycle (heating), the temperature profile is essentially unchanged after 450 seconds elapsed time. Similarly, after 450 seconds of the cooling half of the cycle, the temperatures throughout the metal and insulation have decayed to roughly ambient temperature. The maximum temperature attained at the insulation backwall is 580° K (590° F). Temperature profile histories for the TD NiCr/NiO* composite are almost identical to those presented in Figure 17, since the thermophysical properties of the oxide film are essentially the same.

5.2.4 Coated Cb Thermal Response

Figure 18 illustrates one-cycle temperature profile histories for coated Cb at a heating rate corresponding to a maximum surface temperature of 1590° K (2400° F). The thermal response is similar to that of the TD NiCr/Cr_2O_3* composite. That is, during heating and cooling, the profile attains essentially its steady-state value within 450 seconds elapsed time. The maximum insulation backwall temperature is 650° K (710° F).

5.3 EXPERIMENTAL EVALUATION

The thermochemical and thermal response characteristics of TD NiCr and coated Cb were studied through flowing air tests over a range of reentry simulation test conditions. The experimental procedures presented in Section 4 and the simulation approaches presented in Section 5.1 were employed. The results are presented in the following subsections.

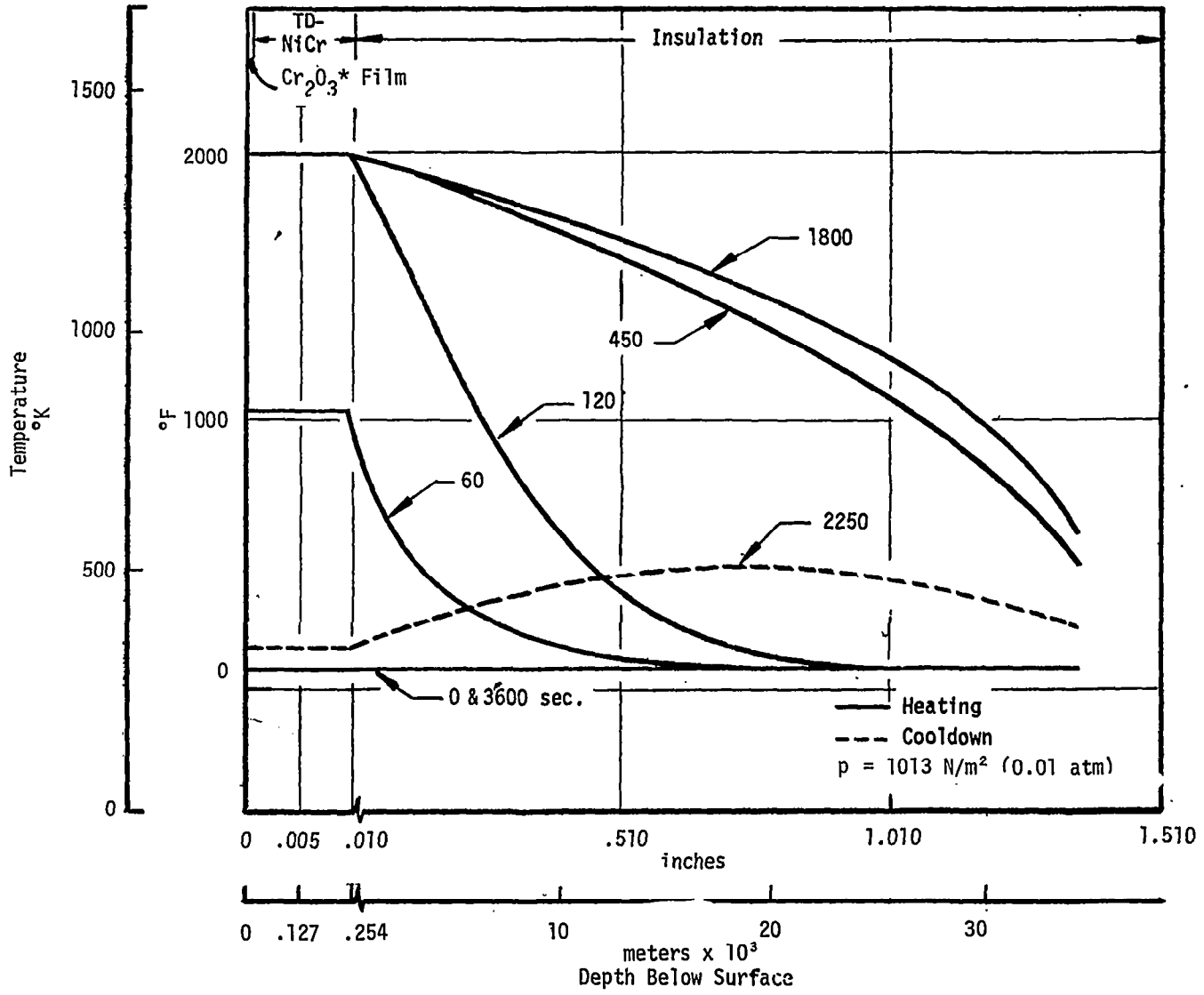

Figure 17. Surface and In-Depth Thermal Response for TD NiCr

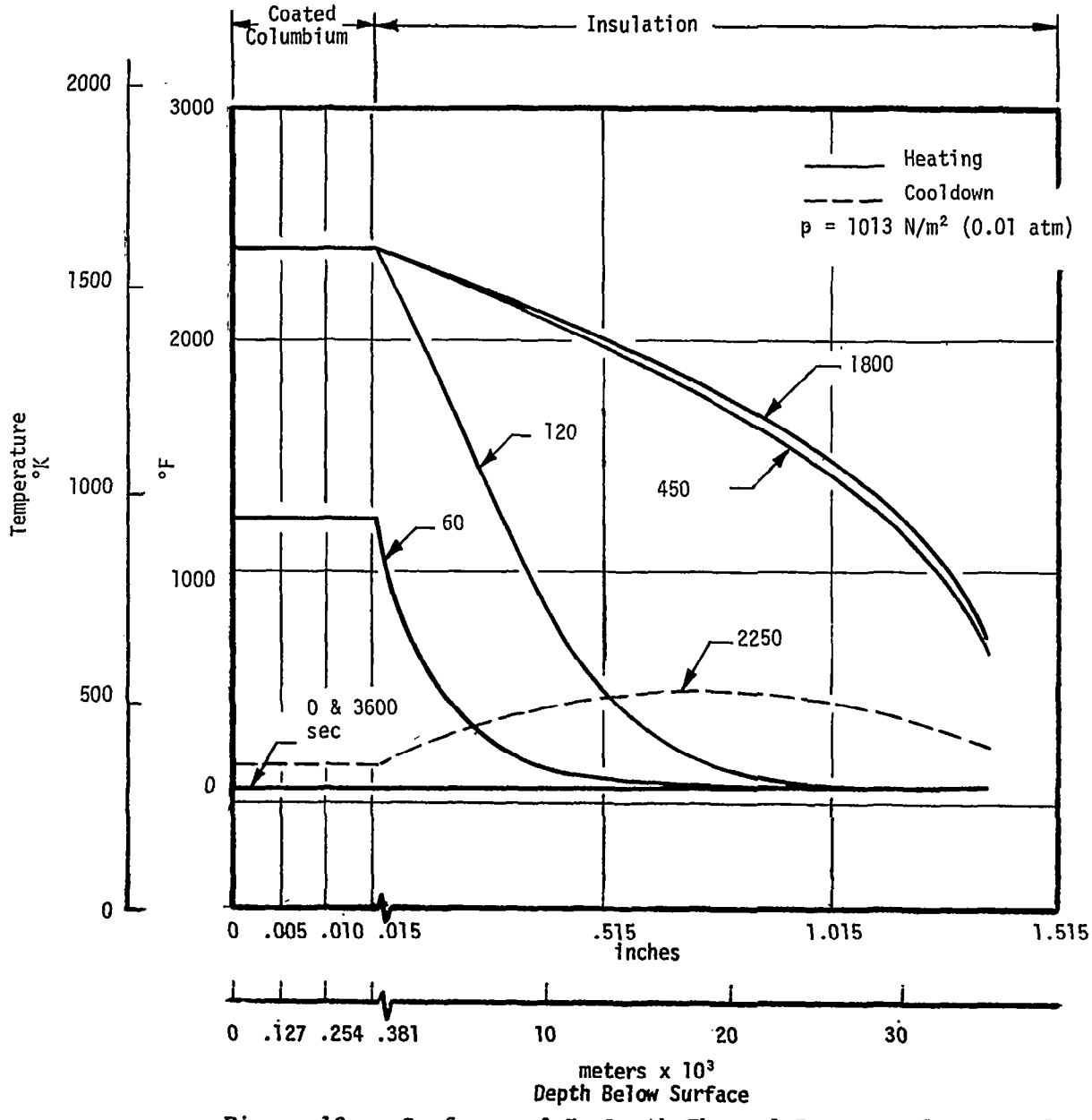

Figure 18. Surface and In-Depth Thermal Response for Coated Columbium

5.3.1 Calibration Tests

The basic test conditions defined by the calibration test series are presented in Tables 7 and 8 for the stagnation point and wedge models, respectively. Typical distributions of properties across the test stream and test models are shown in Figures 19 through 21[1] as follows:

- Test stream distribution, condition 9 - Figure 19
- Model distributions
  - Stagnation point, condition 9 - Figure 20
  - Wedge, condition 5 - Figure 21

The surface catalycity calibration results for all type 1-2 simulation conditions on the 0.121-meter (4.75-inch) diameter stagnation point model are presented in Figure 22.[1] The theoretical minimum heat flux ratio corresponding to a completely frozen boundary layer and a completely noncatalytic wall is also indicated in the figure. Note that the shape of the theoretical limit curve and the curve which was fit to the test data and for which the theoretical curve was used as a guide is related to the two dissociation regimes - O_2 at low enthalpy and N_2 at moderate to high enthalpy.[2] These results are discussed in the following subsection together with the corresponding test sample results.

5.3.2 Sample Tests

The sample test results are summarized in Tables 9 and 10 for the stagnation point and wedge models, respectively. Tabulated test condition and sample response parameters which require additional description are presented in Table 11. A more detailed tabulation of results is included in Appendix C.

In addition to the overall response characteristics presented in Tables 9 and 10, surface temperature response and backup material in-depth temperature response were defined as a function of time through each cycle. Typical surface temperature histories are presented in Figure 23, and a typical temperature distribution through the Silfrax backup material is presented in Figure 24. From the latter figure and the similar results for other tests, the conduction loss to the backup material was always less than 5 percent of the net convective heat flux to the surface. Also from Figure 24, the extrapolation of the in-depth temperatures indicates good agreement with the pyrometrically measured surface temperature. The extrapolated surface temperature is slightly above the measured

---

[1]The complete set of results in included in Appendix C.

[2]These dissociation regimes were defined for the test pressure of 1013 N/m^2 (0.01 atm) by the ACE code.

TABLE 7

CALIBRATION RESULTS FOR NOMINAL STAGNATION POINT MODEL TEST CONDITIONS

a) SI Units

Condition No.	Simulation Type	Desired Test Conditions				Actual Test Conditions			Average Enthalpy (J/kg)		Air Flow Rate (kg/sec)	Arc Heater Current (A)	Test Nos.
		Total Enthalpy (J/kg)	Stagnation Pressure (N/m^2)	Partially Catalytic Wall Heat Flux[a] (W/m^2)	Surface Temp (°K)	Heat Flux Enthalpy (J/kg)	Stagnation Pressure (N/m^2)	Fully Catalytic Wall Heat Flux[a] (W/m^2)	Energy Balance	Mass Balance			
1	1-2	1.42×10^7	1013.2	1.59×10^5	1370	1.38×10^7	1013.2	1.83×10^5	1.10×10^7	1.10×10^7	.0109	411	2058, 2059 2065, 2068
2	3					1.51×10^7		2.01×10^5	1.18×10^7	-			2060, 2066 2067
3	1-2	0.63×10^7		0.64×10^5	1090	0.81×10^7	1114.6	1.10×10^5	0.62×10^7	0.77×10^7	.0172	286	2058, 2059 2065, 2068
4	1	0.84×10^7		0.79×10^5	1370[b]	0.83×10^7		1.13×10^5	0.75×10^7	0.92×10^7	.0150	319	2059, 2065 2068
8	1	4.77×10^7	202.6	2.95×10^5	1590	5.86×10^7	192.5	3.43×10^5	3.87×10^7	3.51×10^7	.0012	896	2063, 2064 2069, 2070
9	1-2	2.47×10^7	1013.2			2.77×10^7	1013.2	3.64×10^5	1.88×10^7	2.26×10^7	.0073	642	2065, 2068
10	3					3.61×10^7	911.9	4.64×10^5	2.20×10^7	-			2066, 2067
11	1-2	3.60×10^7		4.31×10^5	1760	4.87×10^7	1013.2	6.54×10^5	2.41×10^7	3.22×10^7	.0060	814	2059, 2065 2068
12		1.38×10^7		1.48×10^5	1590[b]	1.38×10^7	1013.2	1.83×10^5	1.10×10^7	1.30×10^7	.0109	411	2058, 2059 2065, 2068

a) Indicated heat flux is for a 0.121-meter diameter calibration model; actual sample test model diameter identical except for test conditions 4 and 12 for which model diameter was 0.0318 meters and therefore actual sample test heat flux was a factor of 2 higher.

b) Indicated temperature is for a 0.0318-meter diameter sample test model.

TABLE 7 (CONCLUDED)

b) Conventional Units

Condition No.	Simulation Type	Desired Test Conditions				Actual Test Conditions			Average Enthalpy (Btu/lb)		Air Flow Rate	Arc Heater Current	Test Nos.
		Total Enthalpy (Btu/lb)	Stagnation Pressure (atm)	Partially Catalytic Wall Heat Flux[a] (Btu/ ft²sec)	Surface Temp (°F)	Heat Flux Enthalpy (Btu/lb)	Stagnation Pressure (atm)	Fully Catalytic Wall Heat Flux[a] (Btu/ ft²sec)	Energy Balance	Mass Balance	(lb/sec)	(amps)	
1	1-2	3,400	0.010	14.0	2,000	3,300	0.010	16.1	2,630	3,100	0.024	411	2058, 2059 2065, 2068
2	3					3,610		17.7	2,830		-		2060, 2066 2067
3	1-2	1,500		5.6	1,500	1,930	0.011	9.7	1,470	1,850	0.0380	286	2058, 2059 2065, 2068
4		2,000		7.0	2,000[b]	1,980		10.0	1,790	2,200	0.0330	319	2059, 2065 2068
8	1	11,400	0.002	26.0	2,400	14,000	0.0019	30.2	9,260	8,400	0.0027	896	2063, 2064 2069, 2070
9	1-2	5,900	0.010			6,620	0.010	32.1	4,500	5,400	0.0160	642	2065, 2068
10	3					8,620	0.009	40.9	5,250		-		2066, 2067
11	1-2	8,600		38.0	2,700	11,650	0.010	57.6	5,760	7,700	0.0132	814	2059, 2065 2068
12		3,300		13.0	2,400[b]	3,300	0.010	16.1	2,630	3,100	0.024	411	2058, 2059 2065, 2068

a) Indicated heat flux is for a 4.75-inch diameter calibration model; actual sample test model diameter identical except for test conditions 4 and 12 for which model diameter was 1.25 inches and therefore actual sample test heat flux was a factor of 2 higher.

b) Indicated temperature is for a 1.25-inch diameter sample test model.

TABLE 8

CALIBRATION RESULTS FOR NOMINAL WEDGE MODEL TEST CONDITIONS

a) SI Units

Condition No.	Simulation Type	Desired Test Conditions[a]				Actual Test Conditions[a]				Average Enthalpy (J/kg)		Air Flow Rate	Arc Heater Current	Test No.
		Total Enthalpy (J/kg)	Local Pressure (N/m^2)	Partially Catalytic Wall heat Flux (W/m^2)	Surface Temperature (°K)	Heat Flux Enthalpy (J/kg)	Stagnation Pressure (N/m^2)	Local Pressure (N/m^2)	Fully Catalytic Wall heat Flux (W/m^2)	Energy Balance	Mass Balance	(kg/sec)	(A)	
5	1	4.77+7	202.6	1.59×10^5	1370	4.12×10^7	1114.6	202.6	1.52×10^5	2.41×10^7	--	.0586	387	2156
6	1-2	1.80+7	1013.2			2.05×10^7	2533.1	911.9	1.34×10^5	1.68×10^7	--	.234	483	2148
7	3					2.00×10^7		1013.2	0.98×10^5	1.46×10^7	--	1	486	2149
13	1	4.77+7	608.0	2.95×10^5	1590	4.71×10^7	2127.8	405.3	2.76×10^5	4.66×10^7	--	.0976	895	2148

[a]Local pressure and heat flux are at the central position of the active test sample (s = 0.098 meters, see Figure 8).

TABLE 8 (CONCLUDED)

b) Conventional Units

Condition No.	Simulation Type	Desired Test Conditions[a]				Actual Test Conditions[a]				Average Enthalpy (Btu/lb)		Air Flow Rate	Arc Heater Current	Test No.
		Total Enthalpy (Btu/lb)	Local Pressure (atm)	Partially Catalytic Wall Heat Flux (Btu/ft²sec)	Surface Temperature (°F)	Heat Flux Enthalpy (Btu/lb)	Stagnation Pressure (atm)	Local Pressure (atm)	Fully Catalytic Wall Heat Flux (Btu/ft²sec)	Energy Balance	Mass Balance	(lb/sec)	(amps)	
5	1	11,400	0.002	14.0	2,000	9,850	0.011	0.002	13.4	5,750	-	0.012	387	2156
6	1-2	4,300	0.010			4,900	0.025	0.009	11.8	4,020	-	0.048	483	2148
7	3					4,780		0.010	8.6	3,500	-		486	2149
13	1	11,400	0.006	26.0	2,400	11,250	0.021	0.004	24.3	11,150	-	0.020	895	2148

a) Local pressure and heat flux are at the central portion of the active test sample (s = 3.85 inches, see Figure 8)

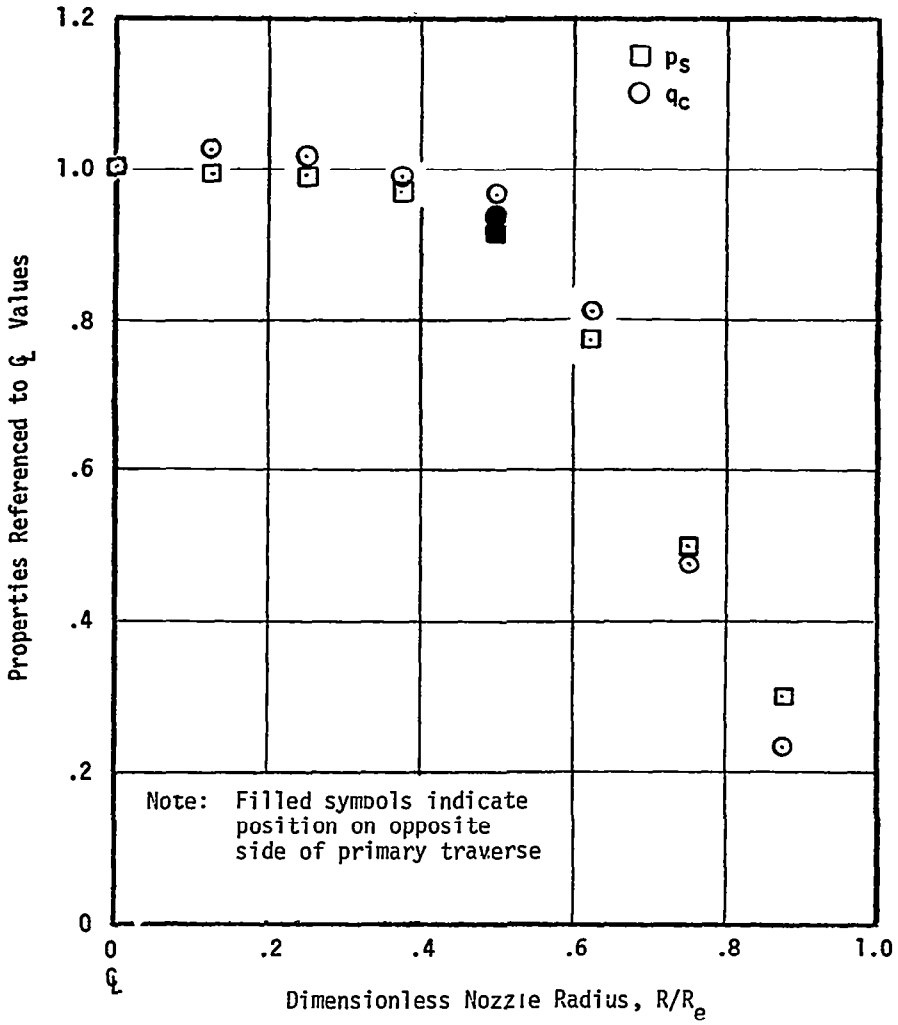

Figure 19. Typical Test Stream Distribution Results (Condition 9)

TEST 2065-4

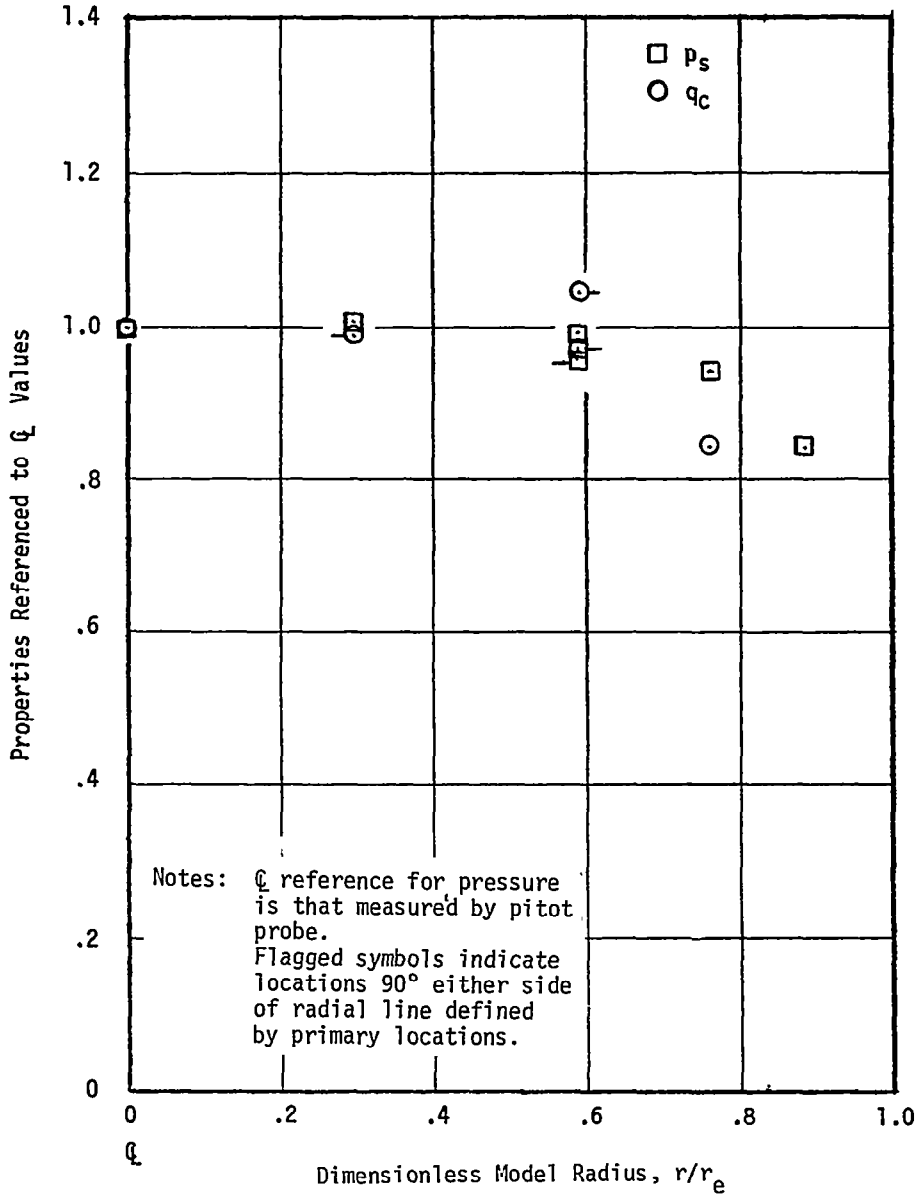

Figure 20. Typical Stagnation Point Model Distribution Results (Condition 9)

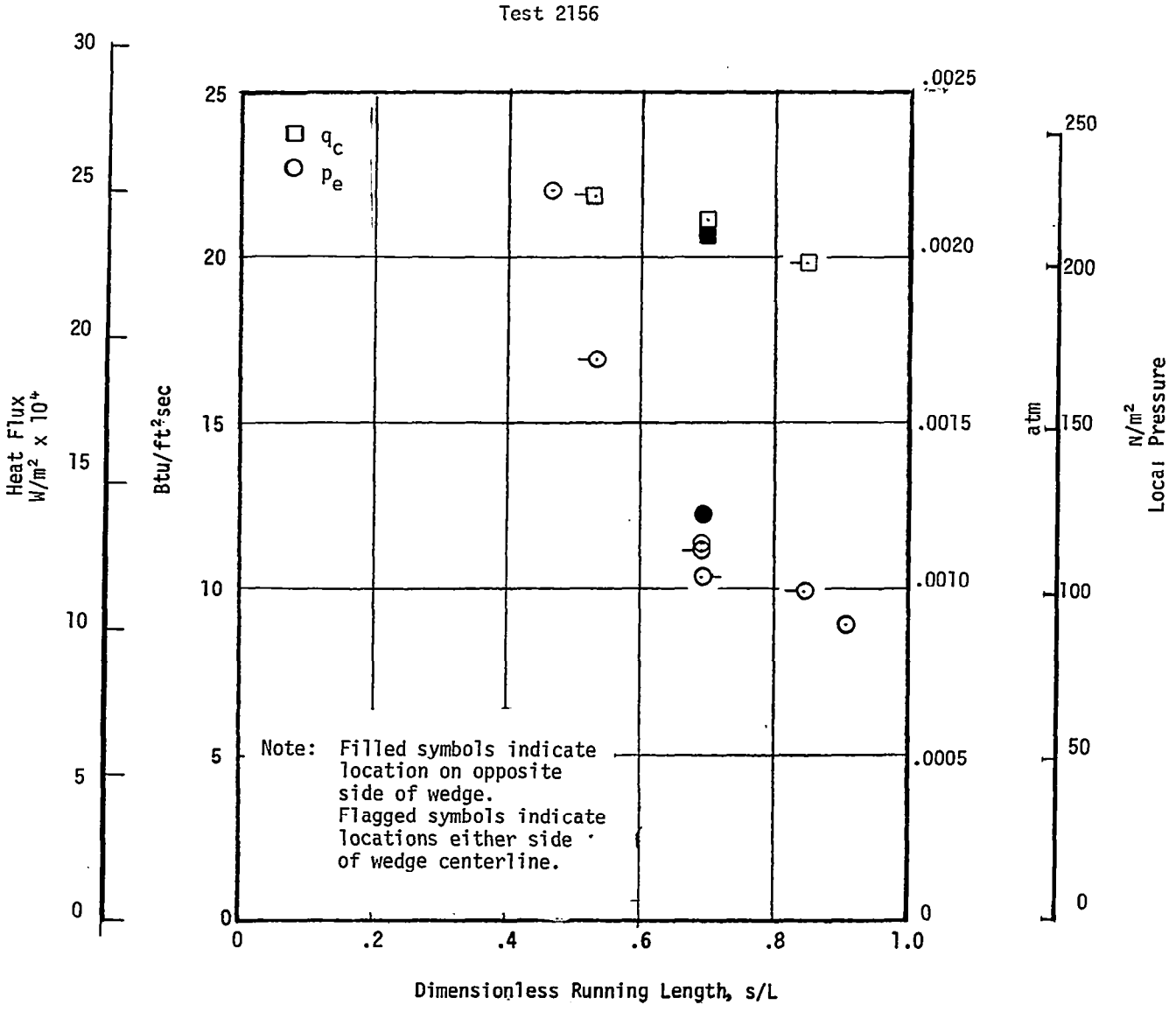

Figure 21. Typical Wedge Model Distribution Results (Condition 5)

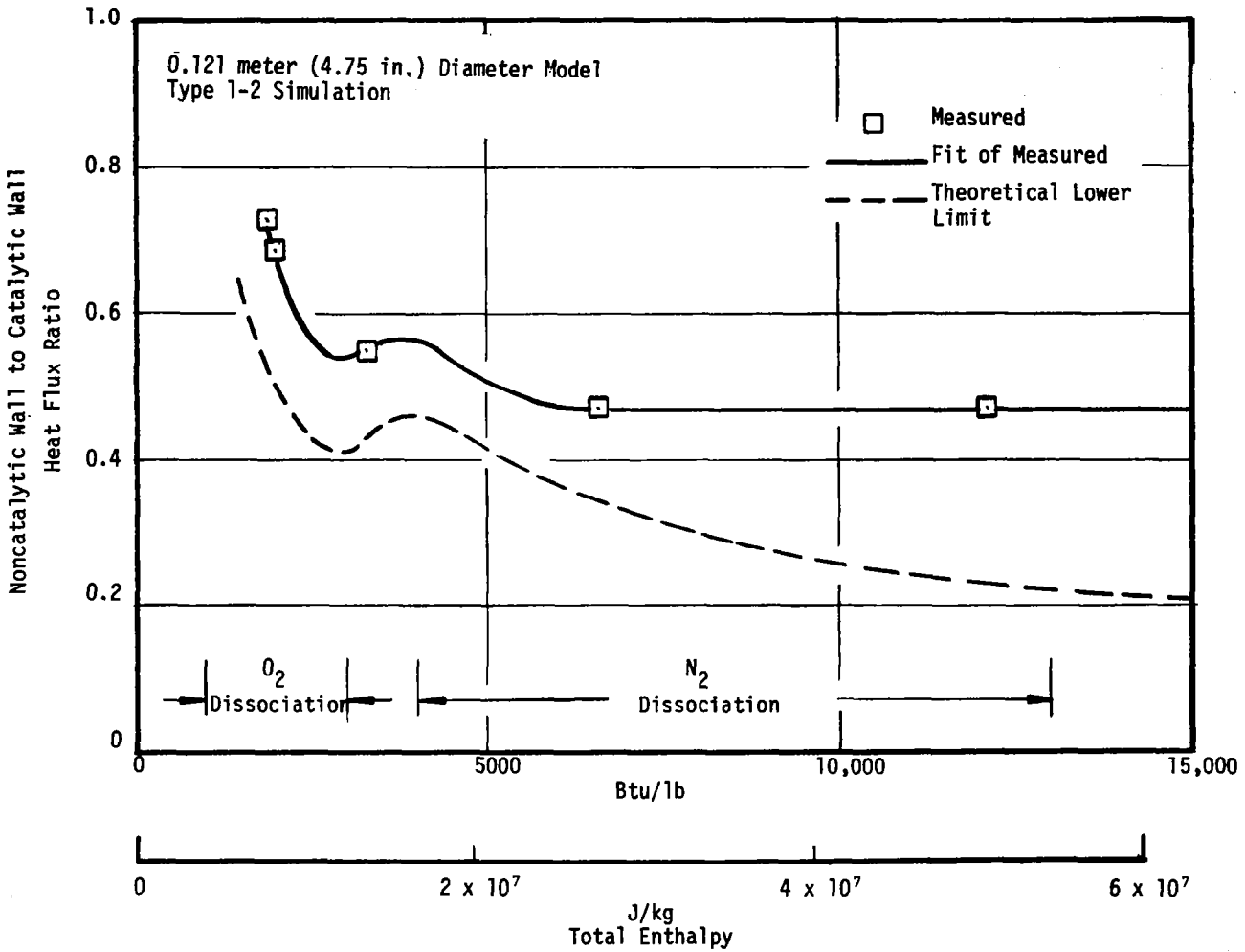

Figure 22. Surface Catalycity Calibration Results

TABLE 9

ITIONS AND RESULTS FOR STAGNATION POINT MODEL TESTS

a) SI Units

Stagnation Pressure (N/m^2)	Oxygen Partial Pressure O/O_2 (N/m^2)	Oxygen Mass Fraction	Heat Transfer Coefficient (kg/m^2sec)	Surface Temperature (°K)	Probable Emissivity (-)	Apparent Net Convective Flux to Wall (W/m^2)	Surface Catalycity Ratio (-)	Average Mass Change Rate (kg/m^2sec)	Average Surface Recession Rate (m/sec)	Comments
9.42×10^2	$2.13 \times 10^2/2.03 \times 10^1$	.232	2.34×10^{-2}	1290	.75	1.17×10^5	.74	3.06×10^{-6}	1.41×10^{-9}	
1.04×10^3	3.44×10^2/ --		2.44 x	1370		1.51	.76	3.06×10^{-5}	-4.23	
				1380		1.55	.82			
1.00	3.34×10^2/ --		2.39 x	1370		1.51	.77			
1.01	3.44×10^2/ --			1360		1.43	.71			
1.03			2.44 x	1370		1.51	.70	-6.22×10^{-5}	-2.12×10^{-9}	Sample failed at 20 min
1.06×10^3	$3.44 \times 10^2/1.01 \times 10^1$	.232	2.44×10^{-2}	1370	.75	1.51×10^5	.81	2.22×10^{-6}	-2.26×10^{-8}	
1.03	3.34×10^2/--						.80			
1.04	$3.34 \times 10^2/1.01 \times 10^1$			1380		1.53	.83			
				1370		1.49	.80			
1.03				1380		1.53	.81	-2.78×10^{-7}	-6.21×10^{-9}	
1.00	1.22×10^2/--	.062	2.39 x	1370		1.51	.69	2.22×10^{-6}	1.41 x	
9.93 x 10^2							.55	2.50 x	-1.69×10^{-8}	
1.06×10^3	$1.01 \times 10^2/1.52 \times 10^2$	.232	2.44 x	1170		0.78	.92	5.56×10^{-7}	7.06×10^{-9}	
				1130		0.70	.82	8.33 x	-8.47 x	
1.04	$1.22 \times 10^2/1.32 \times 10^2$		6.34×10^{-3}	1250		1.03	.56	0	-9.88 x	
	$1.72 \times 10^2/1.01 \times 10^2$		4.88×10^{-2}	1380		1.55	.71		-2.82 x	
1.62×10^2	4.05×10^1/--		9.76×10^{-3}	1460		1.91	.58	1.44×10^{-5}	1.41 x	
1.82			1.02×10^{-2}	1390		1.58	.47	1.44 x	-4.23 x	
				1370		2.38	.65	1.58 x	-9.88 x	
1.72			9.76×10^{-3}	1520		2.22	.61			
1.42	3.04×10^2/--		8.79 x	1500		2.19	.59			
1.52			9.28 x	1530		2.32	.62			
1.42			8.79 x	1580		2.63	.72	4.17×10^{-6}	-7.06×10^{-10}	
2.02×10^1	2.94×10^2/--		2.29×10^{-2}	1510		2.21	.62	-2.19×10^{-5}	-2.26×10^{-8}	
	2.84×10^2/--			1590		2.71	.70	-6.81	0	
9.52×10^2	8.11×10^1/--	.062	2.34 x	1510		2.21	.50	1.94 x	-2.82×10^{-9}	
	7.09×10^1/--			1580		2.68		1.72 x	5.64 x	
1.00×10^3	$2.84 \times 10^2/3.04 \times 10^{-1}$	.232	2.39 x	1290		1.17	.75	1.92 x	-1.27 x	
1.05	3.44×10^2/--		2.44 x	1360		1.46		2.08 x	-4.23 x	
9.73×10^2	2.53×10^2/--		2.34 x	1610		2.86	.46	1.39 x	1.13 x	
1.05×10^3			2.44 x	1620		2.95	.40	-9.44×10^{-6}	-8.47 x	
1.00	3.14×10^2/--		2.39 x	1350		1.41		2.48×10^{-5}	-1.41 x	
1.06	3.44×10^2/--		2.44 x	1570		2.60	.39	3.36 x	-7.06 x	
1.82×10^2	4.05×10^1/--		1.02 x	1360		1.43	.44	5.83×10^{-6}	8.47 x	
1.62			9.76×10^{-3}	1490		2.09	.56	5.00 x	-2.82 x	
1.57			9.28 x	1420		1.74	.47			
1.52				1430		1.79	.48			
1.42	3.04×10^1/--		8.79 x	1420		1.71	.46			
				1390		1.61	.43	8.33×10^{-7}	0	
9.22	2.94×10^2/--		2.54×10^{-2}	1430		1.77	.53	8.61×10^{-6}	-2.12×10^{-8}	
	2.74×10^2/--		2.29 x	1590		2.71	.67	9.17 x	-1.13 x	
9.52	8.11×10^1/--	.062		1410		1.69	.38	4.44 x	1.13 x	
	7.09×10^1/--		2.34 x	1550		2.38	.40	5.28 x	-1.41×10^{-9}	
1.00×10^3	2.94×10^2/--	.232		1270		1.09	.69	5.55 x	-1.27×10^{-8}	
1.05	3.55×10^2/--		2.44 x	1370		1.51	.72	9.17 x	4.23×10^{-9}	
1.01	2.74×10^2/--		2.39 x	1590		2.75	.45	6.11 x	-1.41 x	
1.05			2.44 x	1580		2.68	.39	3.06 x		
1.01	3.34×10^2/--		2.34 x	1300		1.24	.33	2.33×10^{-5}	-5.64 x	
1.07			2.49 x	1580		2.63	.34	1.03 x	-1.55×10^{-8}	

TABLE 9

SUMMARY OF TEST CONDITIONS AND RESULTS FOR STAGNATION POINT MODEL TESTS

a) SI Units

ytic Wall Convective Heat Flux		Stagnation Pressure	Oxygen Partial Pressure O/O_2	Oxygen Mass Fraction	Heat Transfer Coefficient	Surface Temperature	Probable Emissivity	Apparent Net Convective Flux to Wall	Surface Catalycity Ratio	Average Mass Change Rate	Average Surface Recession Rate
: Wall	Hot Wall										
/m²)	(W/m²)	(N/m²)	(N/m²)	-	(kg/m²sec)	(°K)	(-)	(W/m²)	(-)	(kg/m²sec)	(m/sec)
x 10^5	1.58×10^5	9.42×10^2	$2.13 \times 10^2/2.03 \times 10^1$	.232	2.34×10^{-2}	1290	.75	1.17×10^5	.74	3.06×10^{-6}	1.41×10^{-9}
	2.00	1.04×10^3	3.44×10^2/ --		2.44 x	1370		1.51	.76	3.06×10^{-5}	-4.23
	1.88					1380		1.55	.82		
	1.95	1.00	3.34×10^2/ --		2.39 x	1370		1.51	.77		
	2.02	1.01	3.44×10^2/ --			1360		1.43	.71		
	2.17	1.03			2.44 x	1370		1.51	.70	-6.22×10^{-5}	-2.12×10^{-9}
x 10^5	1.86×10^5	1.06×10^3	$3.44 \times 10^2/1.01 \times 10^1$	.232	2.44×10^{-2}	1370	.75	1.61×10^5	.81	2.22×10^{-6}	-2.26×10^{-8}
	1.90	1.03	3.34×10^2/--						.80		
	1.84	1.04	$3.34 \times 10^2/1.01 \times 10^1$			1380		1.53	.83		
	1.85					1370		1.49	.80		
	1.87	1.03				1380		1.53	.81	-2.78×10^{-7}	-6.21×10^{-9}
	1.70	1.00	1.22×10^2/--	.062	2.39 x	1370		1.51	.69	2.22×10^{-6}	1.41 x
	1.78	9.93×10^2							.55	2.50 x	-1.69×10^{-8}
	0.85	1.06×10^3	$1.01 \times 10^2/1.52 \times 10^2$	.232	2.44 x	1170		0.78	.92	5.56×10^{-7}	7.06×10^{-9}
	0.86					1130		0.70	.82	8.33 x	-8.47 x
	1.83	1.04	$1.22 \times 10^2/1.32 \times 10^2$		6.34×10^{-3}	1250		1.03	.56	0	-9.88 x
	2.19		$1.72 \times 10^2/1.01 \times 10^2$		4.88×10^{-2}	1380		1.55	.71		-2.82 x
	3.29	1.62×10^2	4.05×10^1/--		9.76×10^{-3}	1460		1.91	.58	1.44×10^{-5}	1.41 x
	3.32	1.82			1.02×10^{-2}	1390		1.58	.47	1.44 x	-4.23 x
	3.68					1370		2.38	.65	1.58 x	-9.88 x
	3.67	1.72			9.76×10^{-3}	1520		2.22	.61		
	3.70	1.42	3.04×10^2/--		8.79 x	1500		2.19	.59		
	3.76	1.52			9.28 x	1530		2.32	.62		
	3.68	1.42			8.79 x	1580		2.63	.72	4.17×10^{-6}	-7.06×10^{-10}
	3.54	2.02×10^1	2.94×10^2/--		2.29×10^{-2}	1510		2.21	.62	-2.19×10^{-5}	-2.26×10^{-9}
	3.88		2.84×10^2/--			1590		2.71	.70	-6.81	0
	4.43	9.52×10^2	8.11×10^1/--	.062	2.34 x	1510		2.21	.50	1.94 x	-2.82×10^{-9}
	5.31		7.09×10^1/--			1580		2.68		1.72 x	5.64 x
	1.57	1.00×10^3	$2.84 \times 10^2/3.04 \times 10^{-1}$	.232	2.39 x	1290		1.17	.75	1.92 x	-1.27 x
	1.95	1.05	3.44×10^2/--		2.44 x	1360		1.46		2.08 x	-4.23 x
	6.18	9.73×10^2	2.53×10^2/--		2.34 x	1610		2.86	.46	1.39 x	1.13 x
	7.39	1.05×10^3			2.44 x	1620		2.95	.40	-9.44×10^{-6}	-8.47 x
	3.53	1.00	3.14×10^2/--		2.39 x	1350		1.41		2.48×10^{-5}	-1.41 x
	6.59	1.06	3.44×10^2/--		2.44 x	1570		2.60	.39	3.36 x	-7.06 x
	3.28	1.82×10^2	4.05×10^1/--		1.02 x	1360		1.43	.44	5.83×10^{-6}	8.47 x
	3.70	1.62			9.76×10^{-3}	1490		2.09	.56	5.00 x	-2.82 x
	3.70	1.57			9.28 x	1420		1.74	.47		
	3.76	1.52				1430		1.79	.48		
		1.42	3.04×10^1/--		8.79 x	1420		1.71	.46		
	3.71					1390		1.61	.43	8.33×10^{-7}	0
	3.34	9.22	2.94×10^2/--		2.54×10^{-2}	1430		1.77	.53	8.61×10^{-6}	-2.12×10^{-8}
	4.04		2.74×10^2/--		2.29 x	1590		2.71	.67	9.17 x	-1.13 x
	4.39	9.52	8.11×10^1/--	.062		1410		1.69	.38	4.44 x	1.13 x
	6.14		7.09×10^1/--		2.34 x	1550		2.38	.40	5.28 x	-1.41×10^{-9}
	1.58	1.00×10^3	2.94×10^2/--	.232		1270		1.09	.69	5.55 x	-1.27×10^{-8}
	2.39	1.05	3.55×10^2/--		2.44 x	1370		1.51	.72	9.17 x	4.23×10^{-9}
	6.12	1.01	2.74×10^2/--		2.39 x	1590		2.75	.45	6.11 x	-1.41 x
	6.80	1.05			2.44 x	1580		2.68	.39	3.06 x	
	3.73	1.01	3.34×10^2/--		2.34 x	1300		1.24	.33	2.33×10^{-5}	-5.64 x
	7.81	1.07			2.49 x	1580		2.63	.34	1.03 x	-1.55×10^{-8}

Test No.	Test Cond.	Simulation Type	Model Description	Sample No.	Sample Material	Cycle	Cumulative Exposure Time (min)	Total Enthalpy (J/kg)	Catalytic Wall Convect Heat Flux Cold Wall (W/m^2)	Hot Wal (W/m^2)
2073	1	1-2	4-3/4 SP	45	TD NiCr	1	30	1.41×10^7	1.83×10^5	1.58×1
2075								1.73	2.33	2.00
2077				46		2	60	1.62	2.18	1.88
						3	90	1.73	2.24	1.95
						4	120	1.72	2.30	2.02
						5	140	1.83	2.46	2.17
2079	1	1-2	4-3/4 SP	48	TD NiCr	1	30	1.58×10^7	2.16×10^5	1.86×1
2080						2	60	1.61		1.90
						3	90	1.58	2.13	1.84
						4	120			1.85
						5	150	1.62	2.18	1.87
2078	2	3		47		1	30	1.50	1.99	1.70
2081				49				1.57	2.06	1.78
2090	3	1-2		50				0.80	1.09	0.85
2091				51						0.86
2076	4		1-1/4 SP	41				0.86	2.34	1.83
2077				42				1.02	2.78	2.19
2096	8	1	4-3/4 SP	36	R512E/			6.44	3.42	3.29
2097				37	Cb-752			6.07	3.45	3.32
2099				38				6.78	3.77	3.68
2101						2	60	6.94	3.80	3.67
						3	90	7.70	3.82	3.70
						4	120	7.28	3.77	3.76
						5	150	7.61	3.80	3.68
2072	9	1-2		26		1	30	2.84	3.65	3.54
2078				27				3.30	4.22	3.88
2082	10	3		28				3.66	4.74	4.43
2083				29				4.37	5.65	5.31
2086	1	1-2		30				1.38	1.83	1.57
2087				31				11.64	1.21	1.95
2092	11			33				5.00	6.54	6.18
2095				35				5.72	7.76	7.39
2086			1-1/4 SP	5				1.57	4.09	3.53
2087				6				2.67	7.30	6.59
2098	8	1	4-3/4 SP	18	VH-109/			5.98	3.41	3.28
2100				19	C129Y			7.20	3.83	3.70
2103						2	60	7.36	3.81	3.70
						3	90	7.49	3.87	3.76
						4	120	7.74	3.81	
						5	150	7.70	3.87	3.71
2071	9	1-2		10		1	30	2.57	3.65	3.34
2075				11				3.44	4.38	4.04
2084	10	3		12				3.64	4.68	4.39
2085				13				5.00	6.47	6.14
2093	1	1-2		15				1.41	1.83	1.58
2094				17				1.76	2.39	2.39
2104	11			20				4.87	6.49	6.12
2105				21				5.27	7.15	6.80
2093	12		1-1/4 SP	3				1.51	4.09	3.73
2094				4				7.42	8.52	7.81

TABLE 9 (CONCLUDED)

b) Conventional Units

Test No.	Test Cond.	Simulation Type	Model Description	Sample No.	Sample Material	Cycle	Cumulative Exposure Time (min)	Total Enthalpy (Btl/lb)	Catalytic Wall Convective Heat Flux		Stagnation Pressure (atm)	Oxygen Partial Pressure O/O_2 (atm)	Oxygen Mass Fraction
									Cold Wall (Btu/ft²sec)	Hot Wall (Btu/ft²sec)			
2073	1	1-2	4-3/4 SP	45	TD NiCr	1	30	3,380	16.1	13.9	.0093	.0027/.0002	.232
2076				46				4,130	20.5	17.6	.0102	.0034/---	
2077						2	60	3,860	19.2	16.6			
						3	90	4,130	19.7	17.2	.0099	.0033/---	
						4	120	4,120	20.3	17.8	.0100	.0034/---	
						5	140	4,370	21.7	19.1	.0102		
2079	1	1-2	4-3/4 SP	48	TD NiCr	1	30	3,770	19.0	16.4	.0105	.0034/.0001	.232
2080						2	60	3,830	19.0	16.7	.0102	.0033/---	
						3	90	3,770	18.8	16.2	.0103	.0033/.0001	
						4	120			16.3			
						5	150	3,860	19.2	16.6	.0102		
2078	2	3		47		1	30	3,590	17.5	15.0	.0099	.0010/---	.062
2081				49				3,760	18.2	15.7	.0098		
2090	3	1-2		50				1,910	9.6	7.5	.0105	.0010/.0015	.232
2091				51						7.6			
2076	4		1-1/4 SP	41				2,050	20.6	16.1	.0103	.0012/.0013	
2077				42				2,440	24.5	19.3		.0017/.0010	
2096	8	1	4-3/4 SP	36	R512E/			15,400	30.1	29.0	.0016	.0004/---	
2097				37	Cb-752			14,500	30.4	29.3	.0018		
2099				38				16,200	33.7	32.4			
2101						2	60	16,600	33.5	32.3	.0017		
						3	90	18,400	33.7	32.6	.0014	.0003/---	
						4	120	17,400	33.2	32.1	.0015		
						5	150	18,200	33.5	32.4	.0014		
2072	9	1-2		26		1	30	6,800	32.2	31.2	.0092	.0029/---	
2074				27				7,880	37.2	34.2		.0028/---	
2082	10	3		28				8,740	41.8	39.0	.0094	.0008/---	.062
2083				29				10,440	49.8	46.8		.0007/---	
2086	1	1-2		30				3,290	16.1	13.8	.0099	.0028/.0003	.232
2087				31				3,910	19.7	17.2	.0104	.0034/---	
2092	11			33				11,950	57.6	54.5	.0096	.0025/---	
2095				35				13,680	68.4	65.1	.0104	.0026/---	
2086	12		1-1/4 SP	5				3,670	36.0	31.1	.0099	.0031/---	
2087				6				6,380	64.3	58.1	.0105	.0034/---	
2098	8	1	4-3/4 SP	18	VH-109/			14,300	30.0	28.9	.0018	.0004/---	
2100				19	C129Y			17,200	33.7	32.6	.0016		
2103						2	60	17,600	33.6	32.6	.0015		
						3	90	17,900	34.1	33.1			
						4	120	18,500	34.1	33.1	.0014	.0003/---	
						5	150	18,400	33.7	32.7			
2071	9	1-2		10		1	30	6,140	32.2	29.4	.0091	.0029/---	
2075				11				8,220	38.6	35.6		.0027/---	
2084	10	3		12				8,690	41.2	38.7	.0094	.0008/---	.062
2085				13				11,950	57.0	54.1		.0007/---	
2093	1	1-2		15				3,370	16.1	13.9	.0099	.0029/---	.232
2094				17				4,200	21.1	18.5	.0104	.0035/---	
2104	11			20				11,640	57.2	54.0	.0100	.0027/---	
2105				21				12,600	63.0	59.9	.0104		
2093	12		1-1/4 SP	3				3,620	36.0	32.9	.0100	.0033/---	
2094				4				7,420	75.1	68.8	.0106		

Oxygen Mass Fraction	Heat Transfer Coefficient (lb/ft sec)	Surface Temperature (°F)	Probable Emissivity (-)	Apparent Net Convective Flux to Wall (Btu/ft²sec)	Surface Catalycity Ratio (-)	Average Mass Change Rate (gm/cm²hr)	Average Surface Recession Rate (in/hr)	Comments
.232	.0048	1,860	.75	10.3	.74	.0011	.0002	
	.0050	2,010		13.3	.76	.0011	-.0004	
		2,030		13.7	.82			
	.0049	2,010		13.3	.77			
		1,980		12.6	.71			
	.0050	2,010		13.3	.70	-.0024	-.0003	Sample failed at 20 min
.232	.0050	2,010	.75	13.3	.81	.0008	-.0032	
					.80			
		2,020		13.5	.83			
		2,000		13.1	.80			
		2,020		13.5	.81	-.0001	-.0008	
.062	.0049	2,010		13.3	.89	.0008	.0002	
					.85	.0009	-.0024	
.232	.0050	1,640		6.9	.92	.0002	.0010	
		1,580		6.2	.82	.0003	-.0012	
	.0013	1,790		9.1	.56	0	-.0014	
	.0100	2,030		13.7	.71		-.0004	
	.0020	2,160		16.8	.58	.0052	-.0002	
	.0021	2,040		13.9	.47		-.0006	
		2,310		21.0	.65	.0057	-.0014	
	.0020	2,270		19.8	.61			
	.0018	2,250		19.3	.59			
	.0019	2,290		20.4	.62			
	.0018	2,380		23.2	.72	.0015	-.0001	
	.0047	2,260		19.5	.62	-.0079	-.0032	
		2,400		23.9	.70	-.0245	0	
.062	.0048	2,260		19.5	.50	.0070	-.0004	
		2,390		23.6		.0062	.0008	
.232	.0049	1,860		10.3	.75	.0069	-.0018	
	.0050	1,990		12.9		.0075	-.0006	
	.0048	2,440		25.2	.46	.0050	.0016	
	.0050	2,460		26.0	.40	-.0034	-.0012	
	.0049	1,970		12.4		.0093	-.0020	
	.0050	2,370		22.9	.39	.0121	-.0010	
	.0021	1,980		12.6	.44	.0021	.0012	
	.0020	2,220		18.4	.56	.0018	-.0004	
	.0019	2,100		15.3	.47			
		2,120		15.8	.48			
	.0018	2,090		15.1	.46			
		2,050		14.2	.43	.0003	0	
	.0052	2,110		15.6	.53	.0031	-.0030	
	.0047	2,400		23.9	.67	.0033	-.0016	
.062		2,080		14.9	.38	.0016	.0016	
	.0048	2,330		21.6	.40	.0019	-.0002	
.232		1,820		9.6	.69	.0020	-.0018	
	.0050	2,010		13.3	.72	.0033	.0006	
	.0049	2,410		24.2	.45	.0022	-.0002	
	.0050	2,390		23.6	.39	.0011		
	.0033	1,890		10.9	.33	.0084	-.0008	
	.0051	2,380		23.2	.34	.0037	-.0022	

LE 10

D RESULTS FOR WEDGE MODEL TESTS

I Units

ygen rtial ssure 0 /m²)	Oxygen Mass Fraction	Heat Transfer Coefficient (kg/m²sec)	Surface Temperature (°K)	Probable Emissivity (-)	Apparent Net Convective Flux to Wall (W/m²)	Surface Catalycity Ratio (-)	Average Mass Change Rate (kg/m²sec)	Average Surface Recession Rate (m/sec)	Comments
x 10^{1}	.232	.0068	1300	.75	5.11 x 10^{4}	.74	6.33 x 10^{-5}	5.64 x 10^{-9}	
			1330		5.67	.82	9.89	-7.06	
-			1290		4.88	.69			
:			1320		5.45	.77			
			1280		4.65	.65			
			----		----------	---	-2.36 x 10^{-5}	2.82 x 10^{-9}	
-			1340		6.01 x 10^{4}	.85			
;					5.90	.84			
			1320		5.45	.76			
			----		----------	---	-3.30 x 10^{-5}	1.41 x 10^{-9}	
? x 10^{2}	.062	.0117	1310		5.22 x 10^{4}	.59			Sample failed at 12 min 35 sec
3 x 10^{2}	.062	.0117	1260	.75	4.31 x 10^{4}	.48			
3 x 10^{1}	.232	.0088	----		----------	---			Sample failed at 4 min 34 sec
3 x 10^{1}	.232	.0088	----	.75	----------	---			Sample failed prior to 4 min 34 sec
1 x 10^{2}	.232	.0207	1520	.75	1.08 x 10^{5}	.59	1.36 x 10^{-3}	1.41 x 10^{-9}	
2			1510		1.06	.57	1.27	-1.83 x 10^{-8}	
1			1500		1.03	.58			
			1530		1.11	.62		0.70 x 10^{-9}	
			----		----------	---			Sample failed at 30 sec due to momentary vacuum loss
1 x 10^{2}	.232	.0207	1520	.75	1.09 x 10^{5}	.61	3.58 x 10^{-4}		
2 x 10^{1}					1.08	.60			
1 x 10^{2}			1420		7.72	.43			
			1410		7.60	.42	4.87 x 10^{-4}	-2.12 x 10^{-8}	
			1380		6.29	.38			
					6.70	.37			
2 x 10^{1}			1360		6.24	.34	1.11 x 10^{-4}	-2.12 x 10^{-9}	

TABLE

SUMMARY OF TEST CONDITIONS AND

a) SI

Test No.	Test Cond.	Simulation Type	Model Description	Sample No.	Sample Material	Cycle	Cumulative Exposure Time (min)	Total Enthalpy (J/kg)	Catalytic Wall Convective Heat Flux		Local Pressure (N/m^2)	Oxy Part Press O ($N/$
									Cold Wall (W/m^2)	Hot Wall (W/m^2)		
2157	5	1	Wedge	74	TD NiCr	1	30	1.99×10^7	7.72×10^4	6.92×10^4	2.33×10^2	8.11
				75								
2158				74		2	60	2.01	7.83	7.04	2.13	7.09
						3	90				2.03	6.08
						4	120	2.05	7.94	7.14	1.92	
						5	150					
				75		2	60	2.02	7.83	7.04	2.13	7.09
						3	90				2.03	6.08
						4	120	2.05	7.94	7.14	1.92	
						5	150					
2151	6	1-2		76		1	12.5	1.55	1.02×10^5	8.85	5.17	1.72
2151	6	1-2	Wedge	78	TD NiCr	1	12.5	1.55×10^7	1.02×10^5	8.97×10^4	5.17 x	1.72
2152	7	3		81			4.5	1.53	7.60×10^4	----------	8.00	7.09
2152	7	3	Wedge	82	TD NiCr	1	4.5	1.53×10^7	7.60×10^4	----------	8.00×10^2	7.09
2153	13	1	Wedge	67	R512E/	1	30	3.37×10^7	1.99×10^5	1.84×10^5	4.05×10^2	1.11
				66	Cb-752						4.15	1.22
2155						2	60	3.30	1.94	1.79	3.75	1.01
						3	90				3.44	
						4	90.5	----------	----------	----------		
2155	13	1	Wedge	67	R512E/	2	60	3.30×10^7	1.94×10^5	1.79×10^5	3.75×10^2	1.01
					Cb-752	3	90				3.34	9.12
2154				61	VH-109/	1	30			1.80	3.44	1.01
				58	C129Y							
2155						2	60			1.82	3.75	
						3	90				3.44	
						4	120				3.75	
						5	150				3.34	9.12

TABLE 10 (
b) Convent

Test No.	Test Cond.	Simulation Type	Model Description	Sample No.	Sample Material	Cycle	Cumulative Exposure Time	Total Enthalpy (Btu/lb)	Catalytic Wall Convective Heat Flux		Local Pressure (atm)	Oxygen Partial Pressure 0 (atm)
									Cold Wall (Btu/ft²sec)	Hot Wall (Btu/ft²sec)		
2157	5	1	Wedge	74	TD NiCr	1	30	4750	6.8	6.1	.0023	.0008
				75								
2158				74		2	60	4800	6.9	6.2	.0021	.0007
						3	90				.0020	.0006
						4	120	4900	7.0	6.3	.0019	
						5	150					
				75		2	60	4800	6.9	6.2	.0021	.0007
						3	90				.0020	.0006
						4	120	4900	7.0	6.3	.0019	
						5	150					
2151	6	1-2		76		1	12.5	3700	9.0	7.8	.0051	.0017
				78						7.9		
2152	7	3		81			4.5	3650	6.7	---	.0076	.0007
				82								
2153	13	1		67	R512E/		30	8050	17.5	16.2	.0040	.0011
				66	Cb-752						.0041	.0012
2155						2	60	7900	17.1	15.8	.0037	.0010
						3	90				.0034	
						4	90.5	---	---	---	---	---
2155	13	1	Wedge	67	R512E/	2	60	7900	17.1	15.8	.0037	.0010
					Cb-752	3	90				.0033	.0009
2154				61	VH-109/	1	30			15.9	.0034	.0010
				58	C129Y							
2155						2	60			16.0	.0037	
						3	90				.0034	
						4	120				.0037	
						5	150				.0033	.0009

CONCLUDED)

ional Units

e	Oxygen Mass Fraction	Heat Transfer Coefficient (lb/ft^2sec)	Surface Temperature (°F)	Probable Emissivity (-)	Apparent Net Convective Flux to Wall (Btu/ft^2sec)	Surface Catalycity Ratio (-)	Average Mass Change Rate (gm/cm^2hr)	Average Mass Recession Rate (in/hr)	Comments
	.232	.0014	1880	.75	4.5	.74	.0228	.0008	
			1930		5.0	.82	.0356	-.0010	
			1860		4.3	.69			
			1920		4.8	.77			
			1840		4.1	.65			
			----		---	---	-.0085	.0004	
			1960		5.3	.85			
			1950		5.2	.84			
			1910		4.8	.76			
			----		---	---	-.0119	.0002	
		.0024	1900		4.6	.59			Sample failed at 12 min 35 sec
			1810		3.8	.48			
	.062	.0018	----		---	---			Sample failed at 4 min 34 sec
									Sample failed prior to 4 min 34 sec
	.232	.0022	2270		9.5	.59	.4880	.0002	
			2260		9.3	.57	.4600	-.0026	
			2250		9.1	.58			
			2290		9.8	.62		-.0001	
			----		---	---			Sample failed at 30 sec due to momentary vacuum loss
	.232	.0022	2280	.75	9.6	.61	.1288		
			2270		9.5	.60			
			2090		6.8	.43			
			2080		6.7	.42	.1752	-.0030	
			2030		6.1	.38			
			2020		5.9	.37			
			1980		5.5	.34	.0399	.0003	

TABLE 11

DESCRIPTION OF TABLES 9 AND 10

Additional description where required of tabulated parameters in Tables 9 and 10 is as follows:

- Model Description - 4-3/4 SP indicates 0.121 - meter (4.75-inch) diameter point model; 1-1/4 SP indicates 0.0318 - meter (1.25-inch) diameter flat face stagnation point model; wedge indicates 30° half angle wedge model.
- Cycle and Cumulative Exposure Time - one cycle equals 30 minutes exposure at constant incident heat flux.
- Enthalpy - heat flux enthalpy defined from the calibration test results and at the actual current of the sample test.
- Catalytic Wall Convective Heat Flux - cold wall defined from the calibration test results and at the actual current of the sample test; hot wall defined from (Cold Wall) * $(h_o - h_{wc})/h_o$ where h_o is the total enthalpy and h_{wc} is the fully catalytic wall enthalpy.
- Local Pressure (Table 10 only) - pressure at the central measurement station of the wedge model.
- Oxygen Partial Pressure - equilibrium concentrations of atomic/molecular oxygen at the boundary layer edge and at the total enthalpy and stagnation or local pressure (as computed by the ACE code).
- Oxygen Mass Fraction - 0.232 corresponds to air.
- Heat Transfer Coefficient - (Catalytic Cold Wall Convective Heat Flux)/(Total Enthalpy).
- Surface Temperature - measured value where available or interpreted value (in parenthesis) where such interpretation was possible.
- Probable Emissivity - estimated total hemispherical emissivity for the material (see following text).
- Apparent Net Convective Flux to Wall - radiation equilibrium heat flux based on surface temperature and probable emissivity (Equation (2)).
- Surface Catalycity Ratio - (Apparent Net Convective Flux to Wall)/(Catalytic Hot Wall Convective Heat Flux).
- Average Mass Change Rate - average rate of change of mass over the number of cycles indicated; positive number is mass increase.
- Average Thickness Change Rate - average rate of change of sample thickness over the number of cycles indicated; positive number is a thickness increase.

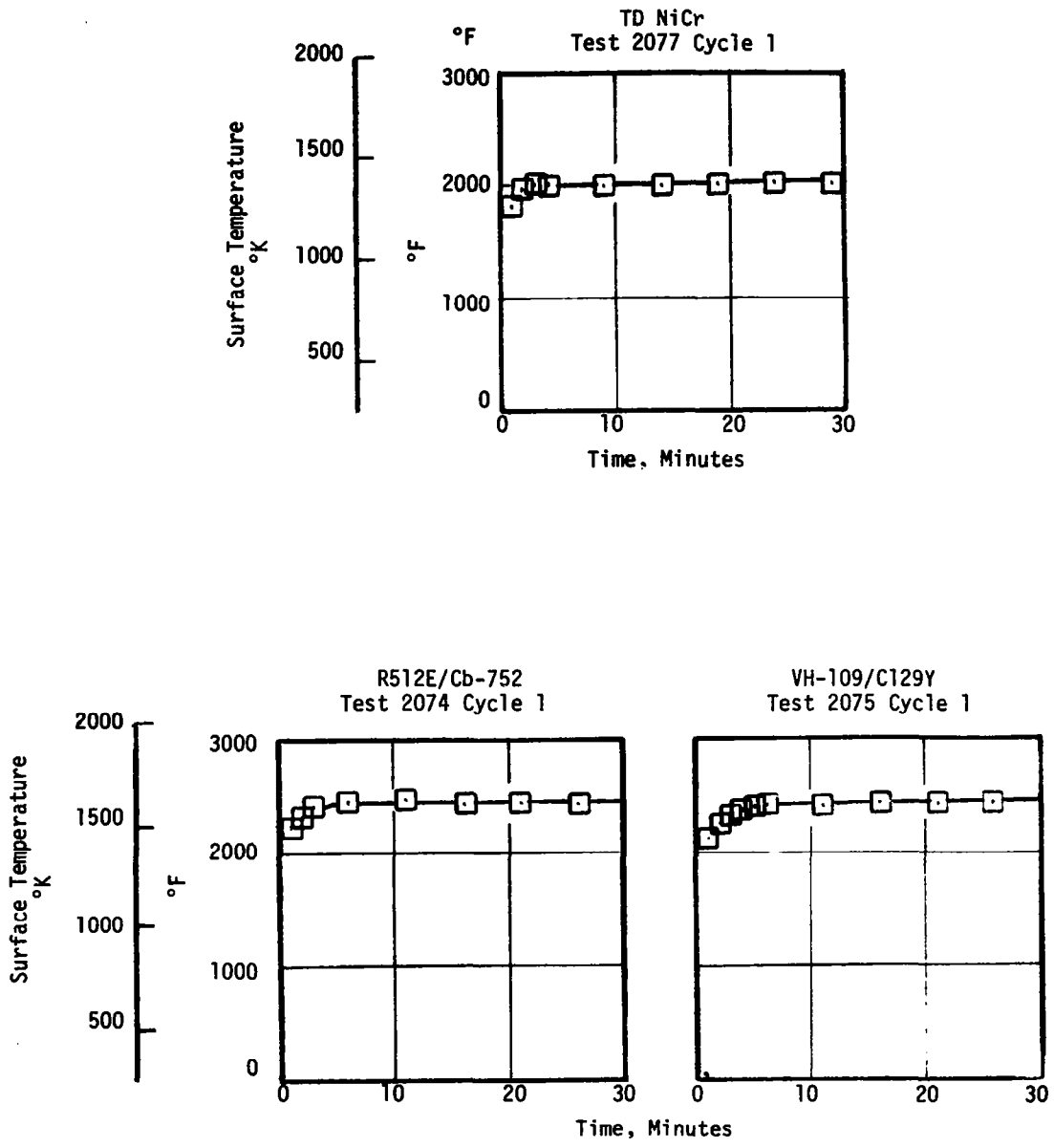

Figure 23. Typical Cyclic Surface Temperature-Time Results

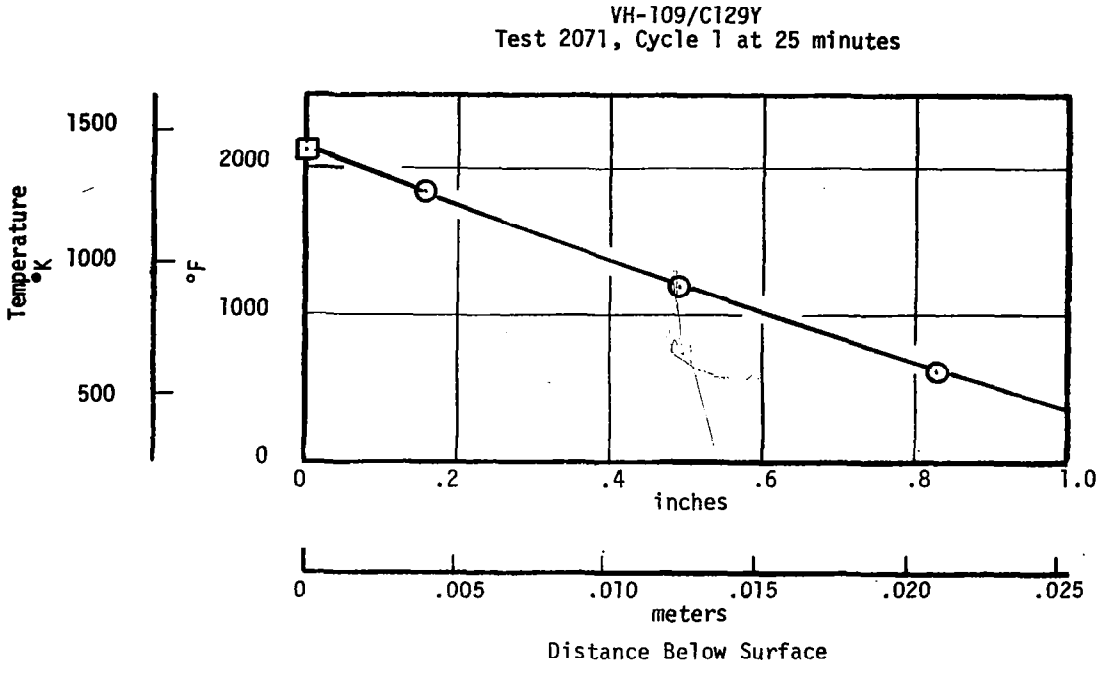

q_{net} = 1.83 x 10^5 W/m^2 (16.1 Btu/ft^2sec)

q_{loss} = 5.67 x 10^3 W/m^2 (0.5 Btu/ft^2sec)

Silfrax Backup, 481 kg/m^3 (30 lb/ft^3)

○ In-Depth Thermocouples

□ Measured Surface Temperature

Figure 24. Typical In-Depth Temperature Distributions in the Backup Insulator

surface temperature, however, which together with other pyrometer results presented in Appendix C implies that the reported surface temperatures for the stagnation point models only (Table 9) may be slightly lower than actual.

The surface catalycity results for the three materials studied are presented in Figure 25 together with the fit of the calibration test results and the theoretical minimum curve from Figure 22. These results are at conditions for which significant calibration and sample test results are available - 0.121-meter (4.75-inch) diameter model and simulation type 1-2. For the calibration results, the measured surface catalycity ratios are higher than the theoretical minimum limit. This implies either or both of the following:

- The surfaces of the calibration models were not fully catalytic and/or fully noncatalytic, and therefore the calibration results do not represent the true minimum catalycity ratio for the test conditions.
- Partial equilibration of the dissociated species occurred in the boundary layer.

An analysis of all results indicates that the latter effect is the principal contributor to the difference in measurement and theory. Therefore, agreement with the fit of the calibration results essentially represents the fully noncatalytic wall case, at least for the test conditions of this program.

From Figure 25, TD NiCr is partially noncatalytic at the low enthalpy levels for which data are available, falling about half way between the fully catalytic case (surface catalycity ratio of 1.0) and the fully noncatalytic case (fit of calibration results). In this same enthalpy range, the coated columbiums exhibit similar noncatalycity but become essentially fully noncatalytic at high enthalpy and pressures typical of flight. VH-109 appears to be somewhat more noncatalytic than R512E in the low and moderate enthalpy range. This same trend is also apparent at high enthalpy and low pressure (simulation type 1) from the results presented in Tables 9 and 10 for both the stagnation point and wedge models. Representative values of the surface catalycity ratios are 0.60 for R512E and 0.45 for VH-109 at these conditions.[1]

These catalycity results indicate that the absolute surface catalycity and the relative surface catalycity between different materials may be affected by the test conditions. The phenomena are sufficiently complex and the catalycity data and boundary layer characterization are sufficiently limited that no definitive guidelines for simulation test condition selection can be defined, however.

---

[1]A more detailed evaluation of these and other Aerotherm surface catalycity results is presented in Reference 9 in which preliminary catalytic efficiencies for both oxygen and nitrogen recombination are presented for coated columbium.

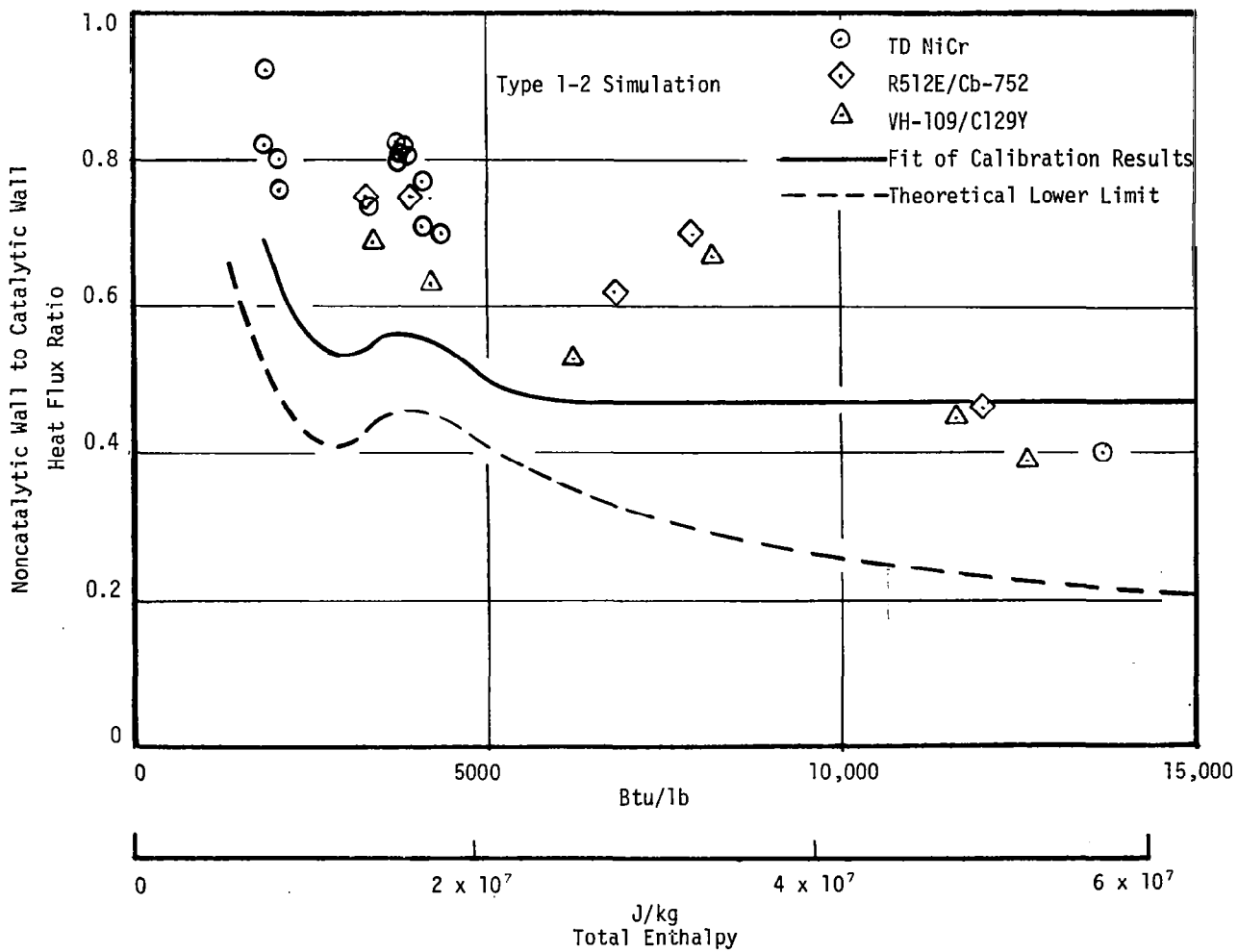

Figure 25. Surface Catalycity Results

The measured rate of change of mass for all materials studied is small (Tables 9 and 10). Because of the small mass change rates, the results exhibit some scatter; the primary trend is the consistently very small mass change rate for VH-109 independent of test conditions. These results for all materials considered indicate that the selection of simulation test conditions may be made independent of mass change considerations, and that the energy of thermochemical reaction at the surface, which may be correlated with mass change, is negligible. This observation does not imply, however, that the surface species or composition and/or the microscopic surface structure is independent of test conditions.

The response characteristics in terms of surface appearance and failure modes were evaluated qualitatively only; no detailed microsocpic or chemical analysis was performed. For TD NiCr at the nominal 1370°K (2000°F) surface temperature, the familiar light green oxide film was apparent in all cases. The thickness of the film and the size of the oxide particles (as determined from microscopic inspection) increased appreciably after 5 cycles as compared to one cycle. The one stagnation point sample that failed exhibited a severe pattern of surface cracks. The failure appeared to be due to catastrophic oxidation related possibly to the cracking, resultant exposure of a crack edge, and then severe heating and oxidation of the exposed edge. For R512E and VH-109, a wide variety of surface conditions was observed under microscopic examination. There was no obvious consistency between surface characteristics and test conditions for either material, however. Both materials exhibited a melt-like surface condition after 5 cycles of exposure. No failures occurred at test conditions for coated Cb materials.

5.4 OVERALL EVALUATION

The analytical and experimental results presented in Sections 5.2 and 5.3 defined the response of TD NiCr and coated Cb to flight and various test environments. These results also provided an assessment of simulation test requirements for valid TPS response results applicable to flight. These response characteristics and test requirements are summarized in the following subsections.

5.4.1 Response Characteristics

The surface thermochemical response of TD NiCr is characterized by subsurface kinetic oxidation of the base material for form an oxide film (Reference 1) and the diffusion controlled surface oxidation of this oxide film. A continuous buildup of this film (and the corresponding continuous depletion of the base material) occurs at a very slow rate for the conditions of interest. The surface thermochemical response of the coated columbium is characterized by the formation

of condensed surface oxides and the volatilization of these oxides. A continuous slow buildup of the condensed oxides occurs at surface temperatures of interest. For both material types, the energy and the mass changes associated with these thermochemical events is small for the surface temperature ranges of interest.

The oxide coating on TD NiCr and the two coated Cb coatings are partially noncatalytic. The relative ranking in order of decreasing surface catalycity is TD NiCr, R512E, and VH-109, although differences between material types are small. Absolute characterization of surface catalycity and its application to flight requires a more basic definition of test and flight boundary layer characteristics, test heat flux conditions, and surface emissivity.

The thermal or surface temperature response is defined by the net heat flux to the surface. This flux is controlled by the surface catalycity and surface emissivity. The energy associated with surface thermochemical reactions is negligible, as noted above, and for typical test and flight configurations the heat loss to be backup material is small. Definitive evaluation of surface emissivity was not part of the test program and therefore was not achieved. Based on the evaluation of test results, however, a total hemispherical emissivity of 0.75 is a reasonable approximation for all three material types.

Definitive failure modes have been identified for TD NiCr only. At high temperature, a crack pattern through the complete panel can occur. This cracking can expose edges of the material, which can result in catastrophic oxidation at the exposed edges.

5.4.2 Simulation Requirements

The macroscopic surface thermochemical response, in terms of mass and energy effects, is dependent on both pressure and surface temperature (or net heat flux). However, the magnitude of these mass and energy effects is sufficiently small that they may be ignored in selecting simulation test conditions. A set of simulation test conditions which closely duplicates heat flux at a pressure and enthalpy within, say, an order of magnitude of those flight is therefore acceptable on macroscopic thermochemical terms. The microscopic thermochemical response, in terms of surface species and surface condition, may vary significantly over this order of magnitude range of conditions, however.

The thermal response is dependent on the net flux to the surface which is a complicated function of surface catalycity, surface emissivity, and boundary layer equilibration. These variables are influenced by the test conditions in terms of enthalpy, pressure, boundary layer characteristics, and resultant surface species, surface condition, and also surface temperature. The definition of flight conditions and the equivalent test conditions must take these effects

into account. Since the functional relations are complex and not accurately characterized, the only test conditions which insure proper thermal response simulation are probably the specific flight conditions themselves.

SECTION 6

CONCLUSIONS

A detailed experimental evaluation, employing flowing air tests, and analytical evaluation, employing computer code techniques, was performed to define the response of TD nickel chromium alloy (20 percent chromium) and coated columbium (R512E on Cb-752 and VH-109 on WC129Y) to shuttle orbiter reentry heating. This evaluation allows the following conclusions to be made:

- The thermochemical response characterizations demonstrated:
  - A small rate of change of mass and a negligible energy contribution for both material types
  - A continuous slow buildup of the surface oxide film and the continuous slow depletion of the base material for TD NiCr
  - A continuous formation and slow buildup of condensed surface oxides and the continuous slow volatilization of these oxides; the surface oxides were Cb_2O_5* for R512E and HfO_2* for VH-109
- The oxide films and coatings are partially noncatalytic; differences in surface catalycity between the three materials are small with a relative ranking in order of decreasing catalycity of TD NiCr, R512E, and VH-109
- The thermal response in terms of surface temperature is controlled by the net heat flux to the surface; this net flux is influenced significantly by the surface catalycity and surface emissivity
- General guidelines for the selection of test conditions for ground test simulation of flight conditions include:
  - Thermochemical response need not be considered as a direct influence on thermal response because of its small or negligible contribution to mass change and energy; however, its affect on surface species and surface condition which in turn can affect surface catalycity and surface emissivity must be considered in selection of test conditions and interpretation of test results (see below)

- Duplication of surface catalytic response is probably not possible in that it probably requires duplication of flight conditions; however, the affect of surface catalycity must be considered in selection of test conditions and interpretation of test results (see below)
- A given fully catalytic wall heat flux results in a thermal response (surface temperature) which depends on surface catalycity and emissivity; or a given thermal response (surface temperature) is achieved at a fully catalytic wall heat flux which accounts for surface catalycity and surface emissivity.

REFERENCES

1. Goldstein, H. E., "An Analytical Model for Hypersonic Ablation of Thoria Dispersed Nickel Chromium Alloy," AIAA Paper 71-34, January 1971.

2. Grumman Aircraft, "Alternate Space Shuttle Concepts Study," Part II, Vol. II, Final Report (B-1) MSC-03810, July 6, 1971.

3. User's Manual, "Boundary Layer Integral Matrix Procedure, Version C (BLIMP)," Aerotherm Corp., UM-70-20, June 1970.

4. Hiester, N. K. and Clark, C. F., "Feasibility of Standard Evaluation Procedures for Ablating Materials," Standford Research Institute, Menlo Park, California, NASA CR-379, February 1966.

5. Boison, J. C., and Curtis, H. A., "On Experimental Investigation of Blunt Body Stagnation Point Velocity Gradients," ARS Journal, Vol. 29, No. 2, February 1959.

6. Kendall, R. M., "An Analysis of the Coupled Chemically Reacting Boundary Layer and Charring Ablator," Part V, "A General Approach to the Thermochemical Solution of Mixed Equilibrium - Non-Equilibrium, Homogeneous or Heterogeneous Systems," Aerotherm Corp., Report 66-7, NASA CR-1064, March 14, 1967.

7. User's Manual, "Aerotherm Chemical Equilibrium (ACE) Computer Program," Aerotherm Corp., May 1969.

8. User's Manual, "Aerotherm Charring Material Thermal Response and Ablation Program (CMA)," Aerotherm Corp., UM-70-14, April 1970.

9. Tong, H., Buckingham, A., Morse, H., "Non-Equilibrium Chemistry Boundary Layer Integral Matrix Procedure," Aerotherm Division, Acurex Corporation, Mountain View, Final Report No. 73-67, April 1973.

APPENDIX A

DEFINITION OF FLIGHT AND TEST BOUNDARY CONDITIONS

A more detailed description of the procedures employed to define the flight boundary conditions for the H-33 vehicle and to define the appropriate test boundary conditions are presented in this appendix.

A.1 FLIGHT CONDITIONS

The evaluation of flight boundary conditions and parameters was performed as outlined in Section 3.1 and as presented in greater detail in this section. In this analysis, the surface of the vehicle was assumed to be smooth and the boundary layer was assumed to be in chemical equilibrium, the latter assumption also corresponding to the fully catalytic wall case.

The stagnation enthalpy and pressure were approximated by the strong shock relations

$$p_s \simeq \frac{\rho_\infty V^2}{g} \tag{A-1}$$

$$h_s \simeq \frac{V^2}{2g} \tag{A-2}$$

for which the static pressure and enthalpy are small and are ignored. These results are included in Table 1.

Since surface pressure distributions are insensitive to chemistry effects, the pressure distributions can be predicted with sufficient accuracy without solving the inviscid flow field. For blunt bodies, modified Newtonian flow approximations suffice, and for downstream regions, tangent wedge or tangent cone approximations provide valid results. Thus for the vehicle symmetry plane, the pressure distribution was approximated by a blending of Newtonian (nose region) and tangent cone (downstream region) pressures and the wing pressure distribution was approximated by a blending of Newtonian and tangent wedge pressures. For the wing, the leading edge pressure was determined by accounting for both the leading edge sweep and angle of attack as described in Reference A-1. For other regions of the fuselage, the pressure was assumed to be Newtonian as determined by the true local surface incidence. For the flight conditions which were

considered, the pressure ratio p/p_s is insensitive to Mach number so that a single distribution was sufficient for all cases. The resultant pressure distributions are shown in Figure 9 for the fuselage symmetry plane and the wing 40 percent semi-span plane.

Boundary layer aerothermodynamic parameters were predicted with the Aerotherm BLIMP computer code (Section 3.1). Since both laminar and turbulent flows were permitted in the analytical procedure, some criteria for transition were required. Substantial effort is presently being expended by various investigators on the effects of various parameters on promoting transition to turbulent flow. These investigations have not been universally conclusive and in fact are indicative of the extremely complex nature of turbulent flows. Thus empirically determined transition cirteria and sound judgement appear at present to be the only practical approach. Therefore on the centerline, transition to turbulent flow was assumed to start at $Re_{\theta_{tr}}/M_e \simeq 170$ and to be essentially fully developed at 2 $Re_{s_{tr}}$ where Re_θ is based on edge conditions but Re_s is based on free stream conditions (References A-2 and A-3). The BLIMP code was then used to calculate fully turbulent heating beginning at $Re_{\theta_{tr}}/M_e = 170$ and the transition zone heating was approximated as

$$q = q_{turb} - (q_{turb} - q_{lam}) \exp\left[-5\left(\frac{s}{s_{tr}} - 1\right)\right] \qquad \text{(A-3)}$$

where the surface coordinate ratio s/s_{tr} is equal to $Re_s/Re_{s_{tr}}$. Transition to turbulent flow was not considered on the wing.

Although the BLIMP code has an entropy layer option, this effect was ignored because the shape of the shock wave surrounding the body is not generally known; instead, the boundary layer edge conditions were determined from an isentropic expansion from the stagnation point or leading edge. Inclusion of an entropy layer would cause an increase in downstream entropy and a corresponding increase in predicted heat transfer rates. Conversely, the predicted Mach number would be higher so that, if $Re_{\theta_{tr}}/M_e$ is a valid transition criteria, transition would be delayed thereby reducing the local heat transfer rate.

The BLIMP code was also used to predict heat transfer rates on the wing by noting that experimental oil flow data indicate that crossflow effects are small except very near the leading edge. Because of the combination of sweep and angle-of-attack, the leading edge stagnation line is not located at a position corresponding to the angle-of-attack of the vehicle. This aerodynamic leading edge was located by assuming that it is a generator of a cylinder inclined at an effective angle-of-attack given by (Figure A-1)

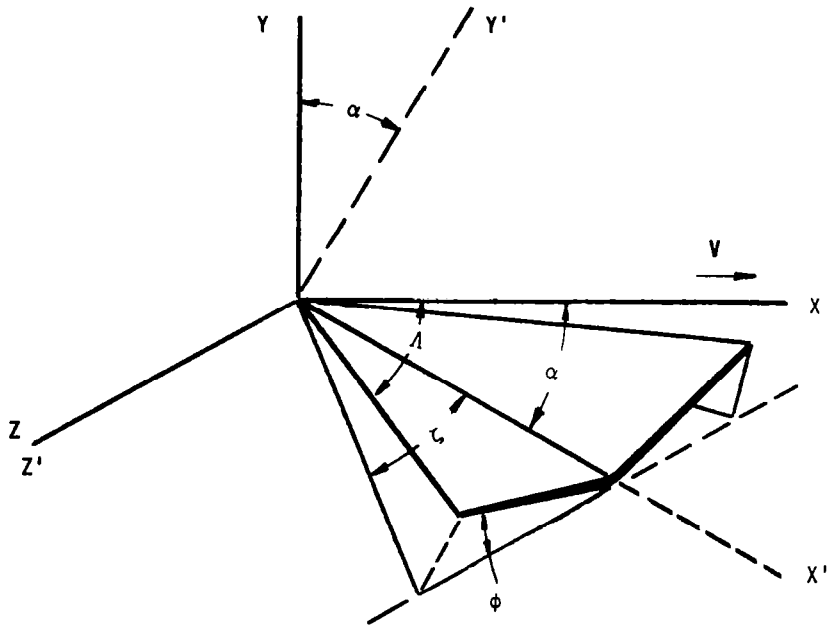

Figure A-1. Delta Wing Flow Field Analysis Parameters

$$\cos \Lambda = \cos \alpha \cos \zeta$$

where

α = vehicle angle-of-attack
ζ = semi-apex angle of wing
Λ = effective sweep angle of leading edge

Then, using the method of steepest descent (Reference A-4), the leading edge is the position which yields an angle corresponding to Λ. For the H-33 vehicle at an angle-of-attack of 29 degrees, the aerodynamic leading edge is located about 59 degrees from the geometric leading edge.

Laminar heat transfer rates to other regions of the windward surface of the forward fuselage were approximated from the known centerline value using swept cylinder theory (Reference A-5). For limited variations in wall temperature this solution can be written as

$$\frac{C_H}{C_{H_{s'}}} \simeq \left[\frac{\left(\frac{p_w}{p_s}\right)\left(\frac{p_w}{p_{w,s'}}\right) u_e^2}{2\int_0^s \left(\frac{p_w}{p_s}\right) u_e \, ds} \right]^{1/2} \frac{1}{\left(\frac{du_e}{ds}\right)_{s'}^{1/2}} \frac{\theta'_w}{\theta'_{w,s'}} \tag{A-4}$$

where C_H is the heat transfer coefficient and the subscripts w, s', and s are for wall, cylinder "stagnation" line, and stagnation point values, respectively. Reference A-5 shows that the ratio $\theta'_w/\theta'_{w,s'}$ does not deviate much from unity. Then defining an equivalent velocity gradient as

$$\left(\frac{du_e}{ds}\right)_{eq} = \frac{\left(\frac{p_w}{p_s}\right) u_e^2}{2\int_0^s \left(\frac{p_w}{p_s}\right) u_e \, ds} \tag{A-5}$$

Equation (A-4) can be written as

$$\frac{C_H}{C_{H_{s'}}} \simeq \left[\frac{\left(\frac{du_e}{ds}\right)_{eq}}{\left(\frac{du_e}{ds}\right)_{s'}} \frac{p}{p_{s'}} \right]^{1/2} \tag{A-6}$$

Results for the fuselage centerline and 40 percent semi-span of the wing are presented in Figures 10 and 11, respectively. Predicted isotherms, for flight condition 2 of Table 1 (approximately maximum heating), on the forward portion of the fuselage are shown in Figure A-2.

A.2 TEST CONDITIONS

Test boundary conditions and parameters were evaluated for the four simulation types and the flat face stagnation point and wedge model configurations defined in Sections 3.1, 4.2, and 5.1. The same basic analysis procedures presented above for flight were employed in the definition of the conditions on the test models. The pressure distribution for the flat face stagnation point models was defined from the blunt body correlation of Reference A-6. The pressure distribution for the wedge was approximated by a blending of Newtonian (nose region) and tangent wedge (downstream) pressures. These distributions were defined for the approximate test stream Mach number of 4.5. The boundary layer analysis was performed using the BLIMP code. Its application was straightforward since the flow is laminar for both model configurations and for all simulation test conditions considered, and the flow is either axisymmetric or one-dimensional.

Typical distributions of properties on the test models are presented in Figures 12 and 13 for the stagnation point and wedge models, respectively. The complete set of results at the reference locations on the test models (Section 5.1.2) are presented in Tables 4 and 5.

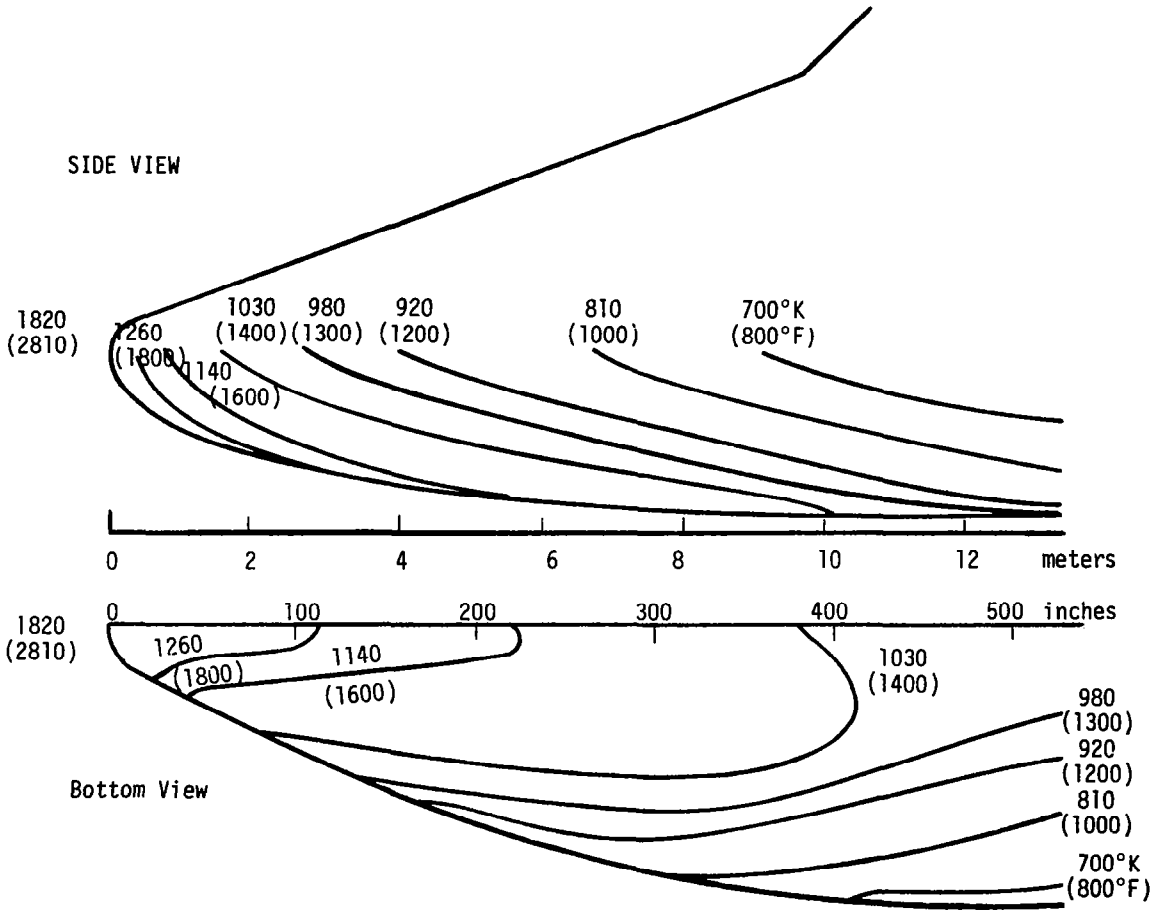

Figure A-2. Temperature Distributions on Fuselage Nose Region at Peak Heating

REFERENCES

APPENDIX A

A-1. Bartlett, E. P., Morse, H. L., and Tong, H., "Investigation of Thermal Protection Systems Effects on Viscid and Inviscid Flow Fields for Manned Entry System," Aerotherm Corporation, Final Report No. 71-38, September 1971.

A-2. Masek, R. V., "Boundary Layer Transition on Lifting Entry Vehicle Configurations at High Angle-Of-Attack," NASA TM X-52876, Volume I, Pages 445-462, July 1972.

A-3. Pearce, B. E., "A Comparison of Simple Turbulent Heating Estimates and Boundary Layer Transition Criteria With Application to Large, Lifting Vehicles," NASA TM X-52876, Volume I, pages 485-507, July 1970.

A-4. DeJarnette, F. R., "Calculation of Inviscid Surface Streamlines and Heat Transfer on Shuttle Type Configurations," NASA CR-111921, August 1971.

A-5. Beckwith, I. E., and Cohen, N. B., "Application of Similar Solutions to Calculation of Laminar Heat Transfer on Bodies with Yaw and Large Pressure Gradient in High-Spped Flow," NASA TND-625, January 1961.

A-6. Moyer, C. B., Anderson L. W., and Dahm, T. J., "A Coupled Computer Code for the Transient Thermal Response and Ablation of Non-Charring Heat Shields and Nosetips," NASA CR-1630, October 1970.

APPENDIX B

ANALYTICAL EVALUATION OF MATERIAL RESPONSE

The thermochemical and transport properties required to carry out the analytical procedure used in this study are briefly summarized in Section 3.3 and are presented in detail in this appendix.

B.1 THERMOCHEMICAL DATA

In order to perform a surface energy balance which includes the energy of surface thermochemical reactions, the free energy and enthalpy of significant molecular species must be known. These quantities are supplied to Aerotherm computer codes by three card sets either directly or through the card output of other Aerotherm codes which use the card sets as input. The sets provide a reference enthalpy, a reference entropy, and specific heat parameters for individual species which allow calculation of the species enthalpy and free energy over a range of temperatures. The three card sets may be constructed directly from data for species for which specific heat parameters are given by an equation of the form

$$c_p = C_1 + C_2 T + \frac{C_3}{T^2} \qquad \text{(B-1)}$$

where C_1, C_2, and C_3 are constants and T is the absolute temperature. In the typical case, the data are not available in this form and the Aerotherm Thermochemical Data code (TC DATA) is used to curve-fit the thermochemical data from whatever form it is available. The minimum data requirements of TC DATA are:

- The heat of formation at 298°K
- Either of the following:
  - A tabulation of free energies
  - A tabulation of entropies
  - A tabulation of enthalpies and an entropy at some temperature
  - An entropy and a tabulation of specific heats

The chemical systems appropriate to the materials of interest and therefore for which data were necessary are:

- TD NiCr
  - Nickel
  - Chromium
  - Thorium
  - Oxygen
  - Nitrogen
- Coated Cb

-VH-109	-R512E	-Other Additional Possibilities
Silicon	Silicon	Tungsten
Hafnium	Columbium	Zirconium
Iron	Iron	
Chromium	Chromium	
Tantalum	Oxygen	
Molybdenum	Nitrogen	
Oxygen		
Nitrogen		

Three card sets for many of the species which may form in the above chemical systems were already on hand at Aerotherm as a result of curvefits of JANNAF data (Reference B-1) made previously. These species consist of the species in Table B-1 which list JANNAF or JANNAF TAPE as sources.

Tantalum, thorium, and molybdenum were omitted from the search for new data as they only existed in trace amounts in any of the chemical systems of interest. The search for the remaining data provided much of that necessary for species not already available. The data sources are indicated in Table B-1 on the title card of each three card set. The source titles listed refer to References B-1 through B-6.

No data or an insufficient amount of data were available for some of the species which were considered to be of importance. These species do not list a source on their title cards in Table B-1, but rather indicate that some part or all of their data were estimated. Table B-2 lists these species for which insufficient data were found and the assumptions that were made in creating the card set for the particular species. In most instances, missing data were substituted with data of a similar species.

TABLE B-1

THERMOCHEMICAL DATA

a) Key

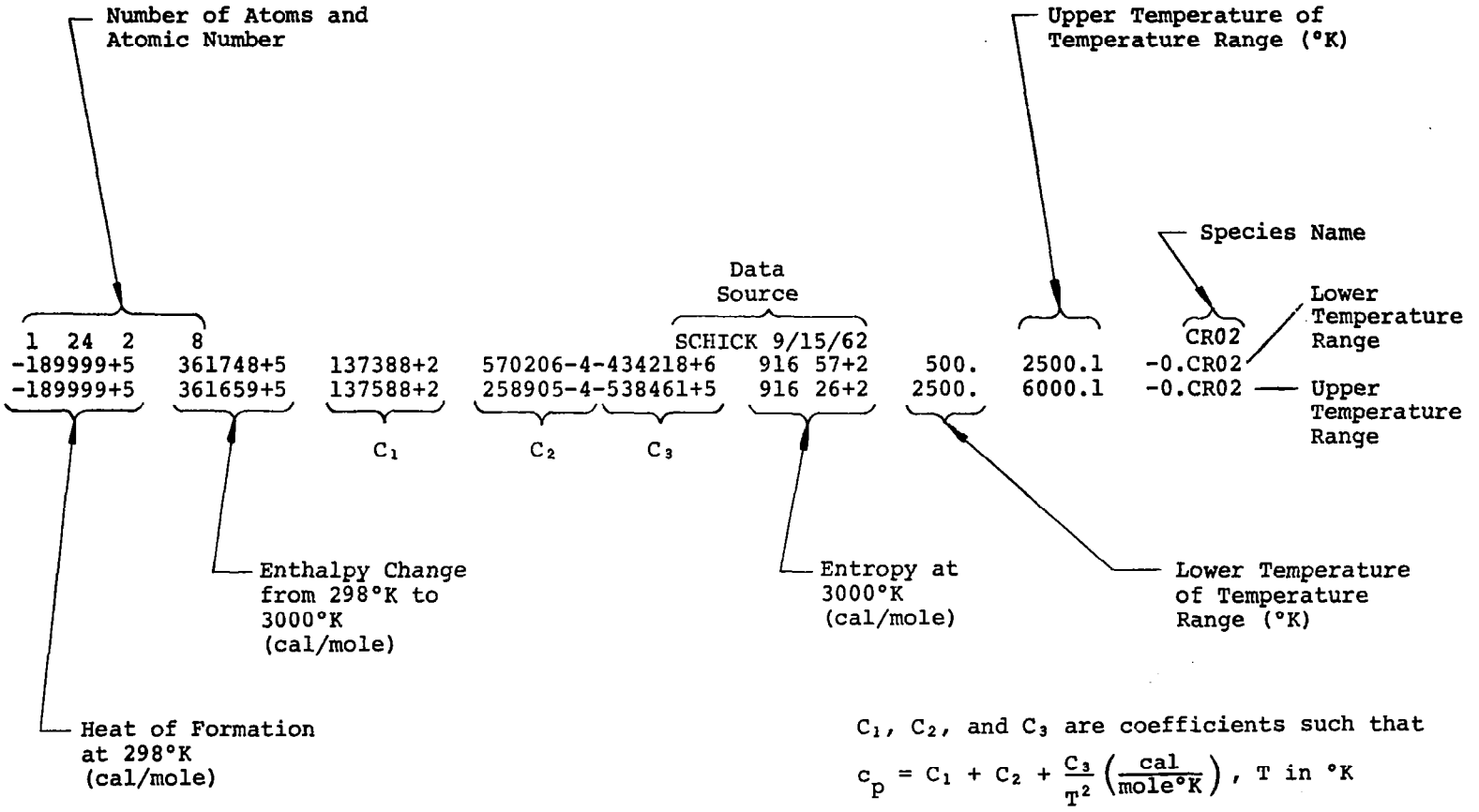

C_1, C_2, and C_3 are coefficients such that

$$c_p = C_1 + C_2 + \frac{C_3}{T^2}\left(\frac{cal}{mole°K}\right), \quad T \text{ in } °K$$

TABLE B-1 (CONTINUED)

b) Data Tabulation

```
  2  8                                        JANAF TAPE 7/71 **/61          02
 574   0+0 234441+5 807265+1 503 78-3-23883 7+6 679715+2  500. 2500.1  -0.02
 574   0+0 234554+5 977777+1 110622-3-47636 7+7 679755+2 2500. 6000.1  -0.02
  2  7                                        JANAF TAPE 7/71 **/61          N2
-110   0+0 222368+5 760394+1 501467-3-23470 8+6 637903+2  500. 2500.1  -0.N2
-110   0+0 221842+5 858948+1 972320-4-78141 1+5 637717+2 2500. 6000.1  -0.N2
  1 26                                        JANAF TAPE 7/71  3/65          FE
 994999+5 152484+5 438984+1 563370-3 359 57+6 562498+2  500. 2500.1  -0.FE
 994999+5 152678+5 272544+1 103743-2 335434+7 562566+2 2500. 6000.1  -0.FE
  1  8  1 14                                 JANAF TAPE 7/71  9/67          OSI
-239999+5 233921+5 862512+1 174322-3-25727 5+6 697544+2  500. 2500.1  -0.OSI
-239999+5 233575+5 768721+1 305160-3 356 33+7 697421+2 2500. 6000.1  -0.OSI
  1 24  3  8                                  SCHICK 9/15/62                CR03
-683999+5 512148+5 194820+2 145166-3-74616 9+6 106225+3  500. 2500.1  -0.CR03
-683999+5 511960+5 197831+2 133129-4-568 72+6 106218+3 2500. 6000.1  -0.CR03
  1 72  2  8                                  SCHICK 9/15/63                HF02
-699999+5 389 47+5 147 96+2 725131-4-41710 2+6 925809+2  500. 2500.1  -0.HF02
-699999+5 388952+5 148597+2 667535-5-32671 3+6 925776+2 2500. 6000.1  -0.HF02
  1 24                                        SCHICK 5/62                   CR
 948199+5 153759+5 308734+1 139753-2 355238+6 539353+2  500. 2500.1  -0.CR
 948199+5 153382+5 175426+1 161778-2 524558+7 539219+2 2500. 6000.1  -0.CR
  1 24  1  8                                  SCHICK 9/15/62                CRO
 499999+5 242750+5 879494+1 171355-3-90883 3+5 770329+2  500. 2500.1  -0.CRO
 499999+5 242687+5 699636+1 602200-3 441827+7 770306+2 2500. 6000.1  -0.CRO
  1 24  2  8                                  SCHICK 9/15/62                CR02
-189999+5 361748+5 137388+2 570206-4-43421 8+6 916 57+2  500. 2500.1  -0.CR02
-189999+5 361659+5 137558+2 258905-4-53846 1+5 916 26+2 2500. 6000.1  -0.CR02
  1 26  1  8                                  JANAF TAPE 7/71  9/66          FEO
 599999+5 240603+5 864969+1 248120-3-14496 1+6 776915+2  500. 2500.1  -0.FEO
 599999+5 241 88+5 938671+1 209395-3-41462 5+7 777 87+2 2500. 6000.1  -0.FEO
  1 72                                        SCHICK 3/15/63                HF
 144923+6 183 99+5 616 15+1 583345-3-40845 7+6 589 78+2  500. 2500.1  -0.HF
 144923+6 182102+5 293328+1 109109-2 118258+8 588724+2 2500. 6000.1  -0.HF
  1 72  1  8                                  SCHICK 6/15/63                HFO
 189959+5 261617+5 104998+2-162980-3-58617 7+6 790385+2  500. 2500.1  -0.HFO
 189959+5 261 60+5 937518+1-489364-4 466132+7 790187+2 2500. 6000.1  -0.HFO
  1  7                                        JANAF TAPE 7/71  3/61           N
 112964+6 134412+5 492461+1 271364-4 956 39+4 480916+2  500. 2500.1  -0.N
 112964+6 134277+5 277722+1 523356-3 567729+7 480868+2 2500. 6000.1  -0.N
  1  7  1  8                                  JANAF TAPE 7/71  6/63           NO
 215799+5 22750 8+5 808175+1 354495-3-27633 6+6 688669+2  500. 2500.1  -0.NO
 215799+5 227145+5 877301+1 726516-4-19288 9+6 688541+2 2500. 6000.1  -0.NO
  1  7  2  8                                  JANAF TAPE 7/71  9/64           NO2
 790999+4 345478+5 128604+2 382 47-3-731 84+6 848188+2  500. 2500.1  -0.NO2
 790999+4 345  4+5 136887+2 329899-4-45391 0+6 848 21+2 2500. 6000.1  -0.NO2
  1  7  3  8                                  JANAF TAPE 7/71 12/64          NO3
 169999+5 498701+5 191696+2 260574-3-11252 5+7 999138+2  500. 2500.1  -0.NO3
 169999+5 498363+5 197111+2 240799-4-81434 0+6 999 18+2 2500. 6000.1  -0.NO3
  1  7  1 14                                 JANAF TAPE 7/71  3/67          NSI
 889999+5 253504+5 764406+1 110914-2-84865 7+5 719821+2  500. 2500.1  -0.NSI
 889999+5 252531+5 118109+2-224515-3-52892 9+7 719478+2 2500. 6000.1  -0.NSI
  1  7  1 40                                 JANAF TAPE 7/71  6/63          NZR
 170499+6 239229+5 886527+1 101730-3-173 80+6 756709+2  500. 2500.1  -0.NZR
 170499+6 239191+5 892486+1 754690-4-13517 0+6 756696+2 2500. 6000.1  -0.NZR
  2  7  1  8                                  JANAF TAPE 7/71 12/64          N2O
 196 99+5 366422+5 133569+2 547758-3-72635 8+6 816233+2  500. 2500.1  -0.N2O
 196 99+5 365783+5 146 28+2 446710-4-65269 2+6 816  7+2 2500. 6000.1  -0.N2O
  2  7  3  8                                  JANAF TAPE 7/71 12/64          N203
 197999+5 618923+5 230372+2 652593-3-12395 1+7 123258+3  500. 2500.1  -0.N203
 197999+5 618123+5 244627+2 562183-4-82999 8+6 123229+3 2500. 6000.1  -0.N203
  2  7  4  8                                  JANAF TAPE 7/71  9/64          N204
 216999+4 787378+5 295602+2 812393-3-17887 6+7 134959+3  500. 2500.1  -0.N204
 216999+4 786374+5 313221+2 705107-4-12088 5+7 134924+3 2500. 6000.1  -0.N204
  2  7  5  8                                  JANAF TAPE 7/71 12/64          N205
```

TABLE B-1 (CONTINUED)

b) (Continued)

```
269999+4 916178+5 352907+2 191 87-3-165360+7 156735+3        2500.1  -0.N2O5
269999+4 915902+5 356432+2 200514-4-118397+7 156725+3 2500. 6000.1  -0.N2O5
 3  7                                  JANAF TAPE 7/71 12/70          N3
989999+5 372936+5 138634+2 376483-3-701306+6 839596+2  500. 2500.1  -0.N3
989999+5 372469+5 146566+2 383 53-4-374915+6 839432+2 2500. 6000.1  -0.N3
 1 41                                  SCHICK                         NB
171835+6 168225+5 548 70+1 249253-3 366715+6 573348+2  500. 2500.1  -0.NB
171835+6 169848+5 645667+1 492200-3-952917+7 573923+2 2500. 6000.1  -0.NB
 1 41  1  8                            SCHICK                         NBO
460169+5 236920+5 872486+1 150294-3-19575 3+6 766880+2  500. 2500.1  -0.NBO
460169+5 236795+5 547152+1 926148-3 801485+7 766835+2 2500. 6000.1  -0.NBO
 1 41  2  8                            SCHICK                         NBO2
-510509+5 406453+5 168 81+2-551854-3-853693+6 943866+2  500. 2500.1  -0.NBO2
-510509+5 406762+5 150598+2-220778-4 179555+7 943975+2 2500. 6000.1  -0.NBO2
 7 28                                  THERMO PROP OF ELMT 1956       NI
101259+5 151356+5 654868+1-500354-3-11785 2+6 567152+2  500. 1700.1  -0.NI
101259+5 153 19+5 550582+1-821911-4 841565+6 567792+2 1700. 3000.1  -0.NI
 1 28  1  7                             FAKED FROM FEO                 NIO
599999+5 240603+5 864969+1 248120-3-144961+6 776915+2  500. 2500.1  -0.NIO
599999+5 241 88+5 938671+1 209395-3-41462 5+7 777 87+2 2500. 6000.1  -0.NIO
 1  8                                  JANAF TAPE 7/71  6/62           O
595589+5 135166+5 496176+1 567346-5 298680+5 500932+2  500. 2500.1  -0.O
595589+5 135210+5 450112+1 133922-3 904980+6 500947+2 2500. 6000.1  -0.O
 1  8  1 74                            JANAF TAPE 7/71  9/66          OW
101599+6 235598+5 873351+1 127136-3-22020+6 781854+2  500. 2500.1  -0.OW
101599+6 235554+5 677 47+1 604741-3 458616+7 781838+2 2500. 6000.1  -0.OW
 1  8  1 40                            JANAF TAPE 7/71 12/65          OZR
139999+5 303 66+5 108827+2 712133-3-101867+7 775393+2  500. 2500.1  -0.OZR
139999+5 299529+5 664731+1 709938-3 254871+8 774139+2 2500. 6000.1  -0.OZR
 2  8  1 14                            JANAF TAPE 7/71  9/67          O2SI
-729999+5 380881+5 143437+2 205481-3-589 33+6 856255+2  500. 2500.1  -0.O2SI
-729999+5 380621+5 147816+2 181596-4-399  4+6 856163+2 2500. 6000.1  -0.O2SI
 2  8  1 74                            JANAF TAPE 7/71  9/66          O2W
182999+5 361197+5 136260+2 114650-3-434 81+6 978690+2  500. 2500.1  -0.O2W
182999+5 360882+5 124732+2 308316-3 374451+7 978578+2 2500. 6000.1  -0.O2W
 2  8  1 40                            JANAF TAPE 7/71 12/65          O2ZR
-683999+5 364113+5 137473+2 608857-4-360 63+6 955360+2  500. 2500.1  -0.O2ZR
-683999+5 364 34+5 138729+2 565448-5-28232 4+6 955332+2 2500. 6000.1  -0.O2ZR
 3  8                                  JANAF TAPE 7/71  6/61           O3
340999+5 360506+5 134949+2 279823-3-60869 4+6 861 14+2  500. 2500.1  -0.O3
340999+5 360308+5 138156+2 140117-3-430343+6 860944+2 2500. 6000.1  -0.O3
 3  8  1 74                            JANAF TAPE 7/71  9/66          O3W
-699999+5 515189+5 195275+2 127749-3-651883+6 110670+3  500. 2500.1  -0.O3W
-699999+5 515 23+5 197920+2 118794-4-494356+6 110664+3 2500. 6000.1  -0.O3W
 6  8  2 74                            JANAF TAPE 7/71  9/66          O6W2
-278199+6 115928+6 436120+2 396799-4-711424+6 196323+3  500. 2500.1  -0.O6W2
-278199+6 115922+6 436910+2 397773-5-647243+6 196321+3 2500. 6000.1  -0.O6W2
 8  8  3 74                            JANAF TAPE 7/71  9/66          O8W3
-408699+6 162 88+6 611916+2 153279-3-137416+7 252703+3  500. 2500.1  -0.O8W3
-408699+6 162 68+6 615 58+2 143643-4-116736+7 252696+3 2500. 6000.1  -0.O8W3
 9  8  3 74                            JANAF TAPE 7/71  9/66          O9W3
-483599+6 177602+6 671350+2 160 79-3-156891+7 267960+3  500. 2500.1  -0.O9W3
-483599+6 177580+6 674625+2 151193-4-135 57+7 267953+3 2500. 6000.1  -0.O9W3
 12  8  4 74                            JANAF TAPE 7/71  9/66          O12W4
-670199+6 240877+6 908630+2 204188-3-193 68+7 345 55+3  500. 2500.1  -0.O12W4
-670199+6 240850+6 912812+2 191577-4-165358+7 345 45+3 2500. 6000.1  -0.O12W4
 1 14                                  JANAF TAPE 7/71  3/67           SI
107699+6 140282+5 463210+1 287580-3 862 99+5 519934+2  500. 2500.1  -0.SI
107699+6 140175+5 581149+1-392 86-4-217894+7 519896+2 2500. 6000.1  -0.SI
 2 14                                  JANAF TAPE 7/71  3/67           SI2
140999+6 271482+5 114 82+2-502556-3-538181+6 774695+2  500. 2500.1  -0.SI2
140999+6 272 72+5 955600+1 137663-3 103517+7 774903+2 2500. 6000.1  -0.SI2
 1  7  2 14                            JANAF 3-31-67                  SI2N
949999+5 390809+5 147854+2 355660-4-370129+6 936880+2   500  30001   -0SI2N
949999+5 390809+5 141298+2 157464-3 223916+7 936880+2  3000  60001   -0SI2N
 3 14                                  JANAF TAPE 7/71  3/67           SI3
```

TABLE B-1 (CONTINUED)

b) (Continued)

```
 151999+6 40084?+5 144776+2 293721-3-10376+6 975739+2  500. 2500.1  -0.SI3
 151999+6 401797+5 161149+2 169399-3-839446+7 976 75+2 2500. 6000.1  -0.SI3
  1 74                                    JANAF TAPE 7/71  6/66          W
 203399+6 212393+5 136361+2-256943-2-158632+7 592576+2  500. 2500.1  -0.W
 203399+6 215927+5 339889+1 105  2-2 584251+7 593825+2 2500. 6000.1  -0.W
  1 40                                    JANAF TAPE 7/71 12/67          ZR
 148299+6 184629+5 493 21+1 974 70-3 307 82+6 585944+2  500. 2500.1  -0.ZR
 148299+6 184525+5 674723+1 488787-3-346672+7 585908+2 2500. 6000.1  -0.ZR
  1 72  2  8                              SCHICK  6/15/63                HFO2  *
-266 59+6 613  2+5 261655+2-434219-4-33689?+6 608415+2 2000. 3173.2  -0.HFO2  *
-266 59+6 862999+5 259997+2 335276-7 102399+4 687204+2 3173. 4900.3  -0.HFO2  *
  1 72  1  7                              SCHICK 12/31/63                HFN   *
-882399+5 389849+5 109244+2 223 84-2-154483+6 410738+2  500. 3583.2  -0.HFN   *
-882399+5 552980+5 160  4+2-717118-7-268799+4 456568+2 3583. 4900.3  -0.HFN   *
  1 72  2 14                              FAKED FROM MOSI2               HFSI2 *
-31400 +5 551759+5 177703+2 185134-2-350906+6 559863+2  300. 1200.2  -0.HFSI2 *
-31400 +5 551759+5 177703+2 185134-2-350906+6 559863+2 1200. 1300.2  -0.HFSI2 *
  2 72  1 14                              FAKED FROM NI2SI               HF2SI *
-50000 +5 57351 +5 158   +2 329   -2 0     +0 574   +2  298. 1000.2  -0.HF2SI *
-50000 +5 57351 +5 158   +2 329   -2 0     +0 574   +2 1000. 1500.2  -0.HF2SI *
  1 24                                    SCHICK 9/15/62                 CR    *
 171  0+0 286119+5 417174+1 361379-2 263972+5 259538+2  500. 2148.2  -0.CR    *
 171  0+0 300649+5 939612+1 101327-5 819199+4 269140+2 2148. 2900.3  -0.CR    *
  1 24  2  8                              SCHICK                         CRO2  *
-139999+6 634416+5 141 33+2 583454-2-21821?+6 570117+2  300.  800.2  -0.CRO2  *
-139999+6 634416+5 141 33+2 583454-2-21821+6 570117+2  800. 1500.2  -0.CRO2  *
  1 24  3  8                              SCHICK                         CRO3  *
-141399+6 833 18+5 180836+2 787144-2-208355+6 801161+2  300.  470.2  -0.CRO3  *
-141399+6 820999+5 290  0+2-558793-8-812499-0 922963+2  470.  900.3  -0.CRO3  *
  1 24  1  7                              B-605                          CRN   *
-294999+5-246993+4 302367+2-173521-1-267145+7 204122+2  400.  800.2  -0.CRN   *
-294999+5-246993+4 302367+2-173521-1-267145+7 204122+2  800. 1700.2  -0.CRN   *
  1 24  2 14                              FAKED FROM MOSI2               CRSI2 *
-30000 +5 551759+5 177703+2 185134-2-350906+6 559863+2  300. 1200.2  -0.CRSI2 *
-30000 +5 55175?+5 177703+2 185134-2-350906+6 559863+2 1200. 1300.2  -0.CRSI2 *
  2 24  3  8                              BULLETIN 605                   CR2O3 *
-272649+6 829857+5 302824+2 661415-3-693337+6 884833+2  500. 1000.2  -0.CR2O3 *
-272649+6 813832+5 391547+2-336825-2-553594+7 880189+2 1000. 1800.2  -0.CR2O3 *
  1 26                                    JANAF TAPE 7/71  3/65          FE    *
   0  0+0 22559?+5 144787+2-290589-2-164500+7 257 95+2  500. 1809.2  -0.FE    *
 313799+4 272949+5 977982+1 400 36-3 511999+3 294422+2 1809. 4500.3  -0.FE    *
  1 26  2 24  4  8                        EVANS                          FECR2O4*
-3419  +6 128832+6 3896  +2 534   -2-762   +6 1351  +3  298. 1000.2  -0.FECR2O4*
-3419  +6 128832+6 3896  +2 534   -2-762   +6 1351  +3 1000. 1800.2  -0.FECR2O4*
  1 26  1  8                              JANAF TAPE 7/71  6/65          FEO   *
-650199+5 413639+5 126376+2 173747-2-196860+6 474991+2  500. 1647.2  -0.FEO   *
-596419+5 412760+5 163  3+2-833533-7-102399+4 508571+2 1647. 5000.3  -0.FEO   *
  1 26  1 14                              EVANS                          FESI  *
-19200 +5 48125 +5 1072  +2 43    -2 0     +0 484   +2  298.  500.2  -0.FESI  *
-19200 +5 48125 +5 1072  +2 43    -2 0     +0 484   +2  500.  900.2  -0.FESI  *
  2 26  1  7                              B-605 1963                     FE2N  *
-899999+3 748385+5 111887+2 972196-2 499632+6 785581+2  500. 1000.2  -0.FE2N  *
-899999+3 748385+5 111887+2 972196-2 499632+6 785581+2 1000. 1800.2  -0.FE2N  *
  2 26  3  8                              JANAF TAPE 7/71  6/65          FE2O3 *
-197299+6 816270+5 493 30+2-958484-2-325 95+7 935541+2  500. 1500.2  -0.FE2O3 *
-197299+6 936480+5 440235+2-248233-2-153431+8 985331+2 1500. 2500.2  -0.FE2O3 *
  2 26  1 14  4  8                        EVANS                          FE2SIO4*
-346000+6 138329+6 3651  +2 936   -2-670000+6 14057 +3  298. 1000.2  -0.FE2SIO4*
-346000+6 13832?+6 3651  +2 936   -2-670000+6 14057 +3 1000. 1490.2  -0.FE2SIO4*
  3 26  4  8                              JANAF TAPE 7/1  6/65           FE3O4 *
-267899+6 12247?+6 624486+2-883379-2-233506+7 14193+3  500. 1700.2  -0.FE3O4 *
-267899+6 131131+6 594339+2-309 70-2-218383+8 145397+3 1700. 3000.2  -0.FE3O4 *
  4 26  1  7                              B-605 1965                     FE4N  *
-254999+4 122 18+6 195521+2 148998-1 111745+7 127 76+3  500. 1000.2  -0.FE4N  *
-254999+4 122 18+6 195521+2 148998-1 111745+7 127 76+3 1000. 1800.2  -0.FE4N  *
  1 72                                    SCHICK 3/15/63                 HF    *
```

TABLE B-1 (CONTINUED)

b) (Continued)

```
-882  0+0 262547+5 631906+1 169410-2-15594 9+4 305814+2  500. 2495.2  -0.HF
-882  0+0 299729+5 800  8+1-149 11-7-31999 9+3 321359+2 2495. 4900.3  -0.HF      \
  1 72  1 14                                  FAKED FROM FESI              HFSI  *
-19200 +5 48125 +5 1072  +2 43    -2 0      +0 484   +2  298.  500.2  -0.HFSI  *
-19200 +5 48125 +5 1072  +2 43    -2 0      +0 484   +2  500.  900.2  -0.HFSI  *
  1  7  1 40                                  JANAF TAPE 7/71  6/61        NZR  *
-872999+5 369549+5 111190+2 167249-2-18053 5+6 384931+2  500. 3222.2  -0.NZR   *
-694889+5 357659+5 139998+2 158324-7 70399 9+3 436571+2 3222. 6000.3  -0.NZR   *
  4  7  3 14                                  JANAF TAPE 7/71  3/67       N4SI3  *
-177999+6 114639+6 327276+2 703 25-2-199 44+7 112842+3  500. 1700.2  -0.N4SI3 *
-17799 9+6 109 39+6 434915+2 560279-3-13110 5+7 110624+3 1700. 3000.2  -0.N4SI3 *
  1 41                                      SCHICK                       NB   *
-604  0+0 195696+5 565999+1 960  0-3  99999+1 246616+2  500. 2741.2  -0.NB    *
-604  0+0 258619+5 799991+1 149 11-7 38399 9+3 269592+2 2741. 5000.3  -0.NB    *
  1 41 11  7                                  SCHICK                       NBN  *
-564999+5 327680+5 124630+3-366 46-1-14131 7+9 387493+2 1700. 2323.2  -0.NBN   *
-564999+5 492319+5 150  0+2-372529-8-95999 9+2 454705+2 2323. 6000.3  -0.NBN   *
  1 41  1  8                                  SCHICK                       NBO  *
-976999+5 373604+5 100402+2 234984-2-78356 4+5 410931+2  500. 2218.2  -0.NBO   *
-976999+5 394539+5 150  0+2-139698-8-31999 9+2 421 96+2 2218. 6000.3  -0.NBO   *
  1 41  2  8                                  SCHICK                       NBO2 *
-190199+6 532354+5 198501+2-698492-7-13999 9+3 563758+2 1200. 2270.2  -0.NBO2  *
-190199+6 683449+5 199999+2 419 95-8 12799 9+3 630255+2 2270. 6000.3  -0.NBO2  *
  1 41  2 14                                  FAKED FROM MOSI2             NBSI2 *
-300000+5 551759+5 177703+2 185134-2-35090 6+6 559863+2  300. 1200.2  -0.NBSI2 *
-300000+5 551759+5 177703+2 185134-2-35090 6+6 559863+2 1200. 1300.2  -0.NBSI2 *
  1 41  2  7                                  SCHICK                       NB2N *
-604999+5 546988+5 170579+2 211155-2-31394 6+6 627547+2  500. 1500.2  -0.NB2N  *
-604999+5 545235+5 165594+2 219983-2 509716+6 626788+2 1500. 2600.2  -0.NB2N  *
  2 41  5  8                                  SCHICK                       NB205 *
-454599+6 120668+6 368998+2 512 15-2-60993 2+6 128430+5  500. 1785.2  -0.NB205 *
-454599+6 154934+6 569999+2 130385-7 25599 9+3 146482+3 1785. 6000.3  -0.NB205 *
  7 28                                      THERMO PROP OF ELMTS 1956    NI   *
-139  0+0 244959+5 579  6+1 190956-2 98843 7+5 262 27+2  700. 1725.2  -0.NI    *
-139  0+0 272700+5 920116+1-327825-6-20479 9+4 280802+2 1725. 5000.3  -0.NI    *
  1 28  1  7                                  B-605  1963                  NIO  *
-572999+5 406315+5 908778+1 523456-2 67793 6+6 413507+2  700. 1800.2  -0.NIO   *
-572999+5 406315+5 908778+1 523456-2 67793 6+6 413507+2 1800. 2700.2  -0.NIO   *
  1 28  1 14                                  B-476  ENTROPY FAKED          NISI *
-20500 +5 40900 +5 10    +2 312   -2 0      +0 4353  +2  298. 1000.2  -0.NISI  *
-20500 +5 40900 +5 10    +2 312   -2 0      +0 4353  +2 1000. 1500.2  -0.NISI  *
  1 28  2 14                                  FAKED FROM MOSI2             NISI2 *
-30000 +5 551759+5 177703+2 185134-2-35090 6+6 559863+2  300. 1200.2  -0.NISI2 *
-30000 +5 551759+5 177703+2 185134-2-35090 6+6 559863+2 1200. 1300.2  -0.NISI2 *
  2 28  1 14                                  EVANS  ENTROPY FAKED         NI2SI *
-33500 +5 57351 +5 158   +2 329   -2 0      +0 574   +2  298. 1000.2  -0.NI2SI *
-33500 +5 57351 +5 158   +2 329   -2 0      +0 574   +2 1000. 1500.2  -0.NI2SI *
  2  8  1 14                                  JANAF TAPE 7/71  6/67        O2SI *
-217699+6 462679+5 174 37+2 299889-3-764 67+6 470401+2  500. 1696.2  -0.O2SI  *
-215739+6 494990+5 205108+2-223191-5-32447 9+5 496114+2 1696. 4500.3  -0.O2SI  *
  2  8  1 74                                  JANAF TAPE 7/71  9/66        O2W  *
-140939+6 572203+5 143968+2 416506-2 16547 8+5 560187+2  500. 1700.2  -0.O2W   *
-140939+6 580777+5 217559+2 234 97-2-12289 5+8 563818+2 1700. 3000.2  -0.O2W   *
  2008 01 40                                  JANAF 06/61                  O2ZR*
-261500+6 487946+5 182127+2-777714-3 68916 8+7 524420+2  500. 2950.2  100.O2ZR*
-245518+6 540370+5 195658+2 831149-4 16793 7+7 596074+2 2950. 5000.3  100.O2ZR*
  3  8  1 74                                  JANAF TAPE 7/71  9/66        O3W  *
-201459+6 682479+5 224874+2 196967-2-52592 0+6 727 53+2  500. 1745.2  -0.O3W   *
-188554+6 784829+5 315  7+2-193715-6-12799 9+4 852428+2 1745. 5000.3  -0.O3W   *
  4  8  1 14  1 40                           JANAF TAPE 7/71  6/65       O4SIZR *
-483735+6 942 63+5 372804+2-340914-3-17957 7+7 964256+2  500. 1700.2  -0.O4SIZR *
-483735+6 940493+5 353393+2 178562-3 12617 9+7 963575+2 1700. 3000.2  -0.O4SIZR *
  1 14                                      JANAF TAPE 7/71  3/67         SI  *
-373  0+0 185854+5 546 41+1 918302-3-85767 9+5 191 90+2  500. 1685.2  -0.SI    *
 115849+5 175619+5 649998+1 279396-6 51999 9+2 256330+2 1685. 4500.3  -0.SI    *
  1 74                                      JANAF TAPE 7/71  6/66          W  *
```

TABLE B-1 (CONCLUDED)

b) (Concluded)

```
 545  0+0 202793+5 254672+1 265820-2 756154+6 23652942  500. 5681.2  -0.W      *
 112229+5 197539+5 84999041 135 41-7 719999+3 265905+2 3681. 6000.3  -0.W      *
  1 74  2 14                                  FAKED FROM MOSI2                WSI2  *
-22400 +5 551759+5 177703+2 185134-2-350906+6 559863+2  300. 1200.2  -0.WSI2   *
-22400 +5 551759+5 177703+2 185134-2-350906+6 559863+2 1200. 1300.2  -0.WSI2   *
  1 40                                        JANAF TAPE 7/71 12/67           ZR    *
 543  0+0 258582+5 990195+1-901510-3-809985+6 290302+2  500. 2200.2  -0.ZR     *
 635 99+4 199589+5 799999+1-901  0+0-809  0+0 292  2+2 2200. 5500.3  -0.ZR     *
  1 40  1 14                                  FAKED FROM FESI                 ZRSI  *
-37000 +5 48125 +5 1072  +2 43    -2 0     +0 484   +2  298.  500.2  -0.ZRSI   *
-37000 +5 48125 +5 1072  +2 43    -2 0     +0 484   +2  500.  900.2  -0.ZRSI   *
  1 40  2 14                                  FAKED FROM MOSI2                ZRSI2 *
-28000 +5 551759+5 177703+2 185134-2-350906+6 559863+2  300. 1200.2  -0.ZRSI2  *
-28000 +5 551759+5 177703+2 185134-2-350906+6 559863+2 1200. 1300.2  -0.ZRSI2  *
  2 40  1 14                                  FAKED FROM NI2SI                ZR2SI *
-50000 +5 57351 +5 158   +2 329   -2 0     +0 574   +2  298. 1000.2  -0.ZR2SI  *
-50000 +5 57351 +5 158   +2 329   -2 0     +0 574   +2 1000. 1500.2  -0.ZR2SI  *
  5 41  3 14                                  FAKED FROM MO5SI3               NB5SI3 *
-630000+5 600000+5 2222  +2                     630000+2  298.  500.2  -0.NB5SI3 *
-630000+5 600000+5 2222  +2                     630000+2  500. 2753.2  -0.NB5SI3 *
```

TABLE B-2

SPECIES WITH ASSUMED PROPERTIES

Species	Ref.	Data Assumptions
NiO(g)	B-1	The thermochemical properties of FeO(g) were used.
$CrSi_2$(s)	B-3, B-7	Specific heat data was generated from a formula for specific heat for $MoSi_2$(s). The heat of formation is an average of the values reported for $MoSi_2$(s) in References B-3 and B-7. The entropy of FeSi(s) at 298°K was used.
HfSi(s)	B-3	The thermochemical properties of FeSi(s) were used.
$HfSi_2$(s)	B-3, B-7	Specific heat data was generated from a formula for specific heat for $MoSi_2$(s). The heat of formation is an average of the values reported for $MoSi_2$(s) in References B-3 and B-7. The entropy of FeSi(s) at 298°K was used.
Hf_2Si(s)	B-3	The thermochemical properties of Ni_2Si(s) were used. The heat of formation is the heat of formation of Zr_2Si(s). The entropy of FeSi(s) at 298°K was used.
$NbSi_2$(s)	B-3, B-7	Specific heat data was generated from a formula for specific heat for $MoSi_2$(s). The heat of formation is an average of the values reported for $MoSi_2$(s) in References B-3 and B-7. The entropy of FeSi(s) at 298°K was used.
NiSi(s)	B-3	In addition to data for NiSi(s) the entropy of FeSi(s) at 298°K was used.
$NiSi_2$(s)	B-3, B-7	Specific heat data was generated from a formula for specific heat for $MoSi_2$(s). The heat of formation is an average of the values reported for $MoSi_2$(s) in References B-3 and B-7. The entropy of FeSi(s) at 298°K was used.
Ni_2Si(s)	B-3	The entropy of FeSi(s) at 298°K was used.
WSi_2(s)	B-7	Specific heat data were generated from a formula for MoSi(s). The entropy of FeSi(s) at 298°K was used.
ZrSi(s)	B-3, B-7	The heat of formation is that of ZrSi(s). All other data used was for FeSi(s).
$ZrSi_2$(s)	B-7	Specific heat data were generated from a formula for MoSi(s). The entropy of FeSi(s) at 298°K was used.
Zr_2Si(s)	B-3, B-7	The heat of formation is that of Zr_2Si(s). All other data used is that of Ni_2Si(s).
Nb_5Si_3(s)	B-3, B-7	The specific heat was assumed to equal the specific heat of Mo_5Si_3(s) at 298°K. The entropy at 298°K was assumed equal to that of FeSi(s).

B.2 OXIDE FILM AND COATING ELEMENTAL COMPOSITIONS

For the ACE code predictions of the thermochemical response of bare TD NiCr, the presence of the trace amount of thorium was neglected and the composition was taken as

Species	Mass Fraction	Mole Fraction
Cr	0.20	0.22
Ni	0.80	0.78

For the predictions of the ablation of the Cr_2O_3* and NiO* films, the surface elemental composition was taken as that implied by the associated molecular formula.

The surface chemical compositions of the R512E and VH-109 coatings considered were obtained from the fabricators (Sylvania and VacHyd) and were converted to elemental compositions for input to the ACE code. These elemental compositions are:

Coating	Element	Mole Fraction
VH-109	Si	0.5066
	Cr	0.1307
	Nb	0.2701
	W	0.0218
	Hf	0.0708
R512E	Si	0.6757
	Cr	0.0080
	Fe	0.0020
	Nb	0.3042
	W	0.0100

B.3 OXIDE FILM FORMATION RATE CONSTANTS

The formation of the oxide film is assumed to occur via the mechanism of parabolic oxidation. As discussed in Section 3.2.1, the empirical parabolic oxidation law used treats the absorption of oxygen and associated formation of oxide scale from a global viewpoint, ignoring the microscopic mechanisms involved in the scale growth. Accordingly, the rate of consumption of oxygen in the formation of the oxide scale (kg O_2/m^2sec) is given by

$$\dot{m}_{O_2} = \frac{B}{y_p} e^{-E_a/\mathcal{R}T_w} \qquad \text{(B-2)}$$

where

y_p = thickness of the oxide scale

E_a = activation energy for formation of the oxide specie, 4.63×10^4 cal/mol

T_w = surface temperature

$\mathscr{R}$ = universal gas constant

and the constant B is given by

$$B = \frac{1}{2} K_o \left[\frac{\nu_{O_2/oxide} M_{O_2}}{M_{oxide}} \rho_{oxide} \right]^{-1} \qquad \text{(B-3)}$$

where

$K_o = 2.57 \times 10^{-3} (kg/m^2)^2/sec \quad (1.08 \times 10^{-4} (lb/ft^2)^2/sec)$

$\nu_{O_2/oxide}$ = oxygen stoichiometric coefficient for oxide formation

M_{O_2} = molecular weight of oxygen

M_{oxide} = molecular weight of oxide

ρ_{oxide} = density of oxide

The values of E_a and K_o were taken from Reference B-8.

For the formation of Cr_2O_3* scale,

$$\nu_{O_2/Cr_2O_3^*} = 3/2$$

$$M_{O_2} = 32$$

$$M_{Cr_2O_3^*} = 152$$

$$\rho_{Cr_2O_3^*} = 5.21 \times 10^3 kg/m^3 \quad (3.25 \times 10^2 lb/ft^3)$$

so that

$B = 0.781 \times 10^{-6}$ kg O_2/m sec

$= (0.526 \times 10^{-6}$ lb O_2/ft sec)

For the formation of NiO* scale

$$\nu_{O_2/NiO^*} = \frac{1}{2}$$

$$M_{O_2} = 32$$

$$M_{NiO^*} = 74.71$$

$$\rho_{NiO^*} = 5.05 \times 10^3 \text{ kg/m}^3 \quad (3.15 \times 10^2 \text{ lb/ft}^3)$$

so that

$$B = 1.19 \times 10^{-6} \text{ kg } O_2/\text{m sec}$$
$$(0.799 \times 10^{-6} \text{ lbm } O_2/\text{ft sec})$$

B.4 DENSITIES, SPECIFIC HEATS, AND THERMAL CONDUCTIVITIES

In order to analyze the in-depth thermal response of the materials of interest, their densities, specific heats, and thermal conductivities as a function of temperature must be known. In the case of TD NiCr, this information for both the oxide film and the pure alloy is required, while for coated columbium, this information is needed for both the base material and the coating. The calculations presented in Section 5.2 were made assuming that each of the metals was backed by 0.038 meters (1.50 inches) of insulation. Density, thermal conductivity, and specific heat is therefore also required for this material. The densities used in the computations were:

Material	ρ, kg/m^3	ρ, lb/ft^3
Cr_2O_3*	5.21×10^3	3.25×10^2
NiO*	5.05×10^3	3.15×10^2
TD NiCr	8.52×10^3	5.32×10^2
$MoSi_2$*	6.00×10^3	3.75×10^2
Cb	9.50×10^3	5.93×10^2
Insulation	0.056×10^3	3.50

where molybdenum disilicide was taken as representative of the columbium coatings considered. The density of TD NiCr was taken from Reference B-8, that for the insulation from Reference B-9, and all other densities from Reference B-10.

The thermal conductivities and specific heats used in the computations are presented in Table B-3. The superscripts in parenthesis in the table indicate references from which the data were taken. Data presented in Reference B-11 indicate that the specific heats and thermal conductivities of Cr_2O_3* and NiO* are essentially identical. Again, molybdenum disilicide was taken as representative of the coatings considered.

B.5 MASS TRANSFER COEFFICIENTS

Since the ACE code provides only nondimensional ablation rates, mass transfer coefficients are required in order to obtain the surface recession rate as a function of surface temperature which is required by the CMA and OFFA codes. The mass transfer coefficients were assumed to be constant at the values presented in Table 3.[1]

Material	C_M, kg/m^2sec	C_M, lb/ft^2sec
TD NiCr	6.35×10^{-3}	1.3×10^{-3}
Coated Cb	1.17×10^{-2}	2.4×10^{-3}

B.6 NODAL NETWORKS

Since the CMA and OFFA codes solve the governing differential equations in finite-difference form, a suitable nodal network must be established. For the TD NiCr problem, the following set of 18 nodal thicknesses was used:

Meters	Inches	
2.54×10^{-6}	0.0001	Initial oxide thickness
5.08×10^{-6}	0.0002	
5.08×10^{-6}	0.0002	
1.27×10^{-5}	0.0005	Initial pure alloy thickness
1.27×10^{-5}	0.0005	
2.54×10^{-5}	0.0010	
2.54×10^{-5}	0.0010	
2.54×10^{-5}	0.0010	
2.54×10^{-5}	0.0010	
2.54×10^{-5}	0.0010	
2.54×10^{-5}	0.0010	
2.54×10^{-5}	0.0010	
2.54×10^{-5}	0.0010	
3.81×10^{-5}	0.0015	

[1] $C_M = C_H Le^{2/3}$ and Le was assumed to be unity.

TABLE B-3

THERMAL PROPERTIES

a) SI Units

Material	Temperature (°K)	Thermal Conductivity ($W/m^2°K$)[a]		Specific Heat ($J/kg°K$)[a]	
Cr_2O_3* & NiO*	500	9.68	(B-11)	1378	(B-6)
	700	6.92		1454	
	1000	4.84		1499	
	1200	4.50		1544	
	1400	4.50		1566	
	1600	4.50		1566	
	1800	4.50		1555	
TD NiCr	278	9.52	(B-11)	798	(B-11)
	1389	2.87		1280	
$MoSi_2$*	278	4.84	(B-11)	753	(B-11)
	556	3.98		866	
	833	3.29		904	
	1111	2.59		941	
	1250	2.25		979	
	1389	2.07		979	
	1667	1.56		979	
Cb	889	66.30	(B-12)	459	(B-12)
	1111	70.65		482	
	1333	76.87		520	
Insulation	256	0.026	(B-9)	2259	(B-9)
	589	0.049		2259	
	811	0.081		2259	
	1033	0.126		2259	
	1256	0.182		2259	

a) *Numbers in parentheses indicate reference sources.*

TABLE B-3 (CONCLUDED)

b) Conventional Units

Material	Temperature (°R)	Thermal Conductivity (Btu/ft sec°R)[a]	Specific Heat (Btu/lb°R)[a]
Cr_2O_3* & NiO*	900	1.555×10^{-3} (B-11)	0.183 (B-6)
	1260	1.112	0.193
	1800	0.778	0.199
	2160	0.723	0.205
	2520	0.723	0.208
	2880	0.723	0.208
	3240	0.723	0.2065
TD NiCr	500	1.530×10^{-3} (B-11)	0.106 (B-11)
	2500	4.61	0.170
$MoSi_2$*	500	7.780×10^{-3} (B-11)	0.100 (B-11)
	1000	6.40	0.115
	1500	5.28	0.120
	2000	4.16	0.125
	2250	3.61	0.130
	2500	3.33	0.130
	3000	2.50	0.130
Cb	1600	1.065×10^{-2} (B-12)	0.061 (B-12)
	2000	1.135	0.064
	2400	1.235	0.069
Insulation	460	0.417×10^{-5} (B-9)	0.3 (B-9)
	1060	0.721	0.3
	1460	1.305	0.3
	1860	2.025	0.3
	2260	2.920	0.3

a) Numbers is parentheses indicate reference sources.

7.62×10^{-3}	0.3	Backup insulation
7.62×10^{-3}	0.3	
7.62×10^{-3}	0.3	
7.62×10^{-3}	0.3	

The following set of 19 nodes was used for the predictions of coated columbium response:

Meters	Inches	
1.52×10^{-5}	0.0006	Coating
3.05×10^{-5}	0.0012	
3.05×10^{-5}	0.0012	
3.18×10^{-5}	0.00125	Base material
3.18×10^{-5}	0.00125	
3.18×10^{-5}	0.00125	
3.18×10^{-5}	0.00125	
3.18×10^{-5}	0.00125	
3.18×10^{-5}	0.00125	
3.18×10^{-5}	0.00125	
3.18×10^{-5}	0.00125	
3.05×10^{-5}	0.0012	Coating
3.05×10^{-5}	0.0012	
1.52×10^{-5}	0.0006	
7.62×10^{-3}	0.3	Backup insulation
7.62×10^{-3}	0.3	
7.62×10^{-3}	0.3	
7.62×10^{-3}	0.3	
7.62×10^{-3}	0.3	

REFERENCES

APPENDIX B

B-1. "JANAF Thermochemical Tables," Dow Chemical Company, Midland, Michigan, 1971.

B-2. Schick, H. L., "Thermodynamics of Certain Refactory Components," Volume II, Academic Press, New York, 1966.

B-3. Kubaschewski, O., and Evans, E. L., "Metallurgical Thermochemistry," Pergamon Press, New York, 1958.

B-4. Stull, D. R., and Sink, G. C., "The Thermodynamic Properties of the Elements," The Advances in Chemistry Series, Volume 18, American Chemical Society, Washington D.C., 1956.

B-5. Kelley, K. K., "High-Temperature Heat-Content, Heat-Capacity, and Entropy Data for Inorganic Compounds," Bureau of Mines Bulletin 476, 1949.

B-6. Wicks, C. E., Block, F. E., "Thermodynamic Properties of 65 Elements - Their Oxides, Halides, Carbides, and Nitrides," Bureau of Mine Bulletin 605, 1963.

B-7. Campbell, I. E., Sherwood, E. M., "High-Temperature Materials and Technology," John Wiley & Sons, Inc., New York, 1967.

B-8. Goldstein, H. E., "An Analytical Model for Hypersonic Ablation of Thoria Dispersed Nickel Chromium Alloy," AIAA Paper 71-34, January 1971.

B-9. Grumman Aerospace Corp., "Alternate Space Shuttle Concepts Study," Part II, Volume II, Final Report (B-2) MSC-03810, July 1961.

B-10. Handbook of Chemistry and Physics, Chemical Rubber Publishing Co., Charles D. Hodgman, M. S., (Editor), Cleveland, Ohio, 42nd Edition, 1960.

B-11. Goldsmith, A., et al., "Thermophysical Properties of Solid Materials," Wright Air Development Center, WADC-TR-58-476, November 1960.

APPENDIX C

EXPERIMENTAL EVALUATION OF MATERIAL RESPONSE

A more detailed description of the test program and the test results for evaluation of material response is presented in this appendix.

C.1 TEST FACILITY

The tests were performed in the Aerotherm 1.5-MW arc plasma facility described in Table C-1. The basic arc heater configuration for both the 300-kw and 1.5-MW units employed is shown schematically in Figure 5. In the arc unit, the energy is added to the primary test gas via a steady electric arc discharge, the arc striking from the tungsten cathode to the downstream diverging copper anode. The primary test gas was high purity nitrogen and was introduced at the downstream end of the cathode module. The secondary gas was high purity oxygen in the proper amount to yield the required test gas compositions and was introduced in the plenum and mixing chamber or in the constrictor column just downstream of the cathode.

The arc heater and associated hardware were cooled with high pressure, deionized water. Power was supplied by a 660-kw continuous duty, 1.5-MW overload saturable reactor controlled DC rectifier. Continuous vacuum pumping capability was provided by a five-stage steam ejector vacuum pumping system.

The model stings were pneumatically actuated to provide a radial motion in and out of the test stream and included variable stop positions for stepwise tranverse of the test stream. The stings were water cooled to provide continuous duty operation at all test conditions. Three stings were employed as follows:

Sting Position	Model Configuration	
	Sample Tests	Calibration Tests
2	Test Sample Model	Pressure Probe
3	Calibration Model	Calibration Model
4	Test Sample Model	Calorimeter

These model configurations are described in subsequent sections.

TABLE C-1

DESCRIPTION OF TEST FACILITY

a) SI Units

• Arc Heater	
Type	Aerotherm 1.5 Mw and 300 Kw Constrictor Arc Heaters
Input Power	1.2 Mw to 50 kw DC, 300 to 10 kw DC
Chamber Pressure	4.05×10^{3} to 3.04×10^{6} N/m^2
Enthalpy	4.18×10^{6} to 3.35×10^{8} J/kg
Gas Flow Rate	9.07×10^{-4} to 6.80×10^{-2} kg/sec
Gas Compositions	N_2,O_2, Air, He, A, H_2, CO_2, CO, H_2O, HCl BF_3, solid particles and mixtures of the above
Stabilization	Gas
Electrodes	Copper/Tungsten, Copper/Copper
• Power Supply	
Type	Rectifier, saturable reactor controlled
Rating	800 Kilowatts for 1 hour, 1 megawatt for 10 minutes
• Nozzle and Test Sections	
Supersonic Nozzles	
Exit Diameter	2.03×10^{-1} to 1.14×10^{-2} meters } 10 combinations
Throat Diameter	2.54×10^{-2} to 8.13×10^{-3} meters } 10 combinations
Area Ratio	64 to 2
Expansion Angle	7.5° and 8.5° half angle, and contoured
Duct Flow Apparatus	
Size	2.54×10^{-1} to 1.27×10^{-2} meters high, 7.62×10^{-2} to 1.27×10^{-1} meters long, 2.54×10^{-2} meters wide
Model Size/Shape	1.27×10^{-2} to 2.54×10^{-1} meters thick/flat or contoured
Sonic Nozzles	
Throat Diameter	7.62×10^{-2} to 2.54×10^{-1} meters
Type	Water cooled or ablating test section
• Test Chamber	
Size	1.07 meters diameter by 4.57 meters long
Chamber Cooling	Cooled diffuser with heat exchanger
Viewing and Access	2 - .305 x .406 meter windows, 4 - .076 meter dia. quartz windows
• Vacuum System	
Type	Steam ejector, 5 stage continuous operation
Capacity	4.54×10^{-2} kg/sec at 1.33×10^{3} N/m^2, 9.07×10^{-3} kg/sec at 2.66×10^{1} N/m^2, 1.81×10^{-3} kg/sec at 6.67 N/m^2
• Model Sting System	
Type	Pneumatic actuated, variable insertion speed,
Capacity	7 stings per test maximum
• Instrumentation	
Enthalpy	Energy balance, mass balance, heat flux potential
Flow Rate	ASME orifice, rotometer
Temperature	Thermocouple, thermopile, pyrometer
Pressure	Strain gauge & reluctance transducers and Bourdon tube gauge
Recording	High Speed 80-channel digital data acquisition system with magnetic tape recording, high speed 36-channel oscillograph, digital and potentiometric recorders, oscilloscopes

TABLE C-1 (CONCLUDED)

b) Conventional Units

• Arc Heater	
Type	Aerotherm 1.5 Mw and 300 kw Constrictor Arc Heaters
Input Power	1.2 Mw to 50 kw DC, 300 to 10 kw DC
Chamber Pressure	0.04 to 30 atm
Enthalpy	1000 to 80,000 Btu/lb
Gas Flow Rate	0.002 to 0.15 lb/sec
Gas Compositions	N_2, O_2, Air, He, A, H_2, CO_2, CO, H_2O, HCl, BF_3, Solid particles, and mixtures of the above
Stabilization	Gas
Electrodes	Copper/Tungsten, Copper/Copper
• Power Supply	
Type	Rectifier, Saturable reactor controlled
Rating	800 kilowatts for 1 hour, 1 megawatt for 10 minutes
• Nozzles and Test Sections	
Supersonic Nozzles	
Exit Diameter	8.0 to 0.45 inch } 10 Combinations
Throat Diameter	1.0 to 0.32 inch } 10 Combinations
Area Ratio	64 to 2
Expansion Angle	7.5° and 8.5° half angle, and contoured
Duct Flow Apparatus	
Size	0.1 to 0.5 inch high, 3.0 to 5.0 inch long, 1.0 inch wide
Model Size/Shape	0.5 to 1.0 inch thick/flat or contoured
Sonic Nozzles	
Throat Diameter	0.3 to 1.0 inch
Type	Water cooled or ablating test section
• Test Chamber	
Size	3.5 ft. diameter by 15 ft. long
Chamber Cooling	Cooled diffuser with heat exchanger
Viewing and Access	2 - 12 x 16 inch windows, 4 - 3 in. diameter quartz windows
• Vacuum System	
Type	Steam ejector, 5 stage continuous operation
Capacity	0.1 lb/sec at 10 torr, 0.02 lb/sec at 0.2 torr, 0.004 lb/sec at 0.05 torr
• Model Sting System	
Type	Pneumatic actuated, variable insertion speed
Capacity	7 stings per test maximum
• Instrumentation	
Enthalpy	Energy balance, mass balance, heat flux potential
Flow Rate	ASME orifice, rotometer
Temperature	Thermocouple, thermopile, pyrometer
Pressure	Strain gauge & reluctance transducers and Bourdon tube gauge
Recording	High speed 80-channel digital data acquisition system with magnetic tape recording, high speed 36-channel oscillograph, digital and potentiometric recorders, oscilloscopes

The test data were recorded on magnetic tape with an 80-channel digital data acquisition system. The magnetic data tape was converted to an unscrambled easily readable format on a second magnetic tape which served directly as the input to the data reduction computer code.

C.2 MODEL AND TEST SAMPLE CONFIGURATIONS

The model configurations employed in the test program were:

- Flat face stagnation point models
  - 0.121 - meter (4.75-inch) body diameter
  - 0.0318- meter (1.25-inch) body diameter
- Wedge Model
  - 30° half angle, 0.0127-meter (0.5-inch) nose radius

As shown in Figures C-1, C-2, 6, and 7. The test models were made of copper and were water cooled to:

- Provide a well defined back wall boundary condition
- Allow continuous operation at all test conditions
- Provide the necessary sample cooldown between cycles

The stagnation point models employed a peripheral copper ring to insure that the test samples were not exposed to any unusual thermal or aerodynamic edge effects. For the wedge model, a Gardon-type calorimeter and a pressure tap were employed in the nose of the model for continuously monitoring the test conditions throughout each test. The backup insulator included two (stagnation point) and 5 (wedge, each side) instrumented thermocouple plugs (Figures C-1 and C-2). Each plug contained 3 Chromel/Alumel thermocouples for in-depth temperature measurement and definition of the backwall heat loss. These thermocouples were on a line offset from but parallel to the axis of the plug; a hole on the plug axis accommodated the spring-loaded thermocouple.

C.3 INSTRUMENTATION AND DATA REDUCTION

Instrumentation was provided and data reduction was performed to define:

- Arc heater and facility operating conditions
- Test stream and model boundary conditions
- Test sample response

All data except for transient calorimetry were recorded on magnetic tape using the 80-channel digital data acquisition system. The data acquisition system

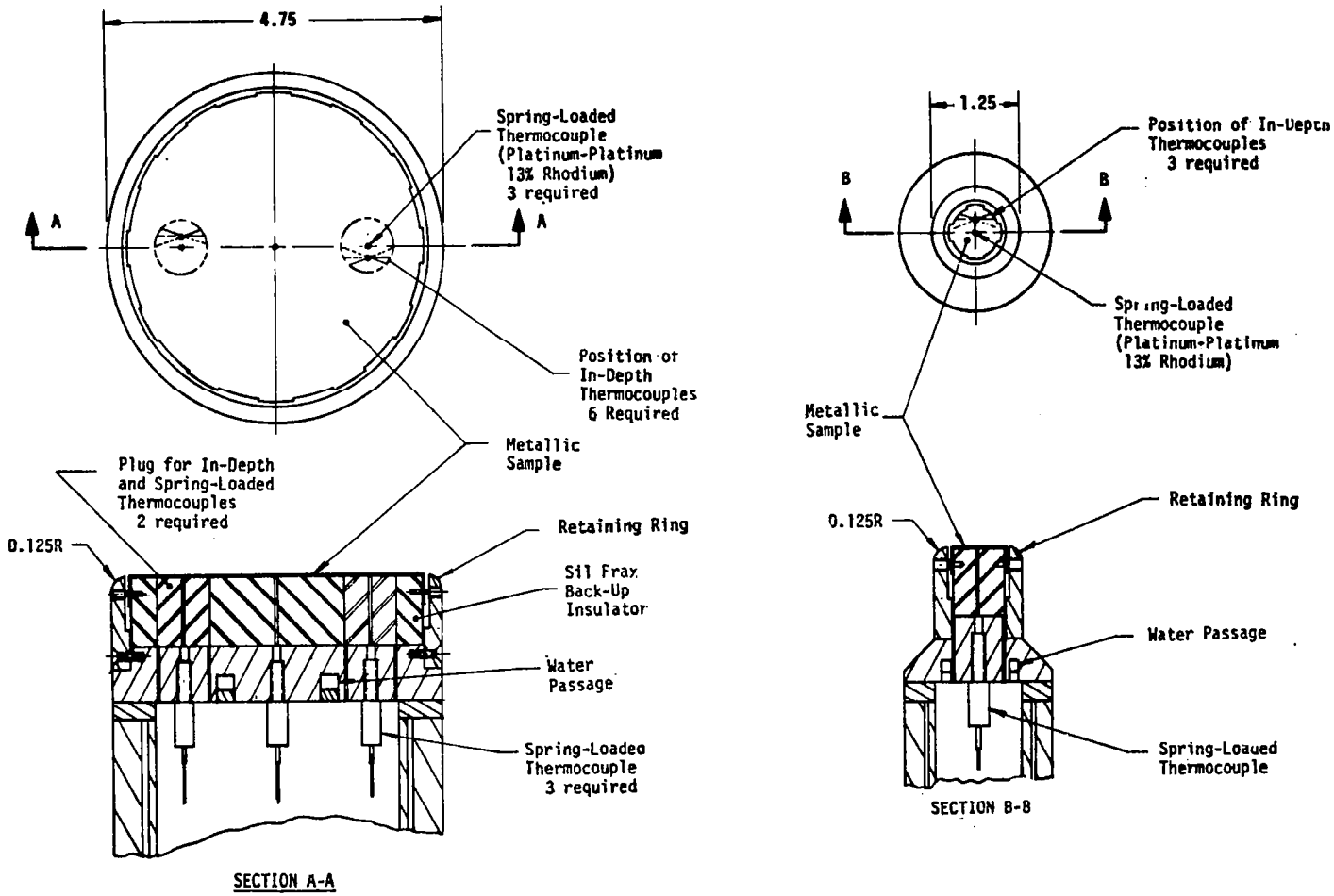

Figure C-1. Stagnation Point Models and Test Samples

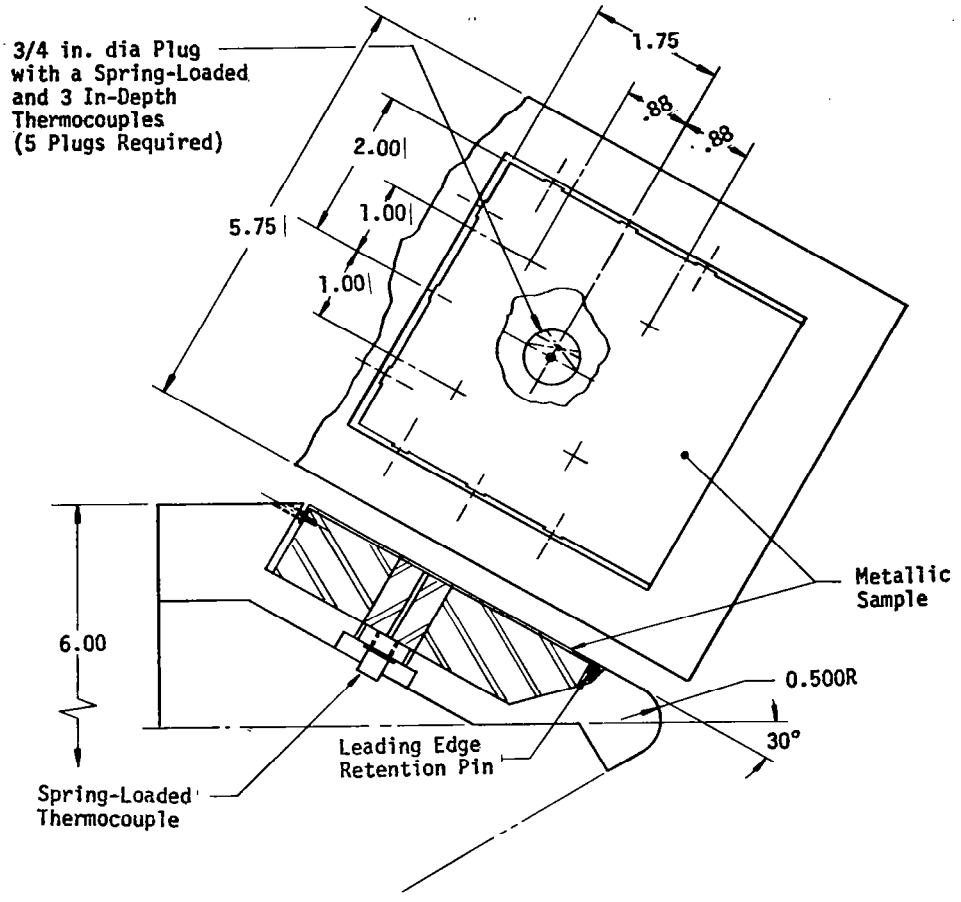

Figure C-2. Wedge Model and Test Sample

was set to trigger every minute and to scan at a rate of 43 channels per second. The unscrambled data tape served as the input to the data reduction code which computed all data in proper units (e.g., °F, atm, Btu/ft^2-sec) and also computed the appropriate multi-variable test and operating conditions (e.g., energy and mass balance enthalpies, efficiency). The output from the transient calorimeters was recorded on a high-speed, 36-channel oscillograph. In some cases, data were recorded by hand from visual indicators, primarily as a backup to the recorded data. The instrumentation and data reduction in the above three categories is presented in the following paragraphs.

C.3.1 Operating Condition Measurements

The following basic operating condition measurements were made to characterize arc heater and facility performance:

- Voltage
- Current
- Gas mass flow rate
- Cooling water flow rate
- Cooling water temperature rise
- Arc chamber pressure
- Test cabin pressure

Table C-2 summarizes the various measuring devices and the standard laboratory methods employed. The flow rates of nitrogen and oxygen were measured separately. Depending on the flow rates, calibrated rotameters or calibrated sharp edge ASME standard orifices were used to set and meter these gas flow rates. A calibrated sharp edge ASME standard orifice was used to meter the cooling water flow rate. The arc heater cooling water temperature rise differential thermopile consisted of a four-pair copper-constantan thermocouple assembly. Arc heater and test cabin pressures were measured by one of several absolute pressure strain gauge transducers depending on operating conditions. The transducer output signal was suitable amplified for recording. Test cabin pressure was also periodically checked with a McLeod gauge and was visually monitored during each test with a thermocouple gauge pressure indicator.

TABLE C-2

OPERATING CONDITION MEASUREMENTS

Type of Measurement	Visual		Recorded	
	Output Device	Type of Output	Output Device	Type of Output
Arc Voltage	Voltage divider	Voltmeter	Voltage divider	0-50 millivolts
Arc current	Shunt	Ammeter	Shunt	0-50 millivolts
Gas mass flow rate	Rotameter or sharp-edge orifice	Percent of full scale or differential pressure	--	--
Cooling water flow rate	Sharp edge orifice	Differential pressure	Δp transducer	0-5 volts
Cooling water temperature rise	Dial thermometer	Deg. Fahrenheit	Differential thermopile	0-20 millivolts
Arc chamber pressure	Pressure gauge	psig or mm Hg	Absolute pressure transducer	0-10 volts
Test cabin pressure	McLeod gauge	Microns	--	--
	Thermocouple gauge	Microns	--	--
	Absolute pressure gauge	mm Hg	--	--

C.3.2 Test Condition Measurements

The boundary conditions to which the test samples were exposed were defined by:

- Enthalpy
- Pressure
- Heat flux
- Surface catalycity effect

Three enthalpy measurement methods were employed:

- Energy balance
- Mass balance (sonic flow)
- Heat flux

The first two methods provided the average stream enthalpy and the last method provided local enthalpy. Energy balance enthalpy was determined from measurements of input power, total energy loss to the cooling water, and gas flow rate from the relation

$$h_{eb} = \frac{Q_{in} - Q_{loss}}{\dot{m}_g} = \frac{EI - \dot{m}_w C_{pw} \Delta T_w}{\dot{m}} \qquad \text{(C-1)}$$

where the measurement of the necessary operating conditions (E, I, $\dot{m}_g$, $\dot{m}_w$, ΔT_w) was presented above. The mass balance enthalpy was determined from the relation

$$\frac{\dot{m}_g}{p_o A_*} = f(h_{mb}) \qquad \text{(C-2)}$$

where this sonic flow parameter (left term) is essentially a function of enthalpy only. This function has been determined in Reference C-1 to enthalpies of 4.15×10^7 J/kg (10,000 Btu/lb), and was refined and extended to higher enthalpies using the ACE computer code (Section 3.2.2). The measurement of the necessary operating conditions ($\dot{m}$ and p_o) was presented above and A_* is the throat area. The heat flux enthalpy was determined from calorimeter measurements of heating rate and the calculation of heat transfer coefficient. This enthalpy is given by

$$h_{hf} = \frac{q_{conv}}{C_H} + h_w \qquad \text{(C-3)}$$

where q_c is the stagnation convective heat flux measured by a catalytic surface calorimeter, C_H is the calculated heat transfer coefficient, and h_w is the enthalpy corresponding to the calorimeter surface temperature. The heat transfer

coefficient was calculated from the relation (Reference 4)

$$C_H = 0.042\sqrt{\frac{p_s}{R_{eff}}} \qquad \text{(C-4)}$$

where p_s is the measured stagnation pressure and

$$R_{eff} = 3.78\ R_B \qquad \text{(C-5)}$$

for a flat face model at moderate to high Mach number (Reference 5).

Heat flux and pressure measurements were made as follows:

- Calibration model of identical geometry to the 0.121-meter (4.75-inch) diameter test model (Figure C-1) for model property distributions - 6 Gardon type calorimeters and 6 pressure taps
- Calibration model of identical geometry to the 0.0318-meter (1.25-inch) test model (Figure C-1) for model heat flux measurements and for stream property surveys - Gardon-type calorimeter
- Calibration model of identical geometry to the wedge test model (Figure C-2) for model property distributions - 7 Gardon-type calorimeters on one side, 1 on the other side, and 1 in the nose; 3 pressure taps on one side, 1 on the other side, and 1 in the nose.
- 0.0095-meter (0.375-inch) diameter pitot probe for stream property surveys
- Calorimeter model of identical geometry to the 0.121-meter (4.75-inch) diameter test model (Figure C-1) for surface catalycity measurements - slug calorimeter

The 0.121-meter (4.75-inch) stagnation point calibration model is shown in Figure C-3 and the wedge calibration model is shown in Figure C-4. The model bodies were copper and were water cooled. The calorimeters for the stagnation point models were individually water cooled and those for the wedge model were cooled by conduction to the body of the copper model. The configuration and assembly details of the calorimeters used for surface catalycity measurements are presented in Figure C-5. The surface treatments employed on these calorimeters were:

- Catalytic - clean, polished copper
- Noncatalytic - teflon coated copper

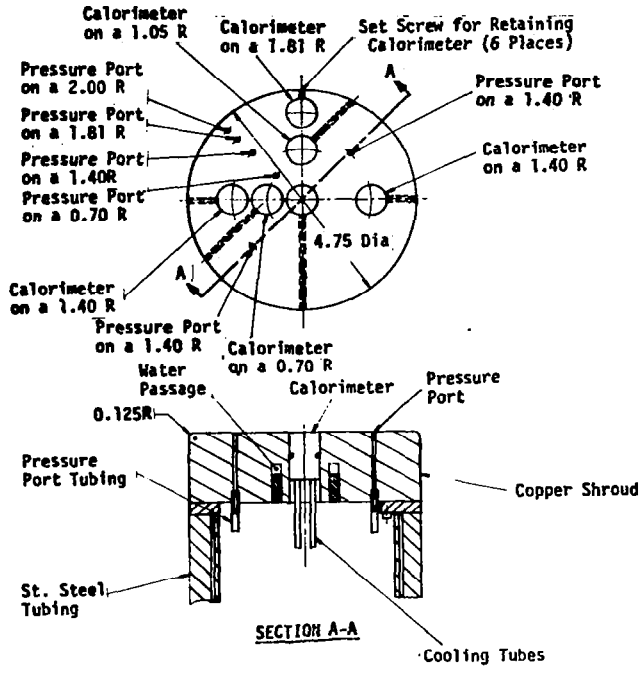

Figure C-3. Stagnation Point Calibration Model

C.3.3 Test Sample Response

The test sample response was defined quantitatively by measurements of surface and in-depth temperatures, surface recession, and weight loss, and qualitatively by photography as presented in Table C-3. The surface temperature was measured pyrometrically with 3 different pyrometers:

- Infrared Industries Thermodot TD-9 Pyrometer - sensing wavelength of 0.8 microns, moderate to high temperatures, relatively insensitive to emissivity
- Infrared Industries Thermodot TD-7 Pyrometer - sensing wavelength range from 1.7 to 2.6 microns, low to moderate temperatures, requires accurate knowledge of emissivity
- Thermogage Miniature Optical Pyrometer - peak sensing wavelength of 0.9 microns, low to high temperatures

The TD-9 pyrometer was used for all tests but those at a nominal surface temperature of 1090°K (1500°F) for which the TD-7 pyrometer was used. Two TD-9 pyrometers were used for the wedge tests to allow simultaneous measurements on both test samples. The primary pyrometer or pyrometers (TD-9 or TD-7 for stagnation point and TD-9's for wedge) were mounted on oscillating mechanisms which indexed the pyrometers every minute. These units described the five position pattern shown below where the a and b dimensions were adjustable to accomodate viewing the model at any angle.

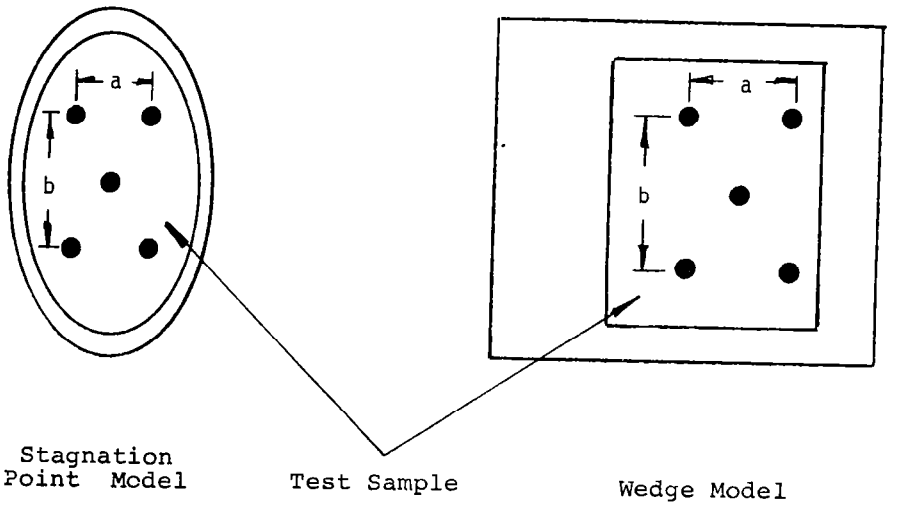

TABLE C-3

TEST SAMPLE RESPONSE INSTRUMENTATION

Variable	Instrumentation
Surface Temperature Primary	TD-9C and/or TD-9F or TD-7 Pyrometers
Secondary	Thermogage, TD-7, and/or TD-9F pyrometers
Backwall Temperatures	Pt/Pt 13% Rh Spring-loaded TC
Backup Insulator In-Depth Temperatures	C/A TC
Surface Recession	Microscope Micrometer
Weight Loss	Semi-Micro Analytic Balance
Qualitative Response	35 mm Color Slides

Backwall temperatures were measured with platinum/platinum 13 percent rhodium spring-loaded thermocouples with a 0.00079-meter (0.031-inch) diameter insulator and 0.000076-meter (3-mil) thermocouple wire. The Silfrax backup insulator was instrumented at each of the measurement locations with three Chromel/Alumel thermocouples as discussed previously.

Surface recession was measured by a special microscope micrometer shown in Figure C-6. This device employed the microscope focus as the surface position indicator. This non-contact technique was necessary to insure no disturbance of the typically delicate surface coatings and oxide films. Weight loss was measured with a conventional semi-micro analytic balance and the qualitative test sample response was defined by pre- and post-test 35 mm color still photography. Surface recession and weight loss measurements and color photography were performed after every sample change.

C.4 CALIBRATION TEST RESULTS

Calibration tests were performed at the nominal test conditions to define the:

- Centerline and bulk average properties
- Distribution of properties across the test stream (stagnation point model conditions only)
- Distribution of properties on the test model
- Catalytic and noncatalytic surface heat flux (stagnation point model conditions only)

The results of the calibration tests are presented in the following subsections.

C.4.1 Centerline and Average Properties

The basic test conditions were defined by measurements of the centerline and average properties as follows:

- Enthalpy
  - Energy balance (average)
  - Mass balance (average)
  - Heat flux (centerline)
- Stagnation (pitot) pressure (centerline)
- Cold wall heat flux (centerline)

These results for the nominal test conditions are presented in Tables 7 and 8. All measurements but heat flux enthalpy and model heat flux were obtained

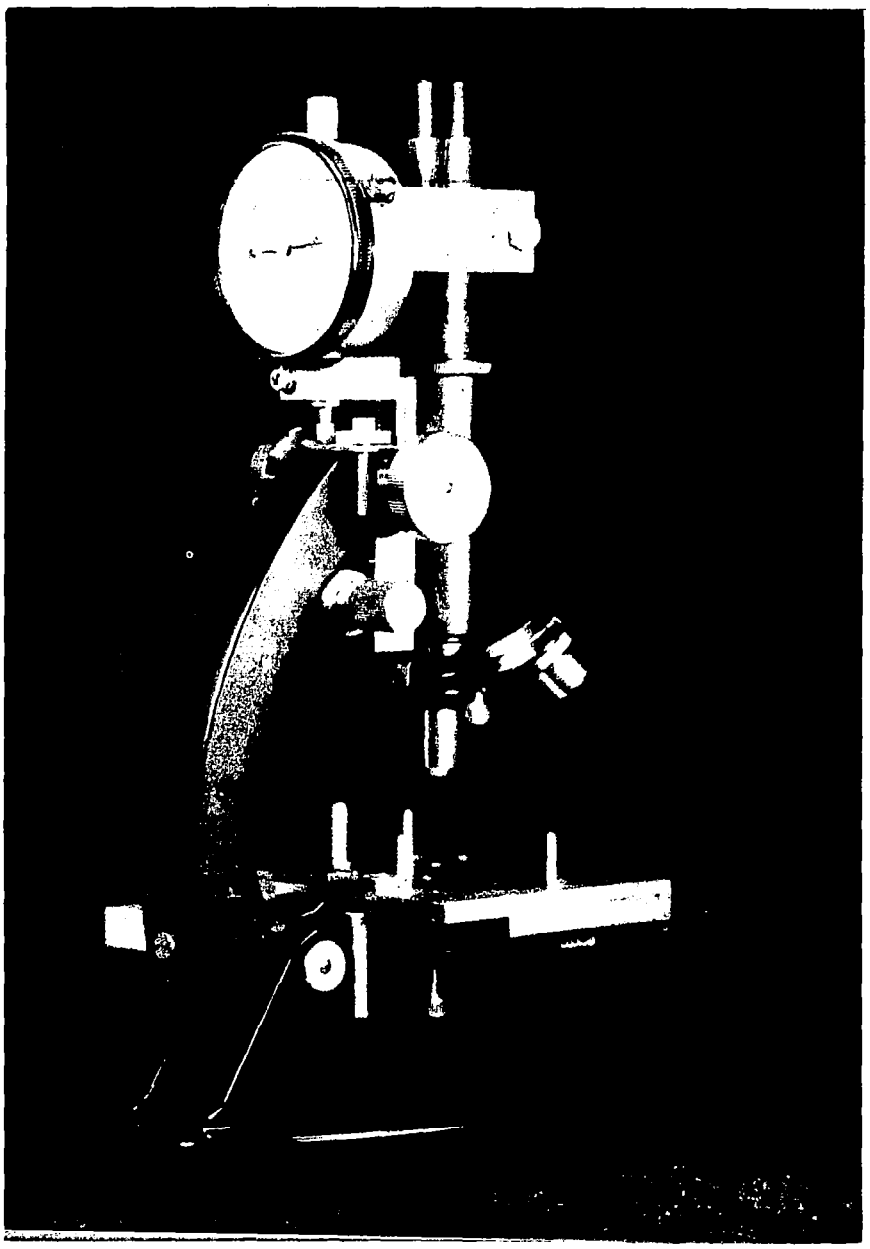

Figure C-6. Microscope Micrometer for Surface Recession Measurement

directly from the data for particular calibration test. Heat flux enthalp- was defined from Equations (C-3) through (C-5) and from the calibration model results obtained during both the calibration and sample test series. This enthalpy was plotted as a function of current, as shown for example in Figure C-7 for test condition 1, and the best-fit line then used to define the enthalpy value for the measured current. The model cold wall heat flux presented in the table was calculated from Equation (1) where $h_o = h_{hf}$ and $h_w = 0$.

The basic test condition seen by the test model was defined by the centerline property values (Tables 7 and 8):

- Heat flux enthalpy
- Stagnation pressure
- Model heat flux

Note that the heat flux enthalpy at the centerline was somewhat higher than the two enahalpies which define the average across the stream.

C.4.2 Stream Distributions

The measured distributions of stagnation pressure and heat flux across the test stream are presented in Figure C-8 for all nominal stagnation point model test conditions. The distributions are essentially flat across the model region for all conditions except test condition 8. The less favorable distribution for test condition 8 was due to the low pressure operating conditions required. This nonuniformity is not as apparent in the model distributions (Section C.4.3) since the stream tube that the model sees is smaller than the model diameter. The measurements on the opposite side of the stream centerline indicate that the test stream is symmetric about the centerline.

C.4.3 Model Distributions

The measured distributions of heat flux and stagnation pressure across the model face are presented in Figure C-9 for all stagnation point model test conditions. The scatter in the heat flux measurements is felt to be due to scatter in the calorimeter performance and not an indication of the actual distribution on the model. Irregularities in the sensor surface and in the surface at its attachment to the calorimeter body and the resultant disturbance to the convective heating are the probable cause. Note that the pressure distributions are uniform. The distributions are relatively flat for all test conditions. The circumferential uniformity (as defined by the pressure measurements) is seen to be excellent at all conditions.

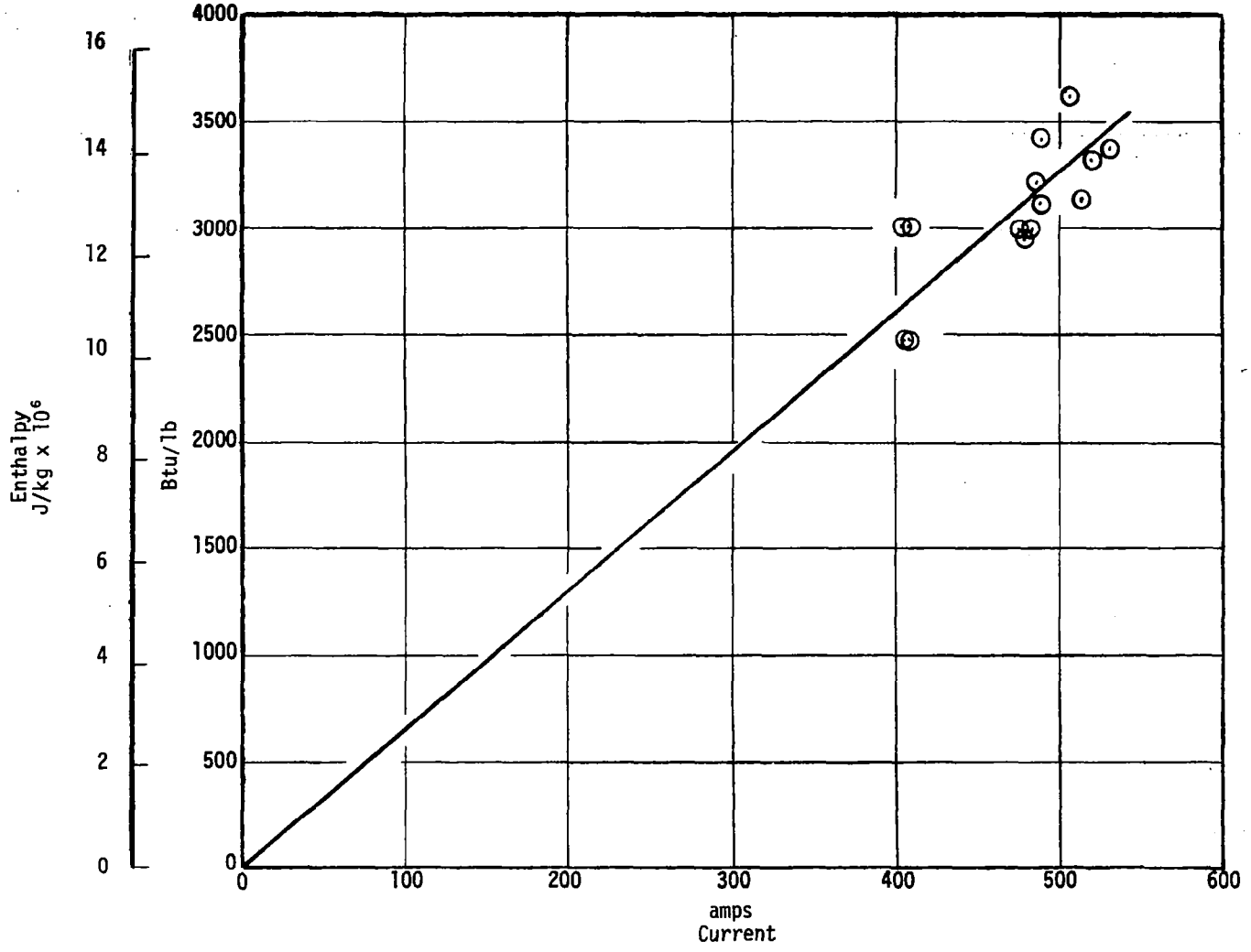

Figure C-7. Typical Heat Flux Enthalpy Calibration Results

TEST 2065-3

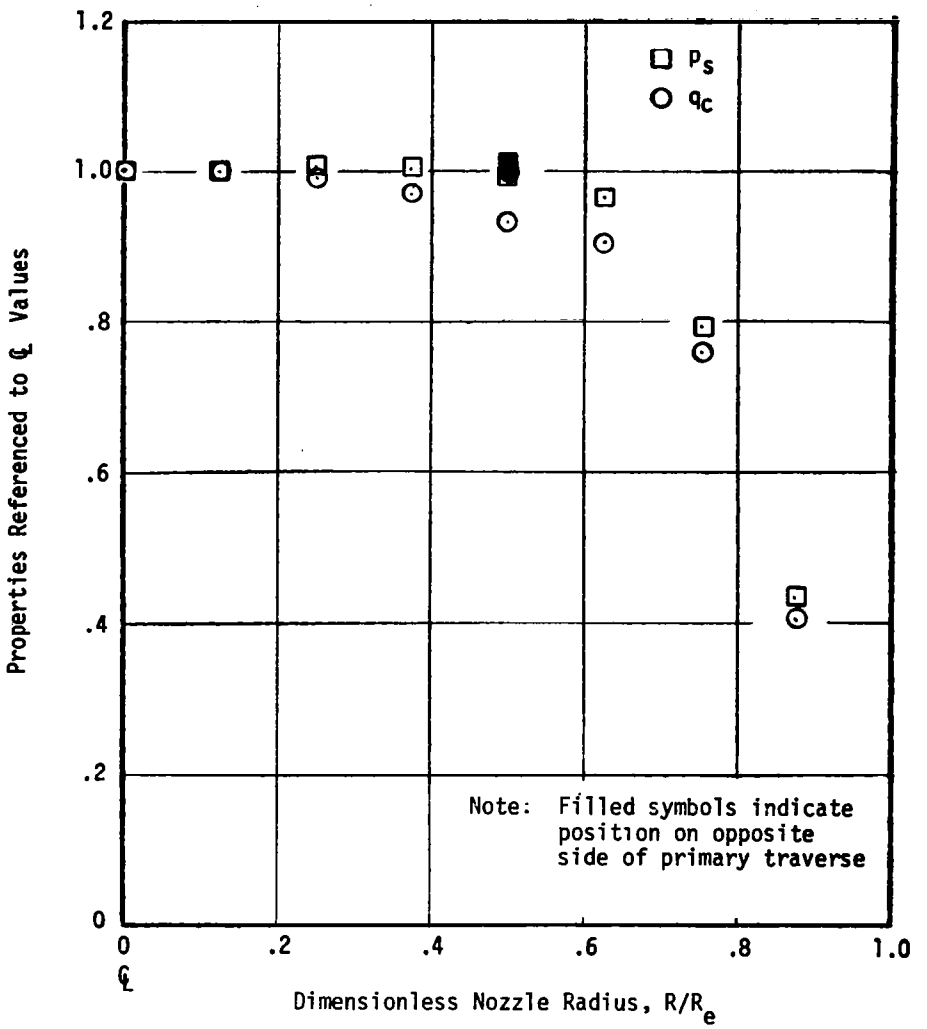

Figure C-8. Test Stream Distribution Results
a) Condition 1, 12

TEST 2066-1

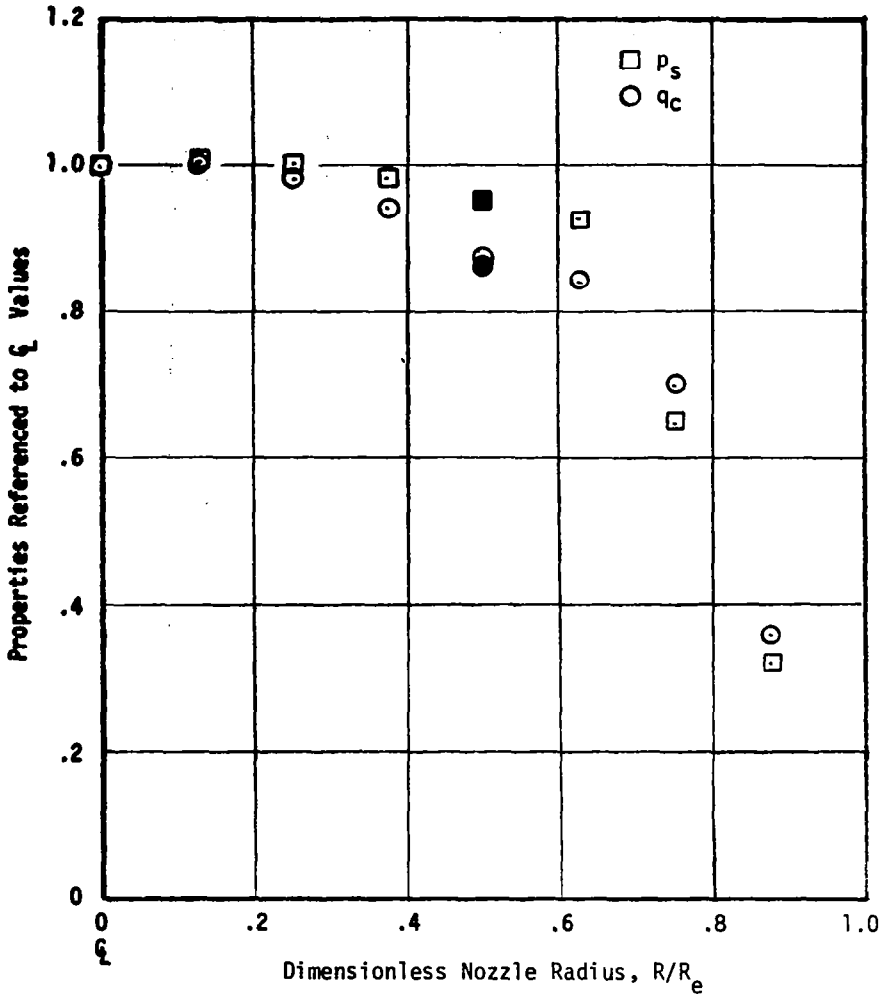

Figure C-8. (Continued)
b) Condition 2

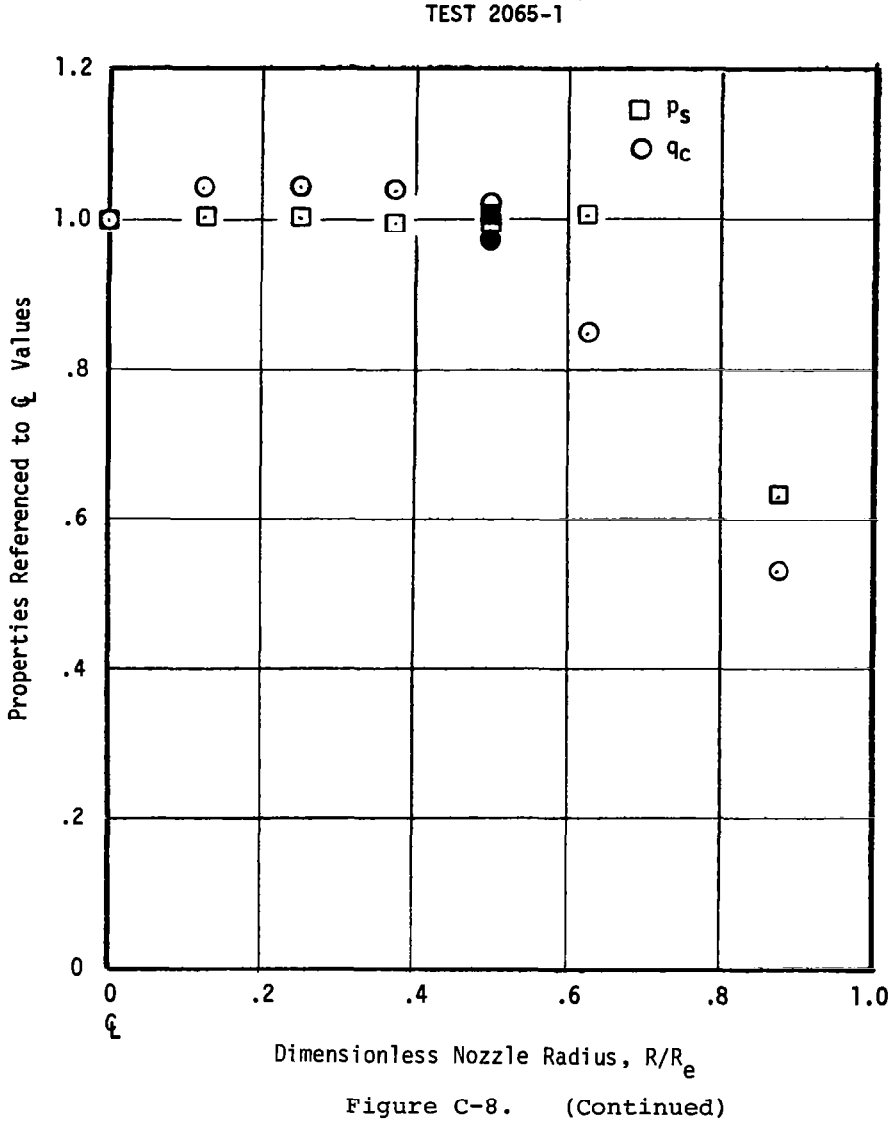

Figure C-8. (Continued)

c) Condition 3

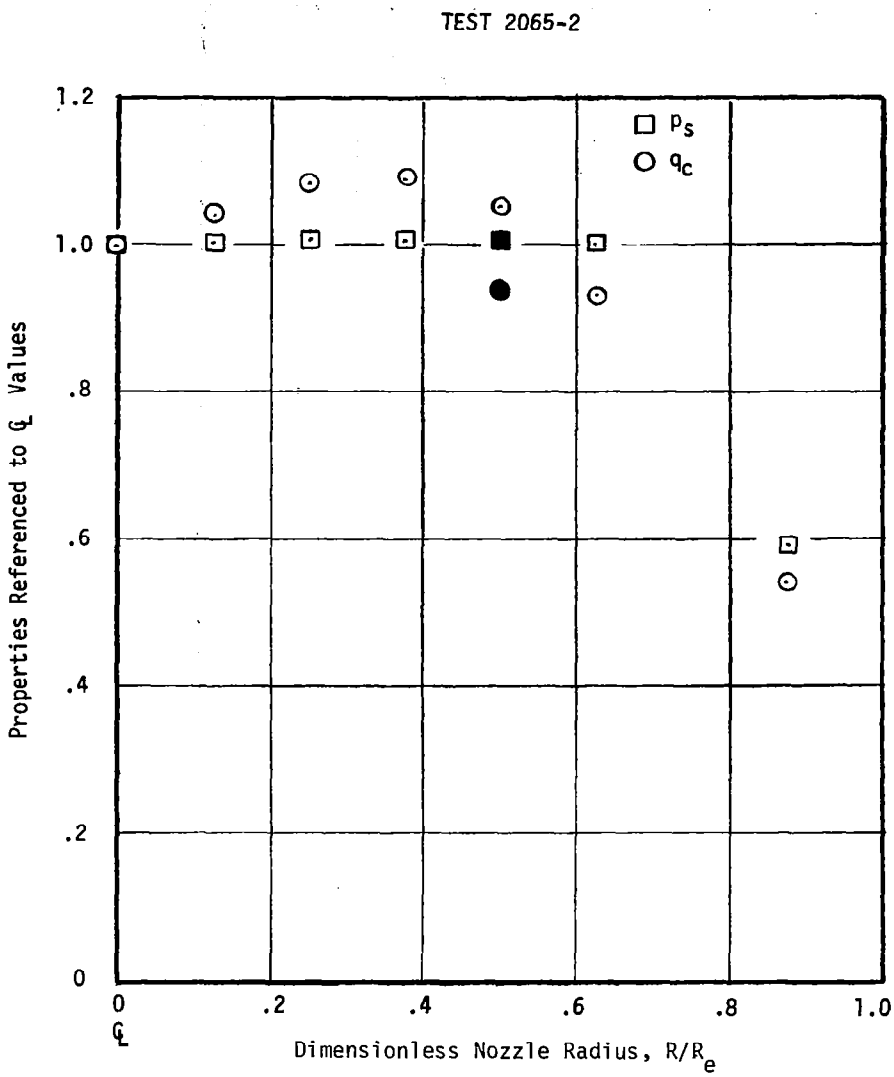

Figure C-8. (Continued)
d) Condition 4

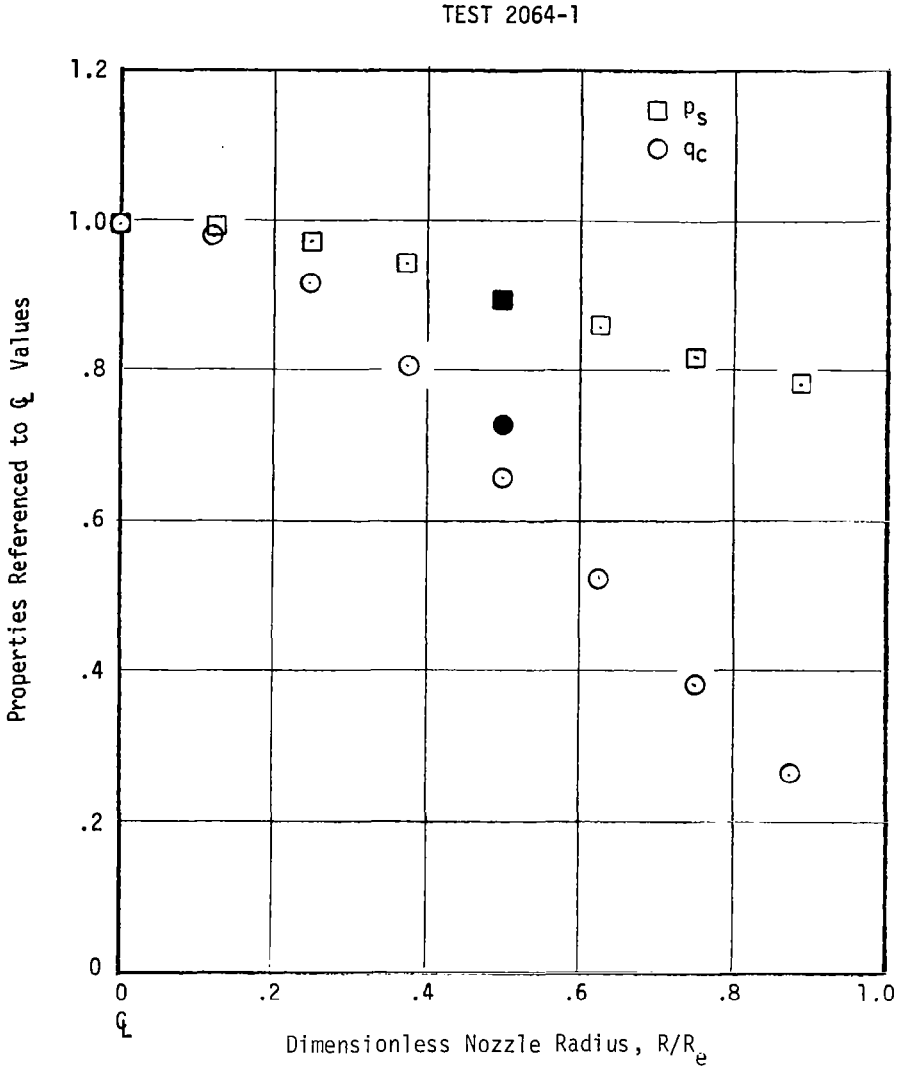

Figure C-8. (Continued)
e) Condition 8

Figure C-8. (Continued)
f) Condition 9 - See Figure 19

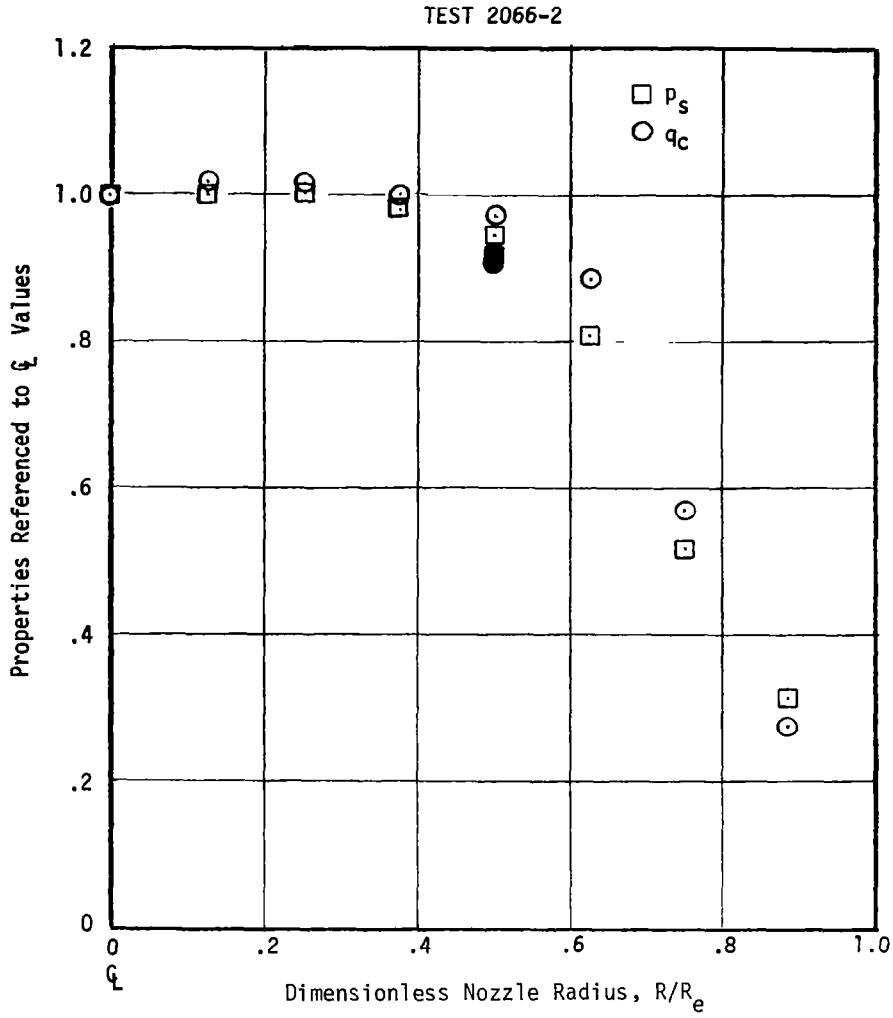

Figure C-8. (Continued)
g) Condition 10

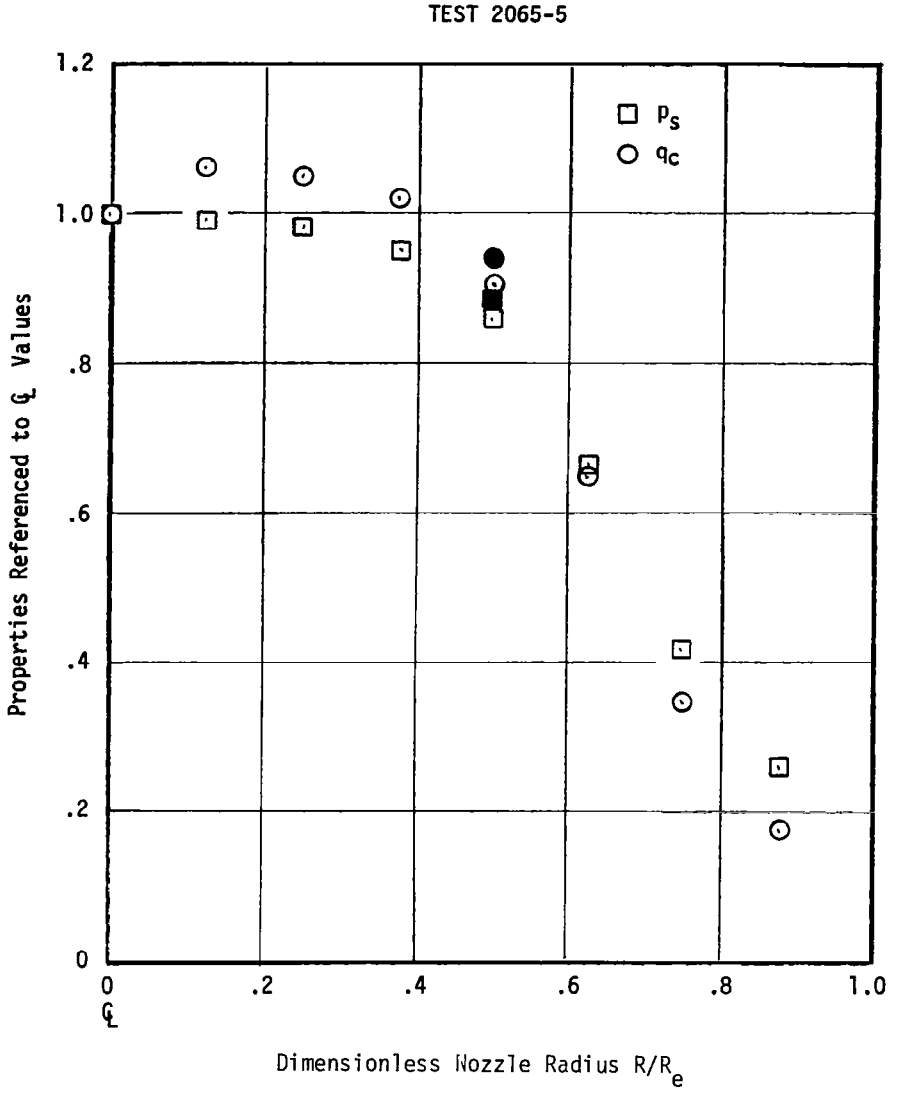

Figure C-8. (Concluded)
h) Condition 11

TEST 2065-3

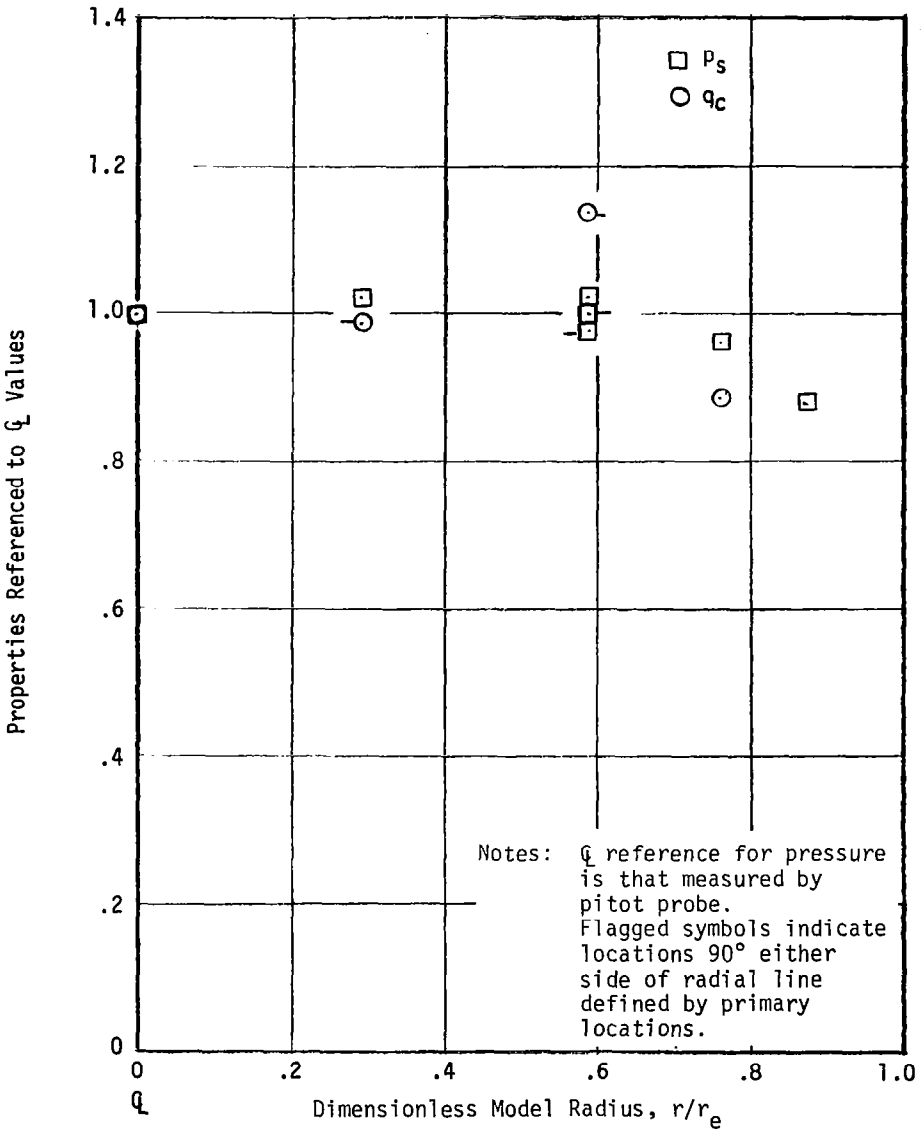

Figure C-9. Model Distribution Results
a) Condition 1, 12

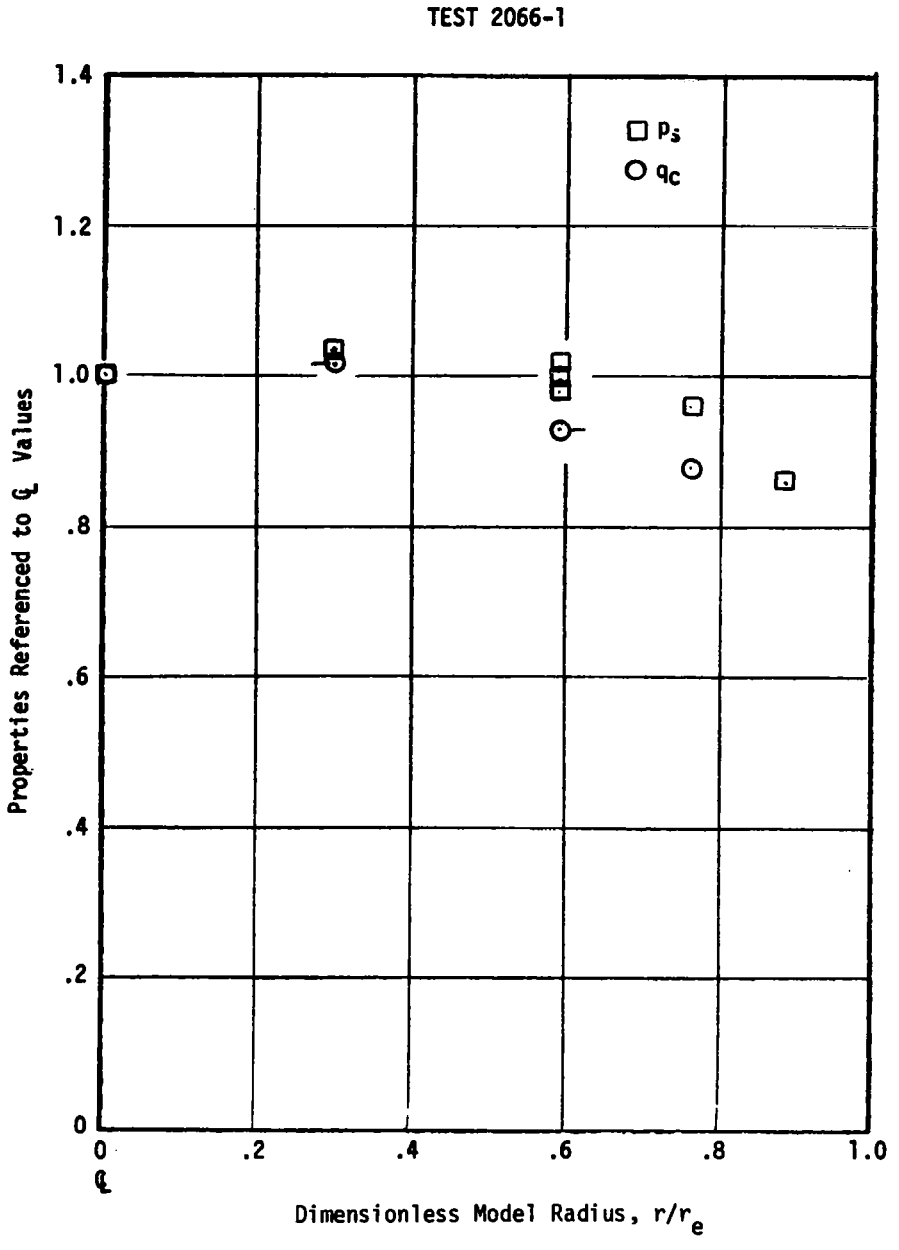

Figure C-9. (Continued)
b) Condition 2

TEST 2065-1

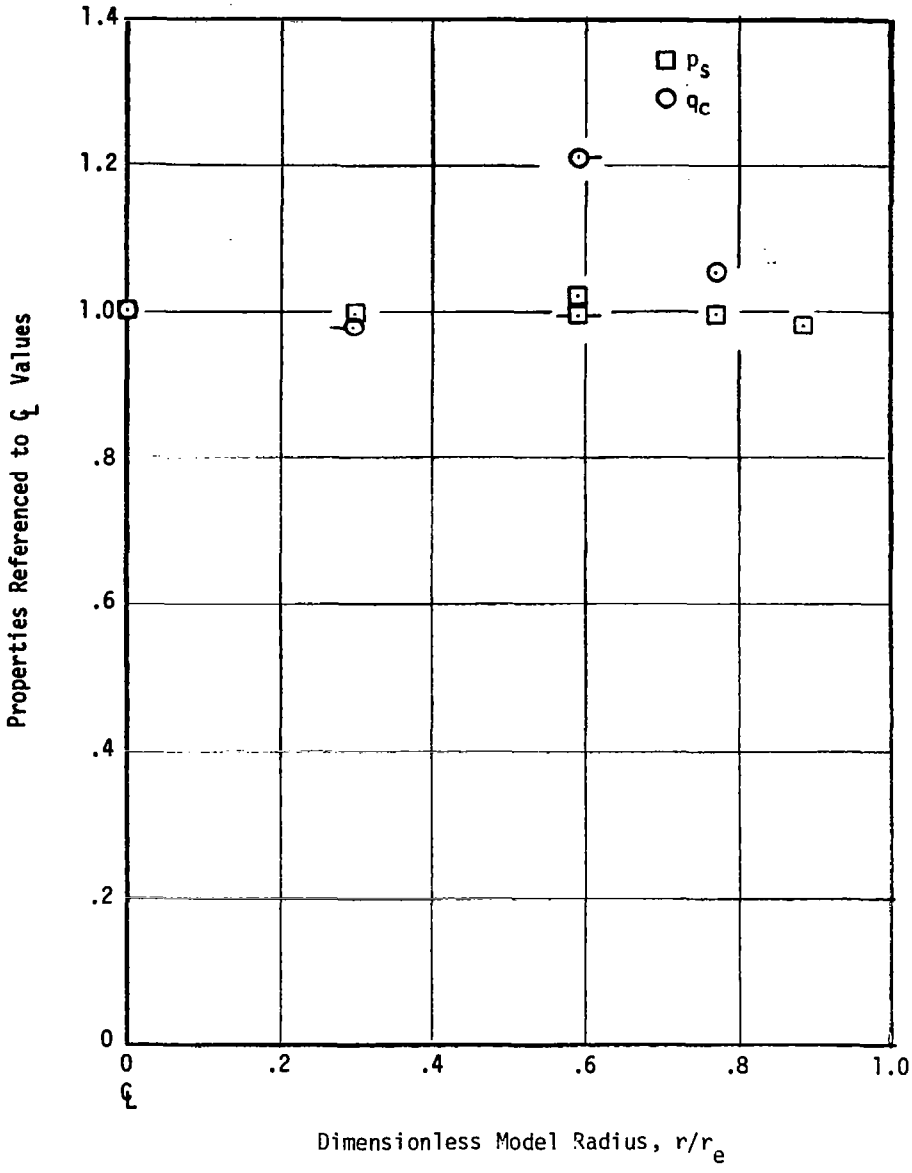

Figure C-9. (Continued)

c) Condition 3

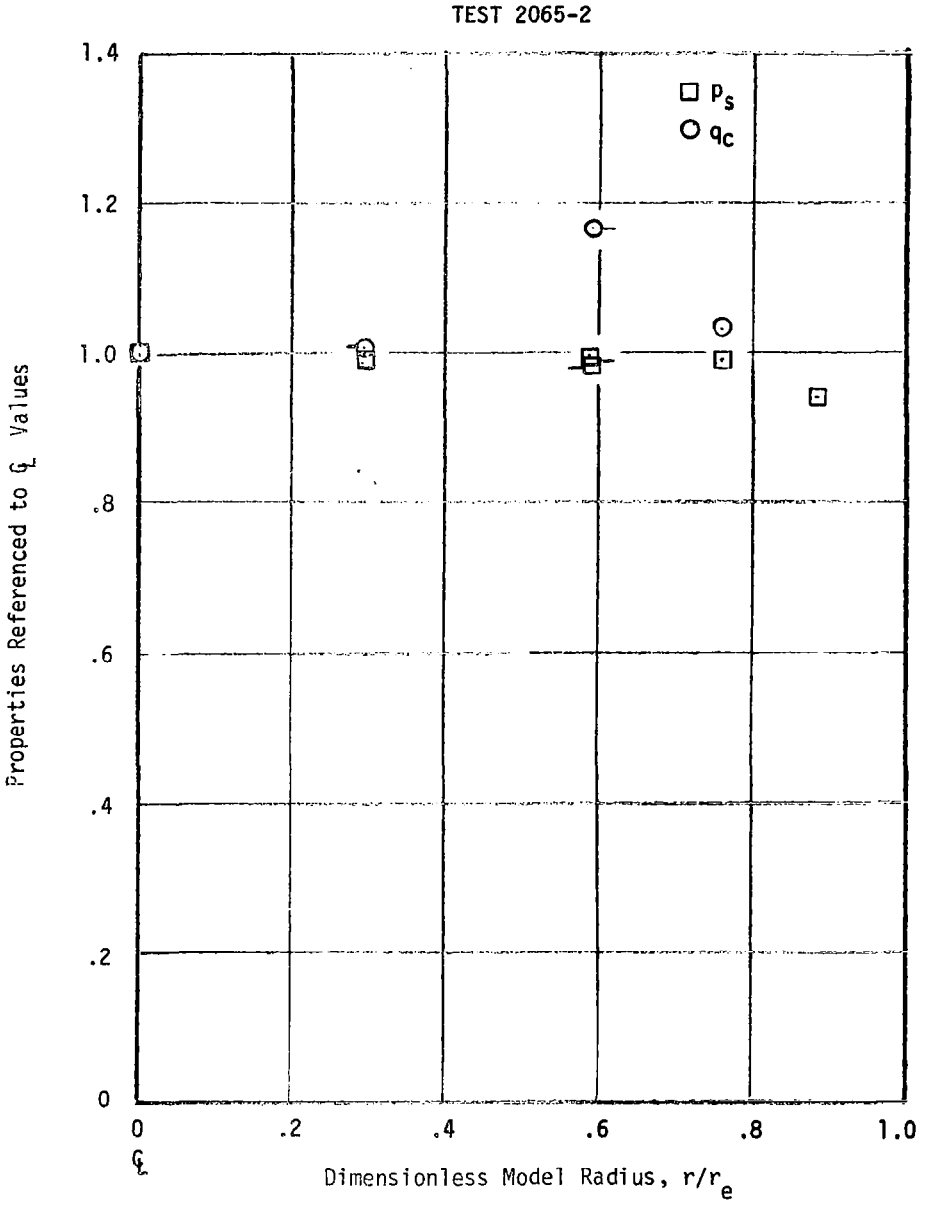

Figure C-9. (Continued)
d) Condition 4

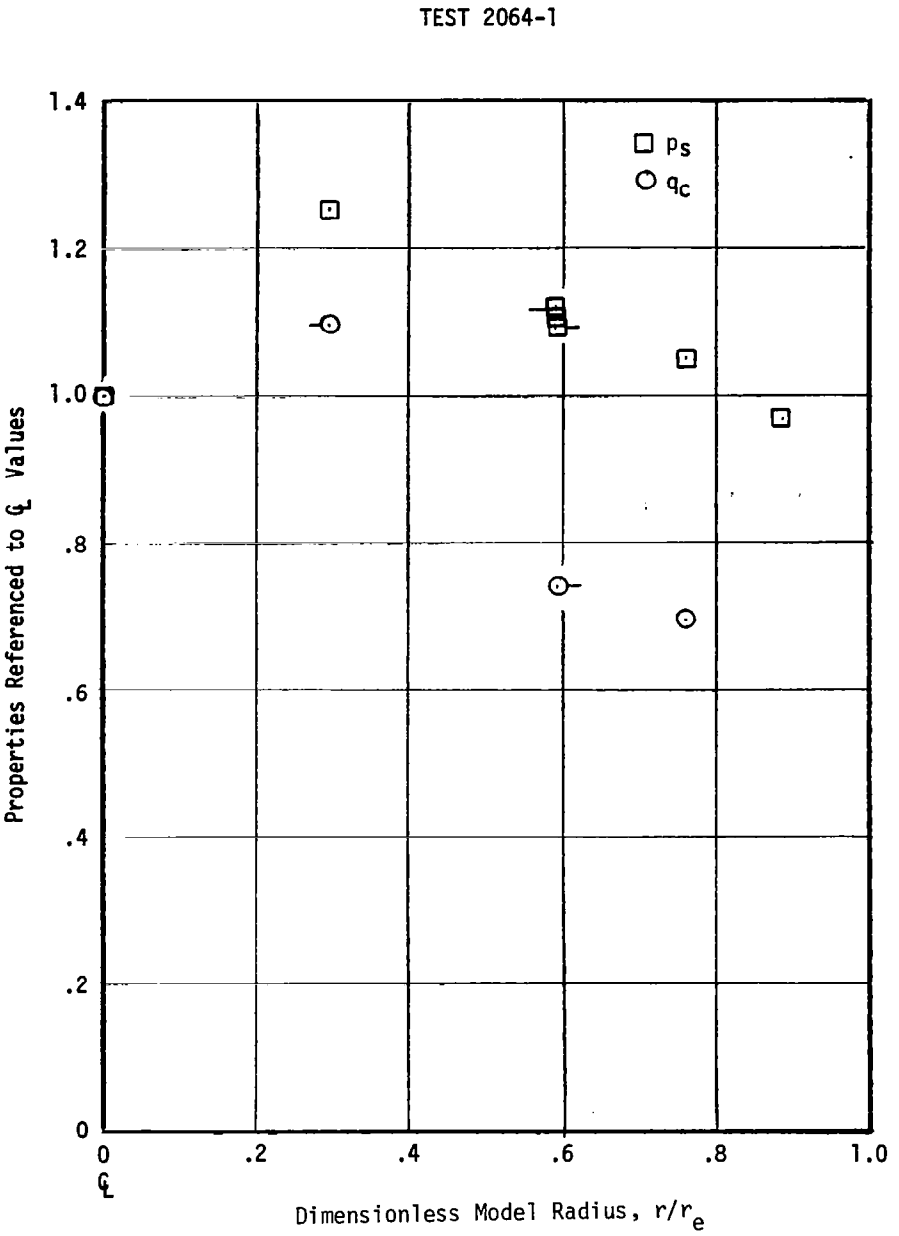

Figure C-9. (Continued)
e) Condition 8

Figure C-9. (Continued)
f) Condition 9 - See Figure 20

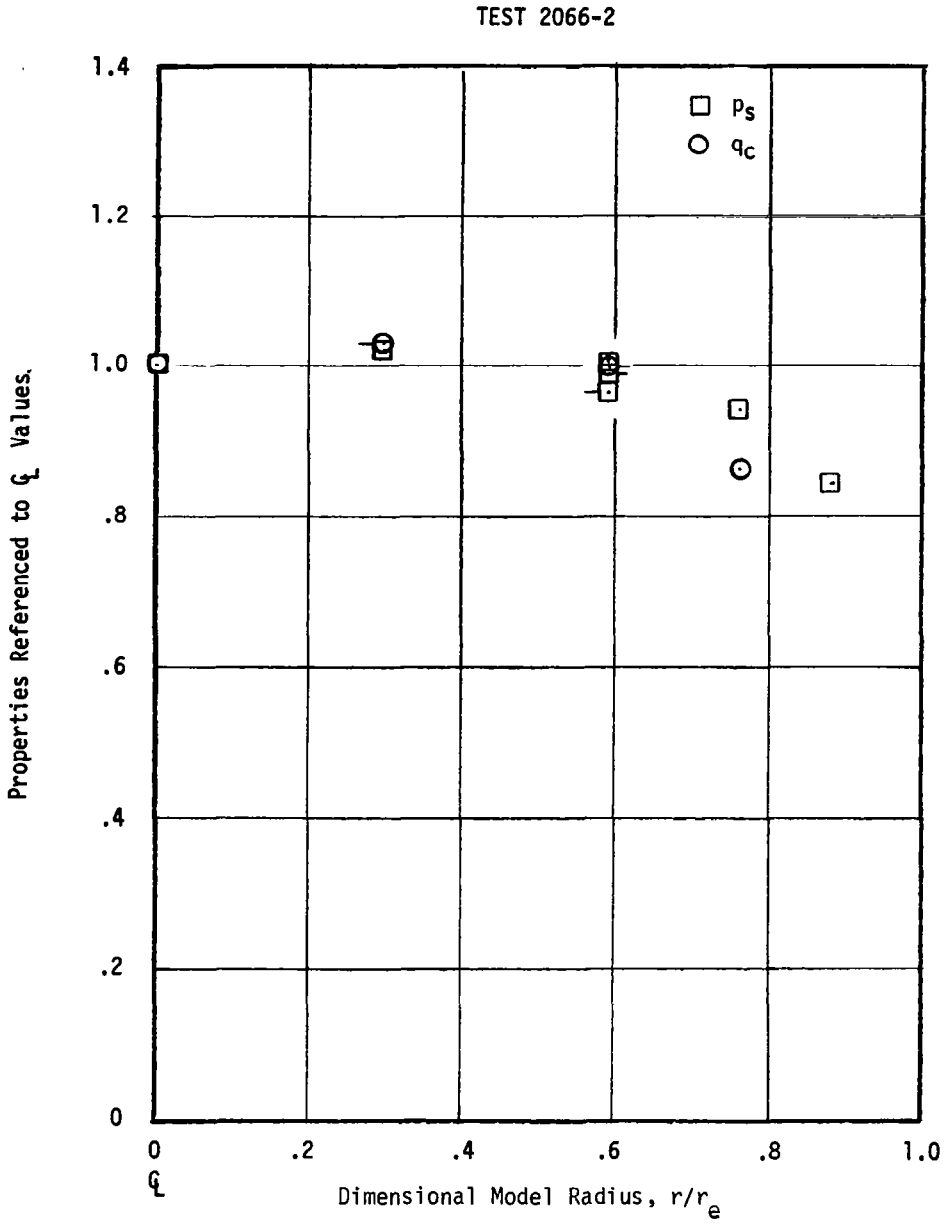

Figure C-9. (Continued)
g) Condition 10

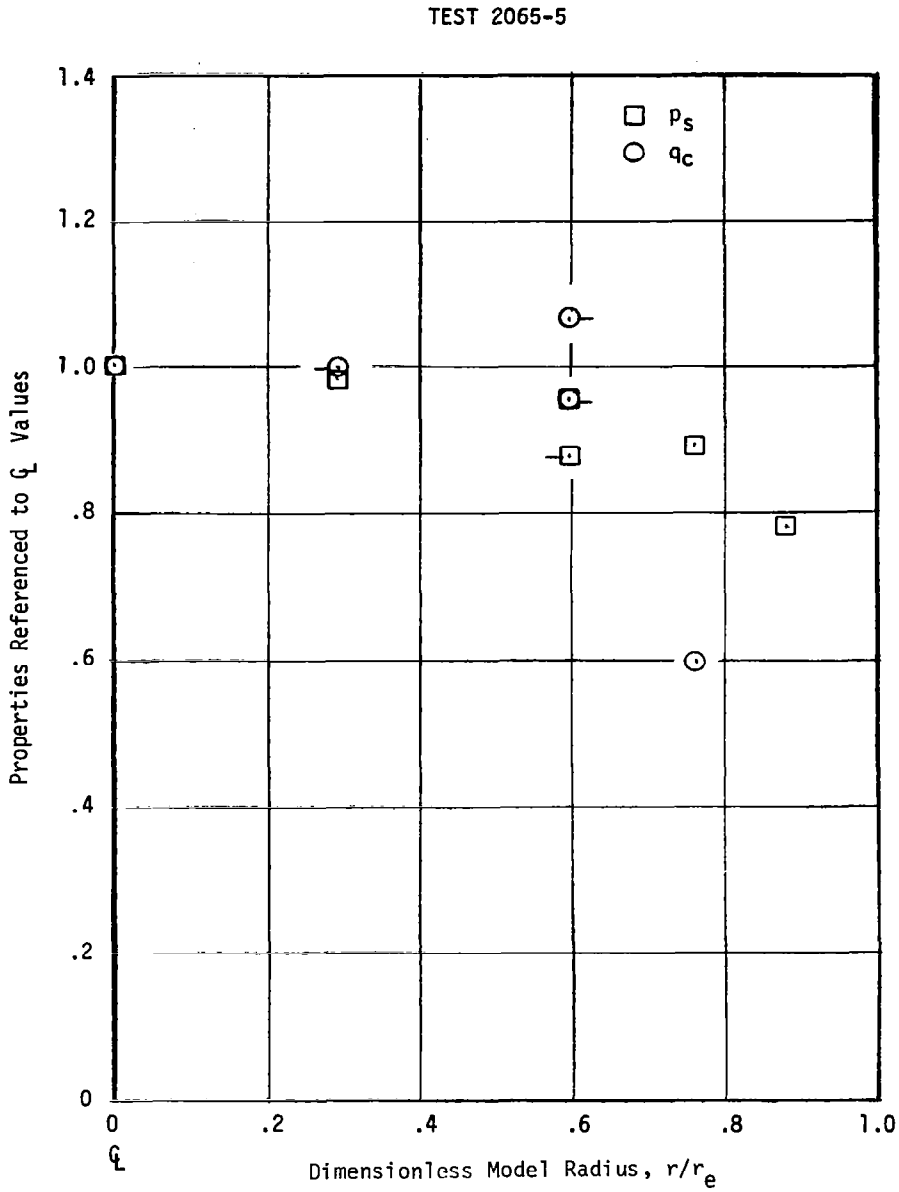

Figure C-9. (Concluded)
h) Condition 11

The measured distributions of heat flux and local pressure on the model surface are presented in Figure C-10 for all wedge model test conditions. The results for test conditions 5 and 13 are consistent but show an unusually large gradient in heat flux. No definitive explanation for this was found. Although the trends correspond to a laminar boundary layer ($q \sim s^{-1/2}$) starting at s/L = 0.35 to 0.40, there is no reason to believe that the boundary layer was somehow tripped at this location. The results for the other two test conditions (6 and 7) exhibit an unusually large scatter. The most logical explanations for this scatter appear to be as follows:

- As indicated in the sketch below, the interaction of the wedge shock and the nozzle exit shock (due to a slightly underexpanded nozzle condition) resulted in an interaction region on the downstream portion of the wedge. This interaction resulted in an increased heat flux in the downstream outboard regions and possibly a decreased flux in the central region

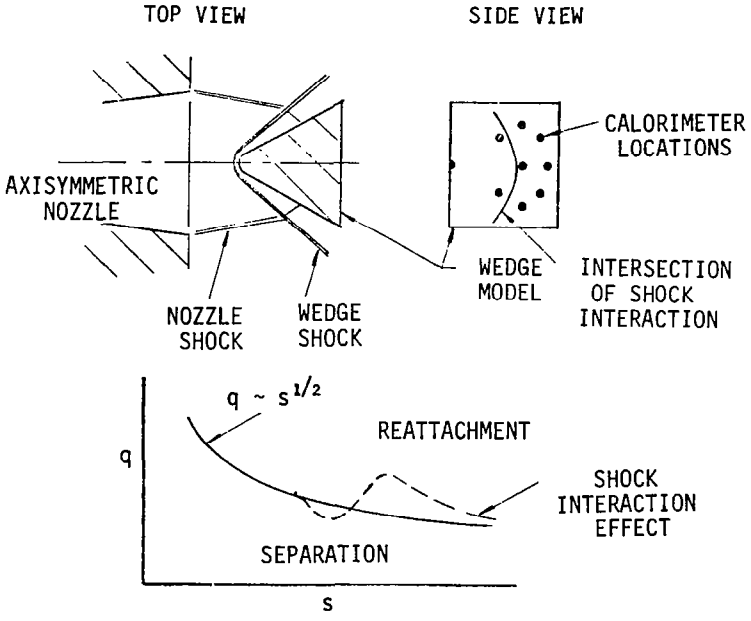

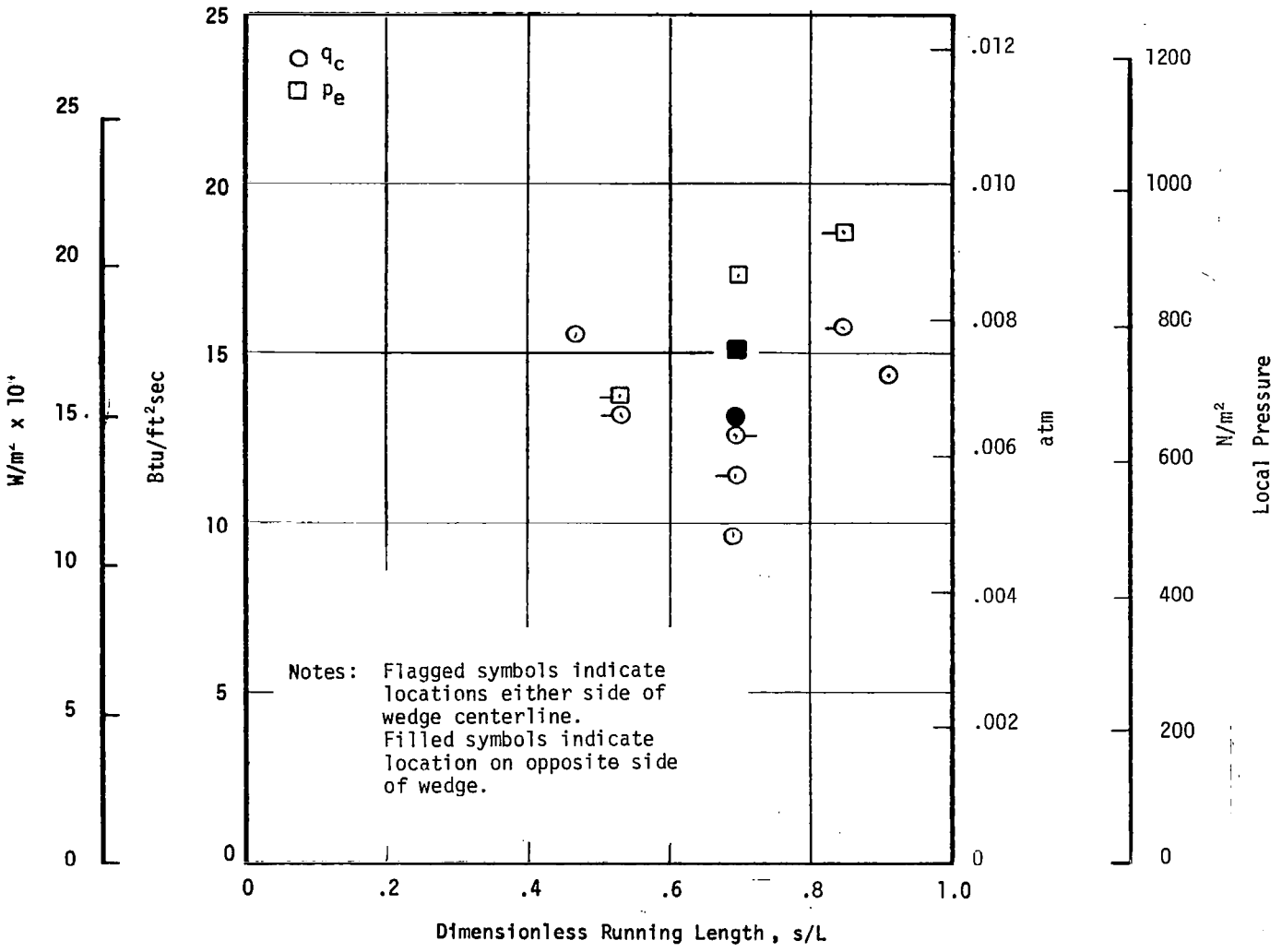

Figure C-10. (Continued)
b) Condition 6

Figure C-10. Wedge Model Distribution Results
a) Condition 5 - See Figure 21

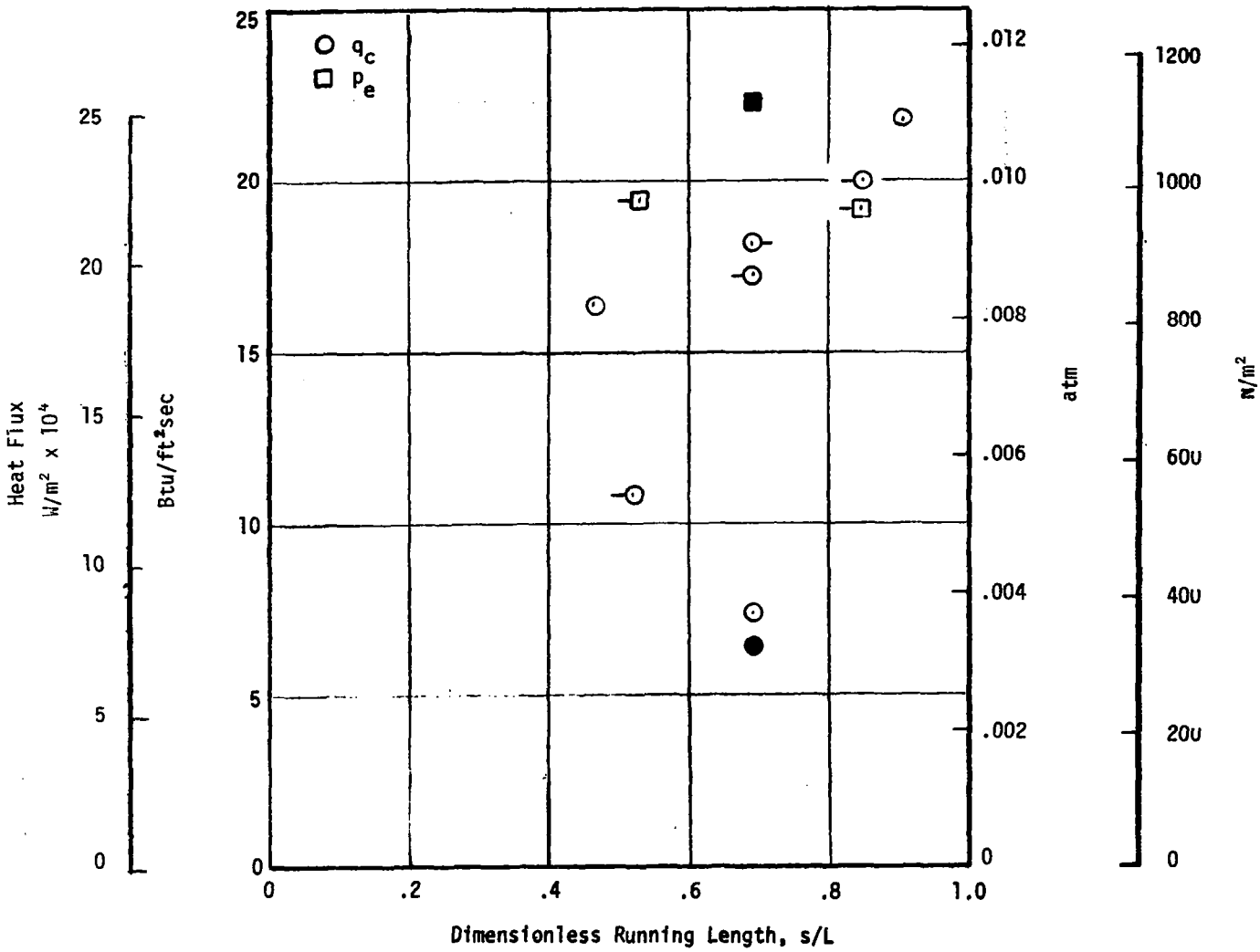

Figure C-10. (Continued)
c) Condition 7

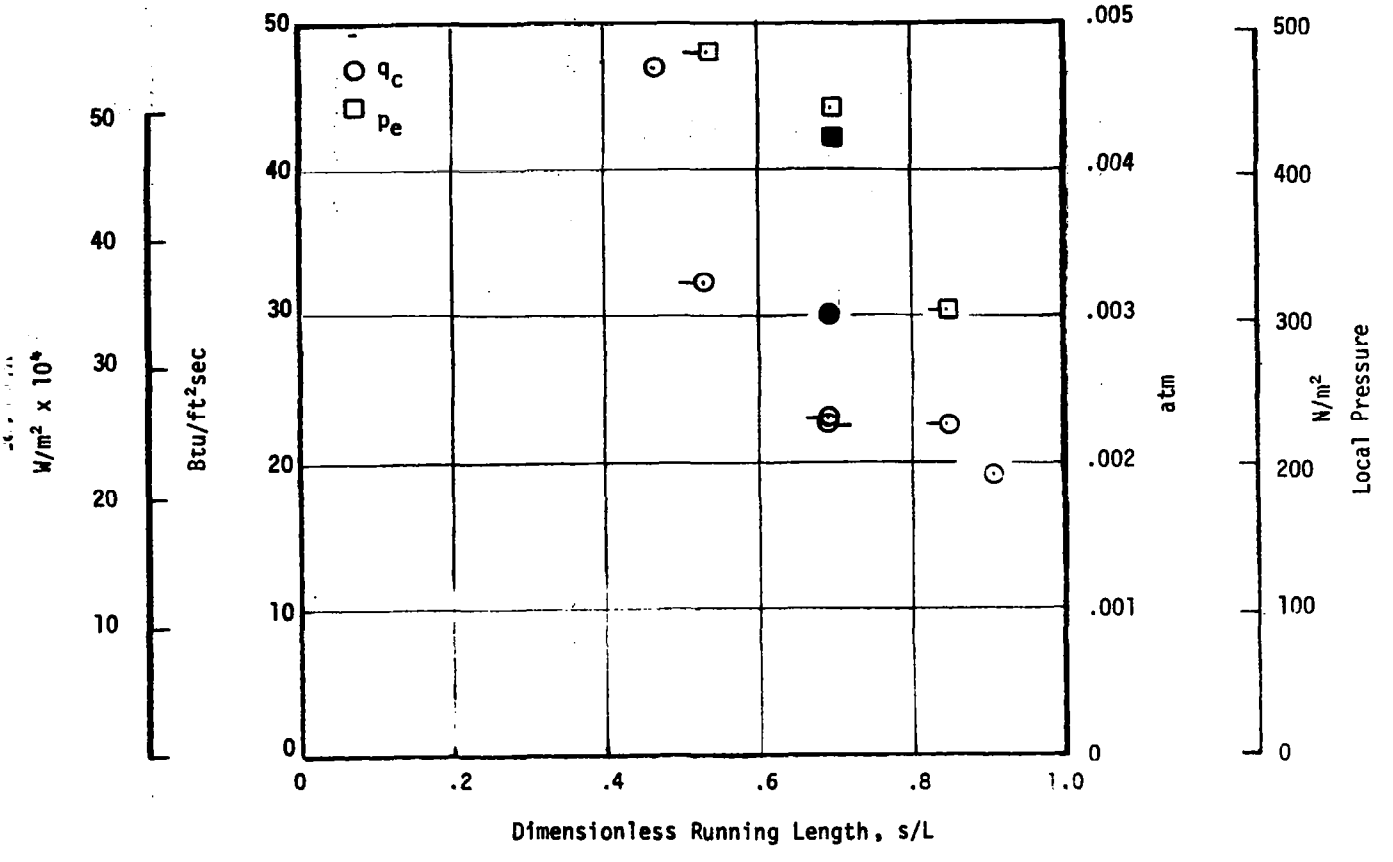

Figure C-10. (Concluded)
d) (Condition 13)

- Measured heat flux in the central region may have been lower than the actual flux due possibly to a calorimeter problem (e.g., calibration error, irregular surface[1]). This conclusion is supported by measurements of char depth in an earlier program which indicated no large central heat flux depression.

The shock interaction has been observed in motion pictures taken in a recent test program, but a quantitative explanation of its effect on the heat flux is not available.

C.4.4 Surface Catalycity

The surface catalycity calibration test restuls are presented in Table C-4 for all stagnation point test conditions[2] and in Figure 22 for all type 1-2 simulation test conditions on the larger stagnation point model configuration.

C.5 SAMPLE TEST RESULTS

All sample test results are summarized in tabular form as follows:

- Tables C-5 and C-8[3] - Test Conditions
- Tables C-6 and C-9 - Surface and Backwall Temperature
- Tables C-7 and C-10 - Mass Loss and Dimension Change Measurements
- Tables 9 and 10 - Summary of Test Conditions and Test Sample Results

The nominal test matrix was accomplished essentially as originally defined. In the stagnation point series an extra 5 cycle set on TD NiCr was performed because of a test sample failure during the fifth cycle of the first set. In the wedge series, four sample failures occurred (three TD NiCr samples due to high temperatures at the sample leading edge and one R512E/Cb-752 sample due to a momentary vacuum loss) but could not be repeated because no spare test samples were available.[4]

---

[1] A slightly dished surface was observed on both of the central region calorimeters.

[2] Note however that no valid results were obtained for test condition 8.

[3] Stagnation point model results and wedge model results, respectively.

[4] All spare TD NiCr and R512E/Cb-752 samples were used in preliminary checkouts of the wedge model and nominal test conditions.

TABLE C-4

SURFACE CATALYCITY CALIBRATION RESULTS

a) SI Units

Condition No.	Test No.	Model Heat Flux (W/m^2)	Heat Flux Ratio Noncat/Cat Wall	Stagnation Pressure (N/m^2)	Heat Flux Enthalpy (J/kg)
1,12	2068-3	1.83×10^5	.552	9.83×10^2	1.39×10^7
2	2067-1	1.97×10^5	.569	9.83×10^2	1.50×10^7
3	2068-1	1.10×10^5	.732	1.06×10^3	0.80×10^7
4	2068-2	1.13×10^5	.686	1.06×10^3	0.83×10^7
8	2069-1	3.40×10^5	-	1.92×10^2	5.85×10^7
9	2068-4	3.63×10^5	.471	9.83×10^2	2.76×10^7
10	2067-2	4.70×10^5	.491	9.42×10^2	3.65×10^7
11	2068-5	6.60×10^5	.476	9.83×10^2	5.02×10^7

Notes: Identical model configuration to test sample model.
Results for stagnation point model configuration only.

TABLE C-4 (CONCLUDED)

b) Conventional Units

Condition No.	Test No.	Model Heat Flux (Btu/ft^2sec)	Heat Flux Ratio Noncat/Cat Wall	Stagnation Pressure (atm)	Heat Flux Enthalpy (Btu/lb)
1,12	2068-3	16.1	.552	(.0097)	(3320)
2	2067-1	17.4	.569	(.0097	(3590)
3	2068-1	9.7	.732	(.0105)	(1920)
4	2068-2	10.0	.686	(.0105)	(1980)
8	2069-1	30.0	-	(.0019)	(13,990)
9	2068-4	32.0	.471	(.0097)	(6600)
10	2067-2	41.4	.491	(.0093)	(8720)
11	2068-5	58.2	.476	(.0097)	(12,010)

Notes: Identical model configuration to test sample model.
Results for stagnation point model configuration only.

TABLE C-5

TEST CONDITIONS FOR STAGNATION POINT MODEL TESTS

a) SI Units

TEST	TEST COND.	SIMULATION TYPE	MODEL DESCRIPTION	SAMPLE	SAMPLE MATERIAL	CYCLE	CURRENT (A)	CENTERLINE TOTAL ENTHALPY (J/kg)	AVERAGE TOTAL ENTHALPY EB (J/kg)	AVERAGE TOTAL ENTHALPY MB (J/kg)	CHAMBER PRESSURE (N/m^2)	GAS FLOW RATE (kg/sec)	OXYGEN MASS FRACTION	CATALYTIC WALL CONVECTIVE HEAT FLUX (W/m^2)[A]		STAGNATION PRESSURE (N/m^2)	COMMENTS
2073	1	1-2	4-3/4SP	45	TDN:CR	1	410	1.41×10^{7}	1.02×10^{7}	1.22×10^{7}	3.77×10^{4}	1.09×10^{-2}	.232	1.63×10^{5}	410	9.42×10^{2}	
2076				46			522	1.73×10^{7}	1.28×10^{7}	1.54×10^{7}	4.15×10^{4}			2.25×10^{5}	520	1.03×10^{3}	
2077						2	489	1.62×10^{7}	1.17×10^{7}	1.44×10^{7}	4.05×10^{4}			2.29×10^{5}	530		
						3	500	1.73×10^{7}	1.18×10^{7}	1.42×10^{7}	4.06×10^{4}			2.11×10^{5}	487	1.00×10^{3}	
						4	517	1.72×10^{7}	1.18×10^{7}	1.44×10^{7}	4.08×10^{4}			2.32×10^{5}	487	1.01×10^{3}	
						5	555	1.83×10^{7}	1.26×10^{7}	1.57×10^{7}	4.19×10^{4}			2.13×10^{5}	512	1.03×10^{3}	SAMPLE FAILED AT 20 MIN
2079				48		1	486	1.58×10^{7}	1.15×10^{7}	1.48×10^{7}	4.09×10^{4}			1.63×10^{5}	414	1.06×10^{3}	
2080						2	484	1.60×10^{7}	1.19×10^{7}	1.46×10^{7}	4.06×10^{4}			2.18×10^{5}	484	1.03×10^{3}	
						3	481	1.58×10^{7}	1.16×10^{7}	1.46×10^{7}	4.08×10^{4}			2.17×10^{5}	476	1.04×10^{3}	
						4	480	1.58×10^{7}	1.16×10^{7}	1.50×10^{7}	4.10×10^{4}			2.13×10^{5}	477		
						5	491	1.62×10^{7}	1.18×10^{7}	1.46×10^{7}	4.13×10^{4}			2.17×10^{5}	482	1.03×10^{3}	
2078	2	3		47		1	410	1.50×10^{7}	1.08×10^{7}	1.09×10^{7}	3.62×10^{4}		.062	2.00×10^{5}	410	1.00×10^{3}	
2081				49			427	1.57×10^{7}	1.11×10^{7}	1.17×10^{7}	3.57×10^{4}			1.97×10^{5}	409	9.93×10^{2}	
2090	3	1-2		50			282	0.80×10^{7}	0.62×10^{7}	0.73×10^{7}	4.94×10^{4}	1.72×10^{-2}	.232	1.08×10^{5}	279	1.06×10^{3}	
2091				51			283	0.80×10^{7}	0.61×10^{7}	0.74×10^{7}	4.91×10^{4}			1.09×10^{5}	281		
2076	4		1-1/4SP	41			316	0.86×10^{7}	0.72×10^{7}	0.82×10^{7}	4.48×10^{4}	1.50×10^{-2}		1.11×10^{5}	312	1.04×10^{3}	
2077				42			386	1.02×10^{7}	0.86×10^{7}	0.97×10^{7}	4.80×10^{4}			1.10×10^{5}	313		
2098	8	1	4-34SP	36	R512E/		892	6.44×10^{7}	3.10×10^{7}	3.65×10^{7}	6.59×10^{3}	1.22×10^{-3}		3.96×10^{5}	889	1.62×10^{2}	
2101				37	CB-752		899	6.07×10^{7}	2.51×10^{7}	3.23×10^{7}	6.28×10^{3}			3.40×10^{5}	899	1.32×10^{2}	
				38			1,000	6.78×10^{7}	3.53×10^{7}	3.21×10^{7}	6.18×10^{3}			3.42×10^{5}	891		
						2	989	7.86×10^{7}	3.65×10^{7}	3.64×10^{7}	6.38×10^{3}			3.31×10^{5}	893	1.72×10^{2}	
						3	1,000	7.70×10^{7}	3.24×10^{7}	3.46×10^{7}	6.48×10^{3}			3.31×10^{5}	1,000	1.42×10^{2}	
						4	986	7.28×10^{7}	4.64×10^{7}	3.87×10^{7}	6.59×10^{3}			3.93×10^{5}	988	1.52×10^{2}	
						5	990	7.61×10^{7}	4.48×10^{7}	3.37×10^{7}	6.28×10^{3}			3.76×10^{5}	986	1.42×10^{2}	
2072	9	1-2		26		1	638	2.84×10^{7}	1.71×10^{7}	2.14×10^{7}	3.16×10^{4}	7.26×10^{-3}		3.68×10^{5}	638	9.32×10^{2}	
2074				27			740	3.30×10^{7}	1.92×10^{7}	2.32×10^{7}	3.28×10^{4}			3.65×10^{5}	645		
2082	10	3		28			(650)	3.66×10^{7}	--	--	3.10×10^{4}		.062	4.58×10^{5}	634	9.52×10^{2}	
2083				29			776	4.37×10^{7}	2.27×10^{7}	2.36×10^{7}	3.29×10^{4}			4.62×10^{5}	--		
2085	1	1-2		30			411	1.38×10^{7}	1.05×10^{7}	1.24×10^{7}	3.84×10^{4}	1.09×10^{-2}	.232	1.09×10^{5}	407	1.00×10^{3}	
2087				31			500	1.64×10^{7}	1.23×10^{7}	1.56×10^{7}	4.19×10^{4}			2.45×10^{5}	502	1.05×10^{3}	
2092	11			33			814	5.00×10^{7}	2.18×10^{7}	3.01×10^{7}	3.00×10^{4}	5.99×10^{-3}		5.20×10^{5}	814	9.73×10^{2}	
2095				35			946	5.72×10^{7}	2.71×10^{7}	3.30×10^{7}	3.13×10^{4}			6.93×10^{5}	947	1.05×10^{3}	
2088	12		1-1/4SP	5			411	1.54×10^{7}	1.08×10^{7}	1.24×10^{7}	3.83×10^{4}	1.09×10^{-2}		2.00×10^{5}	414	1.00×10^{3}	
2087				6			715	2.67×10^{7}	1.66×10^{7}	2.05×10^{7}	4.66×10^{4}			3.54×10^{5}	711	1.06×10^{3}	
2098	8		4-3/4SP	18	VH-109/		887	5.98×10^{7}	3.04×10^{7}	3.54×10^{7}	6.59×10^{3}	1.22×10^{-3}		3.26×10^{5}	882	1.82×10^{3}	
2100				19	C129Y		998	7.20×10^{7}	3.95×10^{7}	3.41×10^{7}	6.38×10^{3}			3.90×10^{5}	887	1.62×10^{2}	
2103						2	995	7.36×10^{7}	3.88×10^{7}	3.58×10^{7}	6.69×10^{3}			3.48×10^{5}	987	1.52×10^{2}	
						3	1,010	7.49×10^{7}	3.71×10^{7}	3.65×10^{7}	6.59×10^{3}			3.89×10^{5}	1,010		
						4	1,010	7.74×10^{7}	3.51×10^{7}	3.53×10^{7}	6.59×10^{3}			3.86×10^{5}	1,000	1.42×10^{2}	
						5	1,000	7.70×10^{7}	3.23×10^{7}	3.18×10^{7}	6.28×10^{3}			3.84×10^{5}	1,000		
2071	9			10		1	643	2.50×10^{7}	1.69×10^{7}	2.12×10^{7}	3.15×10^{4}	7.26×10^{-3}		3.69×10^{5}	643	9.22×10^{2}	
2075				11			765	3.44×10^{7}	1.91×10^{7}	2.36×10^{7}	3.29×10^{4}			3.61×10^{5}	--		
2084	10	3		12			641	3.64×10^{7}	1.98×10^{7}	2.04×10^{7}	3.13×10^{4}		.062	4.57×10^{5}	639	9.52×10^{2}	
2085				13			886	5.00×10^{7}	2.64×10^{7}	2.78×10^{7}	3.51×10^{4}			4.71×10^{5}	640		
2093	1	1-2		15			408	1.41×10^{7}	1.05×10^{7}	1.32×10^{7}	3.91×10^{4}	1.09×10^{-2}	.232	1.99×10^{5}	403	1.00×10^{3}	
2094				17			540	1.76×10^{7}	1.31×10^{7}	1.66×10^{7}	4.31×10^{4}			2.81×10^{5}	560	1.05×10^{3}	
2104	11			20			811	4.95×10^{7}	2.43×10^{7}	2.93×10^{7}	2.96×10^{4}	5.99×10^{-3}		6.88×10^{5}	808	1.01×10^{3}	
2103				21			891	5.36×10^{7}	2.75×10^{7}	3.35×10^{7}	3.13×10^{4}			8.22×10^{5}	892	1.05×10^{3}	
2093	12		1-1/4SP	3			410	1.51×10^{7}	1.05×10^{7}	1.32×10^{7}	3.91×10^{4}	1.09×10^{-2}		2.03×10^{5}	411	1.01×10^{3}	
2094				4			848	3.10×10^{7}	1.84×10^{7}	2.23×10^{7}	4.82×10^{4}			4.31×10^{5}	825	1.07×10^{3}	

A) SECOND NUMBER IS CURRENT IN AMPS AT WHICH TABULATED HEAT FLUX WAS MEASURED

TABLE C-5 (CONCLUDED)
b) Conventional Units

TEST	TEST COND.	SIMULATION TYPE	MODEL DESCRIPTION	SAMPLE	SAMPLE MATERIAL	CYCLE	CURRENT (amps)	CENTERLINE TOTAL ENTHALPY (Btu/lb)	AVERAGE TOTAL ENTHALPY EB (Btu/lb)	AVERAGE TOTAL ENTHALPY MB (Btu/lb)	CHAMBER PRESSURE (atm)	GAS FLOW RATE (lb/sec)	OXGYEN MASS FRACTION	CATALYTIC WALL CONVECTIVE HEAT FLUX [A] (Btu/ft²sec)		STAGNATION PRESSURE (atm)	COMMENTS
2073	1	1-2	4-3/4 SP	45	TD NiCr	1	410	3,380	2,430	2,910	.372	.024	.232	14.4	410	.0093	
2076				46			522	4,130	3,050	3,680	.410			19.8	520	.0102	
2077						2	489	3,860	2,790	3,430	.400			20.2	530		
						3	500	4,130	2,810	3,400	.401			18.6	487	.0099	
						4	517	4,120	2,830	3,430	.403			20.4	487	.0100	
						5	555	4,370	3,020	3,750	.414			18.8	512	.0102	SAMPLE FAILED AT 20 MIN
2079				48		1	486	3,770	2,760	3,550	.404			14.4	414	.0105	
2080						2	484	3,830	2,850	3,480	.401			19.2	484	.0102	
						3	481	3,770	2,780	3,490	.403			19.1	476	.0103	
						4	480	3,770	2,770	3,580	.405			18.8	477		
						5	491	3,860	2,820	3,480	.408			19.1	482	.0102	
2078	2	3		47		1	410	3,590	2,570	2,600	.357		.062	17.6	410	.0099	
2081				49			427	3,760	2,650	2,790	.352			17.4	409	.0098	
2090	3	1-2		50			282	1,910	1,480	1,750	.486	.038	.232	9.5	279	.0105	
2091				51			283	1,910	1,460	1,760	.485			9.6	281		
2076	4		1-1/4 SP	41			316	2,050	1,730	1,960	.442	.033		9.8	312	.0103	
2077				42			386	2,440	2,060	2,330	.474			9.7	313		
2096	8	1	4-3/4 SP	36	R512E/		892	15,400	7,400	8,730	.065	.0027		34.9	889	.0016	
2097				37	Cb-752		899	14,500	6,010	7,710	.062			30.0	899	.0018	
2099				38			1,000	16,200	8,440	7,670	.061			30.1	891		
2101						2	989	16,600	8,720	8,690	.063			29.2	893	.0017	
						3	1,000	18,400	7,740	8,270	.064			29.2	1,000	.0014	
						4	986	17,400	11,100	9,260	.065			34.6	988	.0015	
						5	990	18,200	10,700	8,660	.062			33.1	986	.0014	
2072	9	1-2		26		1	638	6,800	4,090	5,120	.312	.016		32.4	638	.0092	
2074				27			740	7,880	4,600	5,550	.324			32.2	645		
2082	10	3		28			(650)	8,740	--	--	.306		.062	40.4	634	.0094	
2083				29			776	10,440	5,420	5,650	.325			40.7	--		
2086	1	1-2		30			411	3,290	2,520	2,940	.379	.024	.232	17.5	407	.0099	
2087				31			500	3,910	2,930	3,730	.414			21.6	502	.0104	
2092	11			33			814	11,950	5,210	7,200	.296	.0132		45.8	814	.0096	
2095				35			946	13,680	6,480	7,860	.309			61.1	947	.0104	
2086	12		1-1/4 SP	5			411	3,670	2,570	2,970	.378	.024		17.6	414	.0099	
2087				6			715	6,380	3,970	4,910	.460			31.2	711	.0105	
2098	8	1	4-3/4 SP	18	VH-109/		887	14,300	7,270	8,470	.065	.0027		28.7	882	.0018	
2100				19	C129Y		998	17,200	9,430	8,160	.063			34.4	887	.0016	
2103						2	995	17,600	9,280	8,560	.066			30.7	987	.0015	
						3	1,010	17,900	8,870	8,720	.065			34.3	1,010		
						4	1,010	18,500	8,400	8,440	.065			34.0	1,000	.0014	
						5	1,000	18,400	7,710	7,590	.062			33.8	1,000		
2071	9	1-2		10		1	643	6,140	4,050	5,070	.311	.016		32.5	643	.0091	
2075				11			765	8,220	4,560	5,650	.325			31.8	--		
2084	10	3		12			641	8,690	4,730	4,880	.305		.062	40.3	639	.0094	
2085				13			886	11,950	6,310	6,640	.346			41.5	640		
2093	1	1-2		15			408	3,370	2,500	3,150	.386	.024	.232	17.5	403	.0099	
2094				17			540	4,200	3,140	3,960	.425			24.8	560	.0104	
2104	11			20			811	11,640	5,800	7,010	.292	.0132		60.6	808	.0100	
2105				21			891	12,600	6,570	8,090	.309			72.4	892	.0104	
2093	12		1-1/4 SP	3			410	3,620	2,510	3,150	.386	.024		17.9	411	.0100	
2094				4			848	7,420	4,410	5,330	.476			38.0	825	.0106	

A) SECOND NUMBER IS CURRENT IN AMPS AT WHICH TABULATED HEAT FLUX WAS MEASURED

TABLE C-6

TEMPERATURE MEASUREMENTS FOR STAGNATION POINT MODEL TESTS

a) SI Units

TEST	TEST COND.	SIMULATION TYPE	MODEL DESCRIPTION	SAMPLE	SAMPLE MATERIAL	CYCLE	TD-9C			TD-7			TD-9B		THERMOGAGE		BACKWALL TEMPERATURE		COMMENTS
							CENTERLINE (°K)	RANGE (°K)	EMISSIVITY (-)	CENTERLINE (°K)	RANGE (°K)	EMISSIVITY (-)	CENTERLINE (°K)	EMISSIVITY (-)	CENTERLINE (°K)	EMISSIVITY (-)	CENTERLINE (°K)	RANGE (°K)	
2073	1	1-2	4-3/4 SP	45	TD NiCr	1	1290	1500-1270	.75	1280		.61	1280	.75	1360	.75	--	1270-1110	
2076				46			1370	1590-1270		1400			1420		1470		1320	1390-1320	
2077						2	1380	1590-1370		1360			1470		1470		1300	1370-1300	
						3	1370	1550-1370		1360			1460		1470		1290	1330-1290	
						4	1360	1490-1360		1380			1460		1480		--	1310- --	
						5	1370	1610-1370		1410			1480		1510		--	1350- --	SAMPLE FAILED AT 20 MIN
2079				48		1	1370	1520-1370		1390			1450		1470		1330	1360-1330	
2080						2	(1290)	1330-1270		1380			1450		1340		1280	1340-1280	
						3	1380	1510-1370		1370			1450		1350		1290	1340-1290	
						4	1370	1470-1330		1370			1450		1350		1280	1340-1280	
						5	1380	1460-1290		1390			1470		1350		1300	1360-1300	
2078	2	3		47		1	1370	1440-1280		1360			1470		1370		1210	1230-1200	
2081				49			1370	1520-1370		1360			1430		1270		1250	1270-1250	
2090	3	1-2		50			--	--	--	1170	1230-1130		--	--	1180		1050	1090-1050	
2091				51			--	--	--	1130	1220-1090		--	--	1190		1020	1090-1020	
2076	4		1-1/4 SP	41			<1260	--	.75	1290			1300	.75	1180		1160	--	
2077				42			1380	--		1380			1480		1270		1270	--	
2096	8	1	4-3/4 SP	36	R512E/		1460	1560-1320		1450		.75	1560		1540		1460	1460-1330	
2097				37	Cb-752		1390	1390-1260		1390			1480		1420		1330	1330-1270	
2099				38			1540	1540-1270		1500			1610		1540		1490	1490-1390	
2101						2	--	(1470-1330)		(1440)			1590		1370		1470	1470-1380	
						3	1500	1500-1330		1420			1580		1360		1470	1470-1500	
						4	1470	1540-1340		(1400)			1610		1360		1530	1530-1380	
						5	1580	1580-1340		(1400)			1640		1370		1560	1560-1400	
2072	9	1-2		26		1	1510	1590-1450		1490			1580		1580		1500	1500-1480	
2074				27			1590	1690-1520		1540			1660		1670		--	--	
2082	10	3		28			1510	1570-1440		1490			1580		1380		1440	1440-1440	
2083				29			1580	1600-1510		1520			1640		1420		1420	1500-1420	
2086	1	1-2		30			1290	1330-1280		1280			1330		1270		1200	1240-1200	
2087				31			1360	1390-1350		1360			1420		1440		1300	1350-1300	
2092	11			33			1610	1650-1530		1530			1700		1670		1620	1620-1580	
2095				35			1620	1680-1520		1560			1330		1700		1660	1660-1640	
2086	12		1-1/4 SP	5			1350	--		1320			1410		1260		1270	--	
2087				6			1570	--		1490			1640		1420		1560	--	
2098	8	1	4-3/4 SP	18	VH-109/		--	1360-1260		1320			1420		1380		1290	1290-1220	
2100				19	C129Y	1	1490	1490-1260		1450			1540		1340		1460	1460-1370	
2103						2	1420	1430-1300		1370			1520		1400		1420	1420-1320	
						3	1430	1440-1270		1380			1530		1420		1440	1440-1340	
						4	1420	1440-1290		1380			1530		1420		1466	1460-1360	
						5	1390	1420-1290		1350			1510		1400		1430	1430-1340	
2071	9	1-2		10		1	1430	1500-1370	.75	1450			1520		1520		--	1470-1460	
2075				11			1590	1660-1460		1490			1620		1660		--	--	
2084	10	3		12			1410	1480-1370		1400			1470		1340		1340	1340-1330	
2085				13			1550	1580-1460		1520			1320		1390		1520	1520-1500	
2093	1	1-2		15			1270	1370-1260		1300			1330		1350		1200	1260-1200	
2094				17			(1290)	1320-1260		1370			1440		1420		1360	1400-1360	
2104	11			20			1590	1660-1520		1670			1700		1670		1620	1620-1620	
2105				21			1830	1670-1490		1530			1670		1670		--	1590- --	
2093	12		1-1/4 SP	3			1300	--		1300			1380		1230		1130	--	
2094				4			(1320)	--		1530			1680		1380		1620	--	

TABLE C-6 (CONCLUDED)

b) Conventional Units

TEST	TEST COND.	SIMULATION TYPE	MODEL DESCRIPTION	SAMPLE	SAMPLE MATERIAL	CYCLE	TD-9C			TD-7			TD-9B		THERMOGAGE		BACKWALL TEMPERATURE		COMMENTS
							CENTERLINE (°F)	RANGE (°F)	EMISSIVITY (°F)	CENTERLINE	RANGE (°F)	EMISSIVITY (°F)	CENTERLINE (°F)	EMISSIVITY (-)	CENTERLINE (°F)	EMISSIVITY (-)	CENTERLINE (°F)	RANGE (°F)	
2073	1	1-2	4-3/4 SP	45	TD NiCr	1	1860	2240-1820	.75	1850		.61	1850	.75	1990	.75	--	1820-1540	
2076				46		1	2010	2400-2000		2070			2100		2160		1920	20-0-1920	
2077						2	2030	2400-2010		1980			2160		2160		1880	2000-1880	
						3	2010	2330-2060		1980			2170		2160		1860	1940-1860	
						4	1980	2230-1980		2020			2170		2200		--	1900- --	
						5	2010	2440-2000		2000			2210		2260		--	1970- --	SAMPLE FAILED AT 20 MIN
2079				48		1	2010	2280-2000		2040			2150		2120		1940	1990-1940	
2080						2	(1960)	1930-1830		2020			2150		1960		1840	1960-1840	
						3	2020	2260-2000		2010			2150		1970		1860	1950-1860	
						4	2000	2150-1930		2010			2150		1970		1850	1950-1850	
						5	2029	2160-1970		2040			2160		1970		1880	1990-1880	
2078	2	3		47		1	2010	2140-1850		1990			2160		2000		1720	1760-1700	
2081	1	1		49		1	2010	2280-2000		1980			2120		1820		1790	1820-1790	
2083	3	1-2		50			--	--	--	1640	1750-1580		--	--	1670		1430	1500-1430	
2091				51			--	--	--	1590	1750-1[illegible]		--	--	1690		1[illegible]	1510-1380	
2076	4		1-1/4 SP	41			<1800		.75	1860			1690	.75	1680		1630	--	
2077	1			42			2030	--		2030			2200		1710		1820	--	
2086	2	1	4-3/4 SP	36	RS138/		2160	2350-1910		2150		.75	2290		2310		2170	2170-1940	
2087				37	Cb-752		2040	2260-1810		2040			2200		2100		1940	1940-1620	
2089				38			2310	2310-1820		2240			2440		2320		2220	2220-2050	
2101						2	--	(2180-1940)		(2130)			2410		2020		2190	2190-2020	
						3	2250	2250-1940		(2050)			2393		1990		2190	2190-2020	
						4	2290	2310-1990		(2070)			2440		1990		2290	2290-2070	
						5	2330	2330-1990		(2070)			2500		2010		2350	2350-2070	
2072	9	1-2		26		1	2260	2410-2150		2220			2300		2330		2240	2250-2210	
2074				27			2400	2580-2280		2310			2530		2550		--	--	
2082	10	3		28			2260	2580-2140		2220			2350		2020		2140	2140-2130	
2092				29			2350	2430-2260		2280			[illegible]		2100		2100	2250-2100	
2096	1	1-2		30			1860	1930-1840		1840			1940		1830		1710	1780-1710	
2087				31			1950	2050-1970		1930			2100		2140		1880	1970-1880	
2062	11			33			2440	2610-2300		2330			2600		2550		2450	2450-2380	
2085				35			2460	2570-2280		2340			1930		2610		2520	2530-2500	
2068	12		1-1/4 SP	5			1970	--		1920			2080		1810		1830	--	
2087				6			2370	--		2220			2500		2100		2240	--	
2088	8	1	4-3/4 SP	18	WF-103/		--	1920-1810		1920			2100		2030		1860	1860-1770	
2100				19	C129Y		2220	2220-1810		2150			2320		1950		2170	2170-2000	
2103						2	2100	2120-1830		2010			2270		2070		2090	2090-1920	
						3	2120	2130-1800		2020			2290		2030		2140	2140-1960	
						4	2080	2130-1970		2020			2300		2100		2160	2160-1980	
						5	2090	2100-1850		1970			2260		2070		2120	2120-1950	
2071	9	1-2		10		1	2110	2250-2010		2150			2280		2270		--	2190-2170	
2075				11			2400	2530-2160		2220			2460		2530		--	--	
2084	10	3		12			2000	2210-2010		2070			2190		1900		1960	1960-1930	
2095				13			2330	2380-2170		2270			1920		2050		2270	2270-2250	
2093	1	1-2		15			1820	2010-1810		1880			1940		1970		1710	1800-1710	
2094				17			(1800)	1920-1810		2010			2130		2160		1930	2060-1900	
2104	11			20			2410	2520-2270		2250			2610		2540		2460	2460-2450	
2105				21			2390	2550-2220		2280			2500		2540		--	2410- --	
2098	12		1-1/4 SP	3			1880	--		1880			2000		1750		1570	--	
2094	1			4			(1910)	--		2000			2570		2050		2490	--	

TABLE C-7

MASS LOSS AND SURFACE RECESSION MEASUREMENTS FOR STAGNATION POINT MODEL TESTS

a) SI Units

TEST	TEST COND.	SIMULATION TYPE	MODEL DESCRIPTION	SAMPLE	SAMPLE MATERIAL	CYCLE	CUMULATIVE EXPOSURE TIME (min)	MASS CHANGE (kg x 10^3)	CUMULATIVE MASS CHANGE (kg x 10^3)	AVERAGE MASS CHANGE RATE (kg/m^2sec)	DIMENSION CHANGE (meters)	CUMULATIVE DIMENSION CHANGE (meters)	AVERAGE SURF RECESS RATE (meters)	COMMENTS
2073	1	1-2	4-3/4 SP	45	TD NiCr	1	.30	.046	.046	3.06×10^{-6}	2.54×10^{-6}	2.54×10^{-6}	1.41×10^{-9}	
2076				46				.046	.046	3.06×10^{-6}	-5.08×10^{-6}	-5.08×10^{-6}	-2.82×10^{-9}	
2077						2	60							
						3	90							
						4	120							
						5	140	-4.28	-4.23	-6.22×10^{-6}	-1.02×10^{-5}	-1.52×10^{-5}	-2.12×10^{-9}	
2079				48		1	30	.031	.031	2.22×10^{-6}	-4.06×10^{-6}	-4.06×10^{-6}	-2.26×10^{-9}	
2080						2	60							
						3	90							
						4	120							
						5	150	-.049	-.018	-2.78×10^{-7}	-7.62×10^{-6}	-4.83×10^{-5}	-5.64×10^{-9}	
2078	2	3		47		1	30	.032	.032	2.22×10^{-6}	2.84×10^{-6}	2.54×10^{-6}	1.41×10^{-9}	SAMPLE FAILED AT 20 MIN
2081				49				.038	.038	2.50×10^{-6}	-3.05×10^{-5}	-3.05×10^{-5}	-1.69×10^{-9}	
2090	3	1-2		50				.008	.008	5.56×10^{-7}	1.27×10^{-5}	1.27×10^{-5}	7.06×10^{-9}	
2091				51				.011	.011	8.33×10^{-7}	-1.52×10^{-5}	-1.52×10^{-5}	-8.47×10^{-9}	
2076	4		1-1/4 SP	41				0	0	0	-1.78×10^{-6}	-1.78×10^{-5}	-9.88×10^{-9}	
2077				42							-5.08×10^{-6}	-5.08×10^{-6}	-2.82×10^{-9}	
2096	8	1	4-3/4 SP	36	R512E/			.211	.211	1.44×10^{-5}	-2.54×10^{-6}	-2.54×10^{-6}	-1.41×10^{-9}	
2097				37	Cb-752			.209	.209	1.44×10^{-5}	-7.62×10^{-6}	-7.62×10^{-6}	-4.23×10^{-9}	
2099				38				.232	.232	1.58×10^{-5}	-1.78×10^{-6}	-1.78×10^{-6}	-9.88×10^{-9}	
2101						2	60							
						3	90							
						4	120							
						5	150	.079	.311	4.17×10^{-6}	1.02×10^{-5}	-7.62×10^{-6}	-7.06×10^{-10}	
						1	30	.322	.322	2.19×10^{-5}	-4.06×10^{-6}	-4.06×10^{-6}	-2.26×10^{-9}	
2072	9	1-2		26				-.932	-.922	-6.82×10^{-5}	0	0	0	
2074				27				.282	.282	1.94×10^{-5}	-5.08×10^{-6}	-5.08×10^{-6}	-2.82×10^{-9}	
2082	10	3		28				.251	.251	1.72×10^{-5}	1.02×10^{-5}	1.02×10^{-5}	5.64×10^{-9}	
2083				29				.279	.279	1.91×10^{-5}	-2.29×10^{-6}	-2.29×10^{-6}	-1.27×10^{-9}	
2086	1	1-2		30				.305	.305	2.08×10^{-5}	-7.62×10^{-6}	-7.62×10^{-6}	-4.23×10^{-9}	
2087				31				.204	.204	1.39×10^{-5}	2.03×10^{-6}	2.03×10^{-6}	1.13×10^{-9}	
2092	11			33				-.139	-.139	-9.44×10^{-6}	-1.52×10^{-5}	-1.52×10^{-5}	-8.47×10^{-9}	
2095				35				.010	.010	2.58×10^{-5}	-2.54×10^{-5}	-2.54×10^{-5}	-1.41×10^{-9}	
2086	12		1-1/4 SP	5				.013	.013	3.36×10^{-5}	-1.27×10^{-5}	-1.27×10^{-5}	-7.06×10^{-9}	
2087				6				.036	.086	5.83×10^{-6}	-1.52×10^{-5}	-1.52×10^{-5}	-8.47×10^{-9}	
2098	8	1	4-3/4 SP	12	VH-109/			.074	.074	5.00×10^{-6}	-5.08×10^{-6}	-5.08×10^{-5}	-2.82×10^{-9}	
2100				19	C129Y									
2102						2	60							
						3	90							
						4	120	-.013	.061	8.33×10^{-7}	7.62×10^{-6}	2.54×10^{-6}	0	
						5	150	.126	.126	8.61×10^{-6}	-3.81×10^{-5}	-3.81×10^{-5}	-2.17×10^{-9}	
2071	9	1-2		10		1	30	.135	.135	9.17×10^{-6}	-2.03×10^{-5}	-2.03×10^{-5}	-1.13×10^{-9}	
2075				11				.067	.067	4.44×10^{-6}	2.03×10^{-6}	2.03×10^{-6}	2.03×10^{-9}	
2084	10	3		12				.078	.078	5.28×10^{-6}	-2.54×10^{-6}	-2.54×10^{-6}	1.41×10^{-9}	
2085				13				.080	.080	5.56×10^{-6}	-2.29×10^{-5}	-2.29×10^{-5}	1.27×10^{-9}	
2093	1	1-2		15				.134	.134	9.17×10^{-6}	-7.62×10^{-6}	-7.62×10^{-6}	4.23×10^{-9}	
2094				17				.088	.088	6.11×10^{-6}	-2.54×10^{-6}	-2.54×10^{-6}	-1.41×10^{-9}	
2104	11			20				.045	.045	3.06×10^{-6}	-2.54×10^{-5}	-2.54×10^{-5}	-1.41×10^{-9}	
2105				21				.009	.009	2.33×10^{-5}	-1.02×10^{-5}	-1.02×10^{-5}	-5.64×10^{-9}	
2093	12		1-1/4 SP	3				.004	.004	1.03×10^{-5}	-2.79×10^{-5}	-2.79×10^{-5}	-1.55×10^{-9}	
2094				4										

TABLE C-7 (CONCLUDED)

b) Conventional Units

TEST	TEST COND	SIMULATION TYPE	MODEL DESCRIPTION	SAMPLE	SAMPLE MATERIAL	CYCLE	CUMULATIVE EXPOSURE TIME (min)	MASS CHANGE (grams)	CUMULATIVE MASS CHANGE (grams)	AVERAGE MASS CHANGE RATE (gm/cm^2hr)	DIMENSION CHANGE (inch)	CUMULATIVE DIMENSION CHANGE (inch)	AVERAGE SURF RECESS RATE (in/hr)	COMMENTS
2073	1	1-2	4-3/4 SP	45	TD NiCr	1	30	.046	.046	.0011	.0001	.0001	.0002	
2076				46				.046	.046	.0011	-.0002	-.0002	-.0004	
2077						2	60							
						3	90							
						4	120							
						5	140	-4.28	-4.23	-.0224	-.0004	-.0006	-.0003	SAMPLE FAILED AT 20 MIN
2079				48		1	30	.031	.031	.0008	-.0016	-.0016	-.0032	
2080						2	60							
						3	90							
						4	120							
						5	150	-.049	-.018	-.0001	-.0003	-.0019	-.0008	
2078	2	3		47		1	30	.032	.032	.0008	.0001	.0001	.0002	
2081				49				.038	.038	.0009	-.0012	-.0012	-.0024	
2090	3	1-2		50				.008	.008	.0002	.0005	.0005	.0010	
2091				51				.011	.011	.0003	-.0006	-.0006	-.0012	
2076	4		1-1/4 SP	41				0	0	0	-.0007	-.0007	-.0014	
2077				42							-.0002	-.0002	-.0004	
2096	8	1	4-3/4 SP	36	R512E/			.211	.211	.0052	-.0001	-.0001	-.0002	
2097				37	CB-752			.209	.209	.0052	-.0003	-.0003	-.0006	
2099				38				.232	.232	.0057	-.0007	-.0007	-.0014	
2101						2	60							
						3	90							
						4	120							
						5	150	.079	.311	.0015	.0004	-.0003	-.0001	
2072	9	1-2		26		1	30	.322	.322	.0079	-.0016	-.0016	-.0032	
2074				27				-.992	-.992	-.0245	0	0	0	
2082	10	3		28				.282	.282	.0070	-.0002	-.0002	-.0004	
2083				29				.251	.251	.0062	.0004	.0004	.0008	
2086	1	1-2		30				.279	.279	.0069	-.0009	-.0009	-.0018	
2087				31				.305	.305	.0075	-.0003	-.0003	-.0006	
2092	11			33				.204	.204	.0050	.0008	.0008	.0016	
2095				35				-.139	-.139	.0034	-.0006	-.0006	-.0012	
2086	12		1-1/4 SP	5				.010	.010	.0093	-.0010	-.0010	-.0020	
2087				6				.013	.013	.0121	-.0005	-.0005	-.0010	
2098	8	1	4-3/4 SP	18	VH-109/			.086	.086	.0021	.0006	.0006	.0012	
2100				19	C129Y			.074	.074	.0018	-.0002	-.0002	-.0004	
2103						2	60							
						3	90							
						4	120							
						5	150	-.013	.061	.0003	.0003	.0001	0	
2071	9	1-2		10		1	30	.126	.126	.0031	-.0015	-.0015	-.0030	
2075				11				.135	.135	0033	-.0008	-.0008	-.0016	
2084	10	3		12				.067	.067	.0016	.0008	.0008	.0016	
2085				13				.078	.078	.0019	-.0001	-.0001	-.0002	
2093	1	1-2		15				.080	.080	.0020	-.0009	-.0009	-.0018	
2094				17				.134	.134	.0033	.0003	.0003	.0006	
2104	11			20				.088	.088	.0022	-.0001	-.0001	-.0002	
2105				21				.045	.045	.0011	-.0001	-.0001	-.0002	
2093	12		1-1/4 SP	3				.009	.009	.0004	-.0004	-.0004	-.0008	
2094				4				.004	.004	.0037	-.0011	-.0011	-.0022	

TABLE C-8

TEST CONDITIONS FOR WEDGE MODEL TESTS

a) SI Units

TEST	TEST COND.	SIMUL. TYPE	MODEL DESCR.	SAMPLE	SAMPLE MATERIAL	CYCLE	CURRENT (A)	CENTERLINE TOTAL ENTHALPY (J/kg)	AVERAGE TOTAL ENTHALPY EB (J/kg)	AVERAGE TOTAL ENTHALPY MB (J/kg)	CHAMBER PRESSURE (N/m^2)	GAS FLOW RATE (kg/sec)	OXYGEN MASS FRACTION	CATALYTIC WALL CONVECTIVE HEAT FLUX CENTERLINE (W/m^2)	CATALYTIC WALL CONVECTIVE HEAT FLUX RANGE (W/m^2)	CURRENT (A)	LOCAL PRESSURE (N/m^2)	COMMENTS
2157	5	1	WEDGE	74	TDNiCR	1	197	1.99×10^7	1.35×10^7	--	--	5.44×10^{-3}	.232	$1.3\times10^5/1.4\times10^5$	$2.7\times10^5/1.0\times10^5$	390	2.33×10^2	
				75		1												
2158				74		2	200	2.01×10^7	1.36×10^7					$7.6\times10^4/8.5\times10^4$	$1.3\times10^5/6.6\times10^4$	196	2.13×10^2	
						3			1.34×10^7					$8.5\times10^4/8.7\times10^4$	$1.4\times10^5/6.9\times10^4$	222	2.03×10^2	
						4	202	2.05×10^7	1.36×10^7					$8.2\times10^4/8.2\times10^4$	$1.3\times10^5/6.5\times10^4$	201	1.92×10^2	
						5	204		1.35×10^7					$8.4\times10^4/7.9\times10^4$		205		
				75		2	200	2.01×10^7	1.36×10^7					$7.6\times10^4/8.5\times10^4$	$1.3\times10^5/6.6\times10^4$	196	2.13×10^2	
						3			1.34×10^7					$8.5\times10^4/8.7\times10^4$	$1.4\times10^5/6.9\times10^4$	222	2.03×10^2	
						4	202	2.05×10^7	1.36×10^7					$8.2\times10^4/8.1\times10^4$	$1.3\times10^5/6.5\times10^4$	201	1.92×10^2	
						5	204		1.35×10^7					$8.4\times10^4/7.9\times10^4$		205		
2151	6	1-2		76		1	365	1.55×10^7	1.07×10^7			2.18×10^{-3}		$1.06\times10^5/1.1\times10^5$	$1.7\times10^5/1.1\times10^5$	391	$>.17\times10^2$	SAMPLE FAILED AT 12 MIN 35 SEC
				78														
2152	7	3		81			367	1.53×10^7	1.09×10^7				.062	$7.9\times10^5/8.7\times10^5$	$1.7\times10^5/7.8\times10^4$	413	$.70\times10^2$	SAMPLE FAILED AT 4 MIN 34 SEC
				82														SAMPLE FAILED PRIOR TO 4 MIN
2153	13	1		67	R512E/		642	3.37×10^7	2.94×10^7			9.07×10^{-3}	.232	$2.3\times10^5/2.5\times10^5$	$5.6\times10^5/2.2\times10^5$	780	4.05×10^2	34 SEC
				66	CB-752									$2.3\times10^5/2.6\times10^5$	$5.7\times10^5/2.3\times10^5$	793	4.15×10^2	
2155						2	(600-650)	3.30×10^7	--					$2.13\times10^5/2.1\times10^5$	$4.2\times10^5/1.8\times10^5$	--	3.75×10^2	
						3								$2.14\times10^5/2.1\times10^5$	$4.1\times10^5/1.8\times10^5$		3.44×10^2	
						4	--	--						--	--		--	SAMPLE FAILED AT 30 SEC DUE TO
2155	13	1	WEDGE	67	R512E/	2	(600-650)	3.30x10	--	--	--	9.07×10^{-3}	.232	$2.00\times10^5/2.0\times10^5$	$3.7\times10^5/1.7\times10^5$	--	3.75×10^2	MOMENTARY VACUUM LOSS
					CB-752	3								$2.0\times10^5/2.1\times10^5$	$3.8\times10^5/1.7\times10^5$		3.34×10^2	
2154				61	VH-109/	1								$2.0\times10^5/2.1\times10^5$	$4.3\times10^5/1.8\times10^5$		3.44×10^2	
				58	C129Y													
2155						2								$2.13\times10^5/2.1\times10^5$	$4.2\times10^5/1.8\times10^5$		3.75×10^2	
						3								$2.14\times10^5/2.1\times10^5$	$4.1\times10^5/1.8\times10^5$		3.44×10^2	
						4								$2.00\times10^5/2.0\times10^5$	$3.7\times10^5/1.7\times10^5$		3.75×10^2	
						5								$2.0\times10^5/2.1\times10^5$	$3.8\times10^5/1.7\times10^5$		3.34×10^2	

TABLE C-8 (CONCLUDED)

b) Conventional Units

TEST	TEST COND.	SIMULATION TYPE	MODEL DESCRIPTION	SAMPLE	SAMPLE MATERIAL	CYCLE	CURRENT (amps)	CENTERLINE TOTAL ENTHALPY (Btu/lb)	AVERAGE TOTAL ENTHALPY EB (Btu/lb)	AVERAGE TOTAL ENTHALPY MB (Btu/lb)	CHAMBER PRESSURE (atm)	GAS FLOW RATE (lb/sec)	OXYGEN MASS FRACTION	CATALYTIC WALL CONVECTIVE HEAT FLUX CENTERLINE (Btu/ft²sec)	CATALYTIC WALL CONVECTIVE HEAT FLUX RANGE (Btu/ft²sec)	CATALYTIC WALL CONVECTIVE HEAT FLUX CURRENT (amps)	LOCAL PRESSURE (atm)	COMMENTS
2157	5	1	WEDGE	74	TD NiCr	1	197	4750	3220	--	--	.012	.232	11.8/12.7	23.4-9.2	390	.0023	
				75														
2158				74		2	200	4800	3250			.012		6.7/ 7.5	11.6-5.8	196	.0021	
						3			3210					7.5/ 7.7	12.5-6.1	222	.0020	
						4	202	4900	3250					7.2/ 7.1	11.6-5.7	201	.0019	
						5	204		3220					7.4/ 7.0		205		
				75		2	200	4800	3250			.012		6.7/ 7.5	11.6-5.8	196	.0021	
						3			3210					7.5/ 7.7	12.5-6.1	222	.0020	
						4	202	4900	3250					7.2/ 7.1	11.6-5.7	201	.0019	
						5	204		3220					7.4/ 7.0		205		
2151	6	1-2		76		1	365	3700	2560			.048		9.3/ 9.9	15.2-9.3	391	.0051	SAMPLE FAILED AT 12 MIN 35 SEC
				78														
2152	7	3		81			367	3650	2600				.062	6.9/ 7.7	14.6-6.9	413	.0076	SAMPLE FAILED AT 4 MIN 34 SEC
				82														SAMPLE FAILED PRIOR TO 4 MIN 34 SEC
2153	13	1		67	R512E/ Cm-752		642	8050	7020			.020	.232	20.2/21.8	49.1-19.6	780	.0040	
				66										20.4/22.8	50.0-20.3	793	.0041	
2155						2	(600-650)	7900	--					18.8/18.9	37.2-15.9	--	.0037	
						3								18.9/18.6	35.8-15.6		.0034	
						4	--	--						--	--		--	SAMPLE FAILED AT 30 SEC DUE TO MOMENTARY VACUUM LOSS
2155	13	1	WEDGE	67	R512E/ Cm-752	2	(600-650)	7900	--	--	--	.020	.232	17.6/17.9	32.3-15.1	--	.0037	
						3								18.2/18.5	33.3-15.3		.0033	
2154				61	VH-109/ C129Y	1								18.1/18.6	37.7-16.1		.0034	
				58														
2155						2								18.8/18.9	37.2-15.9		.0037	
						3								18.9/18.6	35.8-15.6		.0034	
						4								17.6/17.9	32.3-15.1		.0037	
						5								18.2/18.5	33.3-15.3		.0033	

TABLE C-9

TEMPERATURE MEASUREMENTS FOR WEDGE MODEL TESTS

a) SI Units

TEST	TEST COND.	SIMULATION TYPE	MODEL DESCRIPTION	SAMPLE	SAMPLE MATERIAL	CYCLE	TD-9C			TD-9F			THERMOGAGE		BACKWALL TEMP		COMMENTS
							CENTERLINE (°R)	RANGE (°K)	EMISSIVITY (-)	CENTERLINE (K°)	RANGE (K°)	EMISSIVITY (-)	CENTERLINE (°K)	EMISSIVITY (-)	CENTERLINE (°K)	RANGE (°K)	
2157	5	1	WEDGE	74	TD NiCr	1	1300	1360-1170	.75				1310	.75	--	--	
				75						1340	1440-1180	.75				1030-890	
2158				74		2	1290	1350-1260	.75				1250	.75			
						3	1320	1400-1010					1260				
						4	1280	1300-1270					1250				
						5	--	1300-1290					1210				
				75		2				1360	1430-1270	.75				1010-840	
						3				1350	1440-1330					1020-880	
						4				1330	1350-1310					1030-880	
						5				--	1320-1280					1010-820	
2151	6	1-2		76		1	1310	1550-1280	.75				1240	.75	990	1080-990	SAMPLE FAILED AT 12 MIN 35 SEC
				78						1270	1360-1180	.75			--	1090-1000	
2152	7	3		81			--	1300-1260	.75				1240	.75	900	1100-900	SAMPLE FAILED AT 4 MIN 34 SEC
				82						--	1330-1300	.75			--	970-930	SAMPLE FAILED PRIOR TO 4 MIN 35 SEC
2153	13	1		67	RS12E/ Cb-752		1520	1550-1370	.75				1540	.75	1300	--	
				66						1530	1590-1400	.75				1370-1200	
2155						2	1500	1530-1370	.75				1550	.75	1300	--	
						3	1530	1530-1420					1540		1300		
						4	--	--					--		--		SAMPLE FAILED AT 30 SEC DUE TO MOMENTARY VACUUM LOSS
2155	13	1	WEDGE	67	RS12E/ Cb-752	2	1520	1560-1370	.75				1560	.75	--	--	
						3	1520	1530-1300					1550				
2154				61	VH-109/ C129Y	1	1420	1460-1280					1480		1220		
				58						1420	1470-1270	.75			--	1250-1170	
2155						2				1400	1440-1280					1240-1170	
						3				1390	1460-1280					1250-1160	
						4				1390	1460-1280					1250-1150	
						5				1370	1440-1280					1250-1160	

TABLE C-9 (CONCLUDED)

b) Conventional Units

TEST	TEST COND.	SIMULATION TYPE	MODEL DESCRIPTION	SAMPLE	SAMPLE MATERIAL	CYCLE	TD-9C			TD-9F			THERMOGAGE		BACKWALL TEMPERATURE		COMMENTS
							CENTERLINE (°F)	RANGE (°F)	EMISSIVITY (-)	CENTERLINE (°F)	RANGE (°F)	EMISSIVITY (-)	CENTERLINE (°F)	EMISSIVITY (-)	CENTERLINE (°F)	RANGE (°F)	
2157	5	1	WEDGE	74	TD NiCr	1	1680	1980-1640	.75				1900	.75	---	---	
				75						1950	2140-1660	.75				1400-1150	
2158				74		2	1860	1970-1810	.75				1790	.75			
						3	1920	2060-1860					1800				
						4	1840	1890-1820					1790				
						5	---	1890-1360					1720				
				75		2				1980	2110-1620	.75				1360-1050	
						3				1970	2140-1940					1370-1130	
						4				1930	1970-1900					1400-1120	
						5				---	1910-1840					1360-1020	
2151	6	1-2		76		1	1900	2330-1840	.75				1770	.75	1330	1490-1330	SAMPLE FAILED AT 12 MIN 35 SEC
				78						1830	1980-1660	.75			---	1510-1340	
2152	7	3		81			---	1880-1860	.75				1770	.75	1170	1530-1170	SAMPLE FAILED AT 4 MIN 34 SEC
				82						---	1930-1880	.75			---	1290-1220	SAMPLE FAILED PRIOR TO 4 MIN 35 SEC
2153	13	1		67	R512E/ Cb-752		2270	2330-2000	.75				2320	.75	1890	---	
				66						2290	2410-2060	.75				2010-1710	
2155						2	2250	2290-2000	.75				2330	.75	1880	---	
						3	2290	2300-2090					2320		1880		
						4	---	---					---		---		SAMPLE FAILED AT 30 SEC DUE TO MOMENTARY VACUUM LOSS
2155	13	1	WEDGE	67	R512E/ Cb-752	2	2280	2340-2000	.75				2350	.75	---	---	
						3	2270	2290-1890					2330				
2154				61	VH-109/ C129Y	1	2090	2170-1840					2210		1730		
				58						2100	2190-1830	.75			---	1790-1640	
2155						2				2060	2140-1840					1770-1640	
						3				2040	2170-1840					1790-1620	
						4				2040	2160-1840					1790-1610	
						5				2000	2140-1850					1790-1610	

TABLE C-10
MASS LOSS AND SURFACE RECESSION MEASUREMENTS FOR WEDGE MODEL TESTS
a) SI Units

TEST	TEST COND.	SIMULATION TYPE	MODEL DESCRIPTION	SAMPLE	SAMPLE MATERIAL	CYCLE	CUMULATIVE EXPOSURE TIME (min)	MASS CHANGE ($kg \times 10^3$)	CUMULATIVE MASS CHANGE ($kg \times 10^3$)	AVERAGE MASS CHANGE RATE ($kg/m^2 sec$)	DIMENSION CHANGE (meters)	CUMULATIVE DIMENSION CHANGE (meters)	AVERAGE SURFACE RECESS. RATE (m/hr)	COMMENTS
2157	5	1	WEDGE	74	TD NiCr	1	30	.0114	.0114	6.33×10^{-5}	1.02×10^{-2}	1.02×10^{-2}	2.03×10^{-3}	
				75				.0178	.0178	9.89×10^{-5}	-1.27×10^{-5}	-1.27×10^{-5}	-2.54×10^{-3}	
2158				74		2	60							
						3	90							
						4	120							
						5	150	-.0326	-.0212	-2.36×10^{-5}	2.29×10^{-5}	3.30×10^{-6}	1.02×10^{-3}	
				75		2	60							
						3	90							
						4	120							
						5	150	-.0476	-.0298	-3.31×10^{-5}	1.02×10^{-5}	-2.54×10^{-6}	5.08×10^{-4}	
2151	6	1-2		76		1	12.5							SAMPLE FAILED AT 12 MIN 35 SEC
				78										
2151	7	3		81			4.5							SAMPLE FAILED AT 4 MIN 35 SEC
				82										SAMPLE FAILED PRIOR TO 4 MIN 34 SEC
2153	13	1		67	R512E/ Ca-752		30	.2440	.2440	1.36×10^{-3}	2.54×10^{-6}	2.54×10^{-6}	5.08×10^{-6}	
				66				.2300	.2300	1.33×10^{-3}	-3.30×10^{-5}	-3.30×10^{-5}	-6.60×10^{-6}	
2155						2	60							
						3	90							
						4	90.5							SAMPLE FAILED AT 30 SEC DUE TO MOMENTARY VACUUM LOSS
2155	13	1	WEDGE	67	R512E/ Ca-752	2	120	.0136	.2576	3.58×10^{-4}	-2.54×10^{-6}	.0.0	-1.27×10^{-6}	
						3	150							
2154				61	VH-109/ C129Y	1	30							
				58				.0876	.0876	4.87×10^{-4}	-3.81×10^{-5}	-3.81×10^{-5}	-7.62×10^{-5}	
2155						2	60							
						3	90							
						4	120							
						5	150	.0122	.0998	1.11×10^{-4}	1.78×10^{-5}	-2.03×10^{-5}	7.62×10^{-3}	

TABLE C-10 (CONCLUDED)
b) Conventional Units

TEST	TEST COND.	SIMULATION TYPE	MODEL DESCRIPTION	SAMPLE	SAMPLE MATERIAL	CYCLE	CUMULATIVE EXPOSURE TIME (min)	MASS CHANGE (grams)	CUMULATIVE MASS CHANGE (grams)	AVERAGE MASS CHANGE RATE (gm/cm^2hr)	DIMENSION CHANGE (inch)	CUMULATIVE DIMENSION CHANGE (inch)	AVERAGE SURFACE RECESS. RATE (in/hr)	COMMENTS
2157	5	1	WEDGE	74	TD NiCr	1	30	.0114	.0114	.0228	.0004	.0004	.0008	
				75				.0178	.0178	.0356	-.0005	-.0005	-.0010	
2158				74		2	60							
						3	90							
						4	120							
						5	150	-.0326	-.0212	-.0085	.0009	.0013	.0004	
				75		2	60							
						3	90							
						4	120							
						5	150	-.0476	-.0298	-.0119	.0004	-.0001	.0002	
2151	6	1-2		76		1	12.5							SAMPLE FAILED AT 12 MIN 35 SEC
				78										
2151	7	3		81			4.5							SAMPLE FAILED AT 4 MIN 35 SEC
				82										SAMPLE FAILED PRIOR TO 4 MIN 34 SEC
2153	13	1		67	R512E/ Ca-752		30	.2440	.2440	.4880	.0001	.0001	.0002	
				66				.2300	.2300	.4000	-.0013	-.0013	-.0026	
2155						2	60							
						3	90							
						4	90.5							SAMPLE FAILED AT 30 SEC DUE TO MOMENTARY VACUUM LOSS
2155	13	1	WEDGE	67	R512E/ Ca-752	2	120	.0136	.2576	.1288	-.0001	0.0	-.00005	
						3	150							
2154				61	VH-109/ C129Y	1	30							
				58				.0876	.0876	.1752	-.0015	-.0015	-.0030	
2155						2	60							
						3	90							
						4	120							
						5	150	.0122	.0998	.0399	.0007	-.0008	.0003	

All test condition variables in Tables C-5 and C-8 have been described previously. Note however under the heading catalytic wall convective heat flux that the right hand column is the current at which this flux was measured; this current was not necessarily the current at which the sample test was run. Also the tabulated pressures are those to which the models were exposed - stagnation for the stagnation point model and local at the sample center for the wedge model.

The surface temperature measurements of Tables C-6 and C-9 were made with the following pyrometer assignments:

Stagnation Point Model

- Primary pyrometer on oscillating mechanism
  - TD-9C for all moderate and high temperatures (> 1800°F)
  - TD-7 for low temperatures (< 1800°F)
- Secondary pyrometer (centerline only)
  - TD-9F
  - Thermogage
  - TD-7 for all tests for which TD-9 was the primary pyrometer

Wedge Models

- Primary pyrometers on oscillating mechanisms (one setup for each of the two test samples)
  - TD-9C and TD-9F on identical oscillating mechanisms
- Secondary pyrometer
  - Thermogage

In the case of the primary pyrometers, the centerline temperature and the temperature range defined by the other four positions and centerline (except for the 0.0318-meter (1.25-inch) diameter models) are presented. In all cases, the emissivity values employed for the particular pyrometer/material combinations are indicated in the tables (and are discussed below). The backwall temperature at the sample centerline and the backwall temperature range as measured by spring-loaded thermocouples are also included in the tables (and also discussed below). Note that a problem with the data acquisition system resulted in a loss of centerline surface temperature measurements for two of the stagnation point and two of the wedge model tests, and that failure of spring-loaded thermocouples resulted in the loss of backwall temperature measurements for some tests.

In Tables C-7 and C-10, a positive mass change corresponds to an increase in sample mass and a positive dimension change corresponds to surface recession. For the three sets of variables which describe the mass or dimension change, the first is referenced to the immediately previous measurement, the cumulative is referenced to the pretest measurement, and the last is also referenced to the pretest measurement and is based on the total exposure time and sample surface area. Note for the wedge that all results are also essentially an average for the large temperature range experienced by the test samples. In the cases of sample failures, no results are presented since they resulted in the loss of a significant part of the test samples. The dimension changes in almost all cases were so small that significant scatter in the results can be expected.

Tables 9 and 10 present a summary of all test conditions and test sample response including results from the above table sets and results derived therefrom.

Essentially all test results are discussed in detail in Section 5.3.2. Additional discussion of surface and backwall temperature results and of emissivity is also presented below, however.

The surface temperature results presented in Table C-6 for the stagnation point model tests indicate a significant scatter in the measurements for different pyrometers. Referenced to the primary TD-9C pyrometer:

- TD-7 pyrometer agrees for TD NiCr and is generally lower for coated Cb
- TD-9F and Thermogage pyrometers are higher by as much as about 200°F

The former result is consistent and was expected as discussed below. The latter result was not expected and no explanation is apparent. Also, no such inconsistencies were apparent for the wedge tests as indicated from Table C-9. The primary TD-9C pyrometer results were therefore used as the primary surface temperature measurements for all tests.

The emissivities used in the pyrometer measurements for each material/pyrometer combination are presented in Tables C-6 and C-9. For TD NiCr these values are based on the results of Reference C-2 and preliminary results from NASA Langley Research Center. The approximate variation of emissivity with wavelength for the oxide film on TD NiCr is presented in Figure C-11 which yields the following approximate emissivity values:

- Total Hemispherical emissivity = 0.75
- Emissivity at 0.8 microns (TD-9) = 0.75
- Emissivity in the range of 1.7 to 2.6 microns (TD-7) = 0.61

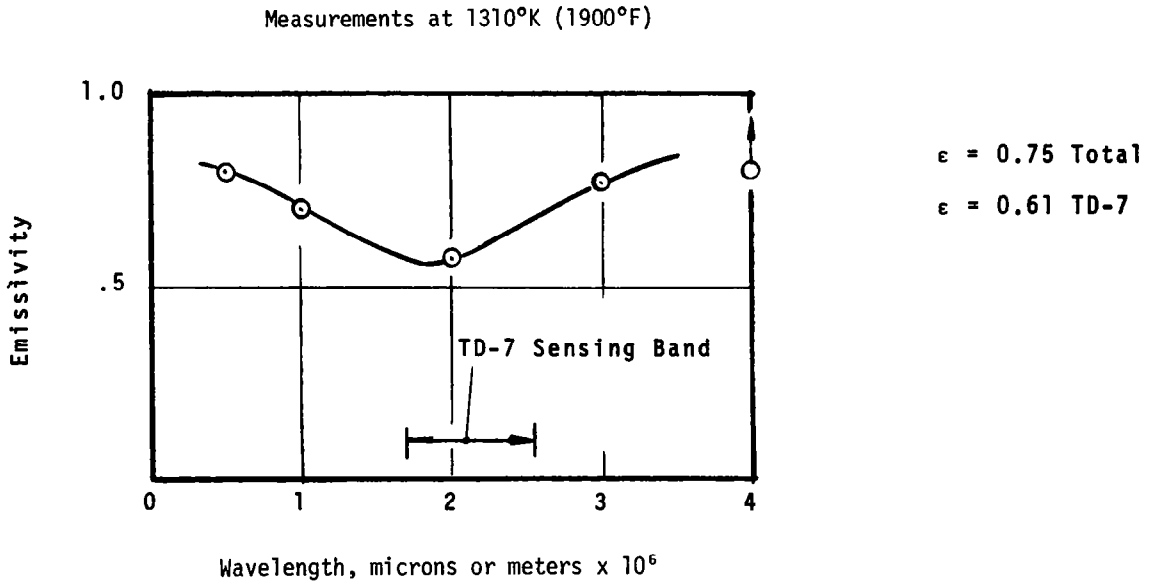

Figure C-11. Preliminary Emissivity Results for TD NiCr Test Samples

No results were available for the columbium coating systems and therefore a value of 0.75 was assumed to be reasonable and was used independent of wavelength. In Reference C-3, a value of 0.85 was used for the pyrometer measurements but the results indicated a lower value at least in the wavelength range of the TD-7 pyrometer. Because of the relative insensitivity of the TD-9 pyrometers to emissivity, the differences in the reported temperatures are small if the emissivity were 0.85 instead of 0.75 as assumed. As shown in Figure C-12, this correction would decrease the reported temperatures by less than 20°K (35°F). A comparison of the results from the TD-9C and the TD-7 for the coated columbiums indicates that the emissivity, at least in the wavelength range of the TD-7 (1.7 to 2.6 microns), is slightly lower than 0.75.

The spring-loaded backwall thermocouples in almost all cases indicated temperatures significantly lower than those measured by the pyrometers. This comparison is consistent with the results of References C-2 and C-3 which indicate errors in such thermocouple measurements ranging from 28°K to 110°K (50°F to 200°F). Smaller errors were found with the coating systems (28°K to 56°K (50°F to 100°F) for R512E) and larger errors with TD NiCr (about 110°K (200°F)). These results are generally consistent with those of this program (Tables C-6 and C-9).

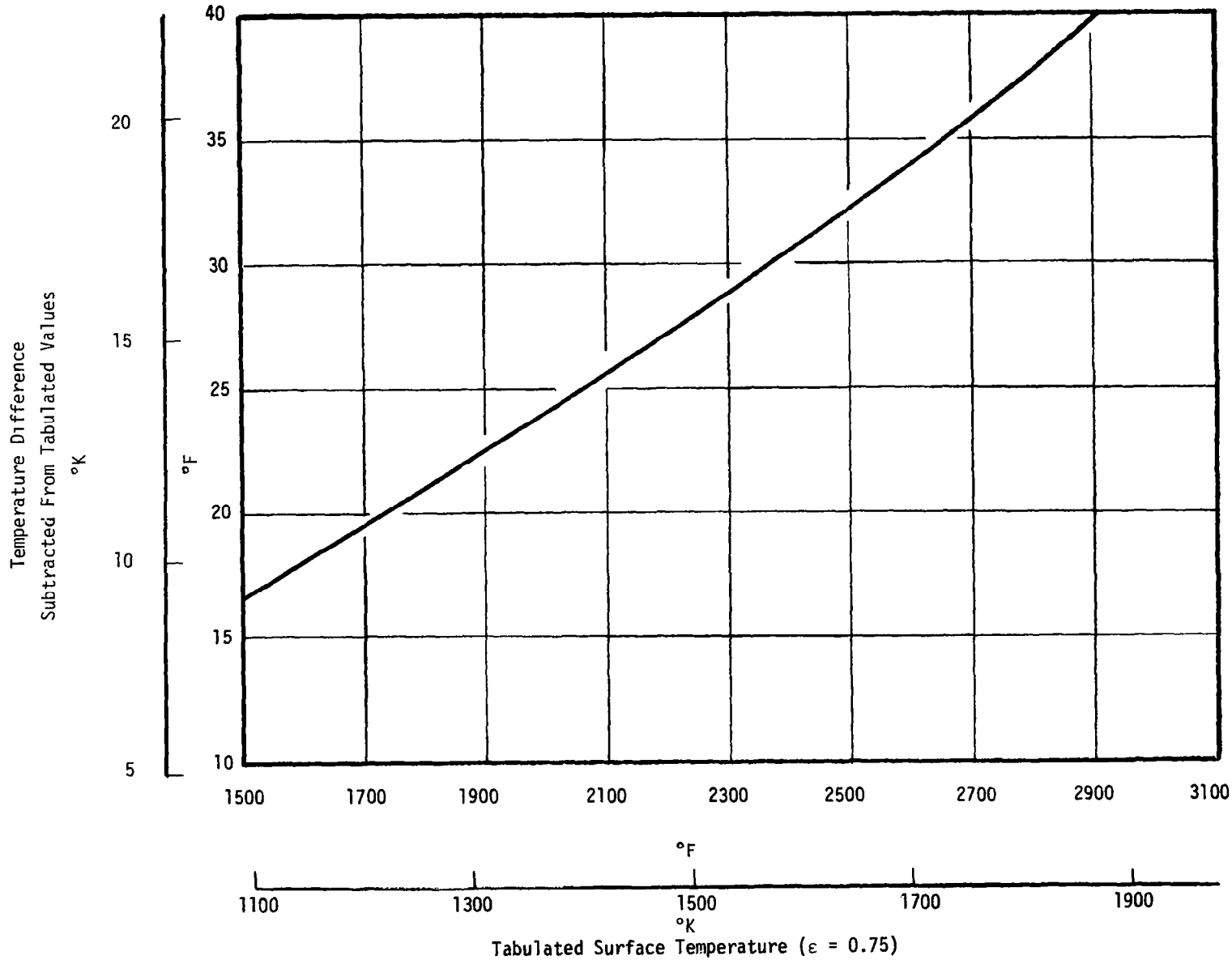

Figure C-12. Surface Temperature Correction from $\varepsilon = 0.75$ to $\varepsilon = 0.85$

REFERENCES

APPENDIX C

C-1. Winovich, W., "On the Equilibrium Sonic-Flow Method for Evaluating Electric-Arc Air Heater Performance," NASA TND-2132, March 1964.

C-2. Schaefer, J. W., "Thermal Screening of Shuttle Orbitor Vehicle TPS Materials Under Convective Heating Conditions, Aerotherm Division, Acurex Corporation, Final Report No. 72-56, Vol. I, NASA CR-114521, August 1973.

C-3. Rinehardt, W. A., Land, D. W., Painter, J. H., and Williamson, R. A., "Cyclical Tests of Selected Space Shuttle Materials in a Plasma Arc Tunnel," McDonnell Douglas Astronautics Company, NASA CR-114459, July 1972.

APPENDIX D

OPTIMIZATION OF TEST PARAMETERS FOR SPACE SHUTTLE SIMULATION TESTING IN THE NASA LANGLEY HYMETS TEST FACILITY

The NASA Langley HYMETS test facility is a nominal 100-kw arc plasma system for simulation of hypersonic flight and reentry heating conditions. The facility has been used extensively to evaluate the response characteristics of candidate metallics for the shuttle vehicle. Present operating capabilities limit the test model size to about 9.53×10^{-3}-meter (0.375-inch) diameter, and in some cases the measured test conditions appear inconsistent. The present facility capabilities and limitations, and the capabilities that could be achieved with minor facility modifications were therefore investigated as related to the shuttle application. The results of this investigation are presented in the following sections.

D.1 DESCRIPTION OF FACILITY

The NASA Langley HYMETS test facility provides reentry convective heating conditions for evaluation of materials in hyperthermal environments. The nominal 100-kw facility consists of:

- Modular constrictor arc heater, 100 kw
- Silicon rectifier moving coil DC power supply, 100 kw
- Vacuum test chamber and pumping system
- Test gas supply systems
- Water cooling system
- Model sting and insertion equipment
- Two conical supersonic nozzles, 0.0318 and 0.0635-meter (1.25 and 2.50-inch) exit diameters
- Control console

as presented in Table D-1. This facility was designed, fabricated and installed by Aerotherm for NASA Langley. The configuration and operation of the arc heater and the functions of the other equipment are as described in Section 4 and Appendix C for the Aerotherm test facility. The facility was originally designed for combined thermal (convective heating) and mechanical (tensile

TABLE D-1

HYMETS ARC PLASMA FACILITY

a) SI Units

• Arc Heater	
Type	Aerotherm 100 kw constrictor arc heater
Input Power	5 to 100 kw
Chamber Pressure	515 to 1.05×10^5 N/m^2
Enthalpy	4.2×10^5 to 1.05×10^8 J/kg
Gas-Flow Rate	3.0×10^{-4} to 6.9×10^{-3} kg/sec
Gas Compositions	N_2, O_2, Air
Stabilization	Gas
Electrodes	Copper/Tungsten
• Power Supply	
Type	Full wave, silicon diode; moving coil current control
Rating	105 KVA at 440V 3 60 cycle continuous operation or 140 KVA for 3 minutes
• Nozzles and Test Sections	
Supersonic Nozzles	
Exit Diameter	9.52×10^{-3} to 3.18×10^{-2} meter
Throat Diameter	1.27×10^{-2} meter
Area Ratio	6.25 and 25.0
Expansion Angle	8.5° half angle
• Test Chamber	
Size	0.610-meter diameter by 0.914-meter long cylinder
Chamber Cooling	Double jacketed and water cooled 0.356 meter
Viewing and Access	Two 0.076 meter quartz view ports, two 0.356 meter hinged access ports with 0.127-meter ciameter pyrex view ports
• Vacuum System	
Type	Mechanical pumps - High vacuum mechanical booster pump and oil seal rotary piston backing pumps, continuous operation
• Model Sting System	
Type	Pneumatically actuated
Capacity	Two stings per test maximum and tensile test equipment
• Instrumentation	
Gas and Water Flow Rates	Rotometer
Water Temperature Rise	Thermopile
Chamber and Cabin Pressures	Precision bourdon tube gauge
Surface Temperature	Disappearing filament pyrometer, thermocouples

TABLE D-1 (CONCLUDED)

b) Conventional Units

• Arc Heater	
Type	Aerotherm 100 kw constrictor arc heater
Input Power	5 to 100 kw
Chamber Pressure	0.005 to 1.00 atm
Enthalpy	1000 to 25000 Btu/lb
Gas-Flow Rate	6.5×10^{-4} to 1.50×10^{-2} lb/sec
Gas Compositions	N_2, O_2, Air
Stabilization	Gas
Electrodes	Copper/Tungsten
• Power Supply	
Type	Full wave, silicon diode; moving coil current control
Rating	105 KVA at 440V 3 60 cycle continuous operation or 140 KVA for 3 minutes
• Nozzles and Test Sections	
Supersonic Nozzles	
Exit Diameter	1.25 and 2.5 inch
Throat Diameter	0.5 inch
Area Ratio	6.25 and 25.0
Expansion Angle	8.5° half angle
• Test Chamber	
Size	24-inch diameter by 36-inch long cylinder
Chamber Cooling	Double jacketed and w ter cooled
Viewing and Access	Two 3 inch quartz ports, two 14 inch hinged access ports with 5 inch diameter pyrex view ports
• Vacuum System	
Type	Mechanical pumps - High vacuum mechanical booster pump and oil seal rotary piston backing pumps, continuous operation
Capacity	2700 cfm nominal at .05 to 10 toor
• Model Sting System	
Type	Pneumatically actuated
Capacity	Two stings per test maximum and tensile test equipment
• Instrumentation	
Gas and Water Flow Rates	Rotometer
Water Temperature Rise	Thermopile
Chamber and Cabin Pressures	Precision bourdon tube gauge
Surface Temperature	Disappearing filament pyrometer, thermocouples

loading) testing of metallics for the hypersonic transport. It however has been used extensively for evaluating the thermal response characteristics of candidate metallic materials for the shuttle vehicle under flowing air conditions. These tests were performed using the .0635-meter (2.5-inch) exit diameter nozzle and a 9.53×10^{-3}-meter (0.375-inch) flat face stagnation point test sample.

D.2 DESIRED TEST CONDITIONS

The desired conditions for the HYMETS facility are those which best simulate the shuttle vehicle reentry heating (Section 5). This implies for the basic size limitation of the facility, the largest possible test model (and test sample). The optimum configuration for the basic tests of interest and consistent with the facility size limitation is a flat face stagnation point model (Section 4). A wedge configuration is also possible but the sample size is small and, because of the $s^{-1/2}$ variation of heat flux in the flow direction, variation in the heat flux along the sample is large.

To insure uniform conditions on the face of the test model, the maximum model body diameter should be 0.5 to 0.6 times the nozzle exit diameter. Within this model size constraint, the best entry simulation (i.e., closest match of enthalpy and/or pressure, Section 5) is attained by using the largest body diameter practical. This trend is displayed in Table D-2 where for the HYMETS configuration ($d_* = 0.0127$ meters (0.5 inches) and $d_e = 0.0635$ meters (2.5 inches)), the operating conditions corresponding to the test conditions for shuttle vehicle reentry simulation are presented for two model diameters. This criteria combined with that for the maximum model diameter indicates that a 0.0318-meter (1.25-inch) model represents the optimum body diameter for simulation testing in the HYMETS facility. The 0.0318-meter (1.25-inch) diameter model was therefore used as the baseline to evaluate facility performance requirements.

The required test conditions for reentry simulation testing for flat face models were presented in Tables 4 and 5 and are summarized in Table D-2 for convenience. These test conditions for the 0.0318-meter (1.25-inch) diameter model and also for a 9.53×10^{-3}-meter (0.375-inch) diameter model appropriate to the HYMETS facility were calculated in Section 5 for all simulation types. The required HYMETS facility operating conditions were then defined as follows:

- Arc heater chamber pressure p_o calculated from the required model stagnation pressure and the constant γ expansion tables for the HYMETS nozzle exit area ratio A_e/A_*
- Test gas flow rate $\dot{m}$ calculated from the sonic flow parameter ($\dot{m}g/p_oA_*$) and the required total enthalpy h_o (see Appendix C)

TABLE D-2

TEST AND OPERATING CONDITIONS FOR HYMETS FACILITY

a) SI Units

Test Parameter	Simulation Type 1				Simulation Type 2			
Model Body Diameter - meter	0.0318	0.0095	0.0318	0.0095	0.0318	0.0095	0.0318	0.0095
Total Enthalpy - J/kg	4.77×10^7	4.77×10^7	4.77×10^7	4.77×10^7	1.30×10^7	8.28×10^6	8.20×10^6	5.61×10^6
Catalytic Wall Convective Heat Flux[a] - W/m^2	2.95×10^5	2.95×10^5	1.59×10^5	1.59×10^5	2.95×10^5	2.95×10^5	1.59×10^5	1.59×10^5
Stagnation Pressure - N/m^2	63.8	19.2	19.2	5.67	1216	1216	1216	1216
Chamber Pressure - N/m^2	1034	314	314	92	19758	19758	19758	19758
Total Flow Rate - kg/sec	12.16	3.65	3.65	1.11	314	375	375	436
Power Required[b] - kw	2.9	0.9	0.9	0.2	20.2	15.6	15.6	12.1

[a] 26 Btu/ft^2sec → typical flux for coated Cb testing

14 Btu/ft^2sec → typical flux for TD NiCr testing

[b] Assumed efficiency = 0.5

TABLE D-2 (CONCLUDED)
b) Conventional Units

Test Parameter	Simulation Type 1				Simulation Type 2			
Model Body Diameter - inch	1.25	0.375	1.25	0.375	1.25	0.375	1.25	0.375
Total Enthalpy - Btu/lb	11400	11400	11400	11400	3120	1980	1960	1340
Catalytic Wall Convective Heat Flux[a] - Btu/ft^{2}sec	26	26	14	14	26	26	14	14
Stagnation Pressure - atm	0.00063	0.00019	0.00019	0.000056	0.012	0.012	0.012	0.012
Chamber Pressure - atm	0.0102	0.0031	0.0031	0.00091	0.195	0.195	0.195	0.195
Total Flow Rate - lb/sec	0.00012	0.000036	0.000036	0.000011	0.0031	0.0037	0.0037	0.0043
Power Required[b] - kw	2.9	0.9	0.9	0.2	20.2	15.6	15.6	12.1

[a] 26 Btu/ft^{2}sec → typical flux for coated Cb testing
14 Btu/ft^{2}sec → typical flux for TD NiCr testing

[b] Assumed efficiency = 0.5

- Arc heater input power calculated from the relation $P_{in} = \dot{m}h_o/\eta$ where the arc heater efficiency η was estimated from previous results

Typical operating conditions for the respective simulation test conditions are presented in Table D-2.

D.3 PRESENT OPERATING CAPABILITY

D.3.1 Arc Heater and Nozzles

The performance envelopes for the HYMETS facility are presented in Figures D-1 through D-3. Figures D-2 and D-3 display the operating characteristics for testing TD NiCr and coated Cb, respectively. From these envelopes it is apparent that the 0.0318-meter (1.25-inch) exit diameter nozzle is not appropriate to shuttle reentry heating simulation. For the 0.0635-meter (2.50-inch) exit diameter nozzle, it is also apparent that flight enthalpy simulation (type 1) is not possible with the HYMETS facility but that flight pressure simulation (type 2) and lower pressure, higher enthalpy simulation (type 1-2) are possible at flux levels appropriate to both TD NiCr and coated Cb. Also, material evaluations for simulation type 2 may be conducted with model body diameters at least in the range 0.0318 meters (1.25 inches) to 9.53×10^{-3} meters (0.375 inch), but as discussed previously, the largest possible diameter is preferred since it represents the best reentry simulation capability of the HYMETS facility.

The ability to achieve or exceed the present capabilities of the arc heater/nozzle combinations above depends on proper performance of other facility systems as presented below.

D.3.2 Diffuser and Vacuum Pumping System

The basic guidelines for diffuser design incorporated into the HYMETS facility based upon an interpretation and combination of the results of References D-1 and D-2 are:

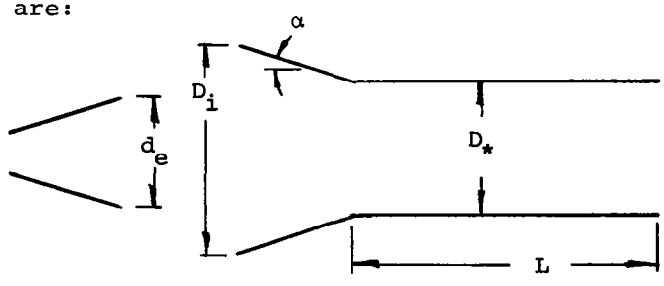

Nozzle

$$\left(\frac{D_*}{d_e}\right)^2 = 1.5$$

Diffuser

$$\frac{D_i}{D_*} \geq 1.35$$

$$30° \geq \alpha \geq 15°$$

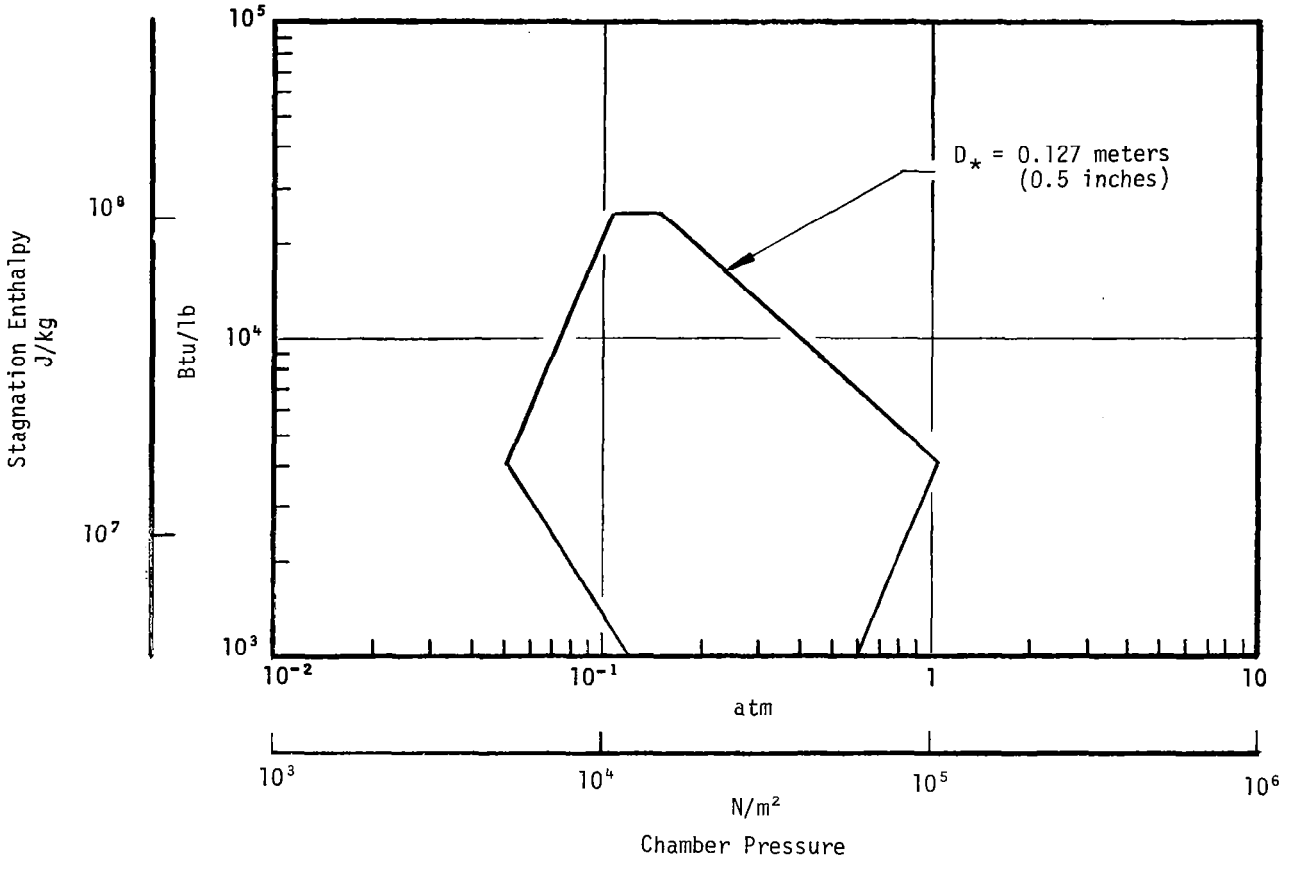

Figure D-1. Chamber Conditions Envelope for HYMETS Facility

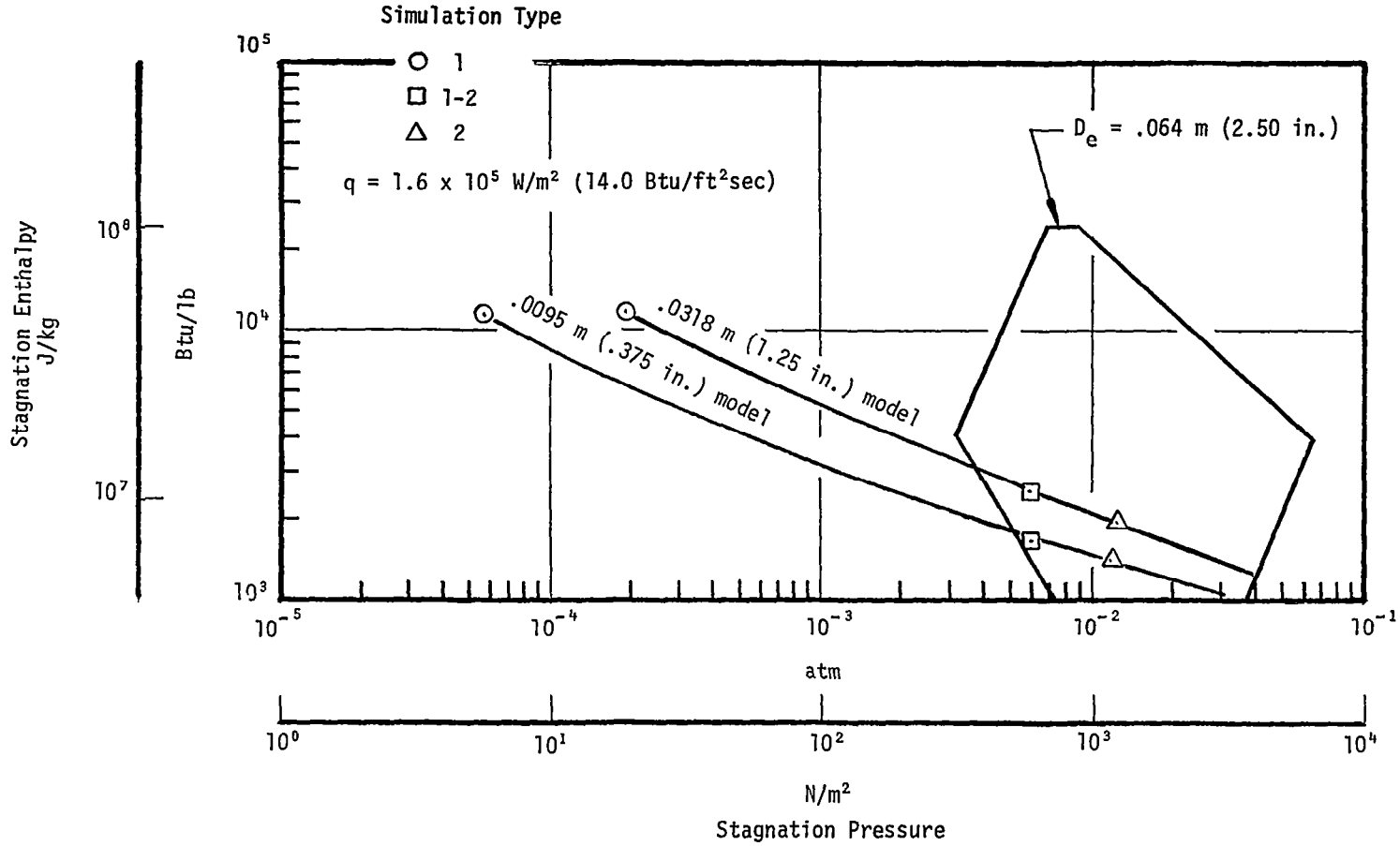

Figure D-2. Model Stagnation Conditions Envelope for HYMETS Facility, TD NiCr Simulation

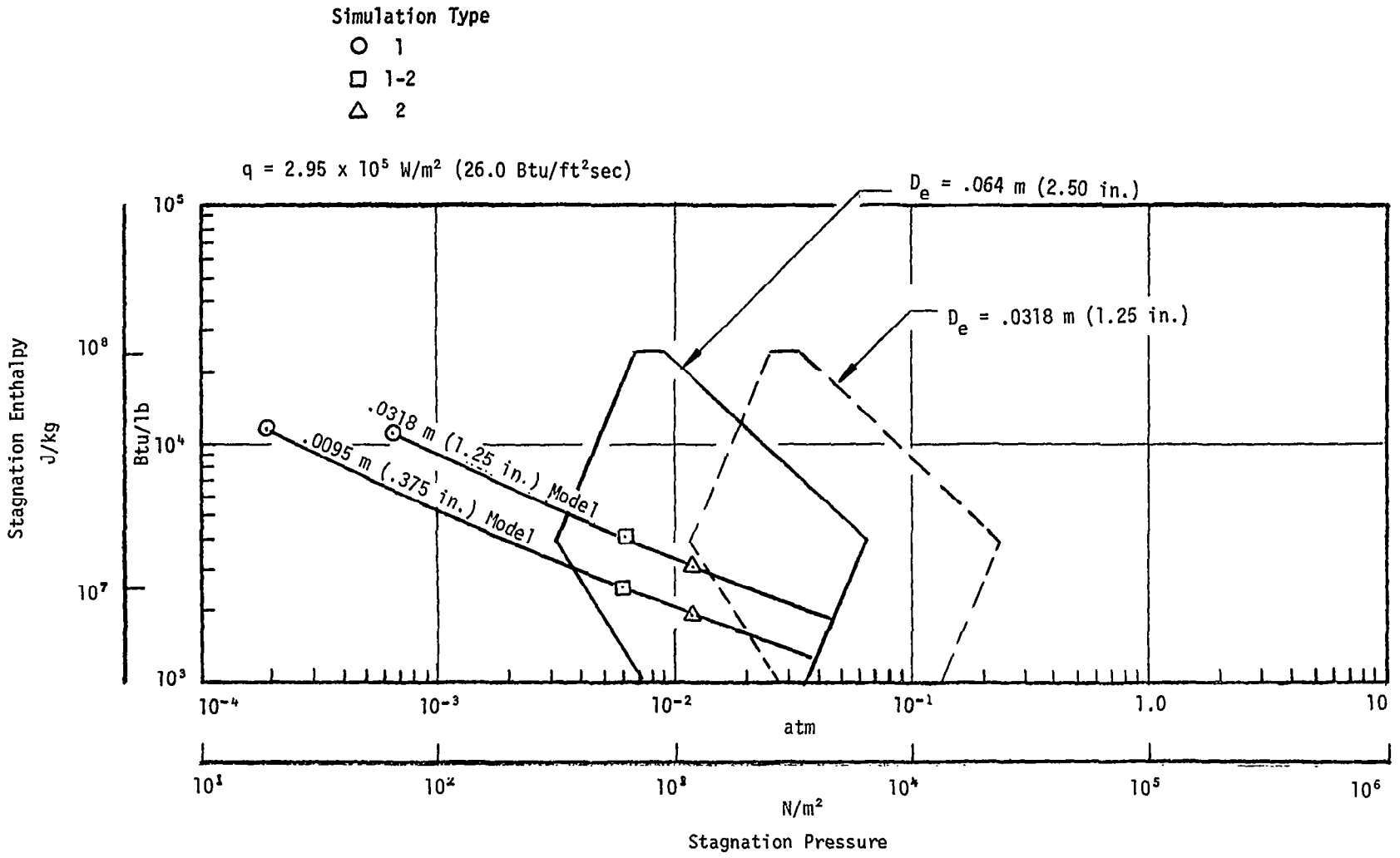

Figure D-3. Model Stagnation Conditions Envelope for HYMETS Facility, Coated Cb Simulation

The diffuser was designed for optimum performance based upon an undisturbed flow without a model in the test stream, but allowance was made for model blockage.

The vacuum pumping system is composed of two types of positive displacement pumps; a high vacuum lobe type mechanical booster pump and two oil seal rotary piston backing pumps. These pumps are interconnected and the resultant pumping system is automatically controlled to operate in the proper vacuum range. The pumping capacity curve for the system is shown in Figure D-4, wherein pumping speed denotes the actual volumetric displacement and suction pressure is the pressure at the pump inlet.

The diffuser/vacuum pumping system was designed to provide a cabin pressure which matched the nozzle exit static pressure required for full nozzle flow. However, when a model is placed in the test stream, full flow is difficult or impossible to maintain. This problem is due to a deficiency either in the vacuum pumping system or in the diffuser performance. Based on analysis of test data from the HYMETS facility and on the resolution of a similar problem in the Aerotherm test facility, the problem is the diffuser. For large model sizes relative to the nozzle exit diameter (e.g., $d_B = 0.5\ d_e$), the ratio of $(D_*/d_e)^2$ should be very large, like 15, instead of 1.5, and optimum performance would probably be achieved with the use of a diffuser centerbody which would result in an annular diffuser configuration.

D.3.3 Instrumentation

Valid test results and a proper interpretation of these results requires an accurate definition of the test conditions. The test conditions of interest include (Appendix C):

- Enthalpy
- Stagnation (model) pressure
- Stagnation (model) heat flux
- Chamber (arc heater) pressure
- Test cabin pressure

The definition of enthalpy should include the energy balance, mass balance, and heat flux values. Therefore in addition to the above parameters, the following arc heater operating measurements are required:

- Voltage
- Current

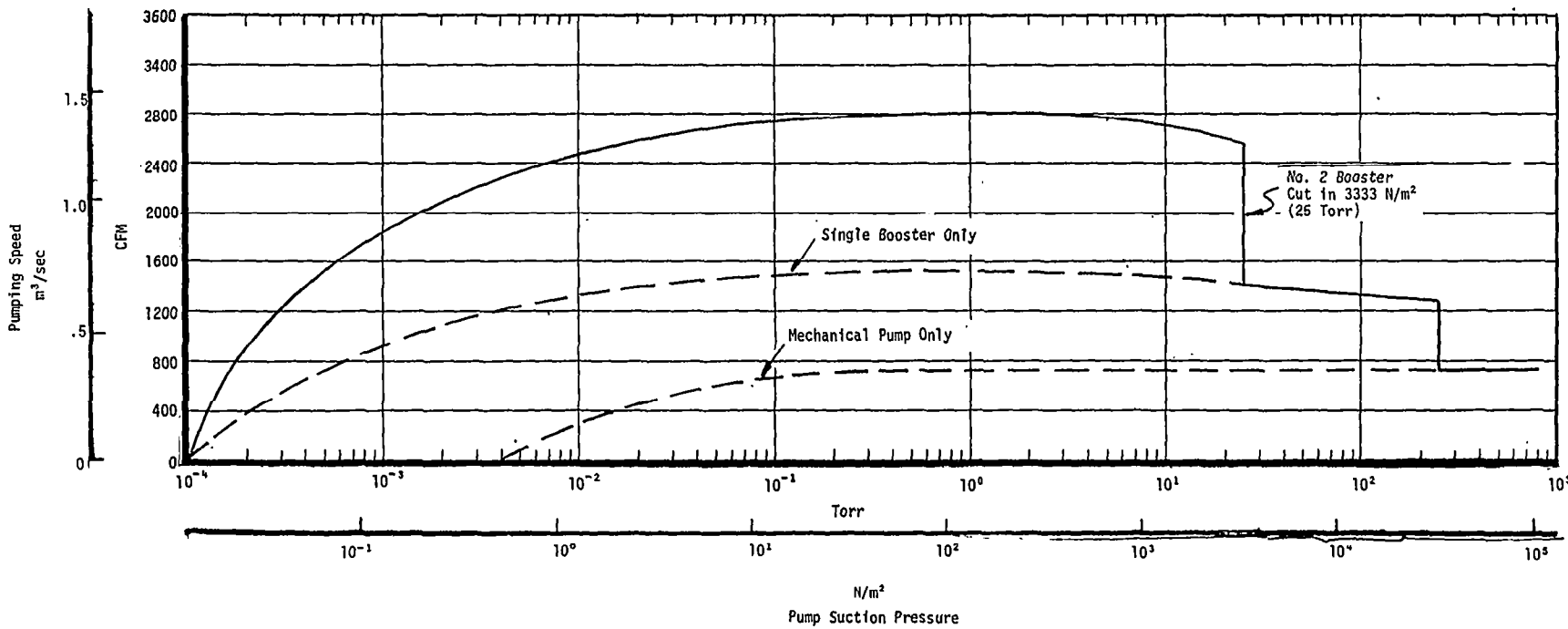

Figure D-4. Vacuum Pumping System Characteristics

- Water flow rate
- Cooling water temperature rise
- Total gas flow rate

The present facility capability includes no stagnation pressure or heat flux instrumentation. The measured energy balance enthalpy has also been somewhat questionable. The potential sources of error in this enthalpy are the measurements of all operating variables listed above. Apparent potential problems with these measurements include:

- Cooling water temperature rise - differential thermopile performance has been erratic; 3 calibrations have yielded 3 different sensitivities, all differing from the theoretical sensitivity
- Total gas flow rate - metered through 3 different systems at low pressure and small rotatmeter scale values, both of which are in the direction of low accuracy

Also the arc heater has been operated in a configuration that results in low efficiency operation. Therefore the energy balance enthalpy is defined by differences in large numbers (Equation (C-1)), and even small errors in the operating condition measurements then result in large errors in enthalpy. A computer analysis using the Aerotherm ARCFLO computer code has demonstrated that this problem can be reduced for typical test conditions in the HYMETS facility by reducing the constrictor column length. A typical computation result is shown in Figure D-5 and indicates a factor of two increase in efficiency by shortening the column length by about 60 percent.

D.4 RECOMMENDED MODIFICATIONS

Based on the above presentation, recommended modifications for reentry simulation testing in the HYMETS facility are:

- Replace the existing diffuser (and extension spool) with a new diffuser assembly
- Add a facility pressure probe and steady state and transient calorimeters
- Add 0.0318-meter (1.25-inch) diameter flat face models which accept appropriate metallic test samples
- Replace the cooling water temperature rise differential thermopile
- Add a second set of gas flowmeters for high accuracy low flow rate metering

I = 140 amps

$\dot{m}_{N_2}$ = 2.44 x 10^{-4} kg/sec (5.4 x 10^{-4} lb/sec) - arc heater only

$\dot{m}_{total}$ = 9.05 x 10^{-4} kg/sec (2.0 x 10^{-3} lb/sec) - arc heater and plenum

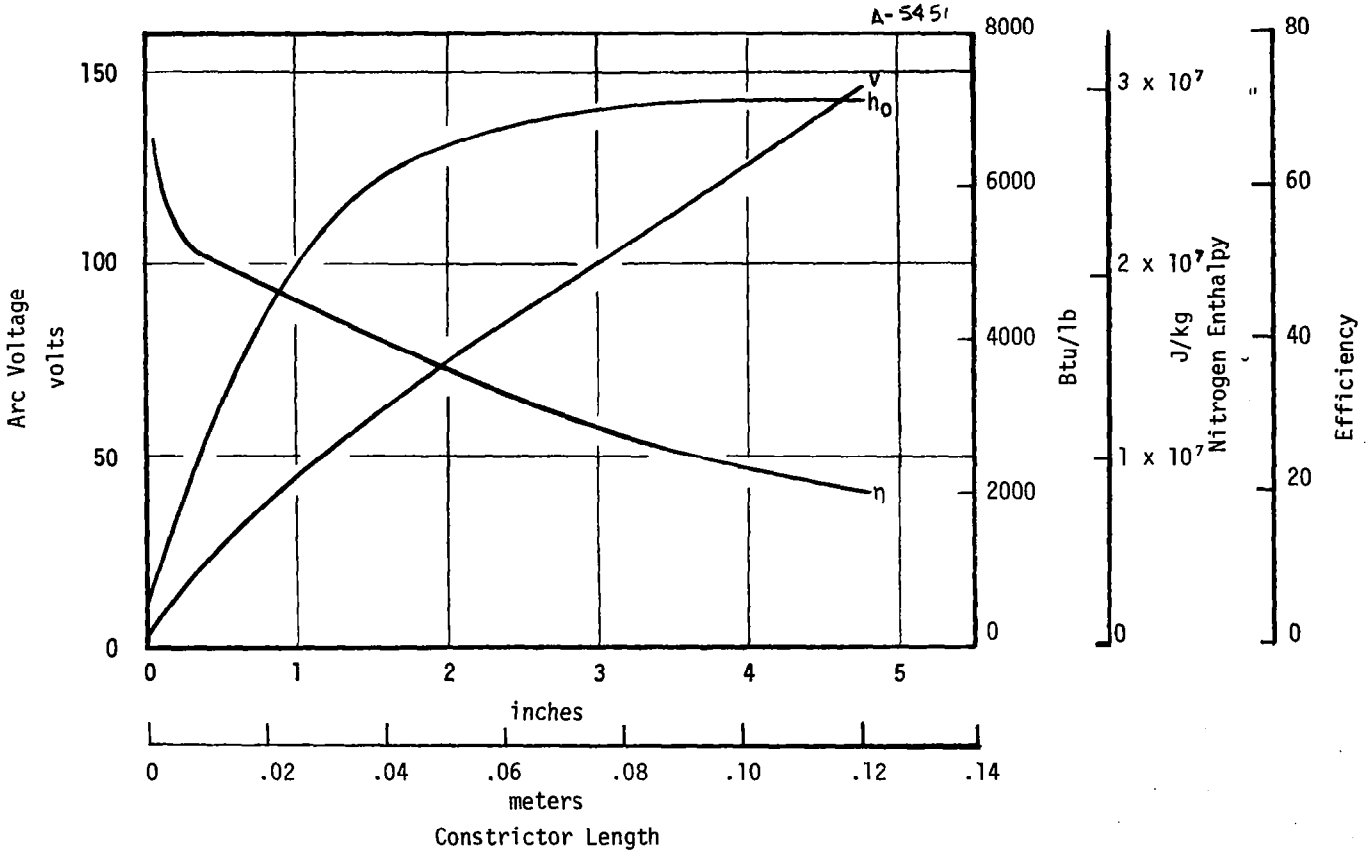

Figure D-5. ARCFLO Computer Code Results for a Typical Test Condition

- Check and/or calibrate all other instrumentation
- Shorten the arc heater constrictor column as defined by analysis for the range of conditions desired for future test requirements

In order to increase the effective vacuum pumping capability with a large model (up to 0.0318-meter (1.25-inch) diameter) in the test stream, the present diffuser must be replaced. A new diffuser system which allows replaceable diffuser sections for diffuser diameter changes and allows removable centerbodies is therefore recommended. The proposed system is shown in Figure D-6. Installation of this system requires elimination of the existing diffuser and extension spool, and modification of the test chamber rear flange and the heat exchanger front flange. The proposed system is sufficiently versatile to accommodate any test condition and configuration within the basic capabilities of the HYMETS facility as defined by the test envelopes of Figures D-2 and D-3.

In order to allow accurate definition of the test conditions to which the test samples are exposed, the following additional instrumentation is recommended:

- Pitot probe and pressure transducer for measurement of model stagnation pressure
- Steady-state, Gardon calorimeter model for measurement of catalytic wall heat flux (0.0318-meter (1.25-inch) body diameter, flat face identical to the test sample model configuration)
- Transient slug calorimeters (at least 2) for measurement of fully catalytic and full noncatalytic wall heat flux (configuration as above)

Also for sample testing, at least two test models similar to those used in this program (Figure C-1) are recommended.

Finally in order to improve the accuracy of operating condition measurements and therefore the accuracy of test conditions defined therefrom, the last four recommendations above should be implemented.

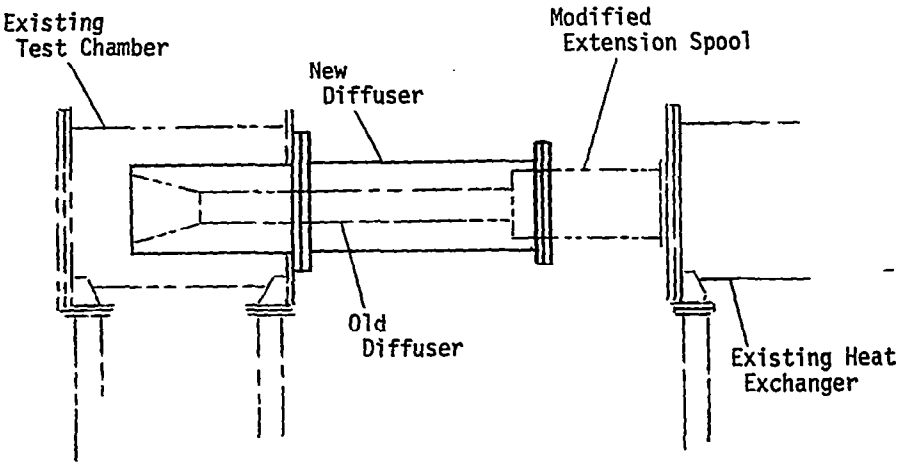

Figure D-6. Proposed Diffuser System
a) Overall View

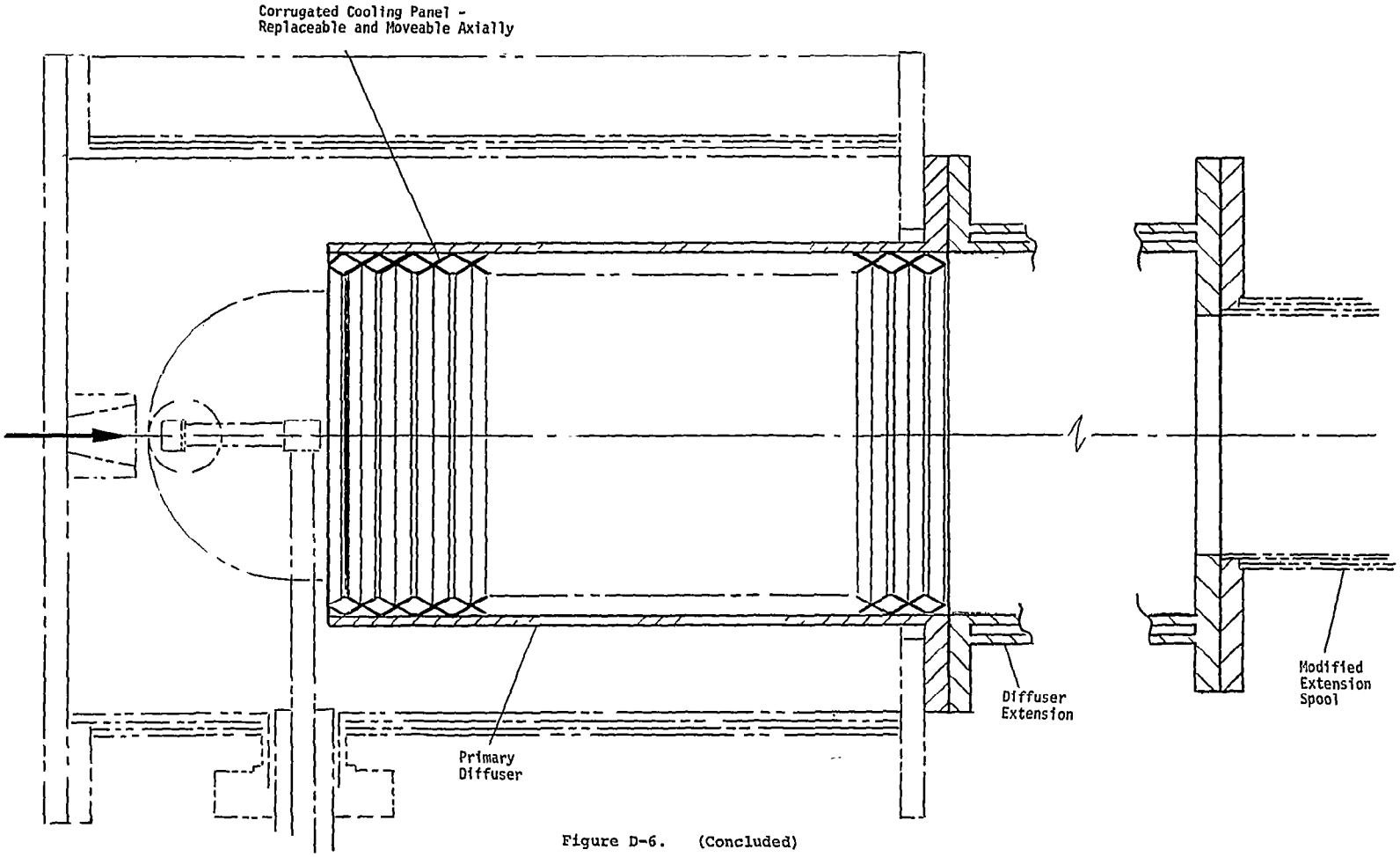

Figure D-6. (Concluded)
b) Detailed View

REFERENCES

APPENDIX D

D-1. Smith, Richard, T., "Experimental Studies of High Temperature Hypersonic Diffusers," Air Force Flight Dynamics Laboratory, Technical Documentary Report No. FDL TDR 64-4, February 1964.

D-2. Boylan, David, E., "An Experimental Study of Diffusers in an Open-Jet, Low-Density, Hypersonic Wind Tunnel," Arnold Engineering Development Center, (AEDC) Air Force Systems Command, AEDC-TDR-64-47, April 1964.

*U.S. GOVERNMENT PRINTING OFFICE: 1975 - 635-275/11